

Dissertation zur Erlangung des Doktorgrades der Fakultät für Chemie und
Pharmazie der Ludwig-Maximilians-Universität München

**Towards the Application and Immobilisation
of a Biomimetic Iron(IV)-oxido Complex
and the Implementation of
Good Research Data Management**

Rachel Janßen

aus Simmerath, Deutschland

2025

Dissertation zur Erlangung des Doktorgrades der Fakultät für
Chemie und Pharmazie der Ludwig-Maximilians-Universität
München

Towards the Application and Immobilisation
of a Biomimetic Iron(IV)-oxido Complex
and the Implementation of
Good Research Data Management

Rachel Janßen

aus Simmerath, Deutschland

2025

Erklärung

Diese Dissertation wurde im Sinne von §7 der Promotionsordnung vom 28. November 2011 von Frau Prof. Dr. Lena J. Daumann betreut.

Eidesstattliche Versicherung

Diese Dissertation wurde eigenständig und ohne unerlaubte Hilfe erarbeitet.

Düsseldorf, 01.08.2025

Rachel Janßen

Dissertation eingereicht am	23.05.2025
1. Gutachterin:	Prof. Dr. Lena J. Daumann
2. Gutachterin:	Prof. Dr. Silvija Markic
Mündliche Prüfung am	10.07.2025

Disclosure of Used Tools

Document Preparation

This thesis was written and processed using the software Texmaker 5.1.4. ChatGPT (GPT-4-turbo) by OpenAI was frequently used to help with used commands and packages.

Figures

All figures (not including analytical spectra) in this thesis were, if not mentioned otherwise, created using Microsoft PowerPoint, Chemdraw 19.1 and the image creator of ChatGPT (GPT-4-turbo) by OpenAI.

Text and Language

For improvement of the text and language several tools were used. If needed, the translator DeepL (<https://www.deepl.com/>) and sometimes ChatGPT (GPT-4-turbo) by OpenAI were used for single word translation from German to English and the website Thesaurus (<https://www.thesaurus.com/>) was used to find more adequate terms or create more variation. In singular cases, whole sentences were optimised using ChatGPT (GPT-4-turbo) by OpenAI. The AI was asked to create better versions of the sentence and from the presented results the sentence was adapted accordingly.

Bibliography

Literature and Citations were managed using Citavi 6.19.

Reviews

This thesis was to a great extent reviewed by Michael Mertens, Sophie Gutenthaler-Tietze and Doreen Reuter. Although only minor corrections were applied, I would like to acknowledge the effort and time they invested.

Disclosure of Participation

I would like to acknowledge that during my research, I often worked in close cooperation with other group members, especially within my subgroup. Therefore, this work was always positively influenced by the input and advice given by my lab mates throughout the different projects. This is mirrored in the shared first authorships in both included publications. In addition to the collaborative work with Violeta Vetsova, Niko Lindlar (né Jonasson) and Annika Menke, I would like to stress that while not visible within this thesis, once she joined the group, Doreen Reuter had a relevant influence in the immobilisation project on silica as we discussed problems within this project and co-supervised the master thesis of Johanna Großmann.

DOMINIK PUTZ was involved in the synthesis of the new pyrroloquinoline quinone derivatives and successfully optimized a crucial reaction step during his internship.

TOBIAS WALTER was involved in the initial phase of the chitosan project during his internship. He helped optimise the chitosan bead formation, investigated the crosslinking with glutaraldehyde and performed several initial experiments of the immobilisation. He also performed the first synthesis of the L1-Cl ligand.

HENRY LAUK investigated the exchange of the outer solution with the inner space of the chitosan gel beads during his internship. He helped optimise the washing procedure to improve the reproducibility of the experiments.

BASTIAN MICHELS performed several experiments towards the direct immobilisation of the complex C2-NH₂ on the chitosan beads during his bachelor thesis.

CLARISSA SONNEMANN performed experiments towards the immobilisation of the L1-NH₂ onto chitosan beads during her internship. She also performed a thorough investigation on the Schiff base formation between the ligand and glutaraldehyde in solution.

JAKOB EWERHARDT performed initial experiments towards the synthesis of the ligand L1-N₃ and the immobilisation *via* copper catalysed azide-alkyne cycloaddition during his internship.

JOHANNA GROSSMANN optimized the synthesis of the ligand L1-N₃ during her master thesis. She performed most of the experiments regarding the immobilisation on MCM41 silica *via* click reaction described in Chapter IV4.3.2.

Acknowledgements

First of all, I want to thank you Lena for guiding me through this thesis. For always having an open door and all the things I was allowed to learn. For being a stronger voice than the tiny impostor in my mind that said I could not do this. For letting me discover how much I enjoy teaching and giving me a place to do it.

I would like to thank Prof. Dr. Silvija Markic and the whole committee for taking the time and interest to read my work.

I want to thank all the people at the analytical facilities at both universities for the time they took to analyse my samples. Thank you to Brigitte Breitenstein in the NMR facility, Werner Spahl for the HR-MS measurements, Peter Meyer for measuring and solving crystal structures and Susanne Ebert and Robert Eicher for elemental analysis at LMU Munich. I also thank the CEMSA@HHU for their NMR and HR-MS measurements, the facility for elemental analysis at HHU Düsseldorf.

I also want to thank Burcu Yücel and Nick Sistig for all the work they do within our group and their support in my both my thesis and teaching.

A special thanks goes to Christoph Singer and Bernhard Veith from the Rechnerbetriebssgruppe at LMU and Philipp Rehs and Alexander Mielke from the ZIM at HHU who advised and helped me setting up our network and storage solutions and countless other IT problems.

I want to thank Thomas Engel from LMU for taking me to the NFDI4Chem Consortium in Hannover and giving me an insight on their work. I would also like to thank Nicole Jung from KIT Karlsruhe for helping me set up the ELN Chemotion and giving me her insights on publishing a FAIR synthesis.

I am very grateful to all the students I supervised for sharing their curiosity and motivation with me. Thank you Dominik, Tobias, Henry, Bastian, Clarissa, Jakob, Johanna and Taima for all the work you did and all the energy you put into your internships. You are a great part of this thesis and often rekindled my own motivation to fix an issue and solve a problem. Thank you for being great cow-workers of mine!

To Britta, Nathi, Tiff and Sonja - Thank you for getting me here. For being there through our studies and all other obstacles I faced. And of course, thank you for all the happy times in Munich and beyond. For being amazing friends that I hope to keep forever.

I want to thank the whole group with all its former and current members. For all the input and discussions, for all the lunch and cake breaks, for all the game nights, for all the time we spent as *Arbeitskollegen*. For sometimes keeping the tidiness I try to implement. Most importantly, I want to thank you for the time we spent as friends and for being the best moving company and pet sitters one could ever hope for.

To Violeta - Thank you for being my supervisor, for being my PQCrew, for being my labmate, for being my friend. For all the time I spent on your windowsill when the science didn't science.

To Ioana - I forgive you for stealing my outfits. Thank you for being an awesome labmate and friend and for teaching me young people stuff.

To Jan - You have been the best interior design collaborator I ever met in a lab. Thank you for the scientific input and all the distractions. No thank you for the teabag-sharing I had to witness.

To Sophie - Thank you for proof reading every little thing I send your way and making it a *schnuff* better every time. You have been my friend, my therapist and even shortly my home when life got in the way. And also, thanks for marrying me an extra friend, nice one!

To Jonathan - Thank you for being that extra friend! For never losing patience with the perfectly shaped crystals I brought you. For every board game we played and will play.

To Mikey - Thank you for being my partner-in-move. For co-working on the Düsseldorf project, setting up our office, lab and homes. For being my friend and labmate. For every coffee, football talk and board game. For watching formula 1 with Chris so I don't have to.

To Doreen - Thank you for being our vanguard at HHU. Please know that I am very grateful for all the preparations you did. Thank you for enduring all the immobilisation setbacks with me. For being 'that team' that shares their hotel room.

To Philippe - I appreciate your help with the lab courses so very much. Thank you for taking work of my plate whenever you could.

Last but not least, I want to thank my family. My parents for making all of this possible and trusting an 18-year old to go out into the world with nothing but a suitcase and a room for three weeks. My siblings for patiently waiting ten years for me to come home. And at last - Chris, thank you for appearing when you did. For being so supportive. For moving with me, so I can do the job that I came to love. For getting up early every morning to make the coffee that gets me through the day. I love you.

Abstract

Ten-eleven translocation (TET) enzymes play a crucial role in gene regulation. They are involved in the demethylation of the epigenetic marker 5-methylcytosine (5mC) which is a factor in gene silencing. In order to facilitate the investigation of the proposed active iron(IV)-oxido species in TET enzymes, biomimetic model complexes are often employed. Previous to this work, it was shown that the model complex $[\text{Fe}^{\text{IV}}(\text{O})(\text{Py}_5\text{Me}_2)]^{2+}$ (C4) can oxidise 5mC as well as 5mC-containing nucleosides and small nucleotides in a biomimetic manner.

In this work, the reactivity of the biomimetic complex C4 towards synthetic DNA bases was investigated (Chapter III). The tested synthetic DNA bases including 1-methylcytosine (1mC), 5-methyl-*iso*-cytosine (5*m*iC) and thymine (T/5mU) have previously been used in the literature to expand the genetic alphabet and create semi-synthetic DNA like the eight-letter "hachimoji" DNA. By this expansion, the information density within DNA has been increased significantly. In other literature procedures, the density of information of DNA has been elevated by adding different layers of information on one DNA strand using epigenetic modifications. The investigations described in this work aimed to take a first step towards combining these approaches to further optimise the possible use of DNA as an informational storage medium. The investigation on the biomimetic oxidation of synthetic DNA bases revealed a difference between C-methylated and *N*-methylated bases wherein the C-methylated bases were oxidised significantly faster. Together with Fabian Zott, these kinetic findings were compared to calculated C-H bond dissociation energies (BDEs) showing a strong alignment of experimental and theoretical values and identifying BDE calculations as a useful tool in reaction rate prediction.

In addition to the application of the complex C4 in substrate oxidation, the immobilisation of the complex was attempted. C4 can be successfully applied in substrate oxidation. However, side reactions like comproportionation of the iron(II) and iron(IV)-oxido species complicate the handling of the complex and the spectroscopic analysis of reaction kinetics. To facilitate the application of C4, thorough investigations towards the immobilisation of the complex were performed. Previous attempts at immobilisation on Merrifield or Tent-a-Gel resin did not yield the desired applicability. Since C4 is primarily used in biomimetic reactions, chitosan was tested as a possible solid support for complex immobilisation as it is commonly used in enzymatic applications and compatible with physiological conditions. The formation of chitosan gel beads, their modification with glutaraldehyde and subsequent reaction with derivatives of Py_5Me_2 and iron(II) complexes thereof was thoroughly investigated.

As a second solid support material, hexagonal porous silica was tested as it is commonly used in catalyst immobilisation. With silica as solid support, immobilisation *via* nucleophilic substitution and ring formation (click) reactions were investigated. While attempts at binding *via* nucleophilic substitution did not yield the desired outcome, preliminary results of the immobilisation of a newly synthesized aza-derivative of the ligand system L1-N₃ using the strain promoted azide-alkyne cycloaddition (SPAAC) reagent DBCO-NHS and subsequent iron(II) complex formation strongly indicate successful immobilisation of Py₅Me₂ ligand system.

Beside the synthetic work, a project towards the improvement of research data management within the group was performed. Together with Violeta Vetsova, a synthetic route towards new Pyrrolloquinoline quinone derivatives was finalised and used to create a publication closely following the FAIR guidelines. Towards this goal, the electronic lab notebook Chemotion was established within the group and the complete datasets including raw data of the synthesis were uploaded in the Chemotion repository and published with the paper. To further improve research data management, an elaborate network and data storage system was created and set up to accommodate modern requirements for better data management, storage and access.

Table of Contents

I. Research Data Management	1
1 Introduction.....	3
1.1 What is Research Data Management?	3
1.2 FAIR Data.....	5
2 Implementation of a Research Data Management System and Describing a Synthesis According to FAIR Principles.....	9
2.1 Improving Research Data Management	9
2.1.1 First Steps Towards a Better Data Management Plan.....	9
2.1.2 Implementation of a Comprehensible and Safe Data Storage System	11
2.2 FAIR applied to the Synthesis of New Pyrroloquinoline Quinone Derivatives	14
2.2.1 The Pyrroloquinoline Quinone Derivatives Project	14
2.2.2 Creating a FAIR synthesis.....	15
2.3 A Publication According to the FAIR Principles	19
II. General Introduction - Biomimetics	25
1 Ten-Eleven Translocation Enzymes.....	27
2 Biomimetic Complexes	29
III. Biomimetic Oxidation of Synthetic DNA Bases	31
1 Introduction.....	33
1.1 DNA Data Storage Systems	33
1.2 Synthetic Expansion of the DNA Alphabet	35
1.3 Epigenetics: An Additional Layer of Information.....	36
2 Motivation and Aim	39
3 Synthesis of 1-Methylcytosine and its Oxidation Products.....	41
3.1 Synthesis of 1mC, 1fC and 1caC	41
3.2 Protection of the Exocyclic Amine in 1mC.....	43
3.3 Initial Experiments Towards the Biomimetic Oxidation of 1mC	45

4	Biomimetic Oxidation of 1-Methylcytosine and Other Synthetic DNA Bases	47
IV. Towards the Immobilisation of Py₅-Ligand Systems on a Solid Support		61
1	Introduction.....	63
1.1	Immobilisation Techniques	63
1.2	Solid Phase Materials.....	65
1.3	Immobilisation of Catalysts.....	67
2	Motivation and Aim	71
3	Synthesis of Ligands and Complexes for Immobilisation.....	73
3.1	Synthesis of Functionalised Ligands	73
3.1.1	Synthesis of L1-NH ₂	74
3.1.2	Synthesis of L1-OH.....	75
3.1.3	Synthesis of L1-Cl.....	76
3.1.4	Synthesis of L1-N ₃	76
3.2	Iron Complex Formation with Functionalised Ligands	77
3.2.1	Iron Complexes of L1-OH.....	80
4	Towards a Functioning Solid Support System	81
4.1	Chitosan Gel Beads	81
4.1.1	Formation of Uniform Gel Beads	81
4.1.2	Functionalisation of Chitosan Gel Beads: Glutaraldehyde Crosslinking ...	84
4.2	Immobilisation of L1-NH ₂ on Functionalised Chitosan Beads (CB-GAs)	86
4.2.1	Investigation on the Schiff Base Formation of L1-NH ₂ and GA.....	92
4.3	Functionalised Silica	97
4.3.1	Immobilisation on Silica by Nucleophilic Substitution.....	98
4.3.2	Immobilisation on Silica Using Click Chemistry.....	103
V. Summary and Outlook		109
VI. Experimental		111
1	General Considerations	113
2	Methods and Materials.....	115
3	Experimental Procedures.....	119
3.1	Epigenetic Substrates.....	119

3.2	Synthesis of $\text{Py}_5\text{Me}_2\text{CH}_2\text{X}$ type Ligands (L1-X).....	123
3.3	Synthesis of Iron Complexes.....	146
3.4	Synthesis of Chitosan Beads and Modifications	152
3.5	Synthesis of modified MCM41 Silica	153
VII	Appendix	155
1	Supporting Information: Modular Synthesis of New Pyrroloquinoline Quinone Derivatives.....	157
1.1	Materials and Methods.....	157
1.2	Synthetic Procedures	158
2	Additional Spectra Chapter III3.....	167
3	Supporting Information: Biomimetic Oxidation of 1-Methylcytosine and Other Synthetic DNA Bases.....	169
3.1	Materials and Methods.....	169
3.2	Product Analysis by HPLC-MS and GC-MS	172
3.3	Bond Dissociation Energy Calculations	185
3.4	Synthetic Procedures	185
4	Additional Experimental Information Chapter IV3	187
5	Additional Spectra Chapter IV4.....	189
6	IR Spectra	201
7	Crystallographic Data	205
8	List of Abbreviations	211
9	Bibliography	215

I. Research Data Management

1. Introduction

In this chapter, the concepts of **FAIR** - **F**indable, **A**ccessible, **I**nteroperable and **R**eusable - Data and Research Data Management especially in the context of a PhD thesis in science will be discussed. As the topic of Research Data Management (RDM) and FAIR Data became more and more important in recent years, our group naturally wanted to adapt our working procedure according to these concepts. During my thesis, I spent a significant amount of time not only doing research but questioning *how* research should be done and thus helping implement the necessary structures to improve our own RDM and creating our first publication with an emphasis on a FAIR synthetic procedure.

1.1. What is Research Data Management?

To understand the term research data management (RDM), it is necessary to define what research data is. In a relatively loose definition, research data is all data that is collected, observed, generated or created to validate research findings. This definition of course includes a vast amount of data types due to the wide range of research fields and areas, which can differ immensely in their used methods to generate and process data. In a specific research field however, the term research data might be understood more easily. As an example, in the field of chemistry research data to a great extent consists of experimental data, such as reaction conditions, as well as analytical data from spectroscopic or spectrometric measurements, respectively. As one could guess, RDM refers to how this data is handled throughout the research process.

For a long time, the way of handling research data was left to the individual without any standardised practices at hand. Although commonly known practices like writing a lab book for example exist, there were no general rules on which and how data was to be recorded. In recent years, RDM has gained more and more relevance as the need for generalised systems became obvious, resulting in task forces creating Europe-wide strategies^[1,2] to guarantee better and more consistent handling of data. For the scientific research fields, the topic became additionally relevant since funding agencies like the European Research Council (ERC) and the Deutsche Forschungsgemeinschaft (DFG) included a suitable data management plan (DMP, Figure I.1) into their conditions for research funding.^[3-5] As described before, guidelines on RDM differ depending on the applied field of research. The DFG provides a general guideline on RDM^[3], but also specific expansions regarding different research fields.

In their guideline for the field of chemistry^[4], they state that a research funding proposal should include an outlook on the kind of data that the project is expected to generate and an outline of how the data will be recorded, documented, processed and stored. In respect to storage, the safety and long-term availability of the data is an additional



Figure I.1.: Research data management (RDM) as the life cycle of a data set. All stations that are passed through by data, from their creation to their access and reuse by other researchers, should be included in a comprehensive data management plan (DMP).

focus. As a side note, it has been found that the accessibility of data rapidly declines with age,^[6] which might be overcome to an extent by improved research data storage systems. If applicable, the data should also be handled according to the FAIR principles (see *vide infra*). In summary, it is a common goal among researchers to implement better RDM strategies and make them as consistent as possible. It should be kept in mind that there is a limit to consistency because of the variety of research fields and data types, which is why RDM guidelines still struggle to give precise instructions rather than general principles to be followed. For example, the ERC asks for 'a sufficiently detailed description' of datasets,^[5] which is very much depending on personal definition.

Throughout the discussion of good research data management, the subsequent question of how to handle the data in terms of sharing arose. Researchers have recognized that sharing data is a relevant pillar on which scientific progress stands, but still have reservations regarding the practice.^[7–11] In order to accelerate and facilitate the process of shifting publication norms towards a more open and reusable standard, discussions of this topic in different research fields are more and more common. They attempt to identify reasons for the reluctance of researchers to share their data^[7–9] and find the necessary incentives^[7,10,11] to support change. There are a few core points which occur repeatedly. First, there simply is a lack of knowledge and training in research data management and sharing data.^[8,9] Scientists are overwhelmed by the demand to change their current behaviour without precise requirements (see *vide supra*) and struggle to find an access point. Especially the form and extent of metadata seems to be a difficult subject.^[9] Secondly, there are concerns about the safety of the data regarding the long-term storage and reuse by others. Information and knowledge about the conditions under which data can be reused by others and how this can be tracked by the original creator is too scarce to induce confidence in repositories.^[9] Third, a common suggestion on how to

encourage more commitment to DMPs and data sharing in general is creating examples. It is believed that researchers can be convinced and animated by providing examples which demonstrate the efficacy of reusing shared data and make these examples widely known.^[8,10]

1.2. FAIR Data

The term and concept of good research data management has gained more and more importance over the last decades in various fields. Not only in the respect to handling data in general, but in regard to enhancing the usability of published results in the science community. Research is always build upon previous findings and can not grow and expand, if these findings are not accessible. The literature review of A. Subaveerapandiyan gives a comprehensive overview on how this topic developed with an emphasis on the role of academic libraries, which play a crucial role in collecting and sharing findings and data.^[12] Although the concept was becoming widely known, discussed, and applied across various fields and universities, it relied on existing systems and methods familiar to the respective researchers. As a result, it failed to establish common rules that could be followed.

Recognizing this issue, a group people with various backgrounds including researchers, publishers and funding agencies banded together to compose the 'FAIR Guiding Principles'.^[13] By bringing together diverse stakeholders in scientific data publishing, they were able to assess and address the needs of everyone involved in the process of creating and sharing research data through publication. Together, they developed the principle of **FAIR** - **F**indable, **A**ccessible, **I**nteroperable and **R**eusable - data as a guideline on how to handle and publish data to make data as useful as possible for the science community. It is emphasized that good data management is not the goal, but rather the necessary base and should nowadays be self-evident. While the FAIR guidelines do not give precise criteria due to the differences in scientific fields, datasets and application, they provide, as the name suggest, guidelines on what makes data useful for future scientific progress. There has been criticism on the loosely defined guidelines and misconceptions of the role the FAIR guidelines want to take on which was addressed by a group of the original authors giving further insight into what the principles intent to be.^[14]

In Figure I.2, a more explicit itemization of the FAIR principles is shown. According to these guidelines, data is *findable*, if the data has a persistent identifier, sufficient metadata and is searchable (F1-F4). More precisely, a published dataset is *findable*, if it is equipped with a Digital Object Identifier (DOI) and registered in a searchable resource like a repository, respectively. Of course the exact criteria for rich and sufficient metadata depends on the research and should be provided by the journals typically publishing this kind of data and additionally examined by the reviewers. The authors also put a strong emphasis on the fact that the FAIR principles do not apply solely to humans. In

To be Findable: F1. (meta)data are assigned a globally unique and persistent identifier F2. data are described with rich metadata (defined by R1 below) F3. metadata clearly and explicitly include the identifier of the data it describes F4. (meta)data are registered or indexed in a searchable resource	To be Interoperable: I1. (meta)data use a formal, accessible, shared, and broadly applicable language for knowledge representation. I2. (meta)data use vocabularies that follow FAIR principles I3. (meta)data include qualified references to other (meta)data
To be Accessible: A1. (meta)data are retrievable by their identifier using a standardized communications protocol A1.1 the protocol is open, free, and universally implementable A1.2 the protocol allows for an authentication and authorization procedure, where necessary A2. metadata are accessible, even when the data are no longer available	To be Reusable: R1. meta(data) are richly described with a plurality of accurate and relevant attributes R1.1. (meta)data are released with a clear and accessible data usage license R1.2. (meta)data are associated with detailed provenance R1.3. (meta)data meet domain-relevant community standards

Figure I.2.: Extension of the FAIR data principles as they are proposed by M. D. Wilkinson *et al.* ^[13]

our modern society, searching for publications and data, as well as the generating and processing of data is done with or by machines. This machine readability should be kept in mind when creating and assigning metadata.

The next term *accessible* is likely the most misunderstood, as it is often equated with open access.^[14] There are reasons to keep data from public access and this need is not neglected by the assessment of accessibility. If the data can be found by using the identifier and the metadata is sufficiently describing the data as well as how the data could be obtained or why it can not, this would be considered *accessible*. In the context of FAIR, *accessible* does not necessarily mean available, just that there is some procedure, which can include authentication or authorization, to access the data.

Interoperable refers to the way data is described and formatted. Again, the exact definitions strongly depend on the type of data and the research field. However, as a basic guideline data is *interoperable* if the used vocabulary to describe the data is in consensus with generally used standards in the field and chosen data formats are operable without limitation to software or procedures of one specific provider.

Similar to accessibility, the term *reusable* is directed towards a protocol for reusing the data, not necessarily allowing unlimited use. Nevertheless, data should always be published with a clear and accessible data usage licence (R1.1). Rich and detailed metadata can already make data *reusable* to a great extent.

In summary, the FAIR principles want to provide a guideline to help manage and publish data in a way that benefits the community the most and allows science to effectively build upon previous results. However, they do not call for unlimited access.

They recognize that sensitive data and unfortunately competitiveness do not concede with open data and therefore do not strive to make all data open, but call for transparency.

An example of how important and productive it can be to openly share data in a FAIR manner was the COVID pandemic, where global collaboration and facilitated access to critical data, such as the virus's genome sequence, enabled researchers to accelerate vaccine development and therefore save lives.^[15,16] On the other hand, commonly implementing the FAIR Guiding Principles could also help with less enjoyable ways of data management, namely data fraud. A prominent example from the Netherlands, where data was faked on a large scale, is the case of Diederik Stapel, which prompted numerous discussions on how data fraud could be prevented or at the least detected early.^[17,18] Following the FAIR principles and assessing published data by these guidelines could help circumvent such issues.

The importance of this is further underlined as the FAIR principles are an integral part of the research and innovation funding programme Horizon Europe and formerly Horizon 2020.^[19,20]

2. Implementation of a Research Data Management System and Describing a Synthesis According to FAIR Principles

2.1. Improving Research Data Management

Before discussing the aspect of your data being in accordance with the FAIR principles in the context of published data, one should ask themselves if your data is even FAIR within your own research group. Do you have access to the data others in your group create(d) or at least does your supervisor? Would you be able to find it? Do you have access to the raw data? Is your data saved in a way to be accessible in a few years?

Besides these questions, from the guidelines of two of the most relevant funding agencies for chemists in Germany, the ERC^[5] and the DFG^[4], the following criteria can be derived for handling data within your research group as part of your data management plan (DMP): 1) Standards for metadata as well as the naming or identifiers of datasets should be set and followed. 2) A methodology on how data is stored and preserved is needed. This includes the safety and a comprehensible sorting system. 3) How can and will data be shared and which restrictions might apply to your group.

In line with this and the previously described concepts and guidelines (see Figure I.1 and Figure I.2), the following changes and improvements to the research data management in our group were applied.

2.1.1. First Steps Towards a Better Data Management Plan



In case of the publication on the PQQ derivatives project (see *vide infra*), we decided to start collecting all the data we had already while finishing the last synthetic steps and used this as a test for our internal DMP. While Violeta and I both retrieved our share of the data, we also tried to find the respective data of the other person in their lab books and computer. It turned out that we were able to find the data but it was not the easiest task, especially for the raw data. Nevertheless, having another person trying to find the data on a specific or even a random experiment you did can give you a very good impression on how good in the sense of *findability* and *accessibility* your system of saving data is for your own group. This prompted the discussion within our group on how, where and with which metadata experimental results and research data are stored and we repeated the experiment of finding someone else's data with the whole group. We found that while the data was in general appropriately named and stored, the systems still differed according to personal preferences. This poses a problem since an explanation of the corresponding person is sometimes necessary to access their data which limits the *findability* and *accessibility* of data. Therefore, we agreed on a common system for the whole group and as a result, basic guidelines were set on *how* to name, save and indicate data. For example, name abbreviations for labelling your experiments should always be a three-letter code, since

two-letters codes, especially when using initials, are quickly repeated and of course the label should always be included when saving data belonging to this experiment. Following the persons identifier is either the number and/or appropriate description of the experiment. Another agreed on identifier for every saved data file is the date. These agreed on guidelines for naming data files fulfils the criterion "1) Standard for naming and identifiers" regarding DMPs for research funding agencies^[4,5] and improved the *findability* within the research group.



The next relevant part of an internal DMP is criterion "2) A comprehensible and safe storage system". Only saving data on one computer is no safe data storage, since data loss due to hardware malfunction or theft is always a possibility. The concept of regularly attaching a hard drive to make a safety copy is time consuming and relies heavily on every group member taking the time and effort. To resolve this issue while at the LMU, we used the possibility of the LRZ Sync and Share instance to establish a common space for every group member to store data that was to be shared and helped them individually to create their own connected folder. This allowed every group member to store their data in regular folders on their computer like they are used to, while the folders are located in an online server which has a backup system. This solution made it possible to simultaneously share data without too much effort and keep your own data on a backed up server. In addition, by the introduction of the commonly shared folder, it's folder structure and naming, a guideline was set which data is generally shared with the whole group, creating a first draft of a sharing policy. However, this solution did not guarantee accessibility of data in personal folders by another person and due to expiring contracts the personal server space of PhDs for example would be deleted at some point. This was circumvented by transferring the full amount of data to an external hard drive once after a contract was finished.

Besides this solution for safe data storage, we also started using an electronic lab notebook (ELN) instead of or more precisely in addition to the paper lab notebooks we used before. We decided to use the ELN Chemotion¹ which is provided by the NFDI4Chem². We opted for this ELN because of the closely connected Repository where data can be stored and made public (see *vide infra*. After the installation of the ELN Chemotion at the LMU Munich, I was included in the administration, tasked with testing the ELN and subsequently teaching other group members in using the instance. The obvious advantages of ELNs regarding DMPs is the safety of the data being stored on a backed-up server instead of either one computer or paper lab notebook, both of which could be irretrievably destroyed or lost due to several causes. In regard to criterion "1) Standards for metadata", an ELN which is updated and maintained by an organisation committed to FAIR data already includes a good standardized metadata system by the data and

¹<https://chemotion.net/>

²Part of the Nationale Forschungsdateninfrastruktur (NFDI) for Germany

2. Implementation of a Research Data Management System and Describing a Synthesis According to FAIR Principles

The screenshot displays the ELN Chemotion interface with the following sections:

- Starting materials:** RAJ-34, N-(2-methoxy-5-nitrophenyl)formam... (15.00 g, 78.47 mmol, 955.9 mmol, 1.000 equiv)
- Reactants:** Pd/C (447.0 mg, 0.00 mmol, 4.200 mmol, 0.05493 equiv), molecular hydro... (0.000 mg, 0.00 mmol, 0.000 mmol, 0.000 equiv)
- Products:** RAJ-35, N-(5-amino-2-methoxyphenyl)forma... (11.00 g, 88.19 mmol, 827.4 mmol, 87% yield)
- Solvents:** Ethanol (80.0 ml, n.d. vol ratio)
- Conditions:** Name, Status (Successful), Temperature (65 °C), Start/Stop times, Duration (3 hours), Type (nitro reduction to amine), Role (Select...), and a detailed Description of the reaction procedure.

Figure I.3.: Excerpt of an entry in the ELN Chemotion displaying parts of the data and metadata of this reaction. This entry corresponds to a reaction in the PQQ derivative synthesis discussed in Chapter I2.3 (see Scheme I.2).

details asked for in the notebook entries. As an example, an excerpt of an ELN entry is shown in Figure I.3. The entries and fields provide a guideline which data and metadata should be added, although this example is specifically relating to a chemical reaction. Also, digital search options are generally faster than flipping through a book resulting in easier *findability* and the ELN Chemotion gives the option to share data directly with other users. This is especially useful when supervising students or when co-working on a project. In addition, the complete ELN can be transferred to your supervisor after finishing your PhD by few clicks, allowing an easy way of future *accessibility*. A disadvantage might be the portability of your computer or use of electronic devices in the lab. Thus, we started switching from desktop computers to portable laptops and created designated chemical free working spaces to make the direct use of the ELN in the lab possible. However, if preferred it is obviously possible to make notes on paper in the lab which can then regularly be transferred to the ELN.

2.1.2. Implementation of a Comprehensible and Safe Data Storage System



When the group moved from the LMU Munich to the HHU in Düsseldorf in 2023, we needed to, but also had the chance to set up a new system for our general data storage building on what we already learned. A few criteria were set using our experiences and preferences as a group. We wanted to create a system that allows group members to save and store data on their personal computer in a way that guarantees the safety of the data in the means of getting lost or corrupted, but also in the means of being protected from unauthorized access. In a

similar way, the system should also allow access to generally shared folders, which are protected accordingly. An additional preference was the connection of personal computers to laboratory instruments in order to access them remotely while keeping the internet access for these instrument restricted due to issues that can occur after automatic updates. It should also be kept in mind that current and future group members have varying technical skills and therefore the complexity as a user should be kept minimal. Taking all these criteria and preferences into consideration, a network and data storage system was created as is depicted in Figure I.4. The set-up was performed in close cooperation with the local Centre for Information and Media Technology (ZIM),³ which manages network and server instances at HHU.

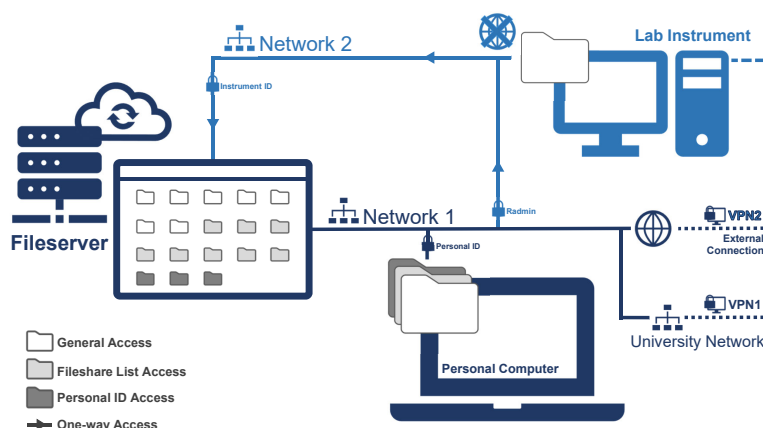


Figure I.4.: Schematic representation of the network solution for data file storage, safety, accessibility and sharing. Network 1 allows access to fileserver content, the internet and the university network according to the restrictions set with the personal ID. This network can be accessed externally using the university general VPN, VPN1. Network 2 is a subnet to network 1 and allows devices to access the fileserver using an instrument ID, which is limited to general access folders. Network 2 can not connect to the university network or the internet. Devices in network 2 can be accessed remotely using the Radmin software. Networks 2 can be access externally using VPN2, which is limited to the personal IDs of group members.

As a base structure, a basic office network (Network 1, Figure I.4) was created which is connected to all network access points in the offices within the group. This network allows access to the general university network and the internet as well as connections between devices within this network. As a next step, a filesaver was created for our group which is located with the ZIM and therefore managed, protected and kept up to date by them, creating a safe and backed-up instance for data file storage. Within this filesaver, we created three levels of accessibility. General Access folders can be seen and edited by every person with access to the filesaver while other folders can only be accessed by IDs on specific fileshare lists. We employed different fileshare lists relating to the employment status (permanent staff, postdoc, PhD, master student, hiwi, intern) which restrict the access to specific folders. In addition, every ID has their own personal home folder which can not be edited or even seen by other users. This layering of access allows us to store and save basically *all* data our group generates in one place while guaranteeing the safety of the data in the sense of corruption or unintended deletion and restricting access where

³<https://www.zim.hhu.de/>

applicable. If necessary, the PI and owner of the files server can be given access to all the data by the ZIM, thus avoiding data by persons who leave the group without sharing their data or password being lost. This guarantees long-term *accessibility* to all data files. Once the connection to the files server is established, it can be used like an internal hard drive allowing easy usage. If not directly connected to the network, for example in home office, a VPN (VPN1 or VPN2, Figure I.4) connection is necessary to access the network and files server, further protecting the data from unauthorized access. In summary, this ID and password protected network and files server set-up already provides a strong system for accessible but safe data file storage. In respect to folder structure and sharing policy, the general system already set was kept but is and will be iteratively improved.

Going one step further, we wanted to include computers in the lab controlling analytical devices to be added to the network. However, as mentioned above, these devices should not be connected to internet access. Therefore, a second network or a subnet (network 2, Figure I.4) was developed which can only access the files server instance, but not the university network or internet. For this purpose, a functional instrument ID was created which allows general access to the files server and thus analytical devices can be set to automatically save measured data in a relating folder on the files server. This has a few major advantages. First, group members do not need to transfer data from the device to their computer but can directly access it through the files server. Secondly, problems stemming from full disk and memory space on the analytical device computers are redundant. And third, by automatically saving measurements on the files server in an general access folder, raw data of all analytical measurements are directly and long-term accessible and therefore fulfil all the criteria for FAIR data. However, generated data can still be copied or transferred and processed data kept in the personal home folders to shield research from unauthorized or premature access, if needed. In order to protect our devices from external manipulation, this subnet can only be accessed *via* a specific VPN (VPN2, Figure I.4), if accessed from an external connection and is restricted to group members' personal IDs. As an additional feature, we use the software Radmin as a remote control solution for devices in network 2, since it can only be used when within the network (by direct connection or VPN2).

2.2. FAIR applied to the Synthesis of New Pyrroloquinoline Quinone Derivatives

2.2.1. The Pyrroloquinoline Quinone Derivatives Project

The synthetic work and relating background project of the synthetic procedures in this section were mainly part of my internship and master thesis^[21], which were done in the group of Prof. Dr. Lena Daumann prior to my doctoral dissertation. Both my internship and master thesis were done under direct supervision or in close cooperation with Violeta Vetsova and the project is described in detail in her doctoral dissertation.^[22] The main aspects of the project will be described briefly in the following. Nevertheless, the synthetic work was finished within the time scope of my dissertation including a crucial step within the total synthesis of the targeted pyrroloquinoline quinone derivatives, which was optimized during the internship of Dominik Putz under my supervision. This synthesis project was used as a first example to apply the concept of FAIR data within our group. Pyrroloquinoline quinone (PQQ) is a redox cofactor found in methanol, glycerol, glucose and other quinoprotein dehydrogenases.^[23–26] Methanol dehydrogenases (MDHs), for example, oxidise methanol to formaldehyde while PQQ is reduced to its quinol form PQQH₂. It has been believed that these enzymes activate the cofactor exclusively with calcium(II) as a Lewis acid, but it was found that lanthanide(III) ions are also used by bacteria and incorporated in functional MDHs.^[27,28] Within our group, several research projects focussed on the cofactor PQQ and its binding to lanthanides instead of calcium.^[22,29–31] One aspect of this work was the investigation of PQQ binding as a free molecule in solution, since there is no surrounding enzyme directing into a specific binding site.^[29] Thus, we synthesized PQQ derivatives containing less possible binding sites to make the enzymatic binding site more preferable.^[32] Figure I.5 shows the probable binding sites of PQQ in free solution (enzymatically relevant binding site in orange) and the targeted PQQ derivatives P_{ME}QQ_{MEM}⁴ and P_KQQ_{MEM}⁵ wherein the third and biologically irrelevant binding site is likely removed.

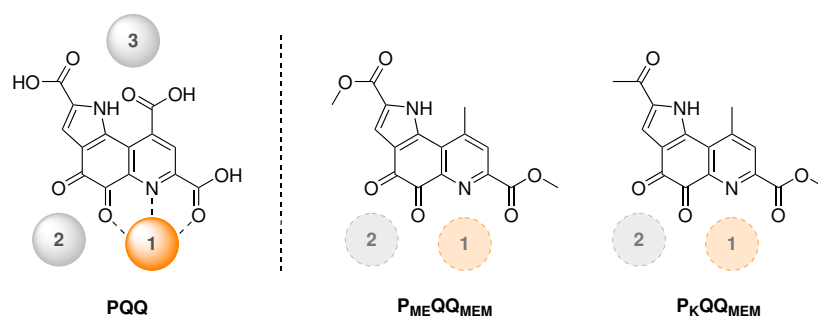


Figure I.5.: Left: redox cofactor pyrroloquinoline quinone (PQQ) with indication of the enzymatic metal binding site^[28,33,34] (1) in orange and additional possible binding sites (2 and 3) in solution^[35–37] outside of an enzymatic environment shown in grey. Right: PQQ derivatives P_{ME}QQ_{MEM} and P_KQQ_{MEM} with indication of probable binding sites (1 and 2) compared to PQQ.

⁴P_{ME}QQ_{MEM} (methyl-ester-substituted pyrrole, methyl-ester- and methyl-substituted quinoline quinone).

⁵P_KQQ_{MEM} (ketone-substituted pyrrole, methyl-ester- and methyl-substituted quinoline quinone).

2.2.2. Creating a FAIR synthesis

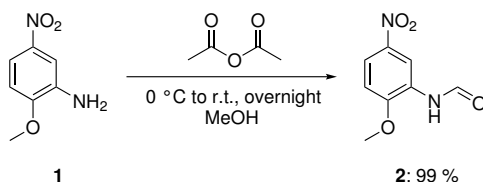
The following section describes the adaptations and improvements we applied to a typical organic synthesis procedure to make it FAIR (see Chapter I1.2).



In order to create a FAIR synthesis one must have two obvious components, a plan for a synthetic procedure and an idea on what FAIR means in this context. As we had most of the synthetic procedure already at hand^[21], we started evaluating and adapting this procedure to make it as FAIR as possible, especially focussing on the 'I' (interoperable) for analytical data and 'R' (reusable) for the synthetic procedures. In this case, reusable can also be interpreted as reproducible as a synthetic procedure is obviously reused to either synthesize the given molecule or adapt the conditions. In our case, the reason for creating a FAIR synthesis partly lies in the fact that the synthesis of an older publication we tried to reproduce and adapt posed a lot of problems and did not work as expected, which we attributed to a lack of information and details. This is thoroughly described in Chapter I2.3.

Hence, striving for a better RDM, we derived a list of necessary data and details for a synthetic procedure from our own standards, the standards given by our targeted journal for publication⁶ and the standards given by the Chemotion Repository,⁷ which we intended to use for publication of the raw data (see *vide infra*). Combining these sources, especially the Chemotion Guidelines, we expected to attain a FAIR synthetic procedure that will be reproducible in the future.

As an example, the first step of our 7-step synthesis in Scheme I.1 shows the generally used depiction of an organic synthesis including the starting material (**1**), product (**2**), reagent (acetic anhydride), temperature (0 °C to r.t.), time (overnight), solvent (methanol) and yield (99 %). All the given attributes are the basic minimum needed to reproduce this specific reaction. The only exception is the yield, which is a measure of effectiveness. To my knowledge, this is a very standardized representation widely used among researchers. While it might be possible to perform the synthesis with this information, a more detailed description is necessary which is generally given as a synthetic or experimental procedure (for Scheme I.1 see Chapter VIII1.2).



Scheme I.1: N-Formylation of 2-methoxy-5-nitroaniline (**1**) resulting in **2** in 99 % yield.

⁶*Synthesis* **2022**, 54, I–VI. <https://www.thieme.de/de/synthesis/author-guidelines-58874.htm>

⁷https://www.chemotion.net/docs/repo/details_standards. Accessed 2022.

However, in the standards given for experimental procedures also affecting the attributes above, the Chemotion Repository, which is directed towards FAIR data publication, differs from the instructions given by the journal *Synthesis*. It is assumed that the standards set by this journal are a good representation of generally applied standards in this field. Table I.1 summarizes these instructions for formulating a typical synthetic procedure for both the journal and the repository.

Table I.1.: Compared standards given for formulating of a typical synthetic procedure for publication by the instruction for authors of a journal and the documentation of a repository including examples for substances, solvents and products.

	<i>Synthesis</i> Journal⁶	Chemotion Repository⁷
Substances	weight, volume ^a and molar units (1.0 g, 10.0 mmol)	weight, volume ^a , molar units and equivalents (10.0 g, 3.50 mmol, 1.00 equiv.)
Solvents	volume MeOH (20 mL)	volume methanol (20 mL)
Products	weight or molar units and %yield, specify pure or crude, physical state and color The crude product (2.0 g, 70 %) was isolated as a colorless solid.	weight, molar units and %yield, specify pure or crude and %purity ^a , physical state and color The crude product ^b (20.0 g, 75 % purity, 7.00 mmol 70 %) was isolated as a colorless solid.
Reaction vessel	- ^c	should be named
Reaction Time	- ^c	explicit number or value
Temperature	- ^c	explicit number or value and type of heating
Purification	include all details	include all details
Abbreviations	use common abbreviations	list of acceptable abbreviations is given

^aIf applicable.

^bAn unambiguous name or IUPAC conform compound name should be given here.

^cNot specified by the Guideline.

Overall, the repository using FAIR data policies includes more detail in their standards and offers less room for abbreviation. In contrast to the journal instructions, the repository demands weight and molar units for both substances and products and requests the equivalents for each substance while this is optional in the journals standards. Similarly, the product description demands more detail especially regarding the purity. Standards for work-up and purification procedures are not given in detail in either guideline likely because they are beyond the scope of the instructions.

Up to this point, the increased demands for detail by the repositories FAIR data policy did not pose a problem as the information was at hand and coincided with our own generally used standards. However, a few points in the repository guidelines did not. Table I.1

shows three empty entries for the journal at reaction vessel, reaction time and temperature as they are not specifically mentioned in their instructions while the repository specifically mentions these points. This is due to very commonly used substitute phrases which are not categorized as FAIR. Among these are the phrases room temperature (r.t.) as a substitute temperature and overnight as a phrase for approximately 14-18 hours. These substitutes are highly imprecise and can vary widely depending on local standard and location. Room temperature is often dependent on the season and surrounding climate and overnight strongly depends on your definition and working hours which can fluctuate even in the same location. Therefore, these phrases do not fulfil the requirement of being reusable or in this context reproducible. In fact, the date when a reaction was performed could also be a relevant information as reactions might be influenced by solar irradiation, respectively.

Going back to Scheme I.1, this reaction actually lacks in a few points of the FAIR requirements, as it uses said substitute phrases. Unfortunately, as we were used to and worked by common standards ourselves, our synthetic procedures also used these phrases and our notes did not deliver the necessary details to give more precise information. After discussion, also including the team of the repository, we refrained from repeating the full synthesis in order to gain the missing data and used the details as they were as we still deemed the experiments reproducible despite this. Nevertheless, we integrated more precise notes regarding reaction time and current room temperature to our standard set of information for future experiments. We also implemented the reaction vessel as a standard information and reassessed the use of ice-baths. More precisely, we aspire to either actually measure the temperature a reaction in an ice-bath adopts or otherwise refrain from assuming 0 °C and give the comment 'an ice-bath or ice-salt-bath was used' with an estimated temperature range. Although this is less precise, it is FAIRer in the sense of being more realistic.



In contrast to the synthetic procedures, we were able to take a big step towards FAIR data regarding our product analysis. The analytical data should foremost be considered for their interoperability ('I'). To achieve this, measured analytical data should be made available as a raw data file in a format that can be used without specific software. As an example, nuclear magnetic resonance (NMR) spectra should be attached as the original (.fid) and a JCAMP-DX^[38] (.dx, .jdx) file instead of a Mestre Nova (.mnova) file, respectively. Although Mestre Nova is a commonly used software for NMR data processing, it is not a freeware and thus not accessible to everyone. While every type of analytical measurement should be assessed individually, the data file format JCAMP-DX and text files (.txt, .csv) are generally interoperable. When using the Chemotion Repository, for example Excel files (.xlsx) are also acceptable as they can be easily converted and made accessible. Using this information, we collected all the raw data files that were available to us (excluding externally measured HR-MS

data) and attached them to the respective reaction entries in the repository⁹. Where applicable, we also added the processed data files in the JCAMP-DX file format.



After the described prework of using the Chemotion ELN and repository to gather as FAIR as possible reaction procedures and attach FAIR data sets, publishing in a FAIR manner is relatively simple. As we published our paper^[32], we additionally uploaded the ELN entries containing the analytical data files *via* the repository⁹ and therefore made all raw data of this synthesis findable and accessible. The terms of reusability are defined by the added Creative Commons CC BY-SA 4.0. Taking the FAIR concepts even further, samples of synthesized molecules can be send the Molecule Archive⁸ where they are tested toward their purity and toxicity towards HeLa cells. Furthermore, the compound samples are stored and available to other researchers upon request and under defined rules.^[39] We send each synthesized compound of the published synthesis to the Molecule Archive. The storage and availability of the compound samples is indicated within the Chemotion Repository entries. In summary, using tools like the Chemotion ELN and repository which are guided by the FAIR principles is a great opportunity to create FAIRer research and publications even if not all the criteria can be met in an instance.

⁸<https://compound-platform.eu/>

2.3. A Publication According to the FAIR Principles

This following section is part of a publication. According experimental procedures can be found in the Appendix (Chapter VIII1). The comprehensive full primary data can be accessed in the Chemotion Repository.⁹

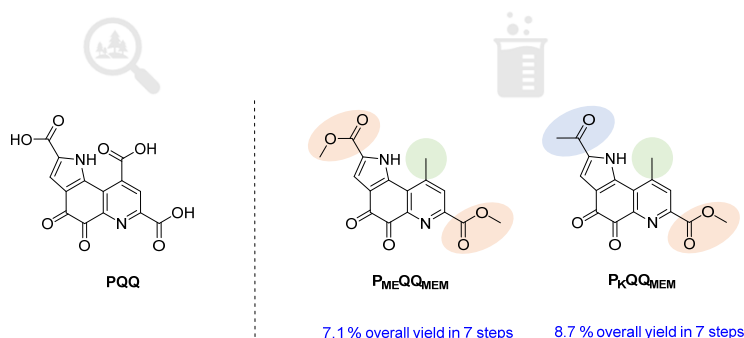
Author Contributions

Violeta Vetsova and Lena J. Daumann developed the project. Violeta Vetsova developed the first steps of the synthesis, while Rachel Janßen developed the remaining synthetic steps. One crucial step in the synthesis was optimised by Dominik Putz during his internship with Rachel Janßen. Violeta Vetsova and Rachel Janßen created the repository entries and wrote the main parts of the manuscript. Lena J. Daumann supervised the project.

Modular Synthesis of New Pyrroloquinoline Quinone Derivatives^[32]

Rachel Janßen, Violeta A. Vetsova, Dominik Putz, Peter Mayer, Lena J. Daumann
Synthesis **2023**, 55, 1000.

Copyright (2023), Rights managed by Georg Thieme Verlag KG Stuttgart, New York.



Abstract Pyrroloquinoline quinone (PQQ) is an important cofactor of methanol dehydrogenases and glucose dehydrogenases. In addition, isolated PQQ is used as a central component in sensors and biomimetic complexes. The synthesis of PQQ derivatives is of interest for developing new alcohol oxidation catalysts and redox sensors. This work describes a modular synthesis for derivatives of PQQ bearing methyl and ketone groups instead of carboxylic acid moieties. These modifications reduce the possible coordination sites of PQQ for metal ions outside the protein environment.

Pyrroloquinoline quinone (PQQ) is an aromatic tricyclic *o*-quinone, which functions as a redox cofactor for many quinoprotein dehydrogenases (Chart I.1).^[23–25,40,41] In methanol dehydrogenase (MDH), for example, PQQ is reduced to its quinol form concurrently to the oxidation of methanol. In addition, PQQ can be found in glucose dehydrogenase,

⁹ The primary Data can be accessed here: https://dx.doi.org/10.14272/collection/RAJ_2022-08-25.

an enzyme that is routinely used as a sensor for glucose or other biomolecules.^[42,43] As well as PQQ, the active sites of these enzymes contain a Lewis acid, like calcium(II) or a lanthanide(III) ion (Ln), for cofactor and substrate activation.^[27,28] PQQ has recently attracted new interest, not only for its role in biological systems together with lanthanides but also as a chelator for Ln separation or as a sensor for Hg(II) or l-fucose.^[30,44,45] In addition, model complex studies have been aimed toward understanding the activation of PQQ by Lewis acids (Ca or Ln).^[29,31,46] In biological systems, PQQ coordinates metal ions in the ONO pocket and can be considered one of the few natural pincer ligands.^[47] It has been shown that outside the protein environment PQQ acts as a versatile ligand, often forming coordination networks or dimers with one or more carboxylic acid moieties.^[30,36,48,49] Thus, for catalyst design and for generating monomeric PQQ-metal complexes, the functionalisation of certain residues, but especially the moieties not involved in metal-ion coordination *in vivo*, is often necessary to modify the cofactor. Hudson and co-workers have previously reported the synthesis of several PQQ isomers, where the pyridine moiety or pyrrole ring were flipped by 180 degrees.^[50] Only one of the isomers retained the ONO pocket and the derivative still featured the carboxylates, which often lead to unwanted dimer or coordination network formation.

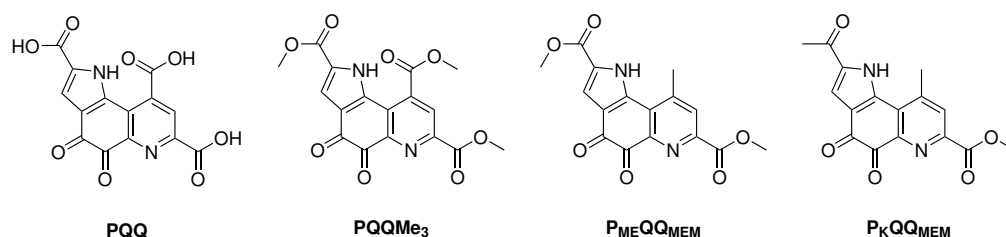
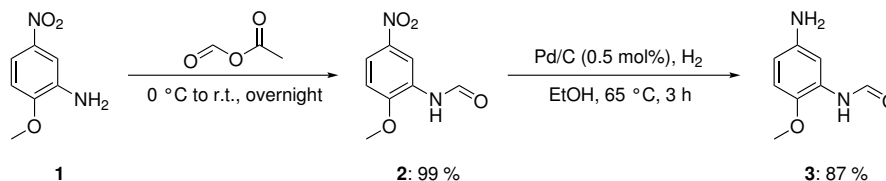


Chart I.1.: PQQ and related derivatives discussed in this study.

In this work, we report the synthesis of two PQQ derivatives, P_{ME}QQ_{MEM} (methyl-ester-substituted pyrrole, methyl-ester- and methyl-substituted quinoline quinone) and P_KQQ_{MEM} (ketone-substituted pyrrole, methyl-ester- and methyl-substituted quinoline quinone), which could be potentially used as ligands in quinoprotein-inspired model complexes or as starting materials for advanced sensor development. Compared to PQQ itself, the derivatives possess fewer alternative coordination sites for metal cations, albeit still retaining the ONO pocket for metal coordination. The synthetic route was adapted from the total synthesis of PQQ published by Corey and Tramontano,^[51] which includes the formation of the trimethyl ester of PQQ (PQQMe₃) as an intermediate; this was previously often used as a model for MDH.^[52–54] In the active site of MDH, the carboxylic functions of PQQ are occupied by interactions with amino acids.^[27] For the trimethyl ester, the literature presents a seven-step synthesis with an overall yield of approximately 22%.^[51] Other authors published partly similar syntheses, as well as alternative approaches,^[55–61] but the PQQ cofactor itself could also be obtained by fermentation.^[62] The derivatives aimed for in this work, however, require adjustments within the synthesis, wherefore we established the adapted procedure described herein.

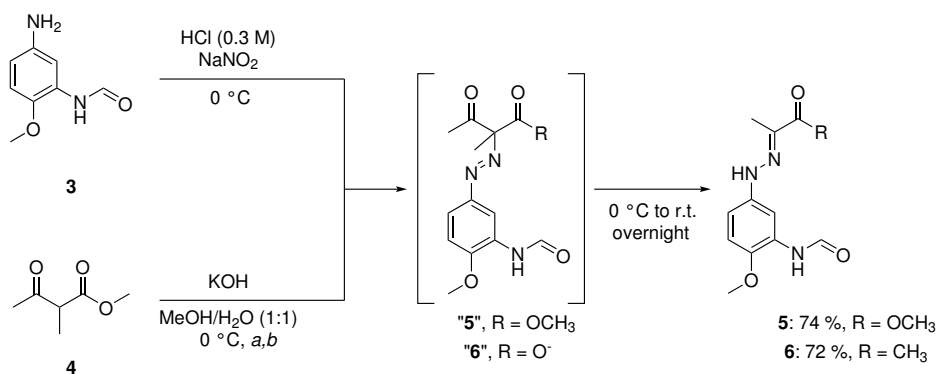
The first step toward the new derivatives was performed according to the PQQ synthesis by Corey and Tramontano^[51] by starting from 2-methoxy-5-nitroaniline (**1**). As described, the amino group was protected with a formyl group by using in situ generated acetic formic anhydride (Scheme I.2). In a difference to the literature report, the paste-like reaction mixture was stirred with an overhead stirrer, resulting in an almost quantitative yield of **2**. Product **2** was then reduced with H₂ and Pd/C to yield the aniline derivative **3** in good yield (87 %, Scheme I.2).



Scheme I.2: *N*-Formylation of 2-methoxy-5-nitroaniline (**1**) and palladium-catalysed reduction of nitro compound **2** to aniline derivative **3**.

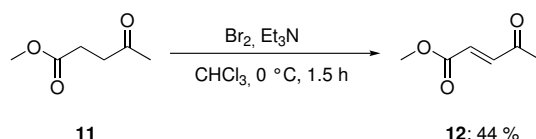
Methyl 3-oxobutanoate (**4**), which was needed for the next step, had to be prepared prior to the synthesis. Therefore, reactant **4** was synthesized according to a literature procedure^[63] and obtained in 65 % yield.

In the literature procedure,^[51] the ensuing Japp-Klingemann reaction of **3** and **4** to form the ester-substituted arylhydrazone **5** was reported to give up to 80 % yield. Various attempts to repeat the published result were discarded for two reasons: either the high yields described in the paper could not be reproduced or the reaction yielded a mixture of the ester- and ketone-substituted hydrazones **5** and **6** that was difficult to separate. While investigating the different outcomes in comparison to the literature, we found that the ester-substituted compound **5** can be synthesized exclusively if the reaction scale is kept under approximately 5 mmol, whereas higher scales led to a mixture of both products. Further optimization of the reaction protocol, such as changes to the addition speed and method, showed that a transfer cannula is most suited to allow constant cooling of the diazonium salt suspension while maintaining a slow addition speed. With this setup, **5** was afforded in 74 % yield (Scheme I.3). Differentiation between the ester- and ketone-substituted products can be achieved by distinct treatment of reactant **4**. To obtain the ketone-substituted product **6** exclusively and in good yield (72 %), precursor **4** was saponified with 1.2 equivalents of potassium hydroxide at 0 °C overnight prior to addition (Scheme I.3). Saponification can also be achieved at room temperature within approximately 1 h. However, the yields are lowered significantly if either solution is not cooled and kept at low temperatures throughout addition. In the case of **5**, the elongated time needed for slow addition and insufficient cooling at higher reaction scales might be why mixtures are obtained because some of reactant **4** could be saponified. It should also be mentioned that higher concentrations of hydrochloric acid lead to deprotection of the formylated amino group in both reactions.



Scheme I.3: Formation of ester- and ketone-substituted arylhydrazones **5** and **6**. Conditions: (a) 0 h for **5**; (b) 6 h for **6**.

In a reaction known from Fischer indole syntheses,^[64] the afforded hydrazones were converted by temperature- and acid-mediated indolization (Scheme I.5). Products **7** and **8** were synthesized in 60 % and 56 % yield, respectively, and subsequent deprotection of the amino group by using hydrochloric acid afforded **9** (84 %) and **10** (79 %). For the introduction of the third ring, Corey and Tramontano^[51] used an α,β -unsaturated carbonyl derived from dimethyl 2-oxoglutarate in a Doebner-Miller type^[65] reaction. As the desired PQQ derivatives contain a methyl group instead of an ester function, a suitable reactant was synthesized by a similar procedure to that described in the literature. Thus, methyl levulinate (**11**) was treated with bromine, and after removal of the resulting hydrogen bromide with a nitrogen gas flow, a double bond was established by an elimination reaction induced by triethylamine, affording product **12** (Scheme I.4).

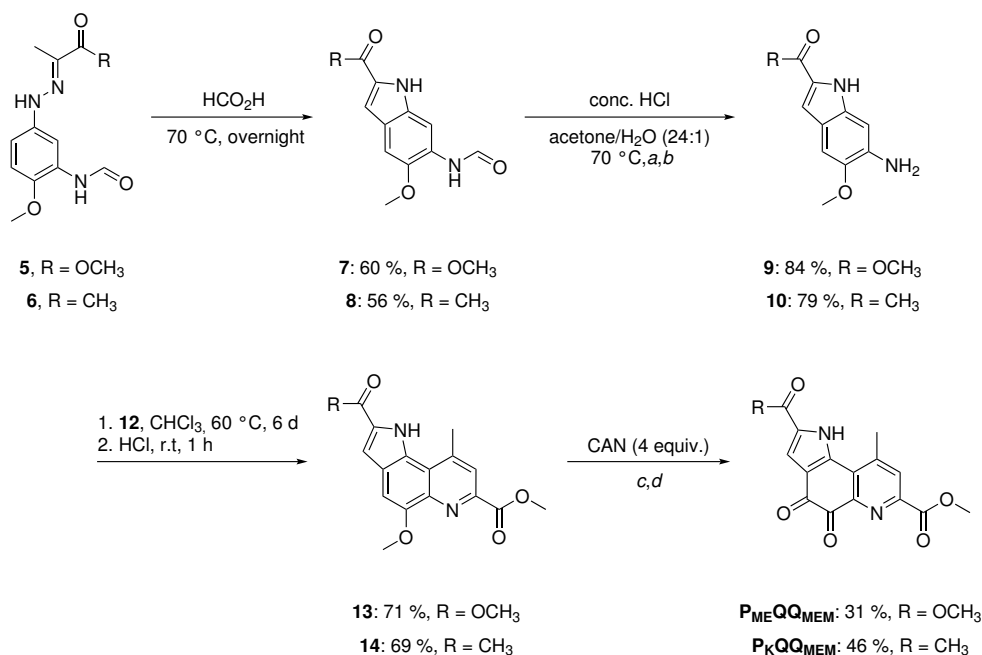


Scheme I.4: Bromination and subsequent elimination of methyl levulinate (**11**) to form **12**.

In contrast to the literature procedure, dry chloroform and reaction under a nitrogen atmosphere afforded better yields than the reaction performed in dichloromethane. The purification of this reaction, however, was nontrivial owing to the low melting point of the product. In solution, product **12** can co-evaporate during removal of solvents in a conventional rotary evaporator at 40 °C. Therefore, the reaction mixture was carefully concentrated in a rotary evaporator at room temperature, but the solvent was not completely removed. The remaining brown liquid was distilled by using a Schlenk tube and a cooling finger, resulting in the disposition of the product as colorless crystals, while the remaining solvent was captured in a connected cooling trap. Once obtained in solid form, the crystals were scraped off and could be dried under high vacuum. Product **12** was obtained in 44 % yield.

With this product at hand, the Doebner-Miller reaction with amino indoles **9** or **10** and

2. Implementation of a Research Data Management System and Describing a Synthesis According to FAIR Principles



Scheme I.5: Fischer indolization of **5** and **6** into amino indoles **7** and **8** and subsequent deprotection of the amine group, Doebner-Miller reaction and subsequent dehydrogenation of **9** and **10** to form precursors **13** and **14**, and oxidation reaction of **13** and **14** to form P_{ME}QQ_{MEM} and P_KQQ_{MEM}. Reaction conditions: (a) 2 h for **9**; (b) 90 min for **10**; (c) acetonitrile/water (4:1), 0 °C, 30 min for P_{ME}QQ_{MEM}; (d) acetonitrile/water (3:1), 0 °C, 40 min for P_KQQ_{MEM}.

12 was performed. It was found that higher temperatures were needed, as previously described; therefore, dichloromethane was substituted with chloroform. In addition, the reaction time was extended to 6-7 days until TLC indicated full consumption of the starting material. To fully convert the intermediate, in situ formed hydrogen chloride was bubbled through the reaction mixture. After purification, the desired tricyclic products **13** and **14** were afforded in yields of 71 % and 69 %, respectively (Scheme I.5).

In the final step, oxidation into the quinones was performed by using ceric ammonium nitrate (CAN). In contrast to the previously reported PQQMe₃, however, the products exhibit lower solubility in water, precipitate from the reaction mixture, and can be filtered off and washed without further purification. The target molecules P_{ME}QQ_{MEM} and P_KQQ_{MEM} were obtained in 31 % and 46 % yield, respectively.

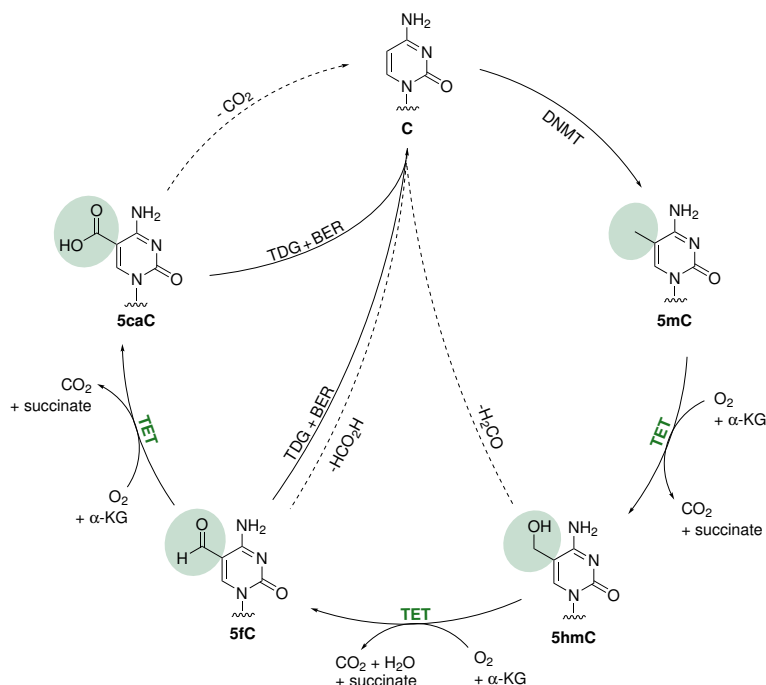
In summary, we have successfully adapted the synthetic route toward PQQMe₃ and present herein two new PQQ derivatives, which may be useful in chemical investigations of the cofactor methoxatin in enzymatic contexts or as sensor moieties. The modification on the quinoline ring reduces the possible coordination sites that the PQQ derivatives can exhibit in solution in addition to the biologically relevant binding sites. The exchange of functional groups on the aromatic structure could also have an impact on the redox properties or kinetics of PQQ for alcohol oxidation.

II. General Introduction - Biomimetics

1. Ten-Eleven Translocation Enzymes

The ten-eleven translocation (TET) enzymes are members of the non-heme iron(II)/ α -ketoglutarate dependent enzyme superfamily which, as the name suggests, uses iron and α -ketoglutarate as cofactors.^[66] The subgroup of the TET enzymes (TET1-3) is involved in the demethylation pathway of epigenetic DNA modifications.

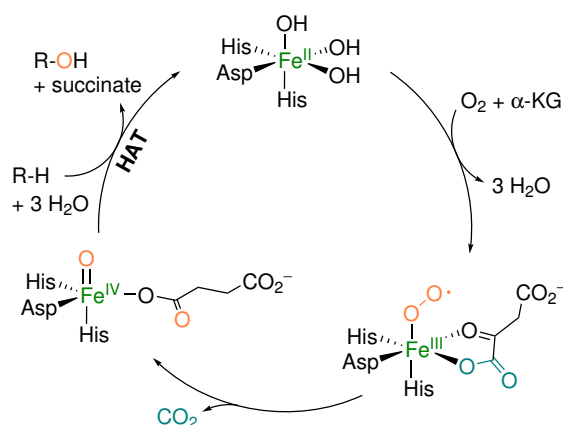
Epigenetics is described as changes in genetic function that are heritable, but do not involve alteration of the DNA sequence.^[67] In this context, functional change often refers to the silencing of specific genes. The respective alterations include the remodelling of chromatin^[68,69] or covalent modifications of histones^[70] and DNA bases.^[71,72] One example is the methylation of cytosine performed by DNA methyl transferases (DNMTs) forming 5-methylcytosine (5mC).^[73] The presence of 5mC as an additional non-canonical base in DNA has been known since 1950,^[74] but its role in epigenetic DNA modifications has only been elucidated in recent years.^[71,72] 5mC makes up 1 % of DNA bases in mammalian DNA and is found in CpG dinucleotides. If CpG nucleotides accumulate, these CpG-rich regions are called CpG islands (CGIs) which are commonly found within promoter regions.^[75] Cytosine (C) methylation forming 5mC in CpG rich promoter regions causes silencing of the respective gene and plays a relevant part in the regulation of gene expression.^[72,76,77] This is why 5mC is referred to as an epigenetic marker.



Scheme II.1: General scheme for the methylation and demethylation of cytosine (C). C can be methylated at the 5-position by DNA methyl transferases (DNMTs) in the context of gene silencing. Upon further gene regulation, the demethylation of the formed 5mC can then be mediated by TET enzymes. Under consumption of α -ketoglutarate and oxygen, 5mC is successively oxidised to 5hmC, 5fC and 5caC. The later products 5fC and 5caC are then removed through a TDG-mediated base excision repair pathway resulting in the reconstitution of C. Dotted lines indicate proposed direct demethylations of the oxidised bases.^[66,77–80]

Another crucial part of gene regulation is the demethylation of 5mC in silenced genes.^[72] The demethylation of 5mC can follow an active or a passive pathway, the active pathway is depicted in Scheme II.1. The passive pathway is attributed to dilution during cell division wherein epigenetic alterations are lost during replication and exchanged by cytosine.^[80] The active demethylation pathway is promoted by the TET enzyme family, members of which are able to successively oxidise 5mC to 5-hydroxymethylcytosine (5hmC),^[78] 5-formylcytosine (5fC) and 5-carboxycytosine (5caC).^[79] Each oxidation is performed under the consumption of α -ketoglutarate and molecular oxygen and the release of succinate and carbon dioxide.^[80] The final products of TET oxidation, 5fC and 5caC, can then be reconstituted as C through the thymine DNA glycosylase (TDG)-mediated base excision repair pathway.^[66,80] However, it is also proposed that direct demodification occurs for 5fC and 5caC.^[77]

As can be seen from the demethylation process of 5mC, the TET mediated oxidation of epigenetic DNA bases is essential to effective gene regulation. It is proposed that the substrates are oxidised by an iron(IV)-oxido species similar to other iron(II)/ α -ketoglutarate dependent enzymes like TauD^[81–83] and that reaction occurs *via* a hydrogen atom transfer (HAT) mechanism.^[84] Scheme II.2 shows the essential oxidation states of the iron in this catalytic cycle. Within the TET enzymes, the iron(II) is bound by a so-called facial triad (two histidine and one glutamate) and coordinates water in the resting state or the co-factor α -ketoglutarate and oxygen.^[85] In the proposed mechanism, the iron reacts with the oxygen to an iron(III) superoxide which forms the reactive iron(IV)-oxido species under release of carbon dioxide and conversion of α -ketoglutarate to succinate. Subsequently, through a hydrogen atom transfer and rebound mechanism, the substrate is oxidised and succinate is released.^[84,86] This cycle is repeated for each oxidation step from 5mC to 5caC and thereby promotes the removal of the epigenetic alteration.



Scheme II.2: Simplified scheme for the catalytic cycle proposed for the TET enzyme family. Shown are the essential oxidation states of the iron center (II–IV). Starting at the top from the iron(II) resting state of the enzyme^[85] which is oxidised to an iron(III) species upon binding oxygen and the cofactor α -ketoglutarate. Under release of carbon dioxide, an iron(IV)-oxido species is formed which can then oxidise the substrate (R-H) in a HAT and rebound mechanism forming the oxidised substrate and succinate.^[84,86]

2. Biomimetic Complexes

Members of the non-heme iron(II)/ α -ketoglutarate dependent enzyme are proposed to oxidise their substrates by an iron(IV)-oxido complex as an active species (*vide supra*). As the extremely short lifetimes of active species in enzymes most often hinder a sufficient analysis, a different method of validation is needed. One method for the investigation of proposed active species is the use of biomimetic model complexes. Towards this, ligand systems and complexes are designed to mirror the coordination sphere in the active site as closely as possible and are then used to investigate the targeted substrate conversion as well as the complex properties.

Following the first obtained crystal structure of a non-heme iron(IV)-oxido species $[\text{Fe}^{\text{IV}}(\text{O})(\text{TMC})(\text{MeCN})]^{2+}$ (see Figure II.1),^[87] a multitude of similar iron(IV)-oxido model complexes has been created.^[88] However, most of these complexes are only stable for short intervals and need to be handled at low temperatures. In 2015, Chantarojsiri *et al.* reported an iron(IV)-oxido complex based on a pentapyridine ligand $[\text{Fe}^{\text{IV}}(\text{O})(\text{Py}_5\text{Me}_2)]^{2+}$ (Figure II.1) which is soluble in water and stable at room temperature for several days.^[89] These features make this iron(IV)-oxido complex an interesting candidate to model biological systems as it can be used under standard physiological conditions.

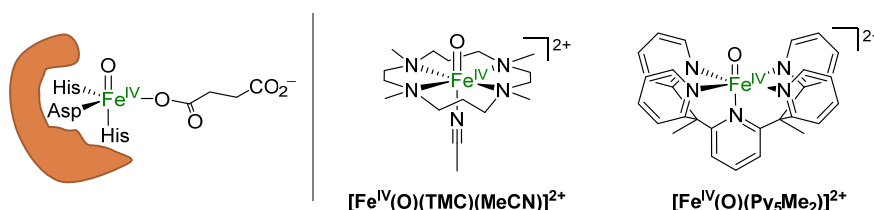


Figure II.1.: Structure of the first non-heme iron(IV)-oxido complex structure $[\text{Fe}^{\text{IV}}(\text{O})(\text{TMC})(\text{MeCN})]^{2+}$ ^[87] and the stable complex $[\text{Fe}^{\text{IV}}(\text{O})(\text{Py}_5\text{Me}_2)]^{2+}$ ^[89] in comparison to the proposed active species in TET enzymes (left).^[81–83] TMC = 1,4,8,11-tetramethyl-1,4,8,11-tetraazacyclotetradecane.

In 2019, Jonasson *et al.* showed that the $[\text{Fe}^{\text{IV}}(\text{O})(\text{Py}_5\text{Me}_2)]^{2+}$ complex (C4) indeed can biomimetically oxidise 5mC in the same successive manner as TET enzymes establishing this complex as a useful model for this member the of α -ketoglutarate dependent enzyme family.^[90] Following investigations further corroborated this by the successful application of this model on nucleosides and oligonucleotides.^[91] These findings, presenting the iron(IV)-oxido complex C4 as a biomimetic model for TET enzyme activity towards the epigenetically relevant base 5mC and its oxidation products, inspired the projects described in this thesis.

III. Biomimetic Oxidation of Synthetic DNA Bases

1. Introduction

As is described in the literature,^[71,77] there is still much to learn about epigenetic markers like 5mC itself and the possible roles of its oxidation products 5hmC, 5fC and 5caC besides their occurrence in the demethylation process. However, while the full extent of the natural role of this additional DNA base has yet to be discovered, scientists have already begun to find alternative uses for the concept of second layer DNA modifications. In the following, a short introduction into the use of DNA as a storage for non-biological information will be given, followed by an overview of the possibilities arising from the combination of these systems with epigenetic modification of DNA.

1.1. DNA Data Storage Systems

In our modern world, digital data storage systems have become an integral part of society, since we produce more and more data every day. The ever-growing amount of data inevitably results in the need for better storage systems.^[92] Two major problems, that accompany this development are the following:

- 1) Regularly changing storage systems due to technical progress, which leads to the necessary equipment for reading the data being discarded in favour of newer systems - have you ever tried watching your grandparents VHS wedding tape in your modern home?^[93] - and nevertheless approach their maximal density.
- 2) The modern technical storage solutions are adapted to our fast-living world where data does not necessarily need to be stored indefinitely, but are not suited for archival long-term storage, for example in the context of keeping historical information, due to their limited longevity.

Regarding the purpose of archival storage of information which is supposed to be indefinite, it is not desirable to enlarge the available storage media physically to provide the required capacity nor is the limited longevity suitable for this task. Therefore, new systems with higher densities are needed while other aspects such as durability and accessibility have to be taken into account as well, which is why scientists have started exploring DNA as a biological storage system for non-biological information.^[94,95] Figure III.1 shows an overview on how the process of storing digital data in DNA generally works.^[94]

One part of the first problem described above is the rapidly changing technical media which pose the danger of losing the means to read them. It is easily understood why using DNA might be an alternative here, since its relevance to our society is most likely infinite. While the techniques around synthesizing, reading, sequencing or manipulating DNA will evolve, the "storage medium" and its basic make-up will stay the same and newer methods should be downward compatible - meaning that new methods should still be able to read older "systems". The second part of this problem is the density current technical solutions can provide. The research of recent years has shown that step by

step, starting from about one megabyte^[96,97] going to 200 megabytes of data^[98], DNA is bound to surpass traditional electronic or magnetic storage media.^[99] In their comment on this, Zhirnov *et al.* estimate that while a Flash memory could achieve a density of $\sim 10^{16}$ bit cm^{-1} cellular DNA should be able to reach $\sim 10^{19}$ bit cm^{-1} .^[100]

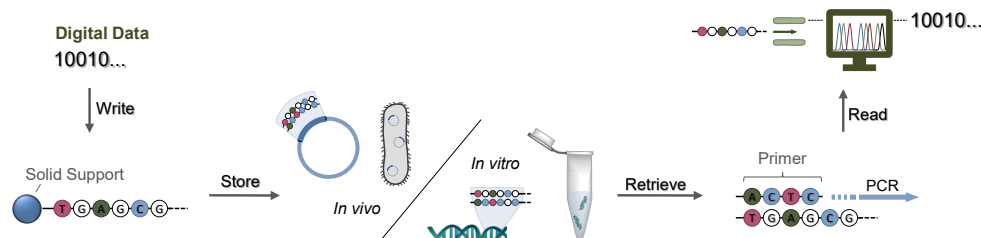


Figure III.1.: The process of storing digital data in DNA involves four general steps. The digital data has to be *written* into DNA code meaning the synthesis of according DNA sequences. This data has then to be *stored* which can be done either *in vivo* or *in vitro*. The *retrieving* of the data can be accomplished with targeted polymerase chain reaction (PCR) processes producing multiple copies of the data which can then be *read* by sequencing methods. For example, this can be achieved by using one of the common techniques like Sanger sequencing,^[101] sequencing-by-synthesis^[102] (e.g. Illumina) or nanopore sequencing^[103,104] (e.g. Oxford Nanopore Technologies). This figure was adapted from Ceze *et al.*^[94]

In respect to the second problem, the longevity of storage media and the contained data, DNA as a storage solution can provide an even higher advantage. Traditional electronic or magnetic storage media are temporary solutions, often incapable of reliably preserving data for the duration of even an individual's lifespan.^[105] Compared to this, DNA has already proven its superior durability. In general, nature keeps the stored information intact by constantly creating copies through reproduction. However, without any intent on storing information in one copy for longer than a lifespan, scientists are able to sequence DNA from several hundred thousands years ago and learn from the gained genetic data of human^[106] and animal skeletons^[107], respectively. Of course these skeletons were preserved by ice and cold temperatures, but it gives an idea on how many years information can be safely stored in DNA under the proper conditions. A study toward this was performed by Grass *et al.*^[97] They used a previously established method to protect the DNA by encapsulating it in a silica sphere^[108] while additionally employing error-correcting codes to overcome problems with decoding errors. With their techniques, they were able to estimate that DNA is able to store information for about 2000 years in central European climate and over 2 million years in a temperature regulated environment (-18°C).

Therefore, it can be concluded that DNA is a highly promising candidate as a long-term solution for data storage. It should be noted that there are still problems to be dealt with and that DNA is not an ideal storage solution for quick access. Nevertheless, it is a promising storage medium to keep vast amounts of knowledge safely stored for the future.

1.2. Synthetic Expansion of the DNA Alphabet

As described in the previous section (III.1.1), DNA has a high density when it comes to information storage. In comparison to binary code, the higher density in DNA stems from the four basic elements, often referred to as canonical bases, cytosine (C), adenine (A), guanine (G) and thymine (T) making up the DNA sequence.^[109] Albeit the already superior density of DNA, scientists are creating even denser systems by expanding the DNA alphabet (CGTA) with synthetic DNA bases. The groups of S. A. Benner and F. E. Romesberg for example, are each following their own approaches toward the synthetic extension of the bases usable in functional DNA. Figure III.2 presents an overview of the natural base pairs (A) compared to examples of synthetic base pairs created by the group of S. A. Benner^[110] (B) and F. E. Romesberg^[111] (C). A characteristic difference in the approaches is the pairing by Watson-Crick-like hydrogen bonding by Benner *et al.* as opposed to Romesberg *et al.* who apply a concept of hydrophobic and steric compatibility.^[109,112]

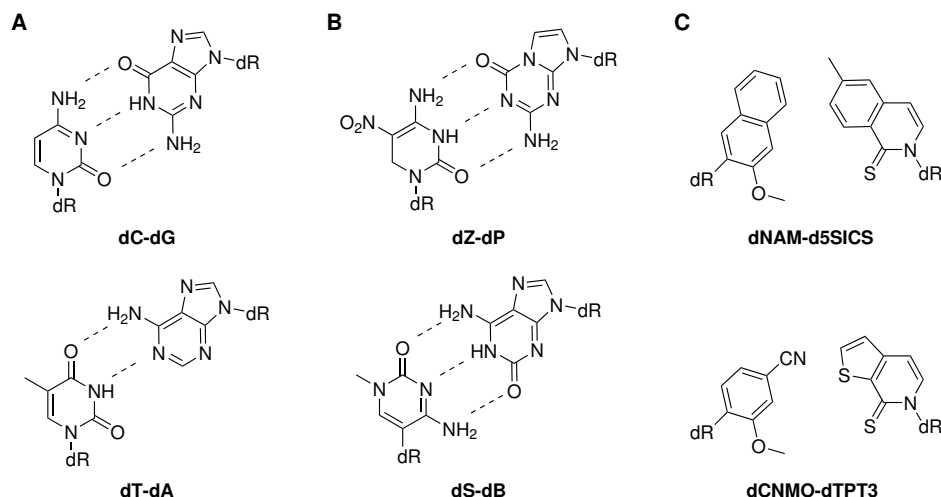


Figure III.2.: A) Canonical base pairs dG-dC and dT-dA naturally occurring in DNA, paired through hydrogen bonding. B) Synthetic base pairs dZ-dP and dS-dB by the group of S. A. Benner, following the Watson-Crick model paired by hydrogen bonding.^[110] C) Synthetic base pairs dNAM-d5SICS and dCNMO-dTPT3 by the group of F. E. Romesberg, which do not exhibit hydrogen bonding.^[111]

Despite their non natural base pairing approach, the group of F. E. Romesberg managed to create a synthetically extended six-letter genetic alphabet (Figure III.2A dC-dG dT-dA and Figure III.2C dNAM-d5SICS) which can be amplified by PCR^[112] and then a semi-synthetic organism that is able to incorporate a third unnatural base pair, transcribe it to RNA and subsequently incorporate respective non-canonical amino acids into proteins.^[111,113] This work is a good example on how the synthetic DNA bases can be integrated in natural DNA, enhancing the information density and further advancing DNA as storage medium (see Chapter III.1.1).

In contrast to this, the group of S. A. Benner lays a stark emphasis on synthetic DNA bases being paired by hydrogen bonding and following the Watson-Crick concept as best

they can. Their intention of staying close to natural conditions also shows in their choice of synthetic DNA bases (see Figure III.2A-B). Starting their work in 1989, when they presented a synthetic base pair made of *iso*-cytidine and *iso*-guanosine as a first expansion of the DNA alphabet^[114] and shortly after submitted a study showing successful *in vitro* translation to non-standard amino acids.^[115] In the following years, they updated their synthetic DNA base library and published their work on a six-letter genetic alphabet after including the bases Z and P^[116] (Figure III.2B).^[109,117,118] In a later addition, the group added a fourth base pair to their collection expanding their DNA alphabet to an eight-letter library (CGATZPSB) including their new synthetic nucleotides dS and dB (Figure III.2B). They successfully integrated this library into DNA-like system they named hachimoji (= "eight letter") DNA.^[110] Hachimoji DNA has a remarkably similar structural to natural DNA, which the authors attribute to the natural hydrogen bonding patterns in their synthetic base-pairs, respectively. Throughout their work, they highlight the structural similarity and the successful transcription to hachimoji RNA.

This eight-letter or hachimoji DNA paves a way for even higher information density in information storage application. It also underlines that in respect to technical storage applications, there is still much to learn and enhance in DNA as a storage medium. Nevertheless, it presents a viable solution without forcing the invention of new materials, but by optimizing one that has been and will be around for a long time.

1.3. Epigenetics: An Additional Layer of Information

Aside from expanding the DNA alphabet synthetically, there is another concept in natural DNA that can help optimize the usability of DNA as a storage solution for data - namely epigenetics. While synthetic biology creates new DNA bases, epigenetics already offers a fifth and sixth letter to the genetic alphabet with the naturally occurring cytosine (C) variants 5-methylcytosine (5mC) and 5-hydroxymethylcytosine (5hmC).^[71] In difference to the synthetic approaches described above, these bases are epigenetic variations of cytosine which still pair with guanine and therefore do not create an additional base-pair. Nevertheless, Mayer *et al.*^[119] reported a method in 2016 showcasing the use of epigenetic DNA bases in information storage systems as they used separate sequencing techniques to allow different readouts from the same DNA, creating a three-layered information system.

The first technique they employed is the deamination of cytosine upon reaction with the bisulfite ion, also called bisulfite sequencing.^[120] This sequencing technique was designed to quantify the amount of 5mC in DNA probes, since 5mC can not be differentiated from cytosine in traditional sequencing. 5mC is relatively inert toward reaction with the bisulfite ion, while cytosine undergoes a hydrolytic deamination which converts cytosine to uracil (Figure III.3B). The DNA probe is sequenced once before the reaction, where

every cytosine and 5mC are recorded as a cytosine, and once after reaction with sodium bisulfite. Here, every cytosine was converted to uracil which causes them to be read out as thymine^[121] while 5mC is still reported as cytosine. It is then possible to determine the difference in cytosine levels before and after bisulfite treatments equalling the amount of 5mC. Yet for this work, the relevant information is the different readout for cytosine and 5mC after bisulfite treatment.

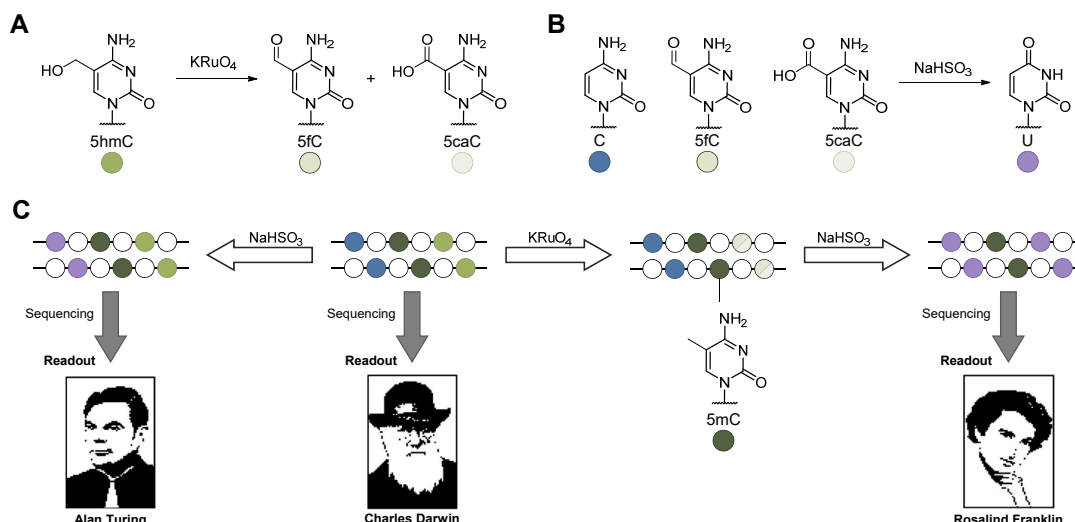


Figure III.3.: A) Oxidation of 5-hydroxymethylcytosine (5hmC) to 5-formylcytosine (5fC) and/or 5-carboxycytosine (5caC) by potassium perruthenate (K₂RuO₄). B) Transformation of cytosine (C), 5-formylcytosine (5fC) or 5-carboxycytosine (5caC) to uracil by sodium bisulfite. C) Simplified depiction of the concept of creating a different readout depending on DNA treatment. A 40 base-pair region of an oligonucleotide was sequenced and read, showing the DNA encoded a binary portrait of Charles Darwin.^[119] Reading the same sequence after bisulfite treatment of the DNA template, thereby exclusively changing the readout for cytosine, produced a portrait of Alan Turing. A third readout is generated by oxidation with potassium perruthenate and subsequent bisulfite treatment, which results in a portrait of Rosalind Franklin by inverting the readout of both cytosine and 5mC. *This figure was adapted from Mayer et al.*^[119]

As a second technique, they introduced oxidation by potassium perruthenate (K₂RuO₄). In this case, both cytosine and 5mC are inert toward oxidation, while 5hmC is not. It should be noted that 5hmC is, however, inert towards the bisulfite ion. As shown in Figure III.3A, 5hmC can be oxidized to 5fC and 5caC using potassium perruthenate, both of which are converted to uracil during bisulfite treatment. This behaviour can be used to create an additional third layer of information by getting a different readout depending on the pre-sequencing treatment of the DNA. In summary, after standard or bisulfite sequencing 5hmC is reported as cytosine. If the DNA is treated with potassium perruthenate prior to sodium bisulfite sequencing, 5hmC is oxidized to 5fC and/or 5caC which react with sodium bisulfite and are therefore converted to uracil and reported as thymine.

Figure III.3C depicts the general system using the example created by Mayer *et al.*^[119]. A DNA strand was created to store a specific data file, in this case a simple black and white portrait of Charles Darwin. When this DNA is sequenced and readout, the picture can be retrieved. When the treatment of the DNA is limited to bisulfite, a second

readout is generated due to cytosine being transformed while 5mC and 5hmC are not, resulting in a portrait of Alan Turing after the readout. If the same DNA strand is reacted with with potassium perruthenate prior to sodium bisulfite treatment, 5hmC will give a different readout then before, revealing a third set of information - a portrait of Rosalind Franklin. With this combination of sequencing techniques and naturally occurring cytosine derivatives, more information density can be created by layering information on the same DNA template.

2. Motivation and Aim

As described above in chapter Chapter III.1, DNA is a promising candidate as a medium for digital information storage that not only has a very high information density, but a superior longevity compared to current silicon based storage media. On top of that, the biological material needed for DNA is an abundant resource. Two different approaches towards the efficient use and optimization of DNA as a storage solution are:

- 1) the expansion of the DNA alphabet by creating additional synthetic base-pairs that can still be recognized for transcription and
- 2) the addition of a second and third layer of information on the same DNA strand inspired by the epigenetic DNA base variants 5mC and 5hmC.

In a previous work in our group, Niko Lindlar (né Jonasson) showed the biomimetic oxidation of 5mC and 5hmC by a TET model complex^[90] in the context of epigenetics. Having this expertise on epigenetic markers at hand, we addressed the idea of combining both approaches towards higher information density of DNA. What if we could add an additional layer of information on a synthetic DNA model using the concepts of epigenetics?

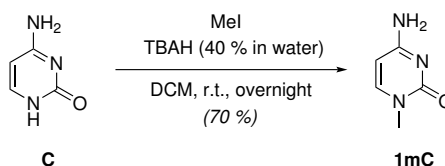
Inspired by the synthetic hachimoji DNA^[110] (see Chapter III.1.2), we wanted to synthesize a small library of synthetic DNA bases bearing methyl groups at different positions and test if these bases were accessible for the biomimetic TET model complex and oxidized in the same manner as 5mC as a first step towards synthetic epigenetics as a tool in DNA storage expansion. This project was embarked upon collaboratively with Annika Menke and Niko Lindlar (né Jonasson) and the synthesis of the targeted molecules (see Figure III.7) was spread amongst the participants. Most of the results regarding this project can be found in the publication shown in 4.^[122] Preliminary experiments will be discussed in the following.

3. Synthesis of 1-Methylcytosine and its Oxidation Products

The first step towards the investigation of synthetic DNA bases as a substrate for biomimetic TET-like oxidation was the synthesis of the base. Additionally, the synthesis of the expected oxidation products as references, to determine retention times for our product analysis *via* HPLC-MS and GC-MS, respectively, was also attempted.

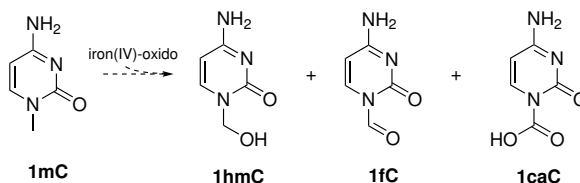
3.1. Synthesis of 1mC, 1fC and 1caC

The synthesis of 1-methylcytosine (1mC) is a literature known procedure which was performed accordingly in similar yields.^[123] An effort was made to improve the yields by elongating the reaction time, which did not alter the result and since this yield was deemed sufficient, no further optimization was attempted. It is possible that the yield might be influenced by the trituration of the product with hot ethanol at the end of the procedure, which is necessary to remove remaining salts, but might also dissolve parts of the product. However, this step is essential since albeit having a clean NMR spectrum before this step, the yield at this point was around 115 % which confirms a significant amount of impurities.



Scheme III.1: Methylation of cytosine at the N^1 -position using methyl iodide under basic conditions according to literature procedure.^[123]

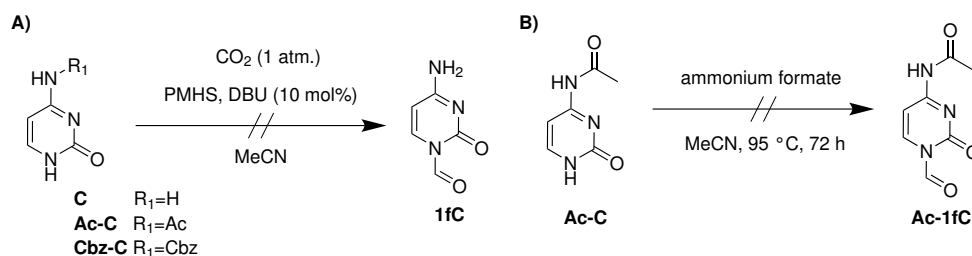
Before undergoing the first oxidation experiments of 1mC with an iron(IV)-oxido complex, an effort was made to have the references of the expected oxidation products at hand, facilitating the product analysis. Naturally, we expected equivalent products as observed for 5-methylcytosine (5mC) by Niko Lindlar (né Jonasson)^[90], namely 1-hydroxymethylcytosine (1hmC), 1-formylcytosine (1fC) and 1-carboxymethylcytosine (1caC) as depicted in Scheme III.2. Due to the fact that the synthesis of 5-hydroxymethylcytosine (5hmC) as a reference was cumbersome and ultimately achieved by reducing the methyl ester of 5-carboxymethylcytosine (5caC)^[124], the synthesis of 1fC and 1caC was approached



Scheme III.2: Expected oxidation products 1-hydroxymethylcytosine (1hmC), 1-formylcytosine (1fC) and 1-carboxymethylcytosine (1caC) of 1mC when reacted with an iron(IV)-oxido complex known to biomimetically oxidise 5mC to the respective oxidised molecules.

first. There obviously is a difference to functionalising a *N*- and a *C*-position, but the possibility to obtain 1hmC by reduction of either 1fC and 1caC was still deemed viable.

Initial attempts at the formylation of the endocyclic nitrogen were performed following literature procedures,^[125,126] although these publications primarily involved exocyclic amine functions. The possibility of formylating either only the exocyclic amine or both positions was taken into account and the experiments were mainly set up to determine whether formylation at the position, in general, is possible. First, a DBU-catalysed *N*-formylation of C using carbon dioxide was tested (Scheme III.3A)^[125] under varying conditions. Using acetonitrile as a solvent and stirring under ambient conditions overnight yielded a highly insoluble product which showed no sign of typical C=O bond signals in an IR spectrum. Repetition of this setup showed the same precipitate, which was then redissolved by carefully heating to 40 °C at which point the solution cleared and after a few hours showed full consumption of the starting material on TLC. Unfortunately, neither NMR or GC-MS analysis helped to determine the exact reaction outcome or showed conversion to the desired product, but indicated that the exocyclic amino function was substituted in the process. Therefore, different protecting groups for the exocyclic amine were investigated (see Chapter III.3.2).

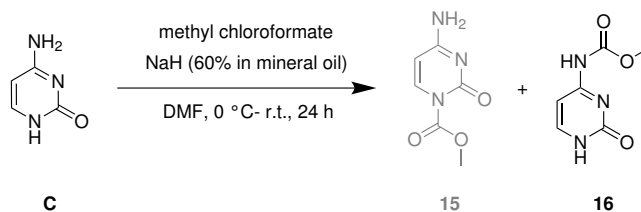


Scheme III.3: A) General reaction scheme of the attempted formylation of cytosine using carbon dioxide under reductive conditions.^[125] B) Attempted formylation of cytosine using ammonium formate.^[126]

The reaction conditions shown in Scheme III.3A were repeated for Ac-C at ambient temperature and at 40 °C over several days. Both reactions showed no formation of the desired product. It is possible that the reaction is not working due to the poor solubility of Ac-C. Therefore, another setup with dimethylformamide as solvent and a reaction temperature of 50 °C was applied in order to increase the amount of dissolved starting material. However, the starting material was mostly suspended instead of dissolved and the reaction showed no conversion of the deployed Ac-C as well. The basic reaction conditions with acetonitrile at ambient temperature using Cbz-C also did not show any consumption of the starting material. Ac-C was also reacted with ammonium formate under the conditions shown in Scheme III.3B^[126], but after 72 h no reaction of the starting material could be detected.

The setup for the carboxylation of the *N*¹ position was adapted from a synthesis by Schwergold *et al.*^[127], where cytosine was functionalised first and the exocyclic amino group protected afterwards. It should be kept in mind that the literature procedure uses

tert-butyl bromoacetate to perform an alkylation while additionally bearing a carboxy function. Nevertheless, a similar reaction with an alkyl halogenformate might work accordingly and was tested as shown in Scheme III.4. While the expected mass could be found by using a direct injection method on an LC-MS system, the according NMR spectra indicates **15** as the sole product. Compared to the NMR spectrum of cytosine, the signal of the exocyclic amine around ~ 7 ppm disappeared while a second signal around ~ 11 ppm arose strongly suggesting functionalisation at the exocyclic amine.



Scheme III.4: Attempted conversion of cytosine (**C**) to the methyl ester of 1-carboxymethylcytosine (**16**) using methyl chloroformate and sodium hydride. Analytics indicate the formation of only the undesired functionalisation at the N^4 position yielding **15**.

A similar procedure by Xu *et al.*^[128], also using *tert*-butyl bromoacetate, but protecting the exocyclic amine beforehand was taken into consideration. Instead of using **C** directly the protected variants Ac-**C** and Cbz-**C** were reacted with chloroformate in dimethylformamide using potassium carbonate as a base instead of sodium hydroxide. While the reaction with Cbz-**C** showed the expected mass after 72 h - both reactions were monitored using direct injection on a LC-MS system - this mass and the desired product could not be detected or purified from the crude product after removal of the solvent.

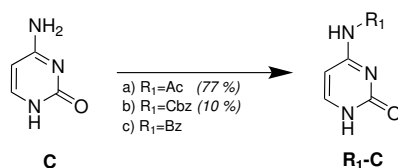
There are further experiments that could be tested to achieve the desired synthesis procedures for 1fC, 1caC and subsequently 1hmC. For 1fC the conditions of the DBU catalysed reaction (Scheme III.3A) can be adapted and the solubility of the starting material might be enhanced by different protecting groups at the exocyclic amine. In the case of 1caC, there are still other literature procedures that could be tested.^[129–131] However, since the synthesis of these references is not necessarily essential to the project, further attempts were put aside to focus on the oxidation of 1mC by the biomimetic iron(IV)-oxido complex C4.

3.2. Protection of the Exocyclic Amine in 1mC

Since one goal of this project was to achieve selective functionalisation of cytosine at the endocyclic nitrogen or N^1 -position, we realized quickly that the protection of the exocyclic amine could not be avoided (see Chapter III.3.1). Hence, different protecting groups were tested. In one respect, we wanted to find the most efficient reaction with good yields. In another respect, different protected variants mean variation in solubility and the conditions under which they can be cleaved off since we can only guess the stabilities of the desired functionalised products. Three commonly known protecting groups were tested

for our purposes: the acetyl- (Ac), the benzyloxycarbonyl- (Cbz) and benzoyl- (Bz) group.

The synthesis towards the acetyl-protected cytosine Ac-C had already been performed in our group by Doreen Reuter during an internship. The reaction was performed according to her procedure (conditions given in Scheme III.5) and gave the product in good yield. This protected cytosine was easily available, but has a very poor solubility and did not result the desired products in further reactions (see Chapter III.3.1). Another aspect was that the acetyl group is generally cleaved under acidic conditions and we were not confident that the N^1 functionalised species would be stable under these conditions.



Scheme III.5: Protection of cytosine at the N^4 position with different protecting groups. Conditions: a) Ac_2O , DMF, 60°C , 1 h, b) CbzCl, pyridine, 0°C to ambient temperature, overnight, c) BzCl, pyridine, 0°C , 45 s (yield was not determined).

A more promising candidate was the benzyloxycarbonyl group (Cbz), which can be cleaved off by hydrogenolysis.^[132,133] As a starting point, the conditions given by Schwergold *et al.*^[127] were applied. They used benzoyl chloroformate in dichloromethane and dimethyl aminopyridine as an additive. Since these conditions did not result in any product formation, a small-scale screen for better conditions was performed. In 1.5 mL centrifuge tubes 250 μmol C were suspended in either water, acetonitrile or dichloromethane. For each solvent, three experiments were performed where each reaction contained 2 equiv. of benzoyl chloroformate and 2 equiv. of either pyridine, triethylamine or DBU as a base. All tubes were placed in a shaker at $35\text{--}40^\circ\text{C}$. Only the reaction with dichloromethane and pyridine showed the desired mass while monitoring the reactions *via* LC-MS both over column and as direct injections. Therefore the reaction was repeated with mixtures of either dichloromethane and pyridine, water and pyridine or pyridine as the sole solvent. Although the product could not be detected in any of these new setups, according to a literature^[134] a scale-up with pyridine as the only solvent was performed and afforded the product in 10% yield. Higher equivalents, longer reaction times and the addition of dimethyl aminopyridine, as done by Schwergold *et al.*,^[127] did not result in higher yields.

Protection of the exocyclic amine was also attempted with benzoyl chloride according to a literature procedure.^[135] The given reactions conditions resulted in a triple-protected product with two benzoyl functions at the exocyclic and one at the endocyclic nitrogen. Thus, the reaction time was reduced from 5 h to 10 min and the reaction kept at 0°C which yielded the double-protected product. Since it was observed that the suspended cytosine or possibly formed Bz-C dissolved upon addition of benzoyl chloride and shortly after a colorless solid precipitated - which might be the less soluble variants with two or three

protecting groups - the reaction was stopped by quenching with methanol immediately after the initial suspension cleared. This procedure yielded the desired single-protected product Bz-C. However, there were challenges with the purity of the product which were not trivial to resolve, as standard methods like flash column chromatography or recrystallisation did not remove the impurities and thus the crude unpurified product had to be used in further reactions. As already described in the previous section, the efforts towards the synthesis of expected oxidation products of 1mC were put to a halt due to the unexpected time the synthetic work consumed and the focus was put on the biomimetic reaction with C4.

3.3. Initial Experiments Towards the Biomimetic Oxidation of 1mC

The first approach towards analysing whether and how the iron(IV)-oxido compound C4 oxidises or reacts with 1mC was done by UV-Vis measurements. The iron complex C4 has a distinctive maximum at 718 nm which can be monitored in UV-Vis measurements. Therefore, an experimental setup with C4 and 1mC was created according to previous methods used within the group.^[124] An aqueous solution of the iron compound C4 was added to and further diluted in a cuvette to achieve a concentration (1 mM) at which the characteristic iron(IV)-oxido d-d band^[89] at 718 nm displays a sufficient absorption intensity. A solution of 1mC was added and the measurement started immediately. However, in contrast to previous experiments with 5mC^[124] where the reaction takes around 30 min before conversion of the complex is nearly complete, no significant decrease in absorption could be detected within this time frame. Therefore, the reaction was repeated and the reaction time was extended to 19.5 h while full UV-Vis spectra were measured every 30 min. The resulting UV-Vis spectra are displayed in Figure III.4A. For comparison, Figure III.4B displays the decomposition of C4 without any added substrate. While this graph shows that the complex is not stable in solution for an extended time

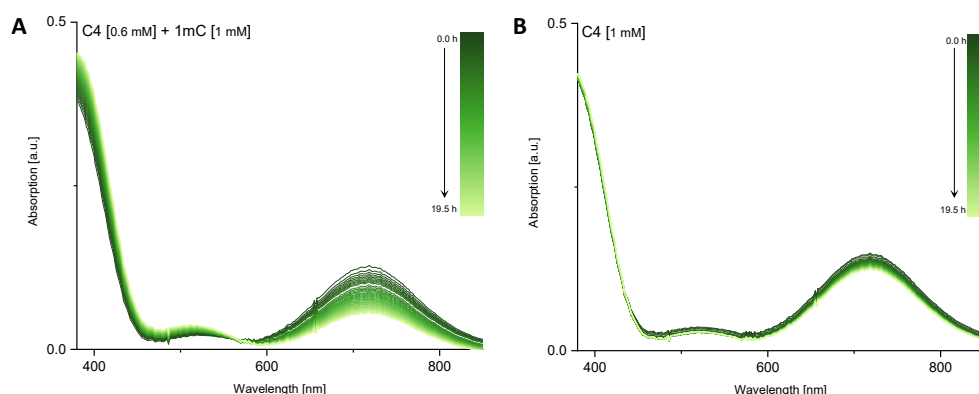


Figure III.4.: A) UV-Vis spectra of the reaction of C4 with 1mC in ultrapure water. The first measurement was done directly after addition of 1mC to C4 (0.0 min). Full spectra were measured every 30 min, the last measurement was done 19.5 h after addition. The decrease in intensity at 718 nm indicates reaction of the iron(IV) complex C4 with the substrate 1mC. The spectrum taken after 5 h was excluded due to irregularities likely caused by a dust particle. B) Control reaction to monitor background without addition of the substrate 1mC showing only side reaction or decomposition of complex C4.

period, the reduction in absorption in Figure III.4A is notably faster and indicates the oxidation of 1mC by complex C4. The fact that the reaction of C4 with 1mC seems to be significantly slower than with 5mC, was further investigated and the results can be found in chapter Chapter III.4.^[122]

Since the UV-Vis measurements indicated consumption of 1mC by the iron(IV)-oxido complex C4, the next step was the detection of possible reaction products. Towards this, an aqueous 1:1 mixture of C4 and 1mC was reacted in a shaker at 27 °C. The reaction was performed as triplicate and aliquots of the reactions were taken after 18 h, 26 h, 42 h, 49 h and 69 h, filtered over silica and lyophilised according to previously established procedures.^[90] A reference solution of 1mC was treated accordingly without the addition of the iron complex. In that case only one aliquot was taken after 69 h. The resulting solids were dissolved in water and measured on an HPLC system equipped with a C-18-PFP column (ACE, 150x4.6 mm). The UV-Vis traces of the measurements after 18 h, 42 h, and 69 h are shown in Figure III.5 (additional spectra can be found in the Appendix, Chapter VII.2). Two distinctive signals were detected at retention times of 1.4 min and 2.0 min. The signal at around 2.0 min was assigned to 1mC by the reference measurement and LC-MS.

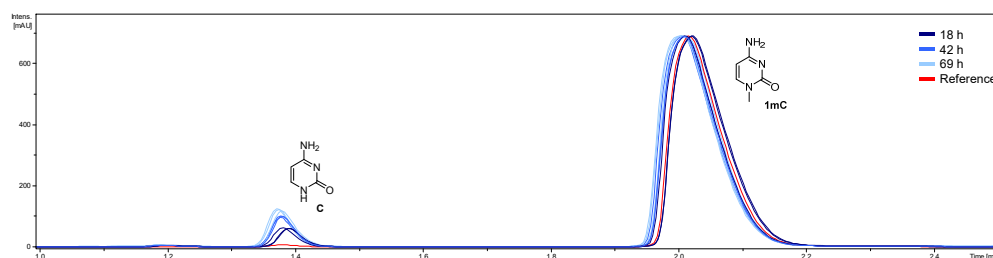


Figure III.5.: UV-Vis traces (280 nm) of reaction aliquots taken after 18 h, 42 h and 69 h. Measured on LC-MS using a C-18-PFP column (ACE, 150x4.6 mm) and a solvent gradient from 100 % A to 99.7 % A and 0.3 % B over 5 min (A = H₂O + 0.1 % formic acid (FA), B = MeOH + 0.1 % FA). Conditions [1mC] = 1 mM, [C4] = 1 mM, 27 °C. Reference conditions [1mC] = 1 mM, 27 °C, 66 h.

The signals show no significant decrease in 1mC concentration, which was expected considering previous UV-Vis analysis showed a comparably slow reaction. The signal at 1.4 min, however, is slightly increasing and not detectable in the reference without C4, indicating a reaction product of 1mC. Surprisingly, this signal was assigned to cytosine (C) by LC-MS (found: 112.3 m/z) instead of the expected reaction products 1hmC, 1fC or 1caC, which could not be found in the corresponding MS spectra. This result prompted the hypothesis that the oxidation products of 1mC might not be stable and undergo further reaction, namely deformylation (see Scheme III.7C) due to the *N*-methylation when compared to 5mC (C-methylated). This theory was further corroborated by DFT calculations in cooperation with the Zipse Group and the results can be found in Chapter III.4.^[122]

4. Biomimetic Oxidation of 1-Methylcytosine and Other Synthetic DNA Bases

Experiments regarding the oxidation of 1mC and following product analysis are part of the following publication. Parts of the supporting information and additional data and spectra can be found in the Appendix (Chapter VII3). All calculations regarding the bond dissociation energies were performed by Fabian Zott and not part of my research and therefore the additional information on this part of the publication (indicated by TableS or FigureS) are not included in the Appendix, but can be found online in the supporting information.^[122]

Author Contributions

Niko S. W. Lindlar (né Jonasson), Rachel Janßen, Annika Menke and Lena J. Daumann developed the project. Niko S. W. Lindlar, Rachel Janßen and Annika Menke performed the syntheses of substrates and iron complexes and were involved in the writing and review process of the manuscript. Niko S. W. Lindlar and Rachel Janßen performed reactions towards analysis of product formation. Niko S. W. Lindlar performed the GC-MS measurements, Rachel Janßen performed the HR-HPLC-MS and LR-HPLC-MS measurements and Annika Menke carried out the UV-Vis kinetic investigations including reaction rate calculation. Fabian Zott did all BDE calculations, wrote the according part of the manuscript and performed the synthesis of 1mU. Hendrik Zipse and Lena J. Daumann supervised this project.

TET-like Oxidation in 5-Methylcytosine and Derivatives: A Computational and Experimental Study^[122]

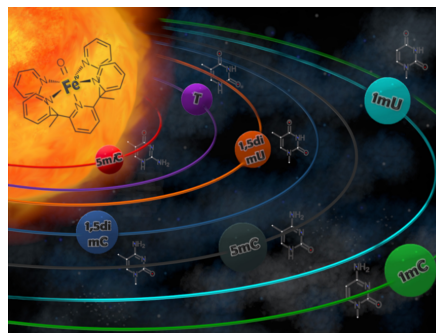
Niko S.W. Jonasson⁺, Rachel Janßen⁺, Annika Menke⁺, Fabian L. Zott, Hendrik Zipse, Lena J. Daumann

ChemBioChem **2021**, *22*, 3333.

Published as Open Access under CC BY-NC-ND 4.0

⁺ The authors wish it to be known that, in their opinion, the first three authors should be regarded as joint First Authors.

Abstract The epigenetic marker 5-methylcytosine (5mC) is an important factor in DNA modification and epigenetics. It can be modified through a three-step oxidation performed by ten-eleven-translocation (TET) enzymes and we have previously reported that the iron(IV)-oxido complex $[\text{Fe}(\text{O})(\text{Py}_5\text{Me}_2\text{H})]^{2+}$ (C4) can oxidise 5mC. Here, we report the reactivity of this iron(IV)-oxido complex towards a wider scope of methylated cytosine and uracil derivatives relevant for synthetic DNA applications, such as 1-methylcytosine (1mC), 5-methyl-*iso*-cytosine



(5*m*iC) and thymine (T/5*m*U). The observed kinetic parameters are corroborated by calculation of the C–H bond energies at the reactive sites which was found to be an efficient tool for reaction rate prediction of C4 towards methylated DNA bases. We identified oxidation products of methylated cytosine derivatives using HPLC-MS and GC-MS. Thereby, we shed light on the impact of the methyl group position and resulting C–H bond dissociation energies on reactivity towards TET-like oxidation.

Introduction

Using DNA as information storage for non-biological data has experienced a considerable development in recent years.^[94,98,136] DNA not only provides an immensely high density of information, but its durability allows to store information over decades and centuries.^[94] Besides the canonical nucleobases C, G, T and A, epigenetics extend the ‘DNA alphabet’ with the epigenetic markers 5-methylcytosine (5*m*C) and 5-hydroxymethylcytosine (5*hm*C) as fifth and sixth letter.^[137] In nature, these additional nucleobases are formed by direct methylation of cytosine which causes the gene to be silenced. Oxidation of the methyl group can alter or remove the epigenetic marker and therefore introduces a second layer of information.^[77] This has also been put to use in DNA information storage systems.^[119] Aside from nature, using unnatural orthogonal nucleobases pairs in synthetic DNA systems has expanded the ‘DNA alphabet’ up to eight letters within one system, called hachimoji DNA, increasing the density of information storable in DNA even further (Figure III.6A).^[110,138] Furthermore, the synthetic nucleoside *N*1-methyl-pseudouridine (1*m*Ψ, Figure III.6B), which consists of a 1-methyluracil (1*m*U) nucleobase fragment bound at its 5 position to ribose, was used in the Covid-19 mRNA vaccines by Pfizer/BioNTech (Comirnaty, BNT162b2) and Moderna (Spikevax, mRNA-1273).^[139] The use of 1*m*Ψ in mRNA has been reported to increase protein expression compared to *pseudo*-uridine Ψ and therefore likely contributes to the high efficacy of the mentioned vaccines.^[140]

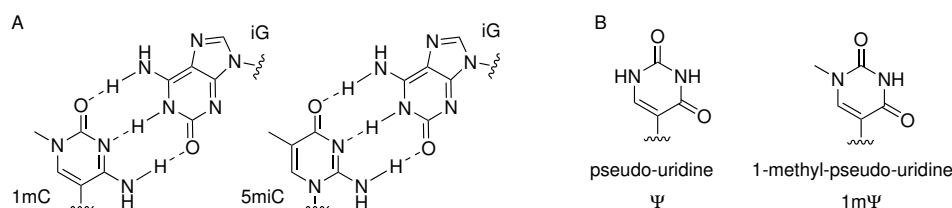


Figure III.6.: A) Base pairs 1-methylcytidine (1*m*C) – *iso*-guanosine (*i*G) and 5-methyl-*iso*-cytidine (5*m*iC) – *iso*-guanosine used in hachimoji DNA and other synthetic DNA applications.^[110,141] B) Nucleobase fragments in *pseudo*-uridine (Ψ) and 1-methyl-*pseudo*-uridine (1*m*Ψ).

Using epigenetic markers or synthetic DNA bases has increased the potential for DNA information storage, however, the idea of epigenetic manipulation of synthetic DNA bases has not been employed yet. In natural epigenetics, ten-eleven translocation (TET) enzymes are involved in the oxidation of the methyl group in 5*m*C. TET enzymes belong to the superfamily of iron(II)/α-KG dependent non-heme enzymes and use an iron(IV)-oxido

moiety as the catalytically active species for the stepwise transformation of 5mC to 5hmC, then to 5-formylcytosine (5fC) and finally to 5-carboxycytosine (5caC). We have recently shown that a synthetic iron(IV)-oxido complex (C4, Figure III.7) is capable of performing the same reaction on nucleobase,^[90] nucleoside, and even nucleotide substrates.^[91] It has been shown that hydroxyl radicals are capable of oxidizing 5mC, however, in addition to hydroxylation of the methyl group yielding 5hmC and/or 5fC, oxidation of the 5,6-double bond in 5mC was observed.^[121,142,143] In epigenetic sequencing applications, 5hmC is oxidized to 5fC with potassium perruthenate (K₂RuO₄). Under these conditions, 5mC is unaffected. In this work, we explored the chemistry of the biomimetic system (C4) towards synthetic DNA bases 1mC and *iso*-cytosine (as methylated 5m*i*C) occurring in hachimoji DNA and RNA, respectively, as well as methylated uracil derivatives. We present data on the diverse reactivity of different methylated nucleobases with the biomimetic compound C4 and present calculations of C–H bond dissociation energies (BDEs) as a viable method to predict the corresponding reactivity. The obtained results open up the possibility to install methyl groups with different reactivity towards oxidation and thus tunability for reaction, as well as to draw conclusions on the suitability of certain methylated DNA species in nature.

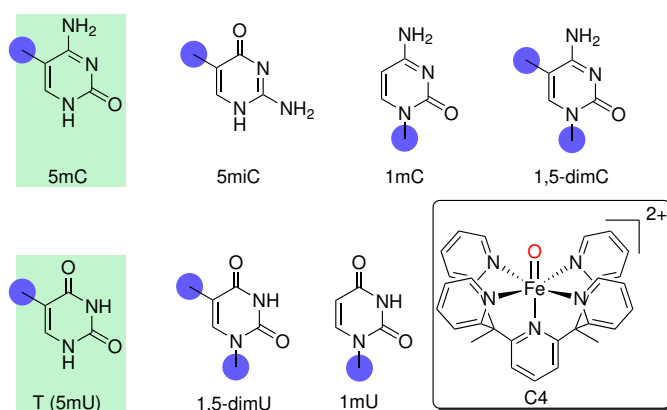


Figure III.7.: Methylated cytosine and uracil derivatives used in this work: 5-methylcytosine (5mC), 5-methyl-*iso*-cytosine (5m*i*C), 1-methylcytosine (1mC), 1,5-dimethylcytosine (1,5dimC), thymine (T), 1-methyluracil (1mU), 1,5-dimethyluracil (1,5dimU). The studied methyl groups are marked with blue circles, the naturally occurring nucleobases have a green background. Used iron(IV)-oxido complex $[\text{Fe}(\text{O})(\text{Py}_5\text{Me}_2\text{H})]^{2+}$ (C4) shown in rounded rectangle.

Results and Discussion

As substrates we used the naturally occurring 5-methylcytosine (5mC) and thymine/5-methyluracil (T/5mU) in addition to the synthetic nucleobases 5-methyl-*iso*-cytosine (5m*i*C), 1-methylcytosine (1mC), 1,5-dimethylcytosine (1,5dimC), 1-methyluracil (1mU) and 1,5-dimethyluracil (1,5dimU, Figure III.7). The cytosine derivatives were also analysed for the products formed when reacted with C4 using HPLC-MS and GC-MS. We evaluate which nucleobases could be useful for synthetic biology and epigenetics with respect to their ability to be further modified by TET enzymes and their biomimetic complexes.

UV-Vis kinetics

We have previously reported that the absorbance of C4 at $\lambda=718$ nm can be used to measure the initial reaction rates (data points used for rate calculation: minute 1-2) and then to determine the rate constants k_S of the individual substrates with C4.^[90] To confirm this is valid for the substrates used in this work, we monitored the observed relative absorbance of each substrate: in all reactions the initial absorbance was not significantly decreased after 2 min reaction time (>85–90 %), indicating that only small amounts of C4 had been consumed. The only exception with 80 % of the initial absorbance of C4 was with the rapidly reacting 5m*i*C (Figure VII.4 and VII.5). As the absorption decrease was still reliably linear within the monitored time frame (Figure III.8B) we deemed this data analysis to be a suitable approximation. Additionally, we analysed the reaction mixture of 5m*i*C and C4 after 2 min reaction time using GC-MS and found mostly unreacted 5m*i*C (see Figure VII.18). For all other substrates the linear consumption of C4 was observed for a much longer time frame. We were therefore confident to monitor almost exclusively the reaction of C4 with the respective starting material and not that of any further oxidized products.

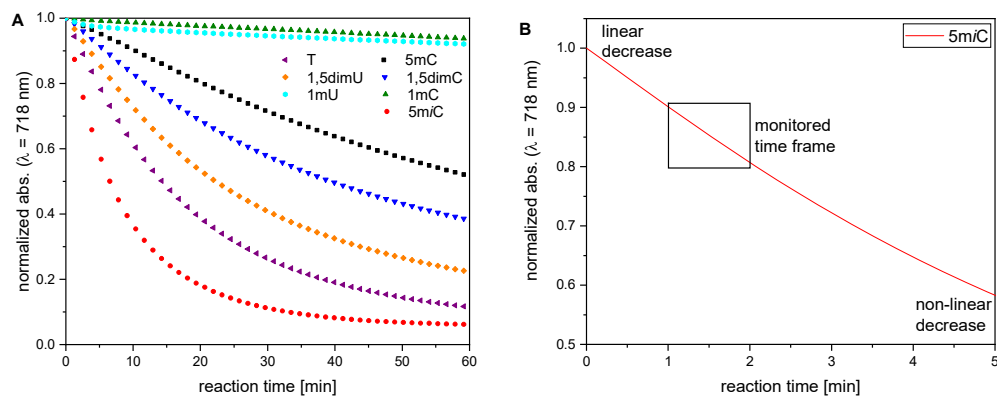


Figure III.8.: UV-Vis spectroscopy kinetics: A) Plot of the development of the absorbance of a series of reactions. B) Linear and non-linear decrease of the absorbance at $\lambda=718$ nm. Conditions: $[S]=1$ mM, $[C4]=5$ mM, H_2O , $30^\circ C$.

For all substrates we found a decrease of the absorbance at $\lambda=718$ nm over the monitored time frame (Figure III.8A, compare also Appendix Figure VII.4 and VII.5 for full UV-Vis spectra and control reactions). Using the method of initial rates, reaction rates were calculated from the observed decrease in absorbance by linear regression. We then calculated the corresponding rate constants k_S (Figure III.9) using the second order rate law found by Jonasson and Daumann for the reaction of 5mC with C4. This rate law was applied for all substrates used in this work (Eq. III.1):

$$v = k_S[S][C4] \quad (\text{III.1})$$

where v is the observed reaction rate, $[S]$ the concentration of the substrates and $[C4]$ the concentration of C4.

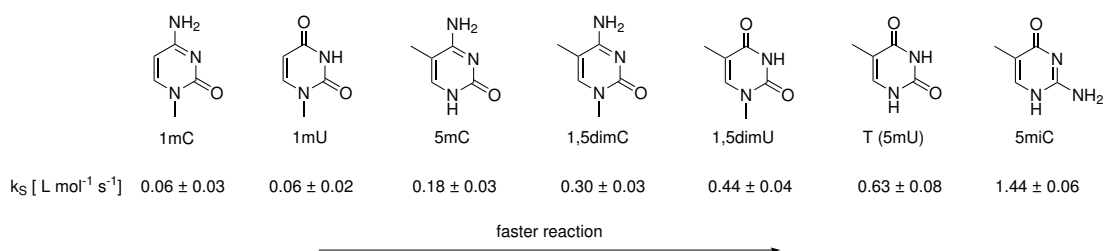


Figure III.9.: Observed rate constants k_S of the substrates at the following conditions: $[S]=1$ mM, $[C4]=5$ mM, H₂O, 30 °C. Rate constants k_S were calculated using a second order rate equation (Eq. III.1).

When the amount of C4 was varied from 1-9 equivalents, a linear dependence of the reaction rates on the amount of C4 (Figure III.10) was observed for all substrates and none showed any saturation behaviour (as had been previously observed for 5hmC).^[90] This confirms that the chosen concentration ranges are suitable for our purposes. The linear increase in reaction rate upon increase of the added amount of C4 indicates a rate law of first order for C4 for all substrates. This agrees with our previous findings concerning the reaction of C4 with 5mC and justifies use of Eq. III.1 for the calculation of k_S .^[90]

The *N*-methylated substrates 1mC and 1mU reacted significantly slower than all other compounds (Figure III.9 and Figure III.10). The uracil derivatives 1mU, T, and 1,5dimU reacted faster than their cytosine counterparts 1mC, 5mC and 1,5dimC, respectively. When comparing mono- vs. dimethylation, a significant difference between uracil- and cytosine derived substrates was noted: The dimethylated compounds 1,5dimC and 1,5dimU showed divergent reactivity: whereas 1,5dimC reacts faster than 5mC, 1,5dimU reacts slower than its monomethylated counterpart T. We found that in the case of dimethylated substrates, reactivity can be attributed almost completely to the methyl group bound to the carbon atom at position 5 (*vide infra* for details). 5*m*iC then shows the fastest reaction rates v by a large margin.

Clearly, the nature of the substituents on the 1, 2, and 4 position influences the reactivity of the methyl groups present. It can be summarized that an amine group at position 4 (as

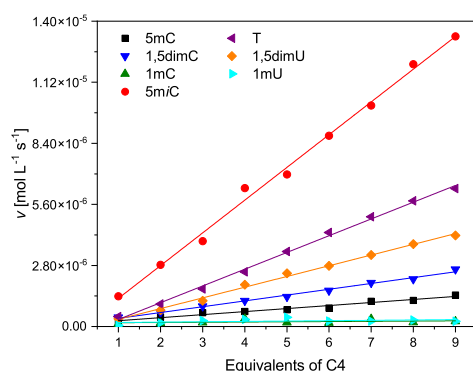
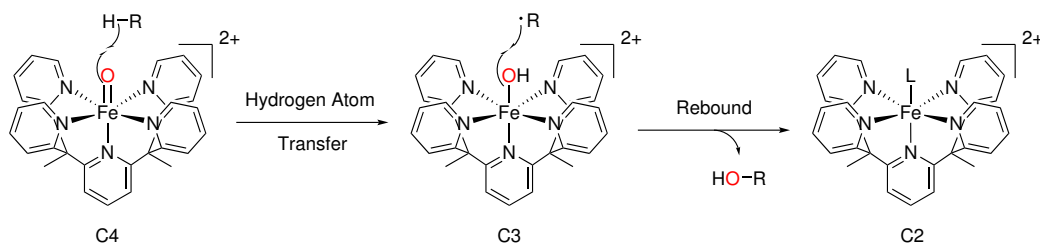


Figure III.10.: Plot of the measured reaction rates v of the reaction of C4 with nucleobase substrates. For a zoomed-in version of 5mC, 1mC, and 1,5dimC results see Appendix Figure VII.6B. 5mC (black squares), 5mC (red dots), 1mC (green triangles), 1,5dimC (blue inverted triangles), T (purple twisted triangles), 1,5dimU (orange diamonds), and 1mU (cyan circles). Conditions: $[S]=1$ mM, $[C4]=1-9$ mM, H_2O , $30^\circ C$. The Appendix contains a second set of measurements for 5mC, 5mC, 1mC, and 1,5dimC (Figure VII.6A).

in 5mC) slows the reactivity, whereas a carbonyl moiety (as in T and 1,5mU) increases it. Also, a guanidine moiety (amine substituent at position 2, as in 5mC) increases reactivity compared to a urea moiety (as in 5mC or T). Methylation of the 1 position can influence the reactivity both ways: in the case of an exocyclic amine on position 4 (as in 1,5dimC), the reaction rate is increased. If, however, two carbonyl functions are present (as in 1,5dimU), the rate is decreased when the 1 position is methylated. These observations imply that the heterocyclic, conjugated ring system is capable of relaying electronic information from the substituents to the methyl groups. Effects stemming from steric interactions and coordination of substrates and products to C4 might also influence the reactivity.

BDE calculation

In a next step, we wanted to rationalize the above described trends. As iron(IV)-oxido compounds both in synthetic^[144–147] and enzymatic context,^[82,86,148] as well as C4 in particular,^[89,90] are reported to react *via* a hydrogen atom transfer from an aliphatic C–H bond (Scheme III.6), BDEs are commonly believed to play an integral part concerning reaction rates.



Scheme III.6: Two-step reaction mechanism for C4 with aliphatic C–H bonds (indicated as R–H) as postulated by Daumann and Jonasson and Chantarojsiri *et al.*^[89,90] The transferred oxygen atom is marked in red. L = solvent, substrate, or product molecule that completes the coordination sphere of C2.

We therefore calculated the relevant BDEs of the substrates (Figure S17^[122]). All quantum mechanics (QM) results are reported at the SMD(H₂O)/DLPNO-CCSD(T)/CBS//(U)B3LYP-D3/6-31+G(d,p) level of theory as stated in the supporting information (for thermodynamic data see Tables S5-10^[122]).^[149–153] A graphical representation of all aqueous phase BDE values at the relevant C–H bonds in the above-mentioned substrates is shown in Figure III.11 (also compare gas phase BDE values, Figures S18-19^[122]).

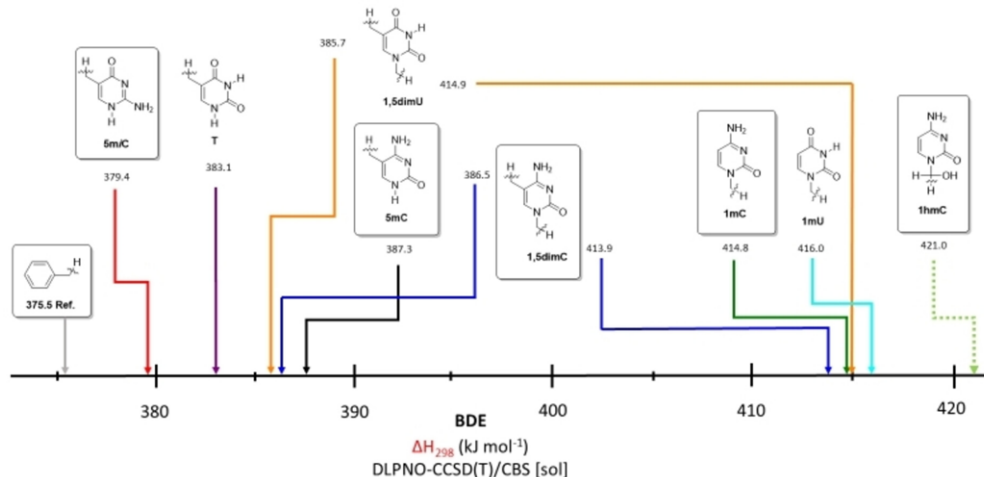


Figure III.11.: Aqueous phase ($\Delta H_{sol} = \Delta H_{298} + \Delta G_{sol}$) RCH₂-H bond dissociation energies (BDEs) of the relevant substrates calculated at the DLPNO-CCSD(T)/CBS level of theory. Dotted lines indicate the BDEs of molecules that were calculated but not included in experiments. For comparison of calculated BDEs of gas and aqueous phase see Figures S18-19^[122].

A significant difference in BDE values can be observed between *N1*- and *C5*-methylated compounds: methyl groups connected to another carbon atom possess BDE values of 379-387 kJ mol⁻¹, whereas the methyl groups situated on the *N1*-nitrogen atom show much higher BDEs of 413-416 kJ mol⁻¹. The BDE of 5mC is somewhat lower than all other compounds, including its closest structural relatives T ($\Delta BDE = 3.7$ kJ mol⁻¹) and 5mC ($\Delta BDE = 7.9$ kJ mol⁻¹). The site-specific BDE values of doubly methylated compounds generally compare to their mono-methylated parent species. The aqueous phase BDE value of 1hmC is the highest of all calculated compounds at 421.0 kJ mol⁻¹, although we note that there is a substantial solvation effect on this value (see Table S2^[122]).

Comparing BDEs to observed rate constants

The calculated BDE values were found to predict reactivity of the substrates perfectly: low BDEs correspond to high rate constants k_S . The only exception from the observed flawless correlation is 1mU, which reacts slightly faster than its BDE reactivity would predict. We hypothesize that this observation is due to the method of data analysis. We used the absorbance values between 1-2 min reaction time for the calculation of reaction time, however, as the reaction of 1mC and 1mU is very slow, small variations (possibly due to uncompleted mixing upon starting the experiment) influence the observed reactivity strongly. When the decrease in absorbance for 1mC and 1mU is compared for

the entire length of the experiment, a very similar behaviour is observed. This would fit very well with the BDEs of 1mC and 1mU being very similar at 415 and 416 kJ mol⁻¹, respectively. Nonetheless, the behaviour of 1mU does fit very well within the broader trend described above, even if the data analysis is not perfectly suited to its behaviour.

The correlation of BDE and k_S is in particular remarkable for the situation in the twice-methylated substrates 1,5dimC and 1,5dimU (Table III.1). As described above we found that *N*-methylation increased the reaction rate in the cytosine derivative whereas the opposite was observed for the uracil derivative. This behaviour is mirrored in the corresponding BDE values: the C–H bond on the carbon-bound methyl group in 1,5dimC is found to possess a lower BDE than 5mC, implying the experimentally confirmed increased reactivity. In the case of 1,5dimU a higher BDE was calculated, matching its lower reactivity compared to T.

Table III.1.: Comparison of calculated BDEs and observed reaction rates.

Substrate	BDE [kJ mol ⁻¹]	k_S [L mol ⁻¹ s ⁻¹]
1mC	414.8	0.06 ± 0.03
1mU	416.0	0.06 ± 0.02
5mC	387.3	0.18 ± 0.03
1,5dimC	386.5	0.30 ± 0.03
1,5dimU	385.7	0.44 ± 0.04
T	383.1	0.63 ± 0.08
5m <i>i</i> C	379.4	1.44 ± 0.06

The perfect correlation of calculated BDEs to observed reaction rates provides further evidence to corroborate the previously postulated two-step reaction pathway of C4 with aliphatic C–H bonds (Scheme III.6).^[90] In the first step in this mechanism, a hydrogen atom is transferred from the substrates R-Me(H) to the iron compound, generating an iron(III)-hydroxido species (**C3**) and a carbon-centred radical. These species then recombine in a rebound step to form the product R-OH and an iron(II)-species (**C2**). It was found that C–H abstraction/hydrogen transfer is the rate limiting step.^[90]

As the hydrogen atom transfer (HAT) step involves the breaking of the C–H bond in the substrate, the BDE should determine the reaction rate. We had previously demonstrated this for both 5mC and 5hmC; in this work we expanded the substrate scope significantly to include 1mC, 1,5dimC, 5m*i*C, T, 1mU, and 1,5dimU.

When plotting the aqueous phase BDE values versus $\ln(k_S)$, a linear Bell-Evans-Polanyi correlation can be observed for 5mC, 1,5dimC, 1,5dimU, T and 5m*i*C (Figure III.12).

1mC and 1mU are outliers, probably due to them being *N*-methylated instead of C-methylated as all other compounds. As mentioned previously, for the doubly methylated compounds the reactivity of the methyl group at the 5-position prevails (*vide infra* for details on how we come to this conclusion). Repeating this type of analysis with gas phase BDE(C–H) values we obtain similar results (see Figure S23^[122]), thus, we conclude that the observed correlation reflects the intrinsic properties of the studied nucleobase substrates.

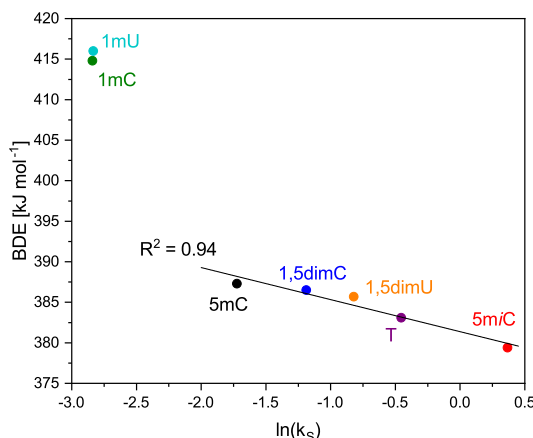


Figure III.12.: Plot of the calculated BDE values in aqueous phase against the observed rate constants k_S on a logarithmic scale ($R^2=0.891$) of the substrates 1mC, 1mU, 5mC, 1,5dimC, 1,5dimU, T, and 5mC. In the case of the demethylated substrates 1,5dimC and 1,5dimU only the BDE of the carbon bound methyl groups are plotted. A similar plot of calculated BDE values in the gas phase against the observed rate constants k_S on a logarithmic scale can be found in Figure S23^[122].

The presented data is a remarkable result, as it both provides evidence to confirm the previously postulated mechanism of C4 and shows that calculated BDEs can be reliably used to predict reaction rates for these types of substrates (in the absence of an enzyme's second coordination sphere). It is noteworthy that the reactivity of the natural nucleobase 5mC is in the middle of the observed spectrum: the *N*-methylated compounds 1mC or 1mU react significantly slower whereas 5mC reacts significantly faster. This could be considered an indication on why 5mC can be considered an ideal epigenetic marker in nature: the reactivity of 5mC towards an iron(IV)-oxido moiety seems to be in a range that is both fast enough for efficient catalytic conversion by an enzyme and still slow enough to be controlled within a biological system. For example, 1mC is oxidized so slowly that even if its oxidized derivatives were stable (*vide infra*) it would not be a suitable substrate for enzymatic conversion. On the other hand, the reactivity of 5mC seems to be so fast that it would be hard to control - an important factor in the delicate methylation equilibrium that is maintained by DNA methyltransferases (DNMT) and TET enzymes.^[79,154–156] Whereas we do not claim that this behaviour of 5mC and the other substrates towards iron(IV)-oxido species has been an evolutionary pressure resulting in the formation of 5mC epigenetics as we know it, we provide evidence that 5mC is indeed a perfect substrate for the task it performs. Regarding applications of natural and artificial methylated nucleobases in synthetic biology and DNA-based storage

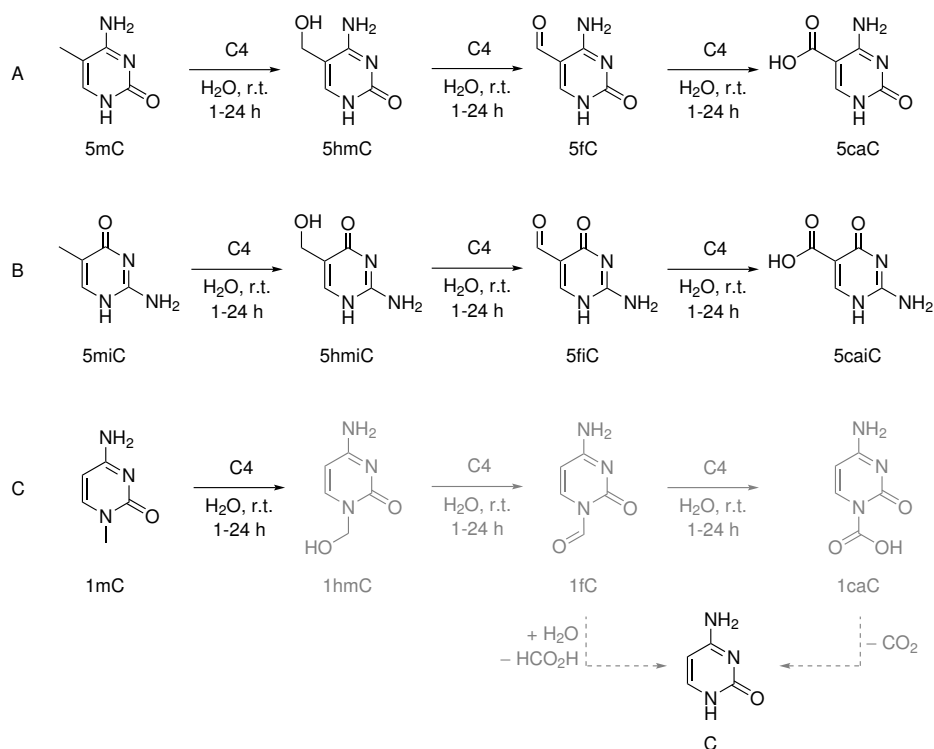
systems, their different reactivities could allow for additional layers of information and tunability. By incorporating two nucleobases of vastly different reactivity towards C4, such as 1mC and 5m*i*C, into an artificial DNA strand, differentiation during oxidative sequencing could be used to drastically increase density of information.

Product Analysis (HPLC-MS/GC-MS)

We used both UHPLC-MS and GC-MS to identify the products formed in the reactions of C4 with the cytosine substrates, as these are most relevant to our research question (see Appendix, Table VII.1 and Figure VII.7-VII.19). We also analysed the product distribution of T oxidation products using GC-MS (see Figure VII.19).

In our recently published work on the reactivity of C4 towards 5mC we identified the oxidized derivatives 5hmC, 5fC, and 5caC, that are also formed by TET enzymes in DNA substrates, using GC-MS.^[90] In this work we corroborated these results with HPLC-MS measurements (Scheme III.7A). In the measurements of the reaction samples we found signals corresponding to all expected products (5hmC, 5fC, 5caC), but did also find an additional signal with a mass-to-charge ratio of 126.0622, which would correspond to 5mC. Due to the longer retention time (~ 13.2 min) than for the reference signal of 5mC (~ 7 min) but equal m/z ratio, we propose that this is a dimer of 5mC, probably formed during lyophilisation (see Figure VII.7 and VII.8).

In fact, a hemi-protonated dimer of 5mC ($5mC-5mCH^+$) has previously been isolated by us and was structurally characterized.^[157] For reactions with 5m*i*C we found signals at m/z values corresponding to 5-hydroxymethyl *iso*-cytosine (5hm*i*C), 5-formyl *iso*-cytosine (5fiC), 5-carboxy *iso*-cytosine (5caiC, Scheme III.7B). When 5 equivalents of C4 were used, no significant difference in product distribution can be observed between the sample taken after 1 h and that taken after 24 h. This indicates that the reaction is complete after 1 h, which agrees with the observed high reaction rates and calculated low BDEs. When changing the substrate to 1mC only small amounts of cytosine (C) could be identified as a product using the standard procedure: conducting the reaction in water, filtration through silica, lyophilisation, UHPLC measurement. However, traces of all oxidation products can be found using HPLC-MS when injecting samples before standard workup procedures were applied. We propose that the methyl group on 1mC is indeed oxidized to the expected products 1hmC, 1fC and 1cC, however, several pathways can lead to a quick decomposition towards cytosine. The first oxidation of 1mC leads to 1hmC which, as an hemiaminal, tends to equilibrate towards cytosine, when removing formaldehyde at reduced pressure (Scheme III.7). This overall process, however, is endergonic (see Figure S21A and B and Table S3^[122]). Oxidation of 1hmC towards 1fC is proposed to be faster compared to the oxidation of 1mC, since the gas phase BDE of 1hmC is 4.3 kJ mol^{-1} lower than for 1mC. In this particular case, we observed that



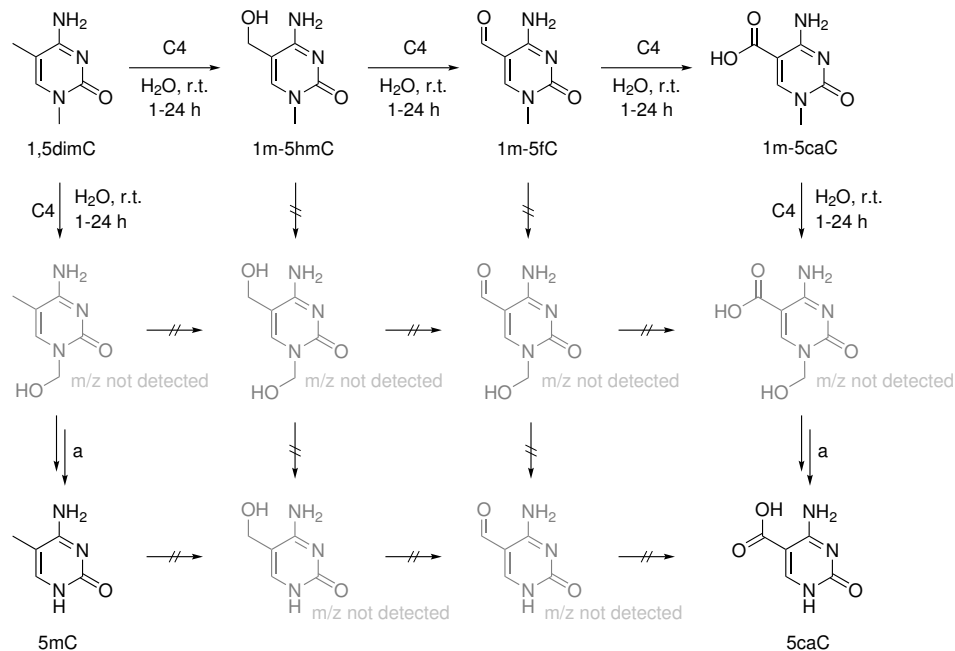
Scheme III.7: Identified products in the reactions of 5mC, 5mzC, and 1mC with C4. All structures in black were detected using HPLC-MS after 1 h and 24 h using both 1 and 5 equiv. of C4, although in different ratios. 5mzC, 5hmiC and 5caiC were also detected using GC-MS with 1 equiv. of C4 after 1 h. All structures in gray were detected on HPLC-MS by injection of the untreated reaction solution with 1 equiv. of C4 after 24 h and 44 h.

the gas phase BDE value represents a better estimation of the reaction trend than in solution phase. This is possibly due to formation of a cyclic hydrogen bond between the hydroxymethyl group and urea moiety (for details, please refer to Figure S20^[122] and subsequent text). The oxidation products that follow, 1fC and 1caC, were both found to be exergonic and therefore unstable (see Scheme III.7C). The calculated solution phase free energies of reaction ΔG for the deformylation of 1fC is $-17.0 \text{ kJ mol}^{-1}$ (Figure S21C^[122]), for the decarboxylation of 5caC it is $-44.9 \text{ kJ mol}^{-1}$ (Figure S21D^[122]).

As a proof-of-concept for this hypothesis, free energies of reaction ΔG were calculated for the literature known deformylation of 6-hydroxymethyladenine (6hmA) and 6-formyladenine (6fA), which are oxidation products of naturally occurring 6-methyladenine (6mA) in mammalian DNA.^[158,159] The deformylation of 6hmA towards adenine and formaldehyde is endergonic ($\Delta G_{298, \text{H}_2\text{O}} = +16.5 \text{ kJ mol}^{-1}$, see Figure S22B and Table S4^[122]), while the deformylation of the following oxidative product, 6fA, is thermoneutral ($\Delta G_{298, \text{H}_2\text{O}} = +1.1 \text{ kJ mol}^{-1}$, see Figure S22C^[122]). It has been reported, that 6hmA and 6fA are transient intermediates of the oxidation of 6mA with hydrogen peroxide.^[160] The aqueous phase BDE(C–H) value of 6mA ($+396.4 \text{ kJ mol}^{-1}$, see Table S2^[122]) is 13.3 kJ mol^{-1} lower than that of 6hmA ($+408.7 \text{ kJ mol}^{-1}$, see Table S2^[122]), which is in support of a consecutive oxidation cascade and therefore also of the proposed pathway

for the oxidative demethylation of 1mC to C.

In the case of 1,5-dimC, the product composition is more convoluted, however, it matches with the expectations based on observed reaction rates and calculated BDEs (Scheme III.8): in addition to the starting material we detected m/z values corresponding to 1-methyl-5-hydroxymethylcytosine (1m-5hmC), 1-methyl-5-formylcytosine (1m-5fC), and 1-methyl-5-carboxycytosine (1m-5caC). These products are expected as the carbon-bound methyl group at position 5 has a lower calculated BDE and should therefore be oxidized more readily. The observed products are also corresponding to those observed for reactions of 5mC and 5mC with C4. However, besides the oxidation products of position 5, we additionally detected both 5mC and 5caC (confirmed by m/z and retention time). We therefore propose, that for 1,5dimC hydroxylation on the 1-methyl group also occurs to some small extent, and this oxidation product then reacts to 5mC (Scheme III.8), corresponding to our proposed mechanism for 1mC (Scheme III.7). Similarly, 1m-5caC only offers the 1-methyl group as a substrate position for C4 to react with, so 5caC is formed *via* hydroxylation and subsequent reaction to 1m-5caC. The amounts of 1m-5hmC and 1m-5fC are too low to represent a significant target for 1-methyl-hydroxylation, therefore no 5hmC or 5fC are detected. Similarly, only small amounts of 5mC are detected and it is, as the calculated BDE values show, less readily oxidized to 5hmC and 5fC as its *N*-methylated counterpart 1,5dimC.



Scheme III.8: Identified products in the reaction of 1,5dimC with C4. All structures in black were detected using HPLC-MS after 1 h and 24 h using both 1 and 5 equiv. of C4, although in different ratios. a: For this step we propose a similar reaction sequence as for 1mC (see Scheme III.7).

Conclusion

We have presented a comprehensive study of the reactivity of the biomimetic iron(IV)-oxido complex C4 towards a number of methylated cytosine and uracil substrates and compared the results to calculated BDE values. Using HPLC-MS and GC-MS we also identified the products of the reaction of C4 with the cytosine derivatives 5m*i*C, 1mC, and 1,5dimC. We also provided a reasonable explanation for the observed decomposition of oxidized 1mC derivatives 1hmC, 1fC, and 1caC by calculating deformylation and decarboxylation energy profiles and comparing these to the literature known pathway in 6hmA/6fA. In the case of 1,5dimC, combining the observed reaction rates, the calculated BDE values and the observations regarding 1mC allowed for a clear interpretation of the observed product distribution. We found that the reported reaction rates are in very good agreement with the calculated BDEs which therefore prove to be a very good predictor for the reactivity of C4 towards a broad range of methylated substrates. In summary, the observed reaction rates towards C4 seemed to be dominated by the reactivity of the C-methylated part of the substrates. 5mC, T and 5m*i*C possess a distinctly different reactivity than the solely *N*-methylated compounds 1mC and 1mU. For the compounds 1,5dimC and 1,5dimU that are both C-methylated and *N*-methylated, their C–H reactivity towards oxidation by C4 is mostly determined by the methyl group bound to the carbon atom. Interestingly, diverging effects were observed for *N*-methylation in 1,5-dimC and 1,5-dimU: in the case of 1,5dimC the reactivity is higher than for its mono-methylated counterpart 5mC, whereas 1,5dimU was observed to react faster than T. The observed rates also suggest that the reactivity of the 5-methyl group on the epigenetic marker 5mC is ideal to fit its purpose in a delicate equilibrium maintained by a series of enzymes. While the low reactivity of 1mU towards C4 is certainly not the reason for the stability of the corresponding nucleoside *pseudo*-methyl-uridine (1mΨ) that is used in some Covid-19 mRNA vaccines, our analysis shows that 1mUs methyl group is rather inert towards oxidation reactions. These observations can be a useful tool in predicting the possibilities of using and manipulating methylated nucleobases in synthetic biology, e. g. data storage, and further understanding the mechanisms of epigenetics.

IV. Towards the Immobilisation of Py₅-Ligand Systems on a Solid Support

1. Introduction

Immobilisation is a useful tool to improve the handling of catalysts or enzymes which are used to convert a specific target molecule into the desired product. When catalysts are used in a homogeneous systems they are efficient, but can also pose problems when it comes to separation. The removal of either the catalyst or the substrate and product can be difficult and is limited by two crucial factors. In some cases, a substrate could be converted multiple times in a sequential manner and the catalysis needs to be stopped at a specific time when the maximum concentration of the desired product is reached. To achieve this, the catalyst and desired product need to be separated as quickly as possible, which is often difficult in a homogeneous system. In addition, for economic and environmental reasons, the catalyst should be recycled for further use and therefore needs to be recovered from the system which can involve several steps of purification.^[161–164] In order to facilitate both the control of reaction time and the recovery and reuse of the catalyst, a heterogeneous system is needed. By immobilising the catalyst on a solid support while substrates and products are in solution, they can be separated in a facile manner by filtration, centrifugation or decanting, respectively, while the catalyst can be purified by simple washing procedures.^[161,162,164,165]

1.1. Immobilisation Techniques

Although immobilisation can improve the issues that can occur in homogeneous systems, the variety of catalysts and enzymes is vast and there is not one immobilisation solution for all homogeneous systems. Over the years, a variety of techniques for immobilisation has been developed to accommodate the different types of catalysts and surrounding conditions^[161–168] since, depending on the system, multiple factors regarding the functionalities of the solid support and the surrounding solvent have to be taken into account.^[163] Nevertheless, several immobilisation techniques have been developed and successfully applied. A generalised overview of these techniques is shown in Figure IV.1. The techniques can be roughly divided into chemical and physical approaches wherein chemical techniques include covalent binding of the catalyst while physical approaches use physical barriers and interactions. In each technique, the catalyst or holoenzyme can either be immobilised directly or the ligand or apoenzyme are immobilised before the metal ion is introduced. Since the properties and reactivity can differ strongly in both cases, this should be considered when designing a heterogeneous system.^[165]

The chemical immobilisation techniques can be further divided in two groups: covalent binding and crosslinking. In covalent binding, the solid support and linker each bare a functional group which can undergo a chemical reaction forming a covalent bond. These bond formations include nucleophilic substitution reactions,^[169,170] Schiff base formation^[171–173] and ring-forming reactions,^[174–177] respectively. In the crosslinking approach,^[178] the catalyst or enzyme do not necessarily react with a solid support.

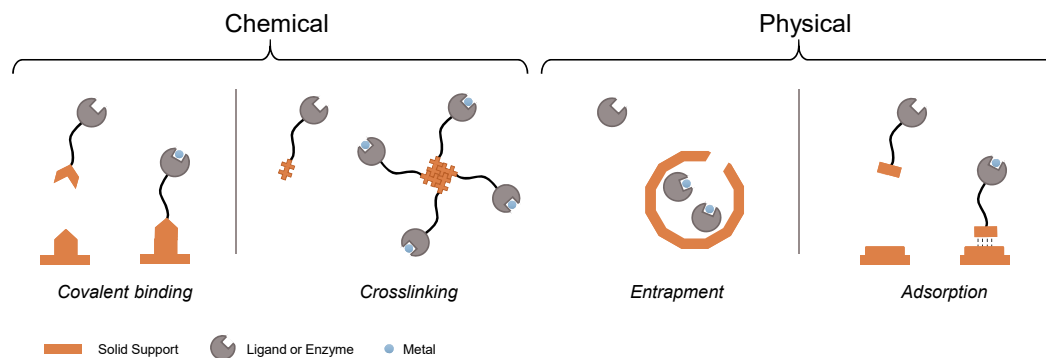


Figure IV.1.: Overview of different immobilisation techniques divided by chemical bond formations and physical interaction. In the covalent bond formation the complex or enzyme is directly bound to a solid support by a specific reaction forming a covalent bond while in crosslinking approaches the complex or enzyme is bound in aggregations of several moieties. In the physical immobilisation the complex or enzyme is either physically entrapped by the solid support or adsorbed through non-covalent binding like van der Waals or electrostatic interactions, respectively.

They are equipped with functionalities that can form multiple bonds and thus aggregate several catalyst moieties which results in insolubility of the formed bulk. This can be achieved by introducing a linker molecule that either binds multiple catalyst moieties or undergoes polymerisation forming a bigger interconnected network of linker molecules bearing the catalyst. The formation of a covalent bond in either case often provides a stable link of the catalyst which is inert to variable conditions and thus prevents leaching of the catalysts into the solution.^[162] Nevertheless, the functionalities used for binding are often not an inherent part of the catalysts or solid support and have to be introduced first. These alterations and the covalent binding itself can have a negative influence on the catalytic activity which needs to be in balance with the advantages of covalent immobilisation.^[163,165,168] In contrast, the physical immobilisation techniques do not always require a functionalisation of the catalyst or enzyme. Especially when using entrapment approaches, the catalytic moiety does not have to be altered. Entrapment can be achieved by different methods including fiber^[179] or gel entrapment,^[180] which are primarily used for enzymes, as well as encapsulation.^[181,182] Here, the solid support is often build *in situ* around the catalytic species although it can also be brought into the solid support step by step and assembled within the material.^[183] Similar to the covalent approaches entrapment effectively avoids leaching of the catalytic species. However, the solid support has to allow for relatively quick and easy permeability of the substrate and product.^[162] In physical adsorption the catalyst and solid support again have to be equipped with matching functionalities or properties allowing for adsorption of the catalysts on the support. These can either be inherent to the molecule or be introduced by functionalisation. The immobilisation can be achieved by van der Waals^[184,185] or electrostatic interactions^[186] or π - π stacking,^[187,188] respectively. An advantage of this approach is the facile immobilisation which does not include a chemical reaction. However, as the physical binding through interactions is generally weaker than covalent binding, these systems tend to create difficulties by leaching the catalytic species into solution.^[162]

1.2. Solid Phase Materials

Similar to the immobilisation techniques, the field of used solid supports includes a vast variety of substances. Depending on the catalytic species that is to be immobilised and the reaction conditions, like the solvent, the solid support has to be chosen according to the given requirements. Table IV.1 depicts an excerpt of commonly used solid supports. They can generally be divided by inorganic and organic materials. While the inorganic materials on average display a higher stability towards surrounding conditions, organic supports are more bio-compatible and especially in the case of bio-polymers more eco-friendly. It should be mentioned that, for practical and economic reasons, solid support systems that are ready to use without further manipulation are preferable, but due to the variety of catalytic species an immediate match of catalyst and support is not always realistic.




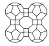
One of the most used solid supports for immobilisation are silica-based systems. This is likely due to the simplicity of the system and the variety of immobilisation techniques than can be applied. As stated in Table IV.1, silica has been used in covalent binding, electrostatic interaction, entrapment and absorption applications emphasizing its versatility.^[167] A frequently used method is the functionalisation of porous hexagonal silicas with silanes bearing a specific functional group that can then be used for covalent binding.^[171,172] Although this method requires an additional synthetic step in the procedure, it can be used to specifically accommodate the catalytic species. Similar techniques are applied to magnetic nanoparticles (MNPs).^[168,189] Most common are iron(III) oxide nanoparticles which can easily be separated from solution through their magnetic properties. They are often functionalised to allow variable covalent binding which is frequently achieved by coating with silica and using the above mentioned methods.^[189] In addition, functional groups like phosphonic acids which have a high affinity towards oxide surfaces can be used for direct covalent modification.^[190] Other inorganic materials are carbon nanotubes (CNTs) which can also be functionalised towards covalent binding. For example, the treatment with nitric acid and thionyl chloride is used to introduced acid chlorides on the CNTs, which can then be used to immobilise the catalytic species.^[170] A unique characteristic of the CNTs is their graphene surface which can efficiently bind catalysts by π - π stacking.^[187,188] This method is, however, limited to catalytic species that are or can be equipped with according functionalities. Non-covalent immobilisations can also be performed by entrapment in zeolites,^[183] which is also constrained due to limitations by pore sizes.

In the group of the organic solid supports, the most commonly used materials are polystyrene based resins.^[191] While polystyrene itself can be used for encapsulation of catalysts,^[192] respectively, several derivatives like Merrifield and TentaGel resins are applied in covalent immobilisation of various catalytic species.^[169,182,193] These resins are commercially available as an derivatised forms of polystyrene with different functionalities.




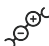
Therefore, they do not always require additional manipulations. Nonetheless, depending on the catalytic species they can be further functionalised. In these respects and with the typical methods used, polystyrene resins serve as the organic counterpart to silica systems. The most environmental friendly solid supports are made from bio-polymers^[180,194] like alginate, cellulose, chitosan and collagen.^[195] They are often used in form of gels or nanofibers to entrap the catalytic species.

Table IV.1.: Examples of the variety of materials used for the immobilisation of catalysts and enzymes. Depicted are general categories of materials and accordingly used methods of immobilisation as well as an indication whether the material has to be functionalised prior to use, which form of immobilisation can be used directly on the material and for which method additional adaptation is necessary. In some cases, the material was used with and without prior functionalisation for the same form of immobilisation. This table does not claim to be exhaustive.

Inorganic

Solid Support		Chemical Manipulation	Form of Immobilisation
Silica ^[167]		yes Functional groups	Covalent binding ^[171,172]
		yes Ion exchange (Si-Al)	Electrostatic interaction ^[196]
		no	Entrapment ^[197]
		no	Adsorption ^[185]
Magnetic nanoparticles ^[168,189]		yes Functional groups	Covalent binding ^[198]
		yes Coating	Covalent binding ^[199]
		no	Covalent binding ^[190]
Carbon nanotubes ^[162]		yes Functional Groups	Covalent binding ^[170,200]
		no	Adsorption ^[187,188]
Zeolites		no	Entrapment ^[183]

Organic

Solid Support		Chemical Manipulation	Form of Immobilisation
Polystyrene resins ^[191]		yes Functional Groups	Covalent binding ^[201]
		no	Covalent binding ^[182]
		no	Encapsulation ^[192]
Bio-polymers ^[166]		yes Functional Groups	Encapsulation ^[179,180]
		yes Functional Groups	Covalent binding ^[194]
		no	Adsorption ^[202]
MOFs ^[181,203]		yes MOF Design	Covalent binding ^[204,205]
		no	Entrapment ^[206]
Ion exchange resins ^[207]		no	Electrostatic interaction ^[208]

Unfortunately, these polymers are often very effective in aqueous solution making them a suitable substrate for enzyme applications,^[195] but limiting their use in immobilisations of inorganic catalysts. In contrast to that, metal-organic frameworks (MOFs) can be a good solid support for chemical catalysts. They can be either incorporated into the framework or be encapsulated as a guest species.^[181,203,205] While it can be effective, this technique requires a specific expertise in designing a MOF either incorporating or encapsulating the target catalyst and is therefore not readily applicable. Another more specific material are ion exchange resins.^[207] As the name suggests, these materials are specifically used in immobilisation *via* electrostatic interaction and are constricted to charged molecules. In addition, this type of interaction is not as inert as covalent binding and thus difficulties with leaching into the solution are common.^[207]

1.3. Immobilisation of Catalysts

As described in the previous sections, depending on application and catalytic species, various combinations of immobilisation techniques and solid supports can be and have been applied successfully. To give a few examples, Figure IV.2 displays four different immobilised catalysts and the according reactions performed after immobilisation. The examples do not necessarily represent the best performing immobilised catalysts but an idea on the different immobilisation methods applied.

Figure IV.2A depicts the immobilisation of a copper(II) acetylacetonate complex ($[\text{Cu}(\text{acac})_2]$) on a hexagonal mesoporous silica by Silva *et al.*^[171] In this procedure, the silica was functionalised by reaction with (3-aminopropyl)triethoxysilane prior to immobilisation. The resulting silica was then reacted with $[\text{Cu}(\text{acac})_2]$ in chloroform under reflux to immobilise the complex by a Schiff base formation between the functionalised silica and the ligand. The immobilised catalyst was then applied in the aziridination of styrene and compared to the homogeneous $[\text{Cu}(\text{acac})_2]$ complex in solution. In a first reaction, the immobilised catalyst displayed a higher conversion (92 %) compared to the homogeneous $[\text{Cu}(\text{acac})_2]$ complex (69 %). However, the turnover frequency (TOF) was significantly smaller and the productivity decreased upon reuse of the material. Nevertheless, this procedure is a typical example regarding immobilisation by covalent Schiff base formation.

Another procedure similarly using a silane for solid support functionalisation is shown in Figure IV.2B. Riente *et al.* used magnetic nanoparticles (Fe_3O_4) and derivatised them by reaction with a silane bearing an azide functional group.^[198] This was then reacted with a MacMillan catalyst by copper catalysed azide-alkyne cycloaddition (CuAAC) forming the immobilised species (Figure IV.2B) by covalent bonding *via* click-reaction. They additionally immobilised the catalyst in a similar manner on Merrifield resin. Here, they substituted the chlorine in the Merrifield resin with sodium azide prior to performing the CuAAC. Both materials were used in Friedel–Crafts alkylations of *N*-substituted pyrroles

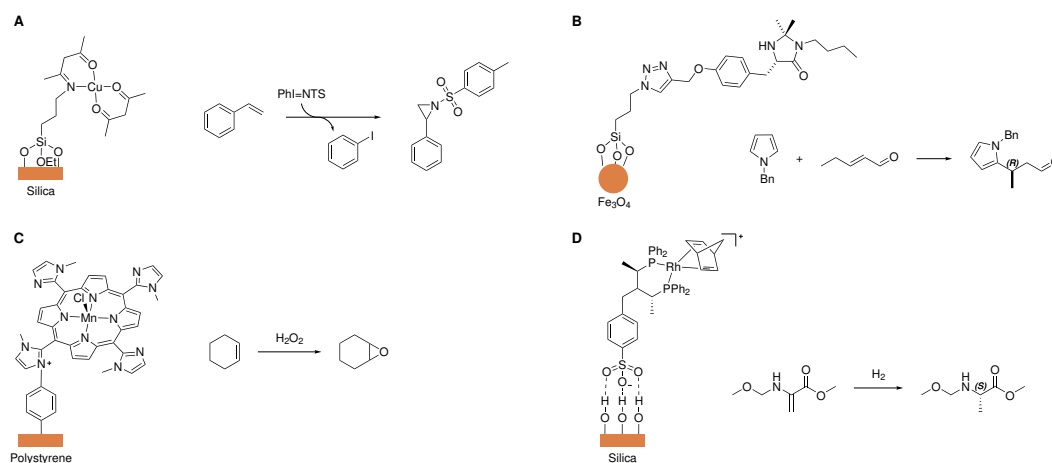


Figure IV.2.: Examples of successful immobilisation of chemical catalysts as an excerpt of the variety of immobilisation techniques and support materials. A) Immobilisation of a $[\text{Cu}(\text{acac})_2]$ complex on a hexagonal mesoporous silica catalysing the aziridination of styrene.^[171] B) Covalent binding *via* CuAAC applied on a functionalised magnetic nanoparticle immobilising a MacMillan catalyst used for Friedel–Crafts alkylations.^[198] C) An immobilised manganese catalyst on polystyrene based Merrifield resin used for cyclohexene oxidation.^[182] D) Immobilisation on a non-functionalised silica by adsorption of a rhodium catalyst used in asymmetric olefin hydrogenations.^[185]

with α,β -unsaturated aldehydes, one example of which is given in Figure IV.2B. With this substrate, both the polystyrene and the MNP supported catalyst reached conversion of 98 % with an enantiomeric excess (ee) of 79 % and 65 %. Although the ee is lower than with the homogeneous catalyst^[209] the authors point out that the immobilised catalyst was used at 0 °C to room temperature while the homogeneous catalyst is used at –60 °C to –30 °C. Additionally, the straightforward removal of the MNPs facilitated reuse of the catalyst showcasing the benefits of immobilisation.

A third example by Paula *et al.* uses a simple nucleophilic substitution to immobilise the catalyst by covalent binding.^[182] They immobilised a manganese porphyrin ($[\text{Mn}(\text{porph})]$) complex directly onto Merrifield resin without additional functionalisation (Figure IV.2C). The resin supported catalyst was then used for different oxidation reactions. In case of the oxidation of cyclohexene by hydrogen peroxide, the immobilised catalyst yielded 98 % average conversion through four cycles of reuse and a product selectivity of approx. 90 %. In general, compared to the homogeneous catalyst the main disadvantage were longer reaction times while the overall performance did not suffer significantly. The same catalyst was additionally immobilised on bromo-silane functionalised silica. However, this silica supported catalyst did not yield satisfactory results. This was attributed to the influence of the linker and synthetic procedure as they did not use hydrogen peroxide in order to avoid water in the system. It should be mentioned that this was done with a silica gel and not a commonly used and more stable hexagonal porous silica.

The immobilisation displayed in Figure IV.2D shows an example of the, in case of catalysts, more rarely used immobilisation by adsorption. Bianchini *et al.* used a rigid

meshed silica (Davison 62) to immobilise a rhodium complex by hydrogen bonding interactions between a sulfonate attached to the ligand structure and the silica.^[185] As is often observed for adsorbed catalysts, dissolution of the hydrogen bonds and thus leaching of the immobilised catalyst was observed in methanol and ethanol, respectively. It should be kept in mind that this is a relevant restriction when using this technique. The immobilised catalyst was used in asymmetric olefin hydrogenations with hydrogen and *n*-heptane as a solvent in comparison to a homogeneous analogue in methanol. With most substrates, like the example given in Figure IV.2D, both catalysts displayed very similar conversion and ee in three consecutive runs.

While many examples of heterogeneous catalysts obtained through immobilisation have been designed, the immobilisation of biomimetic catalysts is a less developed field. As was described earlier (see Chapter II and Chapter III4), biomimetic complexes can be a powerful tool in the investigation of enzyme activity and can be used to reproduce enzymatic reactions in a chemical environment. Creating heterogeneous biomimetic catalysts can additionally widen the applicability of these enzymatic reactions. An examples for successful development of a heterogeneous system is the implementation of an iron(II) site into a MOF system which mimics α -ketoglutarate-dependent dioxygenases by Hou *et al.*^[210] The iron was introduced into the system by exchange of zinc ions in the $\text{Zn}_5\text{Cl}_4(\text{btdd})_3$ structure and the chloride was exchanged with pyruvate to create a close mimic of the reactive site in α -ketoglutarate-dependent enzymes (see Chapter II). They showed that the iron within this MOF structure is able to activate molecular oxygen in a biomimetic manner and thus form an iron(IV)-oxido complex capable of catalytic oxygenation of cyclohexane.

The presented examples give a small insight into the vast field of catalyst immobilisation. While covalent binding is the commonly applied immobilisation technique, there are other viable options depending on the functionalities of the catalyst. Silica is likely the most frequently used solid support due to its availability and straightforward functionalisation. Other materials, like MNPs, offer better separation which is one of the main advantages of immobilisation. In terms of efficiency, supported catalysts often have lower TONs due to lowered diffusion speed but nevertheless can in many cases compete with their homogeneous counterparts.

2. Motivation and Aim

This part of the thesis is aiming towards the immobilisation of the biomimetic iron(IV)-oxido complex C-4 (Figure IV.3). As was previously shown by our group, the complex C4 can mimic the stepwise oxidation of 5mC by TET enzymes.^[90] However, during the reactions performed with this biomimetic complex, two difficulties were observed, complicating the process of performing oxidation reactions.

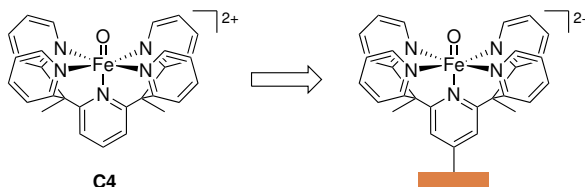


Figure IV.3.: Immobilisation of iron(IV)-oxido complex C4 on a solid support.

First, the iron(IV)-oxido complex can undergo side reactions once the iron(II) species is formed as the comproportionation of both species forming the iron(III) complex is a rapid process.^[211] Second, the removal of the complex from solution needs improving as the currently applied filtration over amorphous silica does work, but in some cases dissolved silica complicates quantification and can precipitate in analytical instruments. The immobilisation of the complex C4 onto a solid support could generate enough rigidity in the system to avoid comproportionation between complexes as well as facilitate the removal of the complex from solution. As described in the previous section, several solid support materials and techniques could be applied. Although bio-polymers are generally used for enzymes rather than catalysts, the complex C4 is designed for the use under biomimetic conditions. Therefore, chitosan was investigated as a solid support material as it is compatible with physiological conditions and a suitable derivative of the ligand systems (L1-NH₂) had already been synthesized within the group. Additionally, the synthesis of ligand derivatives with other functionalities could help widen the scope of possible immobilisation reactions. As an alternative, the immobilisation on hexagonal mesoporous silica *via* functionalisation and subsequent covalent binding was investigated as this is the commonly used approach for catalyst immobilisation (*vide supra*).

As a general concept, the immobilisation was approached in a stepwise manner by first immobilising the ligand before forming the iron(II) species, which could ultimately be oxidised the immobilised iron(IV)-oxido species.

3. Synthesis of Ligands and Complexes for Immobilisation

3.1. Synthesis of Functionalised Ligands

As described in various papers by our group,^[90,91,122,211,212] we are predominantly working with a Py₅-Ligand system (based on five coordinating pyridines) first introduced by Chang,^[213] which is able to form relatively stable iron(IV)-oxido complexes. The parent ligand L1 is shown in Figure IV.4B. To make this ligand system and the corresponding iron complexes suitable for covalent immobilisation, functionalisation of the ligand backbone is needed. The ligands L1-NH₂ and L1-OH (see Figure IV.4A) were previously synthesized by Niko Lindlar (né Jonasson)^[124] according to literature procedure.^[89,213] In this work, the syntheses of these ligands were adapted and optimized. In addition, two new ligands L1-Cl and L1-N₃ were synthesized to widen the scope of possible linking reactions and the functional groups that can be targeted on a solid support. An overview of the intended covalent linking reactions is depicted in Figure IV.4C. While the ligands L1-OH and L1-Cl could be immobilised by nucleophilic substitution, the ligand L1-NH₂ was tested towards immobilisation *via* Schiff base formation. The aza-ligand L1-N₃ was used in test reactions towards linking by click chemistry (*vide infra*).

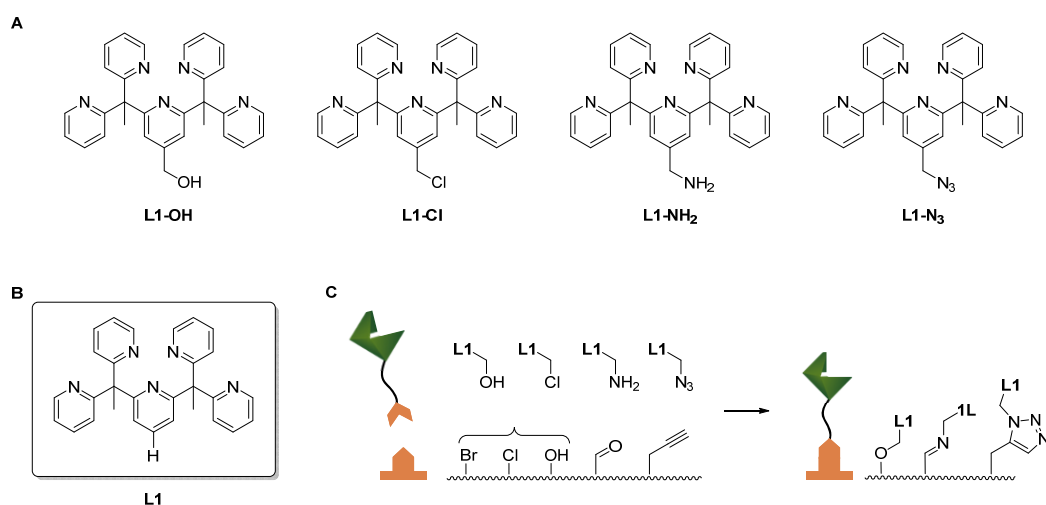
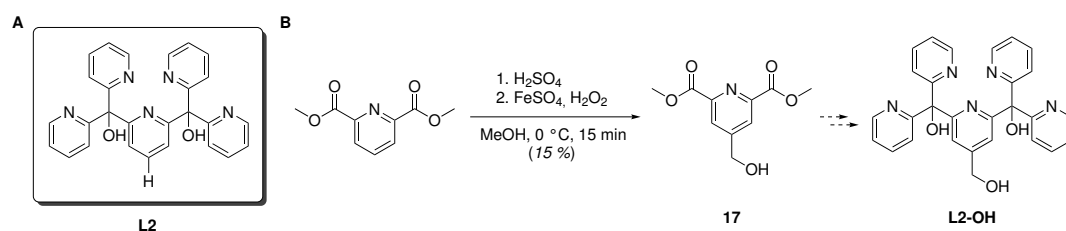


Figure IV.4.: A) Library of *para*-functionalised ligands synthesized for immobilisation applications. The L1-X type ligands were derived from the structure and synthesis of B) Parent ligand L1. C) General overview of intended covalent linking reactions of the L1-X type ligands on a functionalised solid support *via* nucleophilic substitution, Schiff base formation or click chemistry.

It was attempted to synthesize additional L2-X type derivatives in which the methyl groups in the ligand backbone are exchanged for hydroxy groups (Scheme IV.1A) as the additional functional groups could be used for immobilisation and might also display different properties than complexes formed with L1-X type ligands once immobilised.^[211] The general procedure includes the suspension of 2,6-dimethoxycarbonylpyridine in a mixture of sulfuric acid (30 %) and methanol and subsequent addition of hydrogen peroxide (30 %) and a solution of ferrous sulfate with temperatures below 30 °C. The literature states a dropwise addition of the hydrogen peroxide and ferrous sulfate solution, but it is

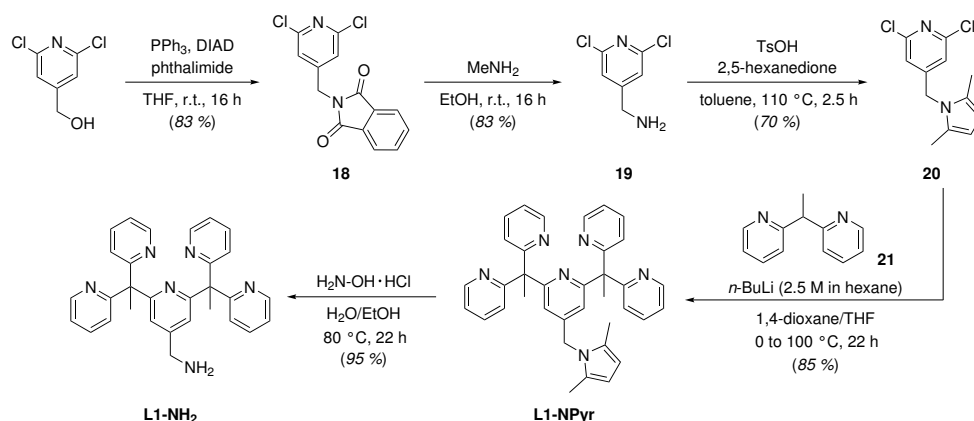
not specified in detail whether this was done successively or simultaneously and if the addition was slow or fast.^[214–216] Therefore, the initial Fenton reaction needed to introduce the axial functionality was tested for adequate reaction conditions (see Chapter VII.4). Unfortunately, this did not result in yields higher than 15 % for **17** (Scheme IV.1B) and proved to not be reproducible under the tested conditions. The following reaction steps were planned to be performed according to literature procedure.^[211,217] Although this synthesis was not pursued further in this work, experiments towards L2-X type ligands will be conducted by Doreen Reuter to be used in immobilisation of pyrene bearing ligand systems on multi-walled carbon nanotubes (MWCNTs).



Scheme IV.1: A) Ligand L2.^[211,217] B) First step of the attempted synthesis towards L2-OH which was not further pursued in this work due to poor reaction outcomes.

3.1.1. Synthesis of L1-NH₂

The ligand L1-NH₂ was obtained in a five-step synthesis starting from (2,6-dichloropyridin-4-yl)methanol (Scheme IV.2) according to a procedure previously performed within the group.^[124] The desired amine function was obtained by converting the alcohol in (2,6-dichloropyridin-4-yl)methanol *via* a Mitsunobu type reaction using triphenylphosphine, diisopropyl azodicarboxylate (DIAD) and phthalimide yielding **18** in 83 % yield. Subsequently, methylamine was used in a Gabriel type synthesis to form **19** in similar yield.

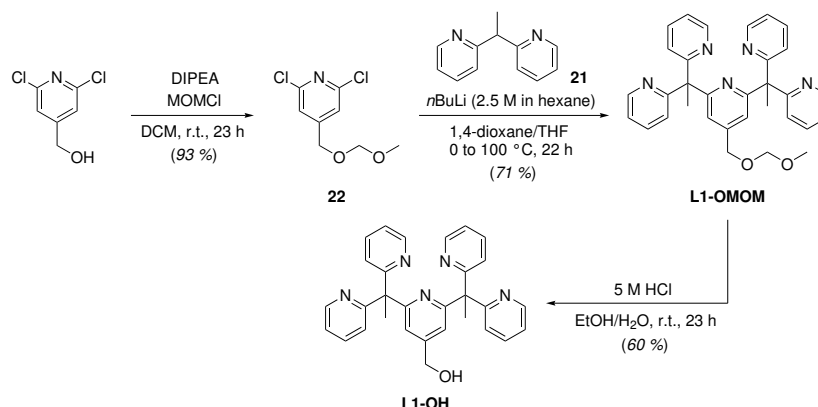


Scheme IV.2: Five step synthesis towards L1-NH₂ starting from (2,6-dichloropyridin-4-yl)methanol. The starting material was converted by a Mitsunobu type reaction using triphenylphosphine, diisopropyl azodicarboxylate (DIAD) followed by a Gabriel type synthesis to form **19**. The amine **19** was protected by a Paal-Knorr Pyrrole Synthesis to form **20** and subsequently reacted with **21** to form L1-NPyr. After deprotection using hydroxylamine hydrochloride L1-NH₂ was obtained in an overall yield of 39 %.

The following steps were performed according to a literature procedure.^[89] The amino function was protected by a Paal-Knorr Pyrrole Synthesis using 2,5-hexanedione and *para*-toluenesulfonic acid resulting in **20** in 70 % yield. With the general procedure used for L1 and L1-X type ligands L1-NPyr was synthesized in 85 % yield by reaction with **21** and *n*-butyl lithium. Finally, L1-NH₂ was obtained by reacting L1-NPyr with hydroxylamine hydrochloride in an overall yield of 39 % over five steps.

3.1.2. Synthesis of L1-OH

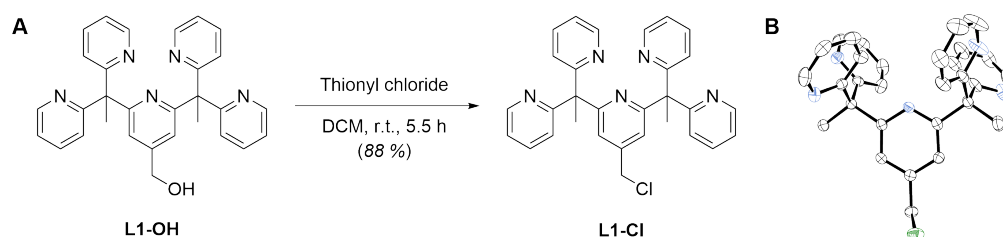
The ligand L1-OH was in general synthesized in a three-step synthesis starting from (2,6-dichloropyridin-4-yl)methanol (Scheme IV.3) according to a procedure previously performed within the group.^[124] Initial protection of the *para*-positioned alcohol function using chloromethyl methyl ether (MOMCl) and *N,N*-diisopropylethylamine (DIPEA) as a base resulted in **22** in 93 % yield. The subsequent reaction of **22** and **21** with *n*-butyl lithium was previously performed over the course of 60 h. However, when this reaction was performed and closely monitored by Tobias Walter during his internship using TLC and GC-MS, it was found that the product is formed faster than anticipated and decomposes over time. Although the synthesis was performed within the group before, this was done as a part of training the student in good research data management (see I) and thereby emphasized that a new reaction should always be monitored and this information should be added to the reaction details as the outcome of a reaction can differ from literature procedures due to different circumstances. In general, reproducing literature procedures can help a student or scientist understand which information are necessary to successfully recreate a synthesis and find access to the research field they are embarking upon.^[218] As a result, by adaptation of the reaction time the yield of L1-OMOM could be improved from 26 % to 71 %. The following deprotection of L1-OMOM using hydrochloric acid resulted in the ligand L1-OH in 60 % yield.



Scheme IV.3: Three step synthesis towards L1-OH starting from (2,6-dichloropyridin-4-yl)methanol. The starting material was protected using chloromethyl methyl ether (MOMCl) forming **22** and subsequently reacted with **21** to form L1-OMOM. After deprotection using hydrochloric acid L1-OH was obtained in an overall yield of 40 %.

3.1.3. Synthesis of L1-Cl

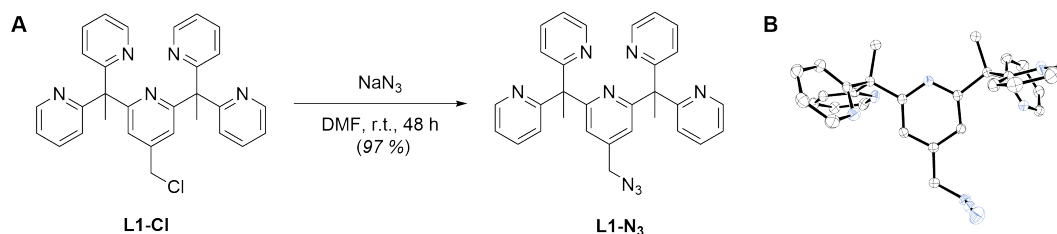
From the previously synthesized ligand L1-OH, a new ligand L1-Cl bearing a chloride at the axial position could be obtained. This was achieved by reacting L1-OH with thionyl chloride at ambient temperature for 5.5 h (Scheme IV.4A) resulting in L1-Cl in 88 % yield *via* a facile chlorination of L1-OH. After washing with saturated aqueous sodium hydrogen carbonate and drying over magnesium sulfate, the solvent was removed *in vacuo* and the ligand L1-Cl crystallized overnight. The obtained crystals were analysed by single crystal X-ray crystallography (Scheme IV.4B). Detailed crystallographic data can be found in the Appendix (Chapter VII7).



Scheme IV.4: A) Chlorination of L1-OH using thionyl chloride at ambient temperature resulting in L1-Cl in 88 % yield. L1-OH was previously synthesized in a three step synthesis as described in Chapter IV3.1.2. B) Graphical representations of the crystal structure of L1-Cl. Ellipsoids are drawn at 50 % probability.^[219] Elements shown in white (C), blue (N) and green (Cl); hydrogen atoms have been omitted for clarity. *Crystal Structure measured, solved and refined by Jonathan Gutenthaler-Tietze.*

3.1.4. Synthesis of L1-N₃

The ligand L1-N₃ was synthesized by simple substitution reaction. The previously synthesized ligand L1-Cl was reacted with two equivalents of sodium azide and the mixture stirred at ambient temperature (Scheme IV.5A) until full consumption of L1-Cl was indicated by LR-MS. As a side note, it is likely that the reaction was completed in quantitative yield in less than 48 h. To avoid formation of hydrazoic acid, remaining azide was quenched by addition of sodium nitrite and sulfuric acid and left in the closed fume hood for 4 h. This should be done at the least as long as the formation of nitrogen or nitrogen monoxide can be detected through forming bubbles. After removing the solvent *in vacuo* and an aqueous work-up, extraction and recrystallization, L1-N₃ was

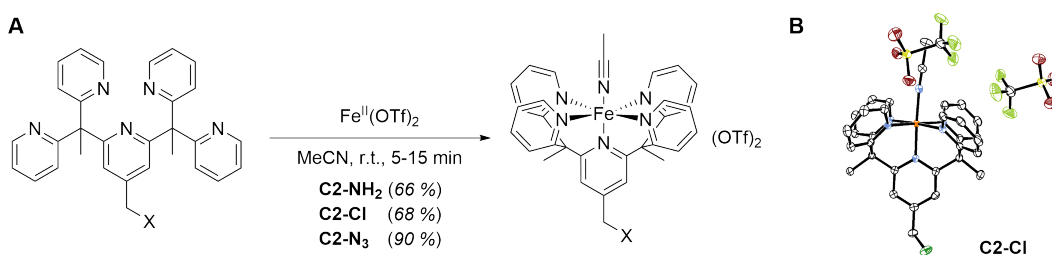


Scheme IV.5: A) Substitution of the chloride in L1-Cl using sodium azide at ambient temperature resulting in L1-N₃ in 97 % yield. L1-Cl was previously synthesized in a four step synthesis as described in Chapter IV3.1.3. B) Graphical representations of the crystal structure of L1-N₃. Ellipsoids are drawn at 50 % probability.^[219] Elements shown in white (C) and blue (N); hydrogen atoms have been omitted for clarity. *Crystal Structure measured, solved and refined by Jonathan Gutenthaler-Tietze.*

afforded in 97 % yield. The obtained crystals were analysed by single crystal X-ray crystallography (Scheme IV.5B). Detailed crystallographic data can be found in the Appendix (Chapter VII7).

3.2. Iron Complex Formation with Functionalised Ligands

In this work, four L1-X type ligands were synthesized (*vide supra*) to use their specific functional groups for immobilisation reactions. The preliminary goal was the immobilisation of the iron(II) species of these ligands (C2-X), which could then be oxidized to the labile iron(IV) species to subsequently perform oxidation reactions. This can be done either by immobilising the ligand and then adding iron to form the desired complexes C2-X or by synthesizing the complexes first and immobilising them directly. Hence, the synthesis of the iron(II) species is essential to use them either as a reference or as a substrate. The iron(II) complexes of L1-NH₂, L1-Cl and L1-N₃ were synthesized according to a previously performed procedure within the group, which was adapted by Chang *et al.*^[89,124] All complexes C2-NH₂, C2-Cl and C2-N₃ can be formed by the addition of iron(II) triflate to a solution or suspension of the respective ligand at ambient temperature (Scheme IV.6A) and subsequent precipitation by addition of diethyl ether and cooling. It is likely that the yield depends more on the completeness of the precipitation rather than the incomplete formation of the iron complexes. All complex formations are accompanied by a deep red colouring of the solution and precipitation resulted in orange powders. For C2-Cl, crystals suitable for single X-ray crystallography were obtained from a solution in acetonitrile from which the solvent was slowly evaporated at 4 °C. The resulting crystal structure is shown in Scheme IV.6B.



Scheme IV.6: A) General procedure for the formation of C2-X type complexes. The respective ligand was suspended in acetonitrile (0.1 mM) and 1.0 equivalent of iron(II) triflate is added. The resulting C2-X complex can be precipitated from the solution by addition of diethyl ether. B) Graphical representations of the crystal structure of C2-Cl. Ellipsoids are drawn at 50 % probability.^[219] Elements shown in white (C), blue (N), dark red (O), green (Cl), light green (F), yellow (S) and orange (Fe); hydrogen atoms have been omitted for clarity. *Crystal Structure measured, solved and refined by Jonathan Gutenthaler-Tietze.*

To gain clearer insight on the formation of the complexes and their spectroscopic properties, a UV-Vis titration experiment shown in Figure IV.5 was performed. For each ligand, a 0.1 mM solution in acetonitrile was prepared and an iron(II) triflate solution was added stepwise. With each addition 0.1 equiv. of iron(II) were added and the solution stirred for approximately 45 s before measurement to allow complex formation. The concentration of the iron triflate solution was adapted so that the addition could be

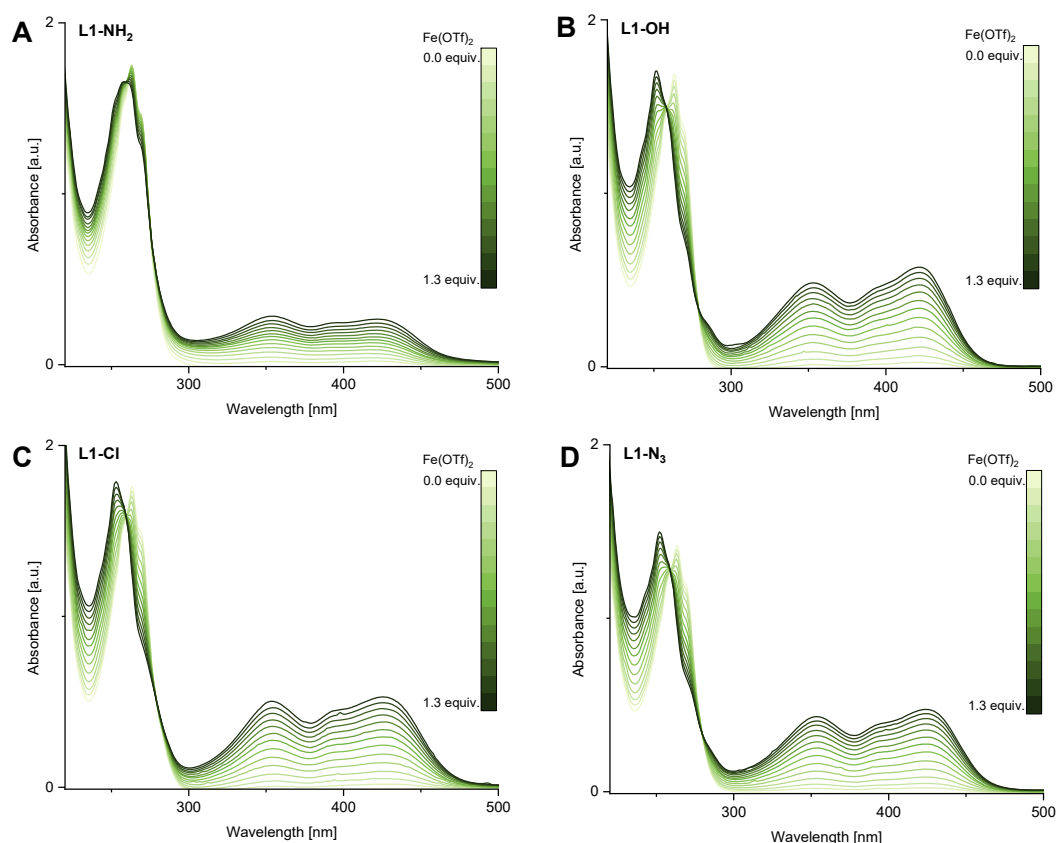


Figure IV.5.: UV-Vis spectra of the functionalised ligands L1-NH₂, L1-OH, L1-Cl and L1-N₃. The measurements show a solution of the respective ligand (0.1 mM in acetonitrile) and the resulting spectra from stepwise addition of a iron(II) triflate solution (0.1 equiv., 4 μ L per step). The mixture in the cuvette was stirred for 45 s after addition and prior to measurement. The spectra show the formation of the C2-X complexes of each ligand. Measurements were performed at 25 $^{\circ}$ C.

performed with small volumes (4 μ L for 0.1 equiv.) in relation to the full volume within the UV-Vis cuvette (2 mL) to avoid dilution effects on the spectra. Although none of the spectra display complete saturation after addition of one equivalent of iron, this is likely attributed to the short reaction time and is expected. As can be seen in Figure IV.5A-D, each ligand spectrum displays a significant shift around 260 nm and the rise of two broad new bands in the region between 300–450 nm. Similar absorption bands occurring in comparable iron(II) systems in the literature are attributed to metal-to-ligand charge transfer bands.^[220] All maxima and the isosbestic point of each complex formation are listed in Table IV.2.

While the maxima of all complexes show no significant deviation, it is noteworthy that the spectra of the formation of C2-NH₂ differ significantly from the other tested systems. In difference to the shift of the absorption maximum around 260 nm with a clear isosbestic point, the shift is less prominent and accompanied by a lowered absorbance. The general absorbance in the region from 300–450 nm is also lower indicating a smaller extinction coefficient for C2-NH₂ or significantly slower formation of the complex. When UV-

Table IV.2.: UV-Vis maxima observed for L1-X type ligands and C2-X type complexes. Maxima were extracted from measurements of the dissolved species in acetonitrile at 25 °C (see Figure IV.5 and Figure IV.6) while the isosbestic points of the iron(II) complex formations of the respective ligands were derived from the titration experiment shown in Figure IV.5.

Complex	Maxima			Isosbestic point
L1-NH ₂	263 nm	-	-	260 nm
C2-NH ₂	252 nm	353 nm	421 nm	
L1-OH	263 nm	-	-	259 nm
C2-OH	252 nm	353 nm	422 nm	
L1-Cl	263 nm	-	-	260 nm
C2-Cl	253 nm	353 nm	425 nm	
L1-N ₃	263 nm	-	-	259 nm
C2-N ₃	252 nm	354 nm	424 nm	

Vis measurements of the C2-X type complexes were performed from solutions of the previously formed complex (Figure IV.6A) at the same concentrations, these differences were not observed. As there are also no extensive deviations in the measured IR spectra (Figure IV.6B), it can be concluded that the differences in complex formation in the titration experiment stem from a slower complex formation when the ligand L1-NH₂ is used. This should be accounted for in later iron(II) complex formations of immobilised species.

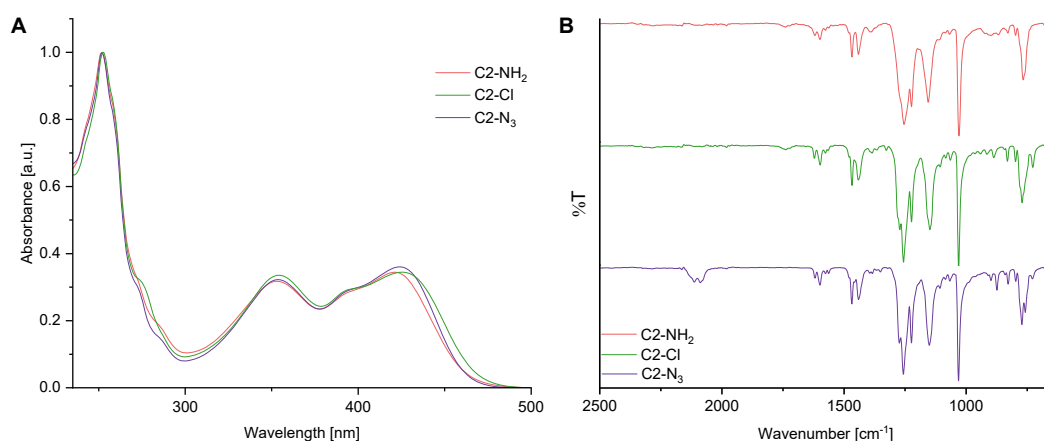
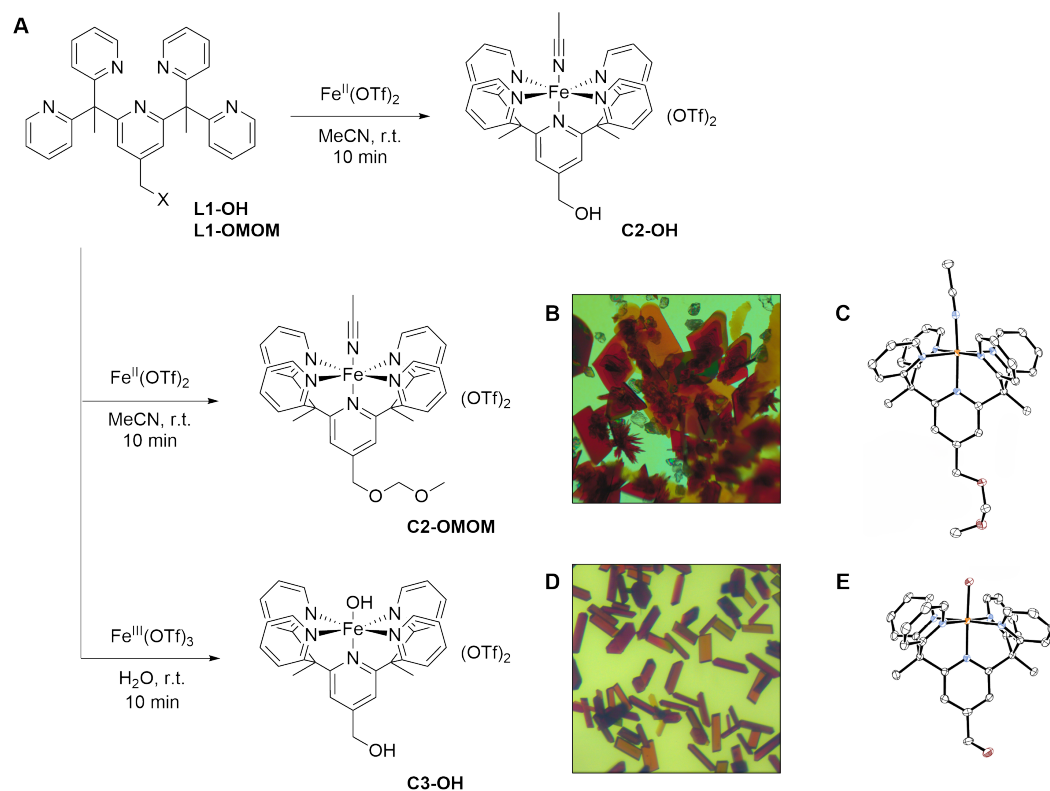


Figure IV.6.: A) UV-Vis spectra of C2-X type iron(II) complexes. Complexes were synthesized according to the experimental procedure and dissolved in acetonitrile and diluted (0.1 mM) for measurements. Measurements were performed at 25 °C. Spectra were normalized for better comparability. B) IR spectra of C2-X type iron(II) complexes.

3.2.1. Iron Complexes of L1-OH

The ligand L1-OH has been previously characterised within our group, when it was used in investigations towards immobilisation of the Py₅ ligand system on TentaGel resin by Niko Lindlar (né Jonasson).^[124] As the approach using TentaGel resin was not further pursued and other solid state materials were used in this work, the ligand L1-OH was mainly a precursor for new ligand systems (*vide supra*). However, within the scope of the internship of Tobias Walter, the iron(II) complexes C2-OH and C2-OMOM, as well as the iron(III) complex C3-OH were synthesized according to literature^[124] (Scheme IV.7A) as references for other complexes (e.g. C2-Cl) derived from this structure. In case of C2-OMOM, crystals suitable for X-ray crystallography (Scheme IV.7B) were obtained by slow diffusion of diethyl ether into the solution at ambient temperature. In addition, C3-OH was crystallized from solution at 4 °C (Scheme IV.7D) and both were characterized by single crystal X-ray diffraction analysis (Scheme IV.7C and E). Details on the crystal structure measurements can be found in the Appendix (Chapter VII7, Chapter VII7).



Scheme IV.7: A) Synthesis of the iron complexes C2-OH, C2-OMOM and C3-OH from L1-OH and L1-OMOM by addition of the respective iron triflate to a solutions of the ligands. B) Crystals of C2-OMOM obtained by diffusion of diethyl ether into the product solution at room temperature. *Picture by Jonathan Gutenthaler-Tietze* C) Graphical representations of the crystal structure of [Fe^{II}(MeCN)(L1-OMOM)](OTf)₂ (C2-OMOM). Ellipsoids are drawn at 50 % probability.^[219] Elements shown in white (C), blue (N), dark red (O) and orange (Fe); hydrogen atoms, counterions and co crystallizing solvents have been omitted for clarity. *Crystal Structure measured, solved and refined by Jonathan Gutenthaler-Tietze*. D) Crystals of C3-OH formed in the product solution at 4 °C. *Picture by Jonathan Gutenthaler-Tietze* E) Graphical representations of the crystal structure of [Fe^{III}(OH)(L1-OH)](OTf)₂ (C3-OH). Ellipsoids are drawn at 50 % probability.^[219] Elements shown in white (C), blue (N), dark red (O) and orange (Fe); hydrogen atoms, counterions and co crystallizing solvents have been omitted for clarity. *Crystal Structure measured, solved and refined by Dr. Peter Mayer*.

4. Towards a Functioning Solid Support System

4.1. Chitosan Gel Beads

Chitosan is derived from chitin, a very abundant biopolymer, which can for example be extracted from the exoskeletons of crustaceans.^[221] Chitin consists of acetylglucosamine units wherein all amino functions bear an acetyl group. Chitosan is produced *via* deacetylation of chitin and is the general name for all deacetylation grades of chitin. Both structures are shown in Figure IV.7. Chitosan was chosen as a solid-phase medium for its bioavailability as a regrowing resource, which makes it a green alternative to synthesized matrices, as well as its stability and insolubility in water, at least at $\text{pH} \geq 7$. For this project, a chitosan powder obtained from shrimp shells with $\geq 75\%$ deacetylation was used.

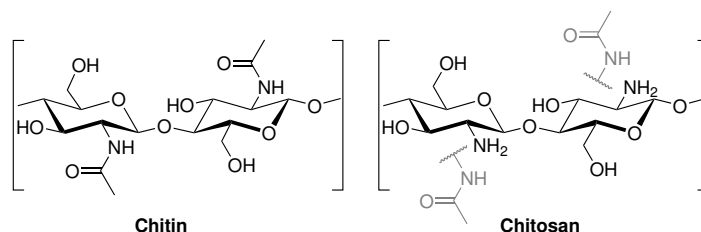


Figure IV.7.: Comparison of the naturally occurring acetylglucosamine polymer chitin and the deacetylated derivative chitosan. Chitosan is a general name for various grades of deacetylation in chitin and therefore an undefined mixture of acetylglucosamine and glucosamine units.

It should be kept in mind that although chitosan will be shown with free amino groups in the following, due to incomplete deacetylation not all amino groups are available for coupling of linkers or ligands. Additionally, the grade of deacetylation ($\geq 75\%$) is not a precise value and can vary within the material which makes it difficult to give exact loading numbers when coupling at this position. However, calculations can be made by estimating the molar mass with 25 % acetylated amino functions.

4.1.1. Formation of Uniform Gel Beads

In order to use chitosan as a solid-phase medium for immobilisation, chitosan can be obtained as flakes or transformed into gel beads, fibers or membranes.^[164,221–223] Since one of the goals of the projects is the facile removal of the immobilised iron complex from solution, it was intended to use chitosan gel beads which can be removed easily and quickly by filtration because of their size (*vide infra*). The gel bead formation described in the following was in great extent tested and established during the internship of Tobias Walter who contributed significantly to this part of the project.

In reported procedures,^[224,225] an acidic solution of chitosan is dropped into a basic bath wherein immediate polymerisation occurs causing the droplets to gel in their current shape. It was desired to implement a procedure which results in uniform shaped beads

to minimize differences between batches. Unfortunately, the literature procedure did not include all necessary details but hinted that elements like the viscosity and dropping height have an impact on the shape. Thus, we tested chitosan solutions ranging from 1.5 % to 3 % (w/v) in 1.5 % acetic acid and dropped them into a constantly stirred 1 M solution of potassium hydroxide (25 % ethanol in ultrapure water) using different syringes, cannulas and dropping heights. The general setup is shown in Figure IV.8A.

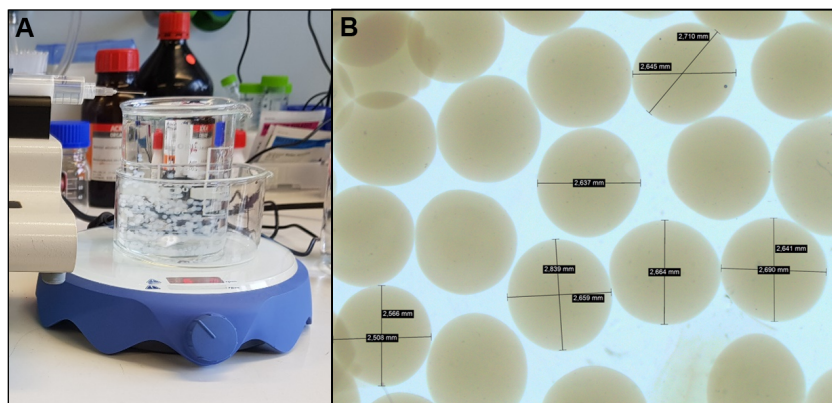


Figure IV.8.: A) Setup for the formation of uniform spherical chitosan gel beads from a prepared viscous solution in diluted acetic acid (1.5 %). The gel is dropped at into a constantly stirred solution of potassium hydroxide (1 M, 25 % ethanol in ultrapure water) at constant speed and dropping height using a syringe pump. B) Microscope picture of the formed and ripened chitosan gel beads ($\varnothing = 2.5\text{--}2.8\text{ mm}$) including measurements showing the uniformity of the beads. *Picture by Jonathan Gutenthaler-Tietze*

It was found that the dissolution of the chitosan powder in acetic acid has to be performed very slowly and the powder has to be finely dispersed on the surface of the acid while stirring so vigorously that a vortex is formed. If the powder is added in bulks, the outer surface forms a gel and the inner part is kept dry and will not dissolve. Remaining solid particles and bubbles can be removed by centrifugation. It was attempted to use syringe filters (0.45 μm) but the viscous gel repeatedly clogged the filters and was generally hard to press through. The gel can be transferred to a syringe by carefully taking it up or decanting it into the opened back without creating air inclusions. The filled luer lock syringe was equipped with a cannula and clamped into a syringe pump. Different cannulas with diameters of 0.4 mm, 0.8 mm and 0.9 mm were tested. The droplets produced by the cannula should be as small as possible, as a high surface to volume ratio is preferable when using the surface as your target area. However, it should be kept in mind that a highly viscous gel is pumped through this cannula possibly leading to the build up of pressure within the syringe which could cause the system to break apart. Starting from a high diameter of the cannula and slow pumping speed to avoid pressure build-up, it was ultimately found that a cannula with a diameter of 0.4 mm at a pumping speed of 20 mL/h resulted in uniform beads ($\varnothing = 2.5\text{--}2.8\text{ mm}$, Figure IV.8B) without problems regarding the pressure. This was tested with syringes of 10-12 mL and 20-24 mL volumes.

While the cannula and pumping speed have an influence on the size of the beads, the shape is influenced mostly by the dropping height. If the dropping height is $< 1\text{ cm}$ or the

droplets immediately contact the surface, they will obtain a teardrop shape. At dropping heights ≥ 2 cm the resulting beads have a disk-like shape due to the impact on the surface. Although the shape of the beads does not necessarily effect the immobilisation, in terms of reproducibility it was desired to accomplish as much uniformity as possible. Here, it was found that a dropping height of 1.0-1.5 cm (tip of the cannula to surface) resulted in uniform spherical beads (Figure IV.8B). Additionally, depending on the amount of produced beads, the surface level of the base can increase enough to result in bead shape variations. To circumvent this, the beaker or glass bottle in which the beads were collected was always filled completely and placed in a crystallisation dish to collect overflowing liquid. To avoid aggregation of beads, the basic solution was stirred constantly during the process.

After the process of forming the beads, they were ripened in the potassium hydroxide solution for 2-3 h to allow complete polymerisation. During this process, the clear gel turns into opaque beads. After ripening the beads were filtered off and washed with water multiple times. However, as it was unclear how permeable the beads surface is and how well the inside of the beads exchanges with the outside solution, this was tested using a pH indicator within the gel beads to visualize the inner spheres pH.

Hence, a small spatula phenolphthalein was added to the acetic acid used to dissolve the chitosan powder and form the chitosan gel. The chitosan gel beads were then formed according to the general procedure (*vide supra*). As can be seen in Figure IV.9, the beads turned bright pink upon dropping into the potassium hydroxide solution within seconds indicating exchange between the gel and outer solution. During the ripening process, the colouring decreased which is due to the indicator phenolphthalein losing colour in a pH >12 . The pH measured in the basic solution was 14 but as this was not a purely aqueous system the pH is not precise. Nevertheless, the experiment showed that the beads are sufficiently permeable to adapt the pH of the outer solution, although this is not an immediate process. Due to this, the washing process after ripening was extended. In addition to washing the beads after filtration, the beads were submerged in ultrapure water and put on a laboratory shaker for 10-15 min. This process was performed twice as the first washing solution had a pH of 14 while the second had a neutral pH.

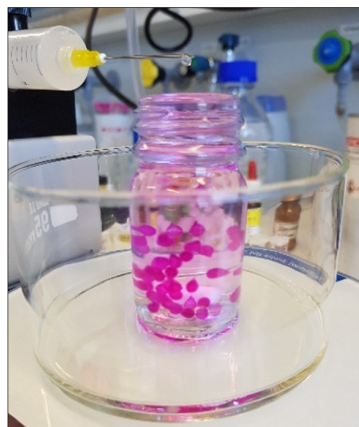
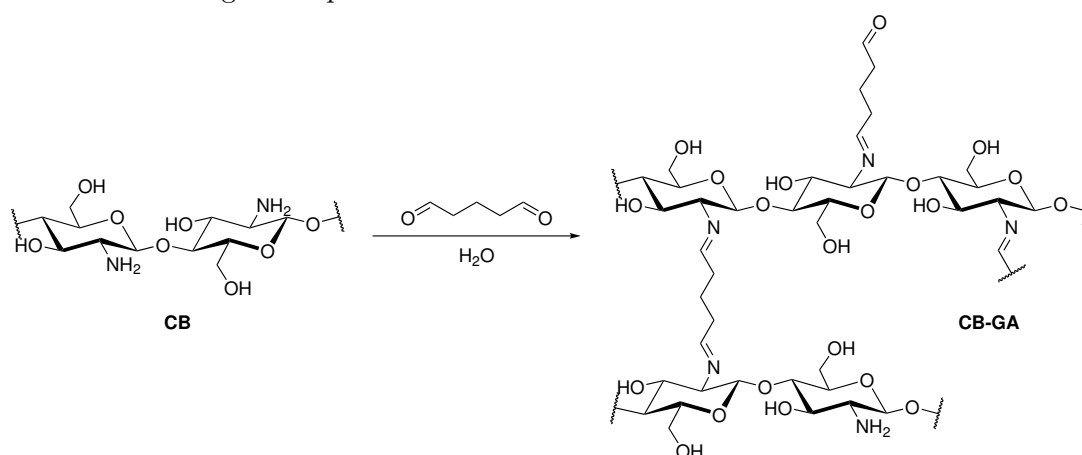


Figure IV.9.: Formation of chitosan beads with added pH indicator (phenolphthalein) in the chitosan gel.

In summary, after testing and adapting several factors of the process, a reproducible procedure for the formation of uniform chitosan gel beads (CB) was accomplished.

4.1.2. Functionalisation of Chitosan Gel Beads: Glutaraldehyde Crosslinking

The previously synthesized uniform chitosan gel beads already include functional groups which could be used for immobilisation due to structure of the glucosamine units (Figure IV.7). Nonetheless, the adapted literature procedure^[225] describes a modification of the chitosan gel beads (CB) by reaction with glutaraldehyde (GA) wherein the aldehyde moieties in glutaraldehyde is reacted with the amino functions of chitosan *via* a Schiff base reaction leaving free aldehyde endings at the surface (Scheme IV.8). In addition, the treatment with glutaraldehyde results in crosslinking between the chitosan monomers and polymer chains which increases stability and decreases the solubility in water.^[224,226] Because of this additional stabilisation and the simple reaction conditions, the CBs were modified according to his procedure.



Scheme IV.8: General scheme of the modification of chitosan gel beads (CB) with glutaraldehyde *via* Schiff base formation.^[225] The reaction results in randomized crosslinking between monomers or polymer chains and free aldehyde functions. These modified chitosan beads with glutaraldehyde are abbreviated as CB-GA.

The modification of the chitosan beads with glutaraldehyde was performed using a stock solution of glutaraldehyde which is diluted with ultrapure water. Two different stock solutions have been used, one with 25 % and one with 50 % glutaraldehyde. In general, the 50 % stock solution seems more advantageous since a smaller amount has to be stored and can be diluted when needed for reaction. But as we suspected that the higher concentrated glutaraldehyde solution might be prone to undergo polymerisation, both solutions were tested, but no difference in the performed reactions to due the used glutaraldehyde solutions could be observed. To check whether and how fast the glutaraldehyde reacts with the formed beads, the following experiment was set up. Approximately 20 beads were put in a centrifuge tube and 4 mL of ultrapure water containing 6.25 wt% glutaraldehyde were added. The falcon was put in an orbital shaker set on 30 °C. A 10 μ L aliquot of the glutaraldehyde solution was taken regularly, diluted with acetonitrile (1:10), filtered (syringe filter, 0.25 μ m) and measured using GC-MS. The resulting spectra are shown in Figure IV.10. The spectra display a significant decrease in glutaraldehyde concentration after 15 min and no further change after 60 min. It should be taken into account that the initial decrease in concentration could be due to exchange of the inner sphere of the

CBs with the solution diluting the glutaraldehyde solution without reaction. However, the additional decrease in concentration between the 15 min and 60 min measurement is likely attributed to the reaction of glutaraldehyde with the CBs.

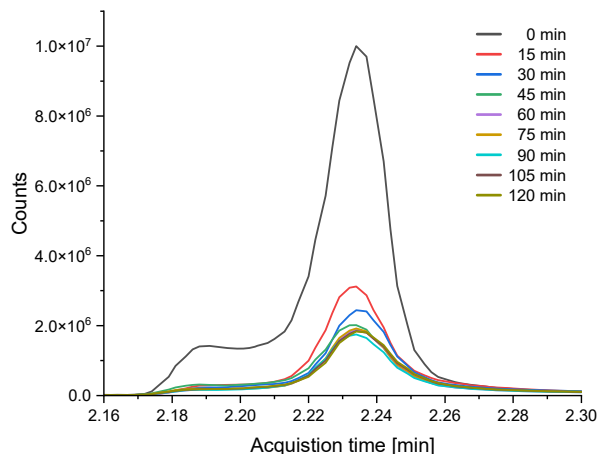


Figure IV.10.: GC-MS traces of glutaraldehyde solution. CBs were submerged into a glutaraldehyde solution (6.25 wt%) and shaken at 30 °C. Aliquots of the glutaraldehyde solution (10 μ L) were taken regularly, diluted with acetonitrile (1:10) and filtered (syringe filter, 0.25 μ m) prior to GC-MS measurements. Column: HP-5ms Ultra Inert, Injection Temp.: 150 °C, Split: 1:100, Oven Temp.: 100 °C (constant-temperature), Runtime: 5 min. Mass spectrum in very good alignment (95 %) with the NIST 2.4 database.

For the following reactions the beads were analysed by IR spectroscopy since most analytical methods are not applicable for the insoluble beads. For all IR measurements, if not stated otherwise, CBs were submerged in water, frozen using liquid nitrogen and then freeze dried by lyophilisation. If the CBs are not frozen in water and freeze dried they will shrink to a very small, hard sphere approximately the size of a needle hat, which are cumbersome to pulverize for measurement. If freeze dried in water, the CBs keep their original size and shape forming brittle, easily pulverized spheres.

Figure IV.11A shows the IR spectra of the used chitosan powder compared to a CB (synthesized and dried according to described procedure, *vide supra*) and in Figure IV.11B different performed reactions of CBs with glutaraldehyde (GA) in comparison to the pure CBs are displayed. Glutaraldehyde modified chitosan gel beads (CB-GAs) were synthesized according to the general procedure (Scheme IV.8) by submerging CBs in a mixture of 6.25 wt% glutaraldehyde in ultrapure water in a Schott glass bottle at ambient temperature and subsequent shaking using a laboratory shaker. The spectra in Figure IV.11B are derived from experiments of different students which indicates that the measurements are reproducible. Unfortunately, the spectra are not in line with the literature^[225] and also show no significant difference between the crosslinked CB-GAs and unmodified CBs. A new band appeared around 1714 cm^{-1} which could be attributed to the C=O stretch of free aldehyde functions.^[227] In addition, a shift of the band around 2931 cm^{-1} in the C-H stretch region is observed, which might stem from free aldehyde functions or the glutaraldehyde in general. The changes in the IR spectra display similar

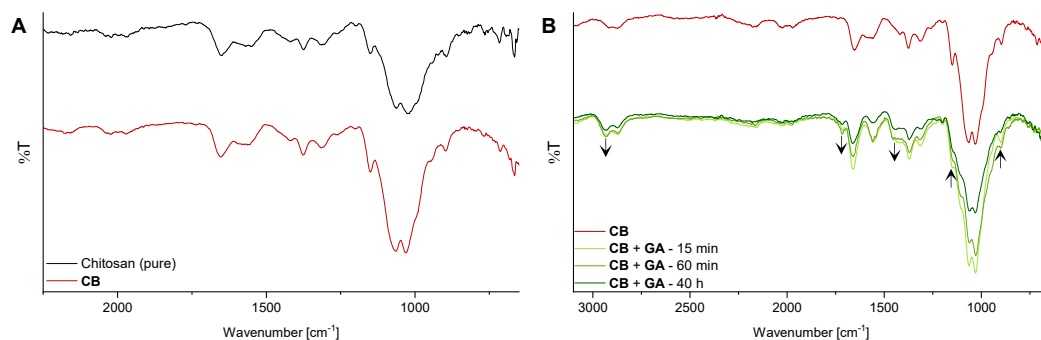
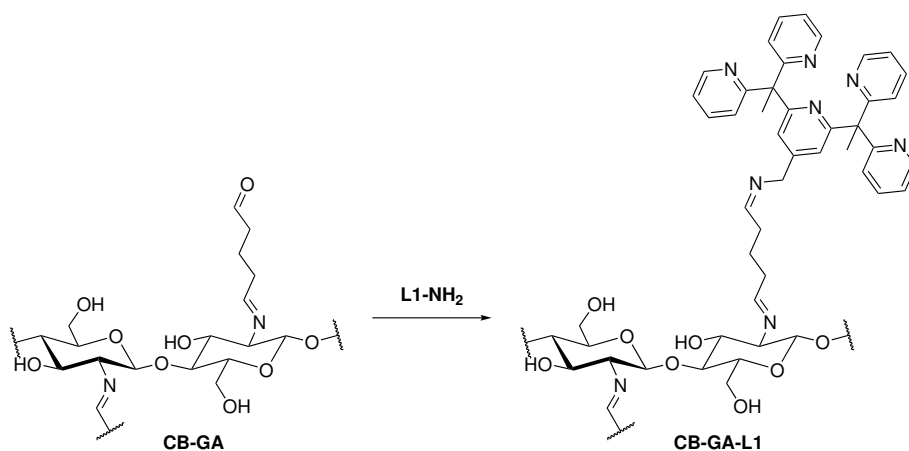


Figure IV.11.: A) Compared IR spectra of chitosan powder ($\geq 75\%$ deacetylated) and synthesized and freeze dried chitosan gel beads (CB). B) Compared IR spectra of pure chitosan gel beads (CB) and reactions of the CBs with glutaraldehyde over different reaction times. Arrows indicate bands that shift or appear ($\nu = 2931\text{ cm}^{-1}$, 1714 cm^{-1} , 1444 cm^{-1}) or change shape or intensity ($\nu = 1149\text{ cm}^{-1}$, 897 cm^{-1}). The shown spectra were baseline corrected and smoothed using the Spectra Manager Version 2 software.

changes as were observed in other literature procedures.^[228,229] Due to this, the results of the GC-MS measurements (Figure IV.10) and obvious changes of the texture of the gel beads, which turned more brittle and broke more easily, the longer they were reacted with glutaraldehyde, it was anticipated that to some extent reaction between the CBs and glutaraldehyde occurred. Therefore, the glutaraldehyde modified chitosan gel beads (CB-GAs) were synthesized as described and used as such in following experiments.

4.2. Immobilisation of L1-NH₂ on Functionalised Chitosan Beads (CB-GAs)

The previously prepared functionalised chitosan beads (CB-GA) were used for the immobilisation of L1-X type ligands according to Scheme IV.9. As the schemes shows, the general concept was to immobilise the amino derivative of ligand L1 (L1-NH₂) by a Schiff base formation with the free aldehyde functions of the CB-GAs.



Scheme IV.9: General scheme of the immobilisation of L1-NH₂ on a functionalised chitosan gel bead (CB-GA) via Schiff base formation between the ligand and free aldehyde resulting from glutaraldehyde functionalisation and crosslinking of the bead.

Initial experiments towards this were performed by Tobias Walter during his internship. In different setups, CB-GAs were submerged in a methanolic solution of L1-NH₂ and put into an orbital shaker. It would have been preferable to perform these reactions in an aqueous solution but the L1-NH₂ was not soluble under these conditions, which is why methanol was used as a solvent. In one setup, a solution of L1-NH₂ was prepared in a UV-Vis cuvette and three CB-GAs were added. The solution above the beads was measured immediately before fastening the sealed cuvette to an orbital shaker. The solution was shaken constantly and measured again after 17 and 41 h. The resulting spectra are shown in Figure IV.12B. As a reference, a range of different concentrations of L1-NH₂ was measured (Figure IV.12A) to use the linear correlation of concentration and absorbance for calculating the amount of ligand immobilised on the beads. Over the first 17 h a significant decrease in the absorbance of the ligands maximum at 264 nm is observed, indicating a lower ligand concentration due reaction with the insoluble CB-GAs. As no further changes appear after 41 h, the reaction appears to be completed within the first 17 h. A similar experimental setup was performed with L1-Cl to test whether the free hydroxy groups of the CB-GAs can be used for immobilisation as well. These experiments were performed in 1,4-dioxane to avoid reaction with the solvent and with addition of either sodium hydride or potassium carbonate as base. However, the spectra of these experiment were partly not evaluable and yielded no indications of successful reactions (see Appendix) and a brown discolouration of the beads. Thus, this was not investigated further.

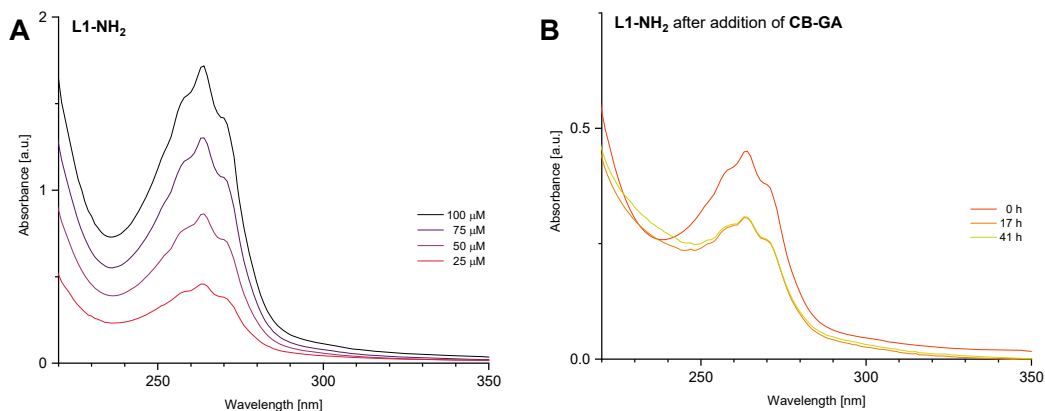


Figure IV.12.: A) Reference UV-Vis spectra of L1-NH₂ at different concentrations in methanol. B) UV-Vis measurements of a 25 μM solution of L1-NH₂ in methanol after addition of CB-GAs and after 17 h and 41 h.

In a second setup, approximately 20 CB-GAs were submerged in a methanolic solution of L1-NH₂ (5 mL, 100 μM) in a 15 mL centrifuge tube and put into an orbital shaker for 24 h at 30 °C. The beads were filtered off and washed with water five times. It should be noted, that the general procedure described in Chapter IV.4.1 was not fully developed at this point in time and these beads were washed by rinsing during which the beads were only shortly submerged and had only short contact time with the washing solution. Subsequently, the beads were freeze dried as described. These beads were then analysed

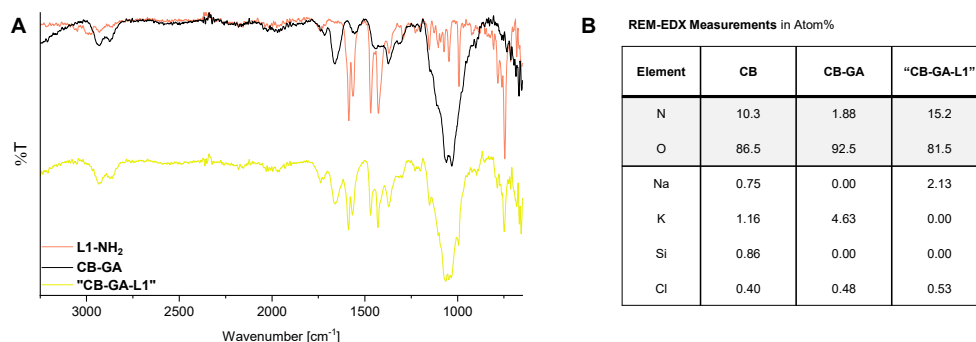


Figure IV.13.: A) IR spectra of the ligand L1-NH₂ and a chitosan bead functionalised with glutaraldehyde (CB-GA) as references compared to the reaction product of CB-GAs that were submerged in a methanolic solution of L1-NH₂ for 24 h (CB-GA-L1) at 30 °C. All beads were freeze dried before measurement. B) SEM-EDX measurement data of the surfaces of a pure chitosan bead (CB) and the functionalised bead (CB-GA) and reaction product CB-GA-L1 described in A. Carbon content could not be determined due to the fixation of the beads on a carbon surface for measurement. Some smaller impurities were omitted for clarity. Full data can be found in the Appendix (Chapter VII5). *EDX measurements were performed by Christian Minke at LMU Munich.*

by IR (Figure IV.13A) and energy dispersive X-ray (EDX) spectroscopy (Figure IV.13B). The IR spectrum of the reacted beads (Figure IV.13A, yellow) displays distinctive features of the CB-GAs at 1000-1200 cm⁻¹ as well as four bands at 1400-1600 cm⁻¹ occurring in the ligand L1-NH₂, respectively, strongly indicating the presence of both in the reaction product. In addition to this, EDX measurements were performed on the product beads as well as on previous states of the reaction. This was done for confirmation and as a proof of concept to verify if the freeze dried beads are suitable for SEM-EDX measurements as X-ray spectroscopy can be destructive towards the substrate. This type of spectroscopy would facilitate later analysis of iron content and distribution on the beads surface. The various chitosan beads proved stable enough for measurements and an excerpt of the resulting data is presented in Figure IV.13B. The measurements show that the nitrogen content on the surface of the beads decreases significantly upon reaction of the CBs with glutaraldehyde while the oxygen content increased. This is in good alignment with the expectation of free aldehyde functions emerging on the surface upon the functionalisation of the beads. Furthermore, when the CB-GAs were reacted with L1-NH₂, the nitrogen content on the surface strongly increased indicating immobilization of the pyridine bearing ligand on the surface indeed forming the expected CB-GA-L1s.

Unfortunately, we were not able to reproduce the results of this experiment. Several approaches were made to repeat and improve the reaction outcome and are described in the following. These experiments were in part performed within the internships of Henry Lauk and Bastian Michels. In the first experiments following the reaction described above, the procedure was in general kept the same, although two different batches of modified beads were used. One of the batches was reacted with glutaraldehyde for a shorter time (15 min) in order to see if an influence on the efficiency of immobilisation could be detected as longer reaction times might cause polymerisation of glutaraldehyde

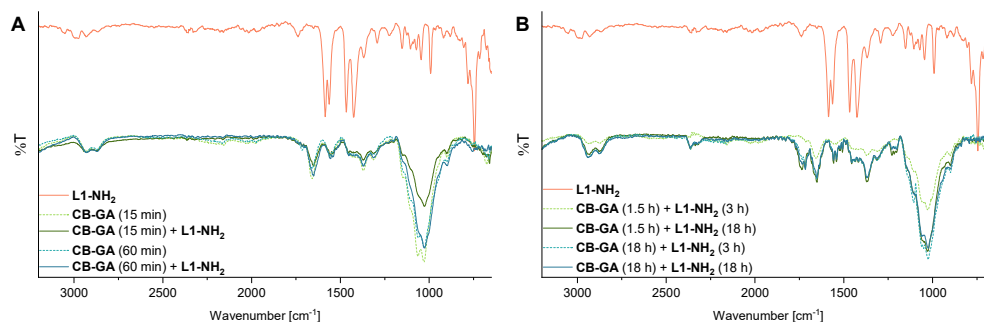


Figure IV.14.: A) IR spectra of the ligand L1-NH₂ as references compared to the reaction product of CB-GAs that were submerged in a methanolic solution of L1-NH₂ for 24 h. CBs were reacted either 15 min or 60 min to form CB-GAs prior to reaction with L1-NH₂. All beads were freeze dried before measurement. B) IR spectra of the ligand L1-NH₂ as references compared to the reaction product of CB-GAs that were submerged in a methanolic solution of L1-NH₂ for either 3 h or 18 h. CBs were reacted either 1.5 h or 18 h to form CB-GAs prior to reaction with L1-NH₂. All beads were freeze dried before measurement. *The shown spectra were baseline corrected and smoothed using the Spectra Manager Version 2 software.*

monomers or other side reactions on the surface of the beads and therefore reduce the amount of free aldehyde groups which can react with the ligand. However, as can be seen in the spectrum (Figure IV.14A), there is no indication of successfully immobilised ligand on the modified chitosan beads. At this point it was considered that dependent on the way of measurement, the ATR-IR spectrometer might not necessarily measure the surface of the beads, where the ligand might be located, since the bead is pressed to a powder prior to measurement. But even carefully scraping off parts of the surface or pressing the bead on the diamond plate directly did not result in different spectra.

Another experiment towards this is shown in Figure IV.14B, which also did not yield a sign of immobilised ligand on the beads. In this experiment longer reaction times with glutaraldehyde were used and the resulting beads were split and two different reaction times with the ligand solution were applied. We opted for an elongation of the reaction time rather than increasing temperatures since the instruments or laboratory shakers available with temperature control were applicable only for small amounts of 4-5 beads. After these experiments, the experiment regarding the pH inside the beads after ripening (Chapter IV.4.1) was performed and we considered that the washing method applied for the beads so far might have been insufficient and inconsistent and therefore, the pH within the beads could have been higher than anticipated in the initial experiments compared to later setups. Due to this, further experiments did include the washing method described in Chapter IV.4.1 during which, after washing three times in the filter, the beads are also put in fresh ultrapure water and put in a laboratory shaker to give the inside of the beads enough time to equilibrate with the outer solution. To test the possible influence of the pH and if there might have been an issue due to using a methanolic solution of the ligand and washing with water, as the poor solubility might cause insufficient washing, an additional experimental setup was performed. Here, CB-GAs from one batch were split evenly and reacted with either a methanolic or an aqueous solution of L1-NH₂. As

already mentioned, the solubility of the ligand in water is very low and treatment with an ultrasonic bath over several hours was necessary to obtain a solution. In addition to the different solvents, both reactions were duplicated and the duplicate treated with sodium hydroxide to mimic the possibly higher pH in the initial experiment (*vide supra*). The resulting IR spectra are depicted in Figure IV.15.

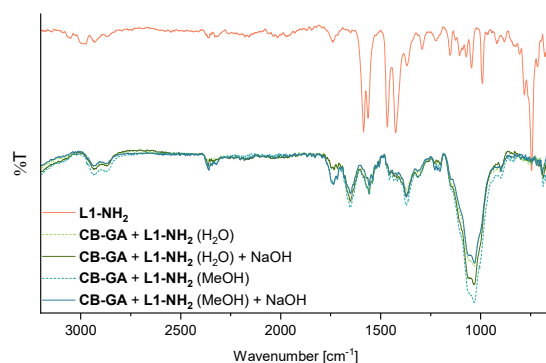


Figure IV.15.: IR spectra of the ligand L1-NH₂ as references compared to the reaction product of CB-GAs that were submerged in a methanolic or aqueous solution of L1-NH₂ for 24 h. The used solvent is indicated begin the ligand. Duplicates of the reactions were performed with added sodium hydroxide solution (2 M, 3 drops, pH 9-10) as base. All beads were freeze dried before measurement. The shown spectra were baseline corrected and smoothed using the *Spectra Manager Version 2* software.

This set of four reactions was performed with CB-GAs that were functionalised with a diluted glutaraldehyde solution stemming from 50 wt% stock solution. As mentioned earlier, we suspected that unintended polymerisation might occur in the higher concentrated stock solution. Thus, the set of reactions shown in Figure IV.15 was also performed with CB-GAs by using the 25 wt% stock solution which, however, did not result in different spectra than shown here.

The previously described experiments were performed at different times and in part by different students. In addition, adjustments and improvements were made throughout the procedures, which in some cases made comparison difficult due to the individual conditions. In an effort to analyse and compare the reaction and reduce the described issues, several experiments were performed simultaneously and from one batch of chitosan gel. In each step, slight differences were applied to be able to detect differences stemming from this part of the procedure. An overview on these experiments is shown in Figure IV.16. In a first step, two batches of chitosan beads A and B were formed from the same gel. These beads were left to ripen in the basic bath for either 10 min (A) or 1.5 h (B). Then, the beads from batch A were split evenly and all resulting batches A1, A2 and B1 were reacted with glutaraldehyde over different time frames. These fractions were each evenly split again and all six fractions were each submerged into a methanolic solution of ligand L1-NH₂ (2 mM) for 16-20 h on a laboratory shaker at ambient temperature. The fractions A1.2, A2.2 and B1.2 were filtered and washed with methanol and water according to the general procedure (Chapter IV.4.1), meaning they were rinsed and additionally submerged and put on a laboratory shaker in the washing solution at least once.

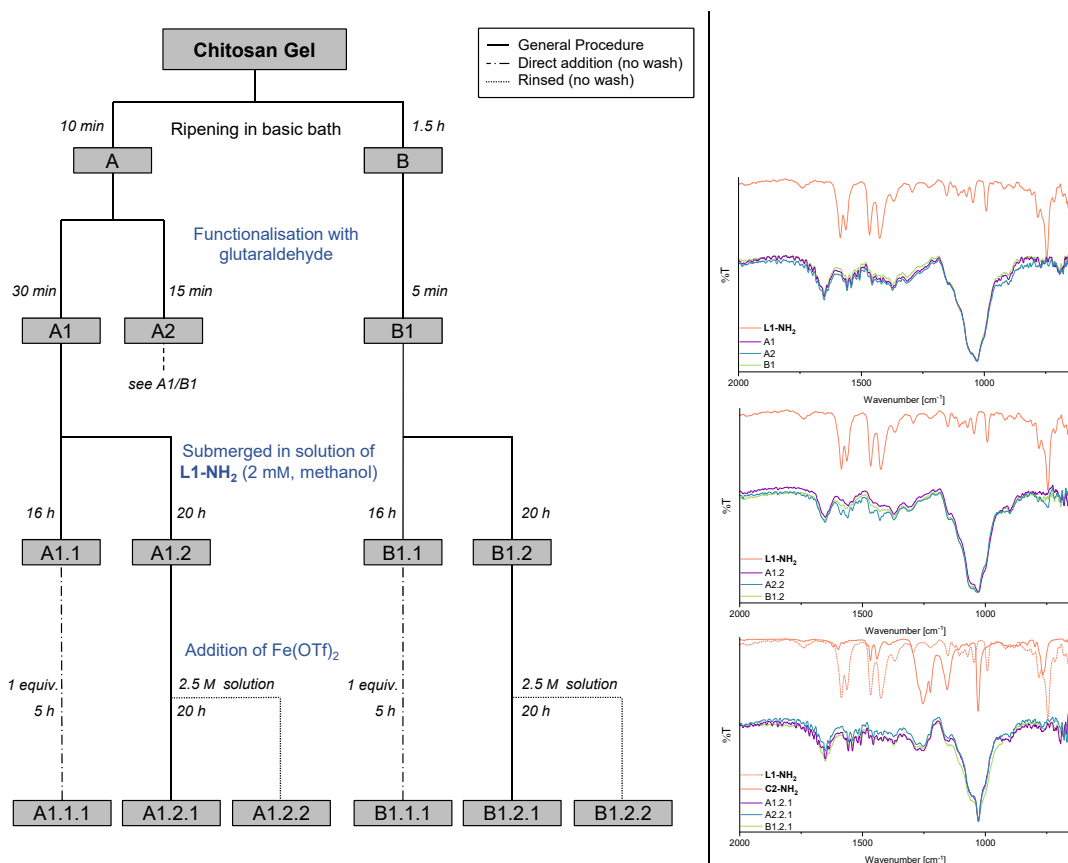


Figure IV.16.: Overview of a series of functionalisations and reactions starting from one batch of chitosan gel. From the gel, two batches A and B were formed according to the general procedure (Chapter IV.4.1) although ripening times in the basic solution were applied as given in the figure. Fraction A was split evenly and all resulting fractions were reacted with glutaraldehyde solution (5 wt%) according to the given times. All resulting fractions were evenly split and submerged in a ligand solution at ambient temperature and put on a laboratory shaker. The fractions were then either washed (A1.2, A2.2, B1.2) and submerged in an iron(II) triflate solution or solid iron(II) triflate was immediately added (A1.1, A2.1, B2.1) without prior washing. IR spectra of the ligand L1-NH₂ or complex C2-NH₂ as references compared to the IR spectra of some fractions are displayed on the right as an example. All additional spectra can be found in the Appendix (Chapter VII.5). All beads were lyophilised before measurement. The shown spectra were baseline corrected and smoothed using the Spectra Manager Version 2 software.

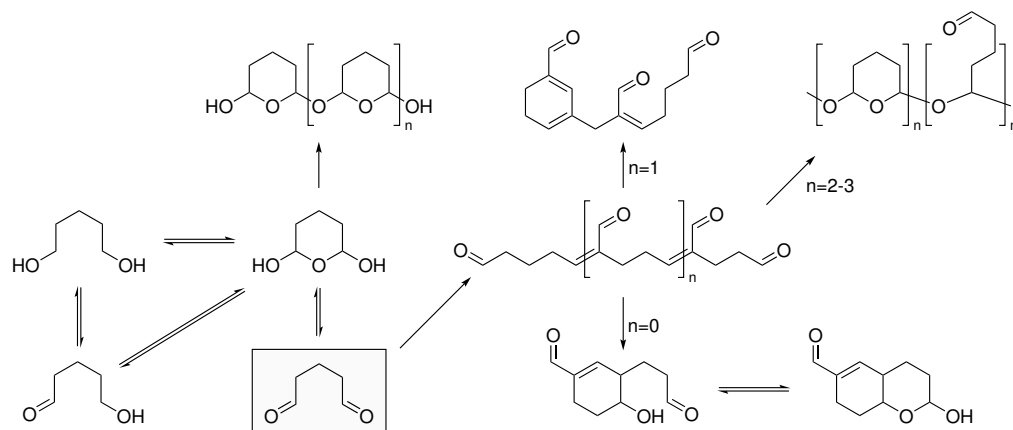
Afterwards, they were each added to a solution of iron(II) triflate (2.5 mM) and put on a laboratory shaker at ambient temperature. Simultaneously, the fractions A1.1, A2.1 and B1.1 were not filtered, but solid iron(II) triflate (1 equiv.) was added directly to the ligand solution around the beads. If no ligand had reacted with the beads so far, these fraction would thus be submerged in a 2 mM solution of C2-NH₂, which might show a different solubility and reactivity towards the beads than the ligand. At each step, six beads were removed from the fraction and freeze dried for analysis. A few selected IR spectra are shown in the overview (Figure IV.16). All other spectra can be found in the Appendix (Chapter VII.5). In general, almost none of the measured spectra indicate the presence or immobilisation of either ligand or complex on the beads. The spectrum of fraction A2.2 displayed some of the distinctive features of the ligand system between 1400-1600 cm⁻¹, but as these features were not present in the spectra of subsequent reaction, we suspect

that this was due to insufficient washing in this case. This is underlined further as beads taken from A2.1 before addition of iron(II) triflate did not display these features although the fractions should have been equivalent at this point in the procedure. It should also be mentioned that the spectra of all fractions after additions of iron(II) triflate either as solid or solution display features of the complex C2-NH₂ as can be seen by the examples A1.2.1, A2.2.1 and B1.2.1 in Figure IV.16. However, as all nine spectra were generally very similar although some of the measured beads were washed thoroughly while others were not, it is questionable if these features are due to covalently immobilised complex or if it was just adsorbed. Additionally, the water added for freeze drying quickly turned yellow upon addition in most cases, suggesting non-covalently bound complex being washed off the beads.

To summarise, we found some smaller indications of successful covalent immobilisation of the ligand or complex. But, these findings were cumbersome to reproduce and generally difficult to interpret. It could be possible, that changing conditions or slight differences in the procedures might be responsible for the different outcomes. We cannot be sure if the initial experiments might have been successful or if the resulting data lead to false assumptions. Either way, at this point no reproducible procedure could be obtained. A possible explanation for the initial data could be that the beads adsorbed ligand from the solution or precipitation of the ligand occurred on the surface or within the beads as the ligand L1-NH₂ is not very soluble in water. This could have led to false positives in the analytical data if the beads were washed insufficiently or a different solvent is necessary in order to remove unbound ligand. Similar concerns can be applied to the experiments shown in Figure IV.16. Unfortunately, the presented experiments could not elucidate this problem. It should also be kept in mind that many indications of successful immobilisation are based on features of the ligand or complex, while no newly appearing features, for example of a formed Schiff base, were found. In order to take a step back and get confirmation if the ligand L1-NH₂ does react with the presumed free glutaraldehyde endings, investigations of this reaction in solution were performed. These are described in the following section.

4.2.1. Investigation on the Schiff Base Formation of L1-NH₂ and GA

As mentioned in the previous section, due to the inconclusive results of the immobilisation attempts of L1-NH₂ on glutaraldehyde modified chitosan beads (CB-GAs), we decided to take a closer look on the Schiff base formation between GA and L1-NH₂. Without the chitosan present, these investigations could be performed in solution, allowing comprehensive analytical investigation *via* mass spectrometry as well as IR and NMR spectroscopy. The resulting IR spectra could then give an indication on the features which should be expected and looked for in future immobilisation attempts of L1-NH₂ on CBs. The following experiments were performed during the internship of Clarissa Sonnemann.



Scheme IV.10: Generalised overview on some possible structures generated from monomeric glutaraldehyde (grey box) in aqueous solution. The formation of the varying species is likely dependent on conditions and pH. A more detailed description can be found in the review by Migneault *et al.* [230]

In initial experiments, the behaviour of GA in solution and its dependence on the surrounding pH was tested. Although there are multiple literature procedures describing varying monomeric and polymeric structures of GA before and after reaction with amino functions, it is debatable which structures occur under specific conditions and which are reactive towards amines. [230] An excerpt of the possible monomeric and polymeric structures of GA is given in Scheme IV.10. As we were not able to detect monomeric glutaraldehyde in solution with a pH ≥ 9 in either GC-MS or NMR measurements (spectra can be found in the Appendix, Chapter VII5), we concluded that polymerisation is occurring in some form and the pH should generally be kept below 9 to avoid side reactions of the GA. As a side note, this might also have an influence on the functionalisation of the chitosan beads if they were not washed and equilibrated sufficiently (*vide supra*) emphasizing the need for a thorough and reproducible procedure.

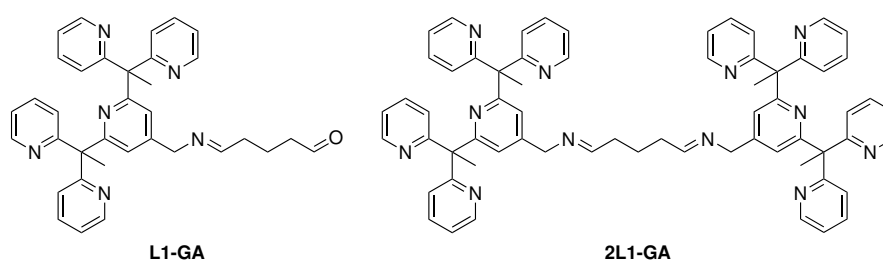
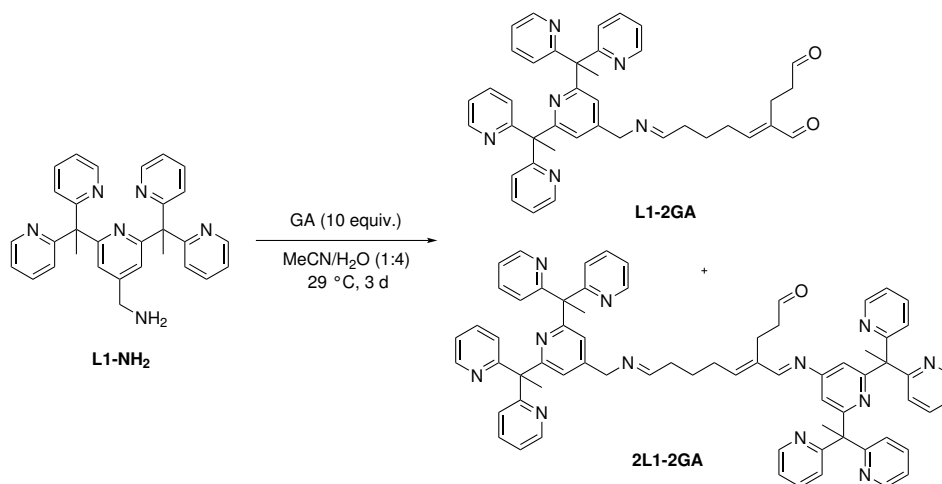


Chart IV.1.: Expected products L1-GA and 2L1-GA from the reaction of the ligand L1-NH₂ with GA in solution.

To test the reaction of GA with the ligand L1-NH₂, three different GA to ligand ratios (1:1, 1:3 and 3:1) were tested. A solution of L1-NH₂ (8 mM in acetonitrile) was prepared and GA was added to obtain the according GA to ligand ratio for each reaction. The mixtures were stirred at room temperature for 4 d and monitored by LR-MS. The measurements showed full consumption of the ligand only in the reaction with excess GA. It was expected to find either one ligand reacted with one GA monomer *via* Schiff base formation (L1-GA)

or GA which reacted on both free aldehyde ends with one ligand each (2L1-GA) forming a "dumbbell" (Chart IV.1). However, neither of these products was detected while other product masses were found in all reactions. Additional small scale reactions at higher pH (9) and temperature (60 °C) were performed, which did not result in different products, but rather an overall decrease in detected masses suggesting unwanted side reactions.

The detected masses correspond to the ligand L1-NH₂ reacted with a GA dimer (L1-2GA) and the same structure reacted with an additional ligand (2L1-2GA) (see Scheme IV.11). As these reactions were performed on small scales which did not yield enough product for NMR analysis, they were scaled up. This reaction (Scheme IV.11) was performed at a constant temperature and with a greater excess of GA (10:1). Additionally, the reaction should be carried out in water to assess the influence of the solvent and to replicate the conditions used with the CBs. However, due to the ligands poor solubility in water, a mixture of acetonitrile and water (1:4) was employed instead.



Scheme IV.11: Reaction of the ligand L1-NH₂ with GA in solution forming L1-2GA and 2L1-2GA. It should be noted that both structures are examples derived from the found mass. Several other isomers are possible and the given structures are not necessarily correct.

As seen in the first experiments, only the products L1-2GA and 2L1-2GA were formed in this reaction. It could not be determined whether the dimerisation of GA occurs prior to the reaction with the first amine or after, as neither the mass for a GA dimer nor L1-GA could be detected throughout the process. We hypothesize that the ligand L1-NH₂ forms a Schiff base with a GA monomer which then immediately reacts with a second GA moiety and that this reaction is very fast. It has been reported in the literature, that the Schiff base product of GA with an amine readily undergoes further reaction with a second GA molecule.^[231,232] It is possible that this is due to a difference in reactivity between the first reacted GA moiety and the subsequently formed dimer. This might be why there is no reaction with a second ligand molecule with only one GA as a linker (2L1-GA). However, this could also be caused by different reaction speeds. Reported GA crosslinking reactions in which two amino group bearing molecules are linked also suggest that at

least a dimer of GA is formed as a linking molecule.^[231–234] It was also proposed that the α,β -unsaturated aldehyde dimerisation product (see L1-2GA, Scheme IV.11) of GA results in stable imine products upon reaction with an amine due to conjugation and therefore is a likely reaction product (see 2L1-2GA, Scheme IV.11).^[232,235] Nevertheless, many literature procedures propose ring formations with the GA polymers in different forms, which is why a cyclic structure could also have formed.^[233,234,236,237] A few examples of possible linker structures derived from dimerisation of two GAs are shown in Chart IV.2.

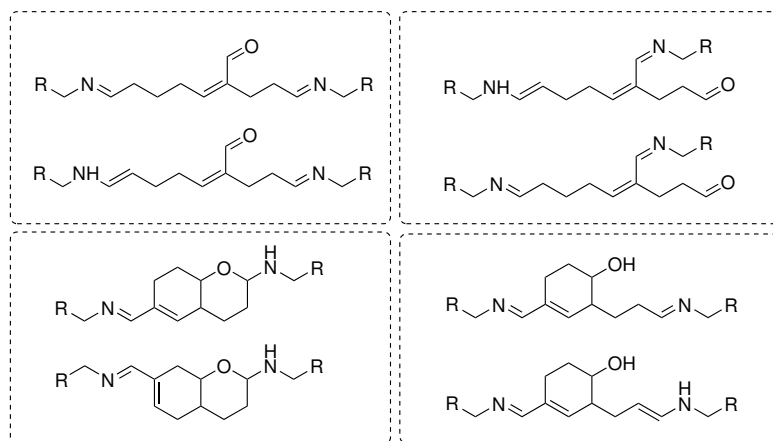


Chart IV.2.: Depicted are possible linker structures that could have formed from two glutaraldehyde monomers after or during the reaction with the ligand L1-NH₂ *via* Schiff base reaction, Michael-type 1,4-addition, aldol condensation or intramolecular aldol cyclisation, respectively. This is only an excerpt of possible structures showing the multitude of isomers possibly belonging to one detected mass. R = ligand L1.

As it is not possible to determine the exact structure only from the detected masses, 2L1-2GA was purified from the reaction mixture by preparative HPLC (ReproSil-Pur 120 C18-AQ, Dr. Maisch, 250x20 mm 5 μ m) and a full NMR analysis including ¹H-NMR, ¹³C-NMR, homonuclear correlation spectroscopy (COSY), heteronuclear multiple-quantum correlation spectroscopy (HMQC), heteronuclear multiple-bond correlation spectroscopy (HMBC), and distortionless enhancement by polarization transfer (DEPT135) was conducted (spectra can be found in the Appendix, Chapter VII5). Unfortunately, despite purification, the NMR spectra indicated more than one species which is likely due to isomeric structures. Besides inconsistent integrals indicating overlapping signals, we also found signals in the proton NMR spectra which likely stem from diastereotopic protons. These signals can be assigned to the same carbon by the HMQC spectra, but their chemical shift differs by $\Delta\delta = 0.47$ ppm, $\Delta\delta = 0.82$ ppm and $\Delta\delta = 1.5$ ppm. However, this might also be due to an equilibrium of different conformations in solution. In general, it can be deduced that the multitude of possible conformations, for example through imine-enamine tautomerism,^[238,239] and different possible dimerisation and polymerisation reactions of GA (*vide supra*) do not allow for a simple structure determination. Unfortunately, similar shifts were not reported in literature on GA crosslinking.^[231–234,236,237] Nevertheless, these experiments showed that the ligand L1-NH₂ does react with GA. But, whether this

reaction is transferable to the modified chitosan beads remains elusive, as we do not know whether dimerisation of the GA is generally necessary for a second amine reaction to bind and which form the GA acquires once immobilised on the beads. Thus, unfortunately, the performed experiments were not able to elucidate on how and if immobilisation according to the described methods is likely to succeed.

In summary, the immobilisation of the ligand L1-NH₂ on chitosan did not result in the desired product, yet. Also, the investigation and observation of the reaction proved to be a cumbersome task and poses questions and problems that would take a lot of additional effort to solve. Thus, this project was so far not pursued further and a different solid support system was investigated instead.

4.3. Functionalised Silica

After the previously discussed investigations on chitosan as a solid support system for ligand or complex immobilisation turned out to be challenging and did not yield the expected outcome, we decided to investigate a different support system as well. As the literature on chitosan procedures are focussing on protein and enzyme immobilisation,^[240–243] we decided to focus on a material that has been used for chemical structures more similar to our ligand system. Thus, we chose silica as an alternative solid support. As described in Chapter IV1.2, silica has been used as a matrix for immobilisation in numerous chemical applications, including the fixation of complexes or catalysts. More specifically, we opted for the mesoporous hexagonal silica MCM41 (Figure IV.17A),^[244–246] which has been used in different applications including immobilisation,^[247–250] because this calcinated silica can be used in aqueous solvent systems.



Figure IV.17.: A) Graphical representation of the mesoporous hexagonal silica MCM41 with free binding functions inside the tube-like pores. B) Functionalisation of MCM41_X by reaction with TESP-Cl or TESP-NH₂. Two different forms of MCM41 silica were used in these reaction. One was bought in powdered form (pow) and one in pressed pellets (pel).

In order to make the MCM41 accessible for immobilisation, it can be modified by reaction with silanes bearing functional groups. As they were commercially available, we used a powdered (MCM41_{pow}) and a pelleted (MCM41_{pel}) form of MCM41 as they might provide different advantages in later use. The powdered form is less voluminous while the pelleted form should allow a better flow if, for example, packed into a column or syringe while solutions of substrate are added or pumped through. According to the literature,^[251–256] (3-chloropropyl)triethoxysilane and similar silanes can be used to functionalise silica. They will be abbreviated as TESP-Y (tri-ethoxy-silyl-propyl-Y) in the following. As shown in Figure IV.17B, we reacted the MCM41 with TESP-Cl and TESP-NH₂ in order to create two different types of silica to which different functionalities can be attached by, for example, nucleophilic substitution. As described in the literature,^[254] MCM41_X was suspended in toluene, the according silane was added and the mixture heated for several days. It was then filtered, washed thoroughly in dichloromethane using a soxhlet apparatus and dried in a vacuum drying cabinet at 40 °C. It should be mentioned that the pelleted MCM41 did not withstand the procedure in its original form due to stirring and was also received in a powdered form after the procedure. Nevertheless, both were analysed by elemental analysis (see Chapter VI3.5) and IR spectroscopy. The IR spectra of the experiments conducted with the powdered silica (MCM41_{pow}) are shown in Figure IV.18. The according spectra derived from the pelleted silica did

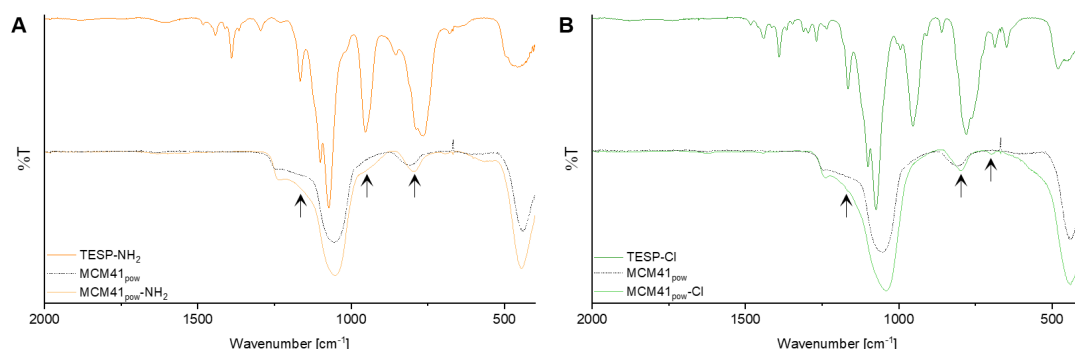
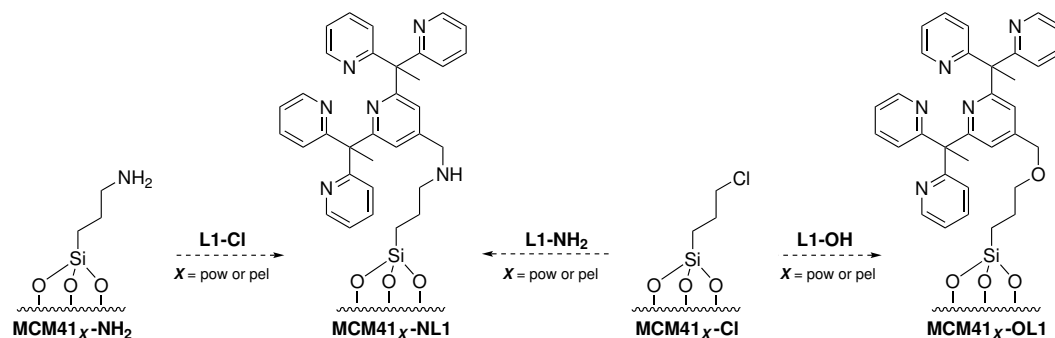


Figure IV.18.: A) IR spectrum of the functionalised MCM41_{pow}-NH₂ in comparison to MCM41_{pow} and TESP-NH₂. B) IR spectrum of the functionalised MCM41_{pow}-Cl in comparison to MCM41_{pow} and TESP-Cl. Indications of successful addition of TESP-Y are marked by arrows.

not display significant differences and can be found in the Appendix (Chapter VII5). Although the IR spectra of MCM41_{pow}-NH₂ and MCM41_{pow}-Cl do not show strong signals of the respective TESP-Y silane, this was anticipated and is in accordance with the literature.^[251] As shown in Figure IV.17A, the possible binding sites of the MCM41 are within the pores of the structure, which might not be detected with the attenuated total reflection (ATR) IR that was used. This is due to the synthetic process of the mesoporous silica in which the silica is condensed around rod-like micelles previously formed from tetraalkylammonium halides.^[245,247] The negatively charged silicate species accumulate on the positively charged surface of the micelles and thus this innermost layer of silicate does not undergo full condensation. However, as the elemental analysis showed an increase of carbon and hydrogen content, while the silica percentage decreased (see Chapter VI3.5), it is very likely that the functionalisation was successful.

4.3.1. Immobilisation on Silica by Nucleophilic Substitution

In order to immobilise our ligand system L1-X on MCM41, we took inspiration from Haensch *et al.*^[254] who used MCM41_{pow}-Br as their base and immobilised ligands and linkers bearing amino functional groups by substitution. Additionally, the same concept was applied in previous immobilisation attempts within the group^[124] on TentaGel and



Scheme IV.12: Overview on the possible products MCM41_X-NL1 and MCM41_X-OL1 from the reaction of MCM41_X-Y with the ligands L1-NH₂, L1-Cl and L1-OH by nucleophilic substitution.

Merrifield resin, which bear either amino or bromide functions as binding sites. With the ligand systems at hand, including the new L1-Cl ligand and the two types of silica MCM41_X-NH₂ and MCM41_X-Cl, two types of linking moieties could result (see Scheme IV.12). The ligand can be bound either *via* an amine (MCM41_X-NL1) or an ether (MCM41_X-OL1) function. To test the general reactivity and which of these combinations leads to the desired product or, if several do, gives the best loading on the silica, different screens of the possible reaction conditions and combinations were performed.

Table IV.3.: Overview of tested reactions of L1-NH₂ with MCM41_X-Cl. In each reaction, 20 mg of MCM41_X-Cl was added to a 1.5 mL centrifuge tube and suspended in the respective solvent (1 mL). The ligand (5 mg) and base (2 equiv.) were then added directly to the mixture. All reactions were put in an orbital shaker (750 rpm) and reacted for 90 h at 30 °C. The reactions were each filtered through a syringe barrel with a cotton wool plug, washed several times (2x1 mL water, 2x1 mL methanol, 2x1 mL dichloromethane, 2x1 mL methanol, 2x1 mL water) and dried in a vacuum drying cabinet at 40 °C. All reactions that yielded enough material were measured by elemental analysis. Values which deviate from expected trends are marked in red. Reactions which display expected values are marked in blue.

		Ligand	Silica	Solvent	Base	Elemental Analysis		
						C	H	N
References			MCM41 _{pel} -Cl			4.89	1.80	0.00
			MCM41 _{pow} -Cl			4.63	1.42	0.00
1a	L1-NH ₂	MCM41 _{pel} -Cl	MeOH	NEt ₃	-	-	-	-
2a	L1-NH ₂	MCM41 _{pel} -Cl	H ₂ O	NEt ₃	7.70	2.44	0.55	
3a	L1-NH ₂	MCM41 _{pel} -Cl	DCM/MeOH	NEt ₃	-	-	-	-
4a	-	MCM41 _{pel} -Cl	MeOH	NEt ₃	6.74	2.17	0.37	
5a	L1-NH ₂	MCM41 _{pow} -Cl	MeOH	NEt ₃	3.98	1.72	0.26	
6a	L1-NH ₂	MCM41 _{pow} -Cl	H ₂ O	NEt ₃	5.28	2.11	0.66	
7a	L1-NH ₂	MCM41 _{pow} -Cl	DCM/MeOH	NEt ₃	-	-	-	-
8a	-	MCM41 _{pow} -Cl	MeOH	NEt ₃	3.79	1.79	0.25	
9a	L1-NH ₂	MCM41 _{pel} -Cl	MeOH	K ₂ CO ₃	-	-	-	-
10a	L1-NH ₂	MCM41 _{pel} -Cl	H ₂ O	K ₂ CO ₃	6.91	2.11	0.23	
11a	L1-NH ₂	MCM41 _{pel} -Cl	DCM/MeOH	K ₂ CO ₃	-	-	-	-
12a	-	MCM41 _{pel} -Cl	MeOH	K ₂ CO ₃	5.97	1.96	0.00	
13a	L1-NH ₂	MCM41 _{pow} -Cl	MeOH	K ₂ CO ₃	3.01	1.91	0.16	
14a	L1-NH ₂	MCM41 _{pow} -Cl	H ₂ O	K ₂ CO ₃	2.78	2.23	0.22	
15a	L1-NH ₂	MCM41 _{pow} -Cl	DCM/MeOH	K ₂ CO ₃	3.29	1.83	0.20	
16a	-	MCM41 _{pow} -Cl	MeOH	K ₂ CO ₃	2.46	1.91	0.00	

In a first experiment, the reaction of L1-NH₂ with MCM41_X-Cl was tested. The intent was to compare the powdered and the pelleted silica and find a suitable solvent and base for the reaction. As the ligand L1-NH₂ is poorly soluble in water other organic solvents, namely methanol and a 1:1 mixture of dichloromethane and methanol, were tested as well. The reaction conditions and procedure are presented in Table IV.3. Reactions which were not measured by elemental analysis did not yield enough product for the method. It is suspected that the reaction of the pelleted silica with the ligand leads to a higher solubility of the silica, as this was observed for reaction 1a, 3a, 9a and 11a (see Table IV.3, which all include ligand, pelleted silica and a base, while the reference reactions without ligand in methanol (4a and 12a) did not lead to dissolution. While this might be an indication of successful reaction, for the concept of immobilising the ligand on a solid support, this is not feasible. Additionally, both reference reactions (4a and 12a) show an increase in carbon, hydrogen and nitrogen (only 4a) content which is likely due to the respective base sticking to the silica despite the washing procedure. In case of the powdered silica, only reaction 11a resulted in the loss of the solid. However, most reactions with the powdered silica (5a, 8a, 13a-16a) showed a decrease in carbon content, which is not expected and might be explained by the loss of the attached TESP-Cl functions instead of the addition of the ligand. The only reactions yielding the expected increase in carbon, hydrogen and nitrogen content are 2a, 6a and 10a (marked in blue). But, as these are the reactions in water, in which the ligand L1-NH₂ is poorly soluble, this might be caused by undissolved ligand which did not wash off sufficiently. IR spectra could only be measured from the reactions yielding enough product for both EA and IR measurements. No significant changes could be observed in the spectra (see in the Appendix, Chapter VII.5). From this experiment, we deduced that the powdered silica MCM41_{pow}-Y is more stable under the tested conditions in terms of insolubility and thus, solely the powdered silica was used in future experiments despite the possible loss of TESP-Cl.

In a second experiment, the ligands L1-NH₂, L1-Cl and L1-OH were reacted with the respective silica and a water and acetonitrile mixture was used as a solvent to minimise the possibility of false positives through precipitated ligand without risking dissolution of the silica in organic solvents like methanol. In order to gain more insight if ligand might stick to the silica without covalently binding to the linker, the reactions were also performed with unfunctionalised MCM41_{pow}. The elemental analyses are shown in Table IV.4. The results of the EA of reactions 1b-6b are all averages of two measurements which include values that deviated strongly in case of 1b-4b. Therefore, these results can not be taken as a strong indicator for any assumptions. However, from the overall measurements it can be deduced that it is very likely that the carbonate is not sufficiently washed of the silica since the reference reactions 4b and 6b show an increase in carbon content while no nitrogen was detected, which is why this can not stem from the ligand. These reactions were washed within a syringe barrel by letting the washing solution flow

Table IV.4.: Overview of tested reactions of L1-X with MCM41_{pow}-Y. In each reaction, 100 mg of MCM41_{pow}-Y was added to a 10 mL round bottom flask and suspended in a water and acetonitrile mixture (1:5, 12 mL). The ligand (25 mg) and potassium carbonate (5equiv.) were then added. All reactions were stirred for 5 h at 21-23 °C. The reactions were each filtered through a syringe barrel with a cotton wool plug, washed several times with (2x2 mL methanol, 2x2 mL water, 2x2 mL methanol) and dried in a vacuum drying cabinet at 40 °C. All EA values are averages of two measurements. Values marked in grey are averages which deviated by > 20 %.

Ligand		Silica	Elemental Analysis		
			C	H	N
References					
		MCM41 _{pow}	0.01	0.85	0.00
		MCM41 _{pow} -Cl	4.63	1.42	0.00
		MCM41 _{pow} -NH ₂	6.78	1.93	1.81
1b	L1-NH ₂	MCM41 _{pow}	5.13	1.28	0.41
2b	L1-NH ₂	MCM41 _{pow} -Cl	6.23	2.16	0.20
3b	L1-OH	MCM41 _{pow}	6.50	1.37	0.00
4b	L1-OH	MCM41 _{pow} -Cl	5.86	1.62	0.10
5b	L1-Cl	MCM41 _{pow}	6.05	1.23	0.00
6b	L1-Cl	MCM41 _{pow} -NH ₂	7.17	2.83	2.21

through which should therefore be avoided in the future. It should be tested whether stirring, shaking or sonication in a washing solution and subsequent centrifugation or filtration yield better results. Nevertheless, reaction 5b shows the expected elevation in carbon, hydrogen and nitrogen content which do not appear in the reference reaction 6b, especially for nitrogen. Thus, it is likely that the reaction of MCM41_{pow}-NH₂ with L1-Cl was successful. The IR spectra of 5b and 6b and of the reactions with the ligand L1-NH₂ (1b and 2b) are shown in Figure IV.19.

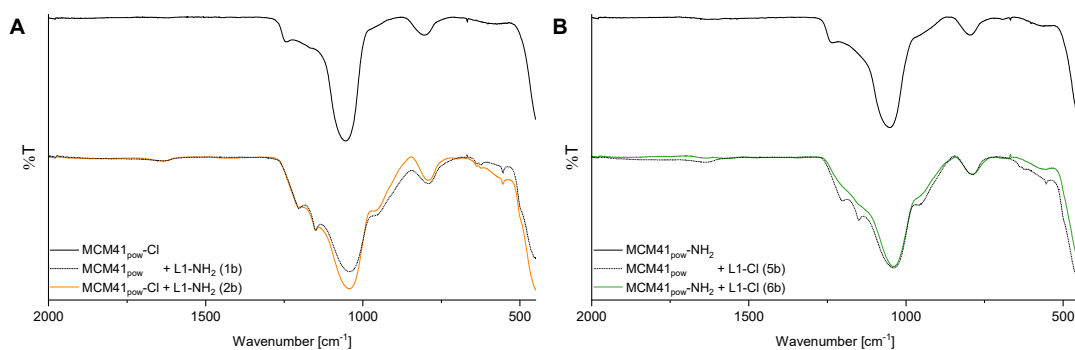
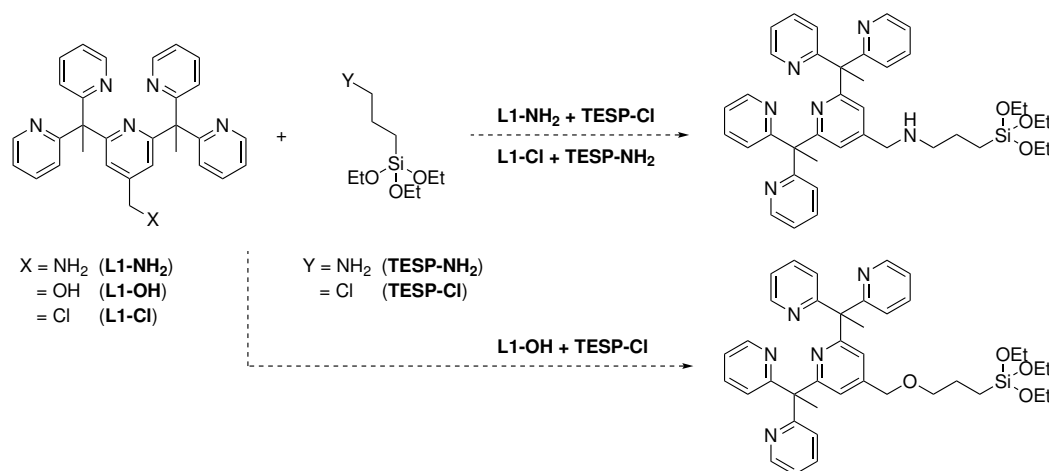


Figure IV.19.: A) IR spectra of the reaction of the ligand L1-NH₂ with MCM41_{pow}-Cl (2b) and MCM41_{pow} (1b) in comparison to MCM41_{pow}-Cl. B) IR spectra of the reaction of the ligand L1-Cl with MCM41_{pow}-NH₂ (6b) and MCM41_{pow} (5b) in comparison to MCM41_{pow}-NH₂. All numbering refers to Table IV.4.

Unfortunately, no new signals, that could be assigned to immobilised ligand, could be observed in the spectra which might again be due to the binding sites being positioned within the pores of the MCM41. This is further corroborated as the carbonate impurity, which is very likely present in all products, can also not be detected in the IR spectra. For a carbonate, a very broad signal in the region around 1400 cm^{-1} would be expected, however, this impurity is likely also situated within the pores and therefore not detectable with the ATR-IR technique. In all products despite 6b, absorption bands at 950 cm^{-1} , 1150 cm^{-1} and 1205 cm^{-1} were observed which could not be attributed yet. But, as they only appear in the products which according to EA were deemed unsuccessful, they were not investigated further so far.

In addition to the experiments on MCM41, all ligands were reacted with the according TESP-Y in solution as we learned from the chitosan project that it might be useful to test the reaction of linker and ligand in free solution. The general scheme is shown in Scheme IV.13. In this experiment, each ligand (L1-NH₂, L1-Cl or L1-OH) was reacted with the according TESP-Y in dimethylformamide with potassium carbonate or triethylamine. The reactions were monitored for two days at ambient temperature ($24\text{ }^{\circ}\text{C}$) using LR-MS and then heated to $60\text{ }^{\circ}\text{C}$ for 5 d. The mass spectra showed no indication of product formation. To test a different analytical method, the reactions of ligand L1-Cl were diluted with water and the mixtures extracted with ethyl acetate before the solvents were removed *in vacuo* and the products measured by NMR. Unfortunately, none of the reactions showed indication of either the expected product mass or NMR signals nor was any precipitation due to insolubility observed.



Scheme IV.13: General reaction scheme of the ligands L1-NH₂, L1-Cl and L1-OH with TESP-NH₂ or TESP-Cl forming either the amine or ether bound product. All reactions were performed in dimethylformamide, with 2.0 equiv. of TESP-Y and 3.0 equiv. of base (triethylamine or potassium carbonate). The reactions were stirred 2 d at $24\text{ }^{\circ}\text{C}$ and subsequently 5 d at $60\text{ }^{\circ}\text{C}$.

In summary, regarding the described experiments, the combination of ligand L1-Cl on MCM41_{pow}-NH₂ is the best candidate for successful immobilisation by nucleophilic substitution. It is likely that ATR-IR is not the right method to investigate the MCM41

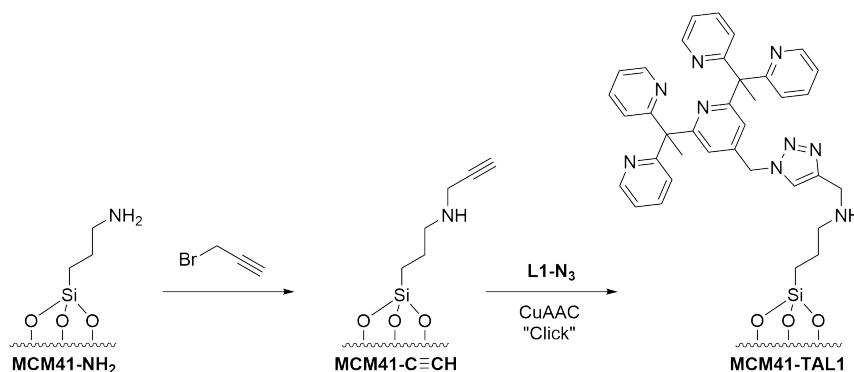
products due to the binding sites positioned within the pores. If possible, it will be attempted to measure transmission IR spectra of the products in the future.

4.3.2. Immobilisation on Silica Using Click Chemistry

In addition to the nucleophilic substitution approach, literature procedures also implement click chemistry to immobilise ligands. In general, mostly either copper catalysed azide-alkyne cycloaddition (CuAAC)^[176,177,198,257] or strain promoted azide-alkyne cycloaddition (SPAAC)^[258,259] are used towards this. Thus, to be able to test click chemistry towards our immobilisation of L1-X on MCM41, the ligand L1-N₃ was synthesized (see Chapter IV3.1.4). Although this was partly done preliminary, the experiments and reactions within this section were to a great extent part of the master thesis of Johanna Großmann and more details can be found in her work.^[260] The aim of this first part of the project was to initially test all relevant steps separately in solution and find indication, if the reactions are successful. This was, as already mentioned (*vide supra*), done since the analysis of the solid material is somewhat restricted and more difficult to interpret.

Copper Catalysed Azide-Alkyne Cycloaddition (CuAAC)

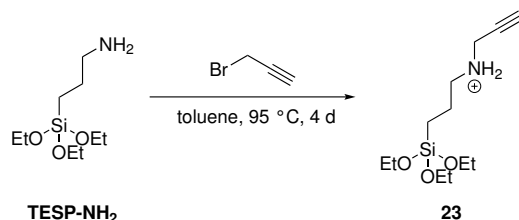
As it is a widely known and overall facile reaction, we wanted to test the CuAAC on our system first. A general scheme of this is shown in Scheme IV.14. In order to click the azide ligand L1-N₃ onto the MCM41, the silica has to be functionalised with an alkyne group. This is done by reaction of MCM41-NH₂ with propargyl bromide in the literature.^[254,261]



Scheme IV.14: General scheme for the modification of silica using propargyl bromide and subsequent CuAAC click reaction immobilising ligand L1-N₃ via a triazole (TA) function forming MCM41-TAL1.

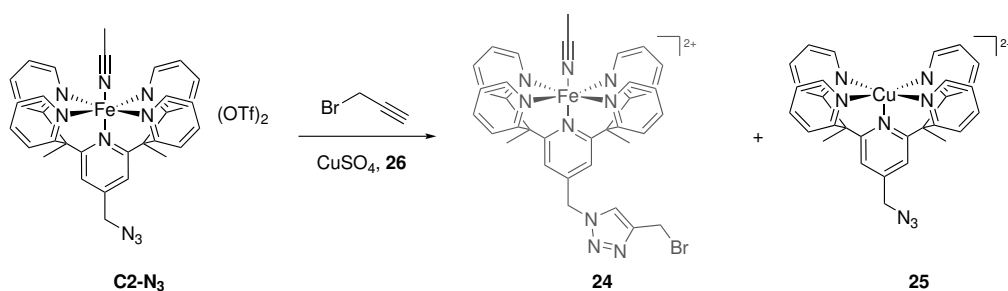
To test the reaction between the silane and propargyl bromide and get more insight into the optimal reaction time, TESP-NH₂ was reacted with propargyl bromide in solution (Scheme IV.15). The procedure was adapted from Lee *et al.*^[261] TESP-NH₂ was dissolved in toluene and the propargyl bromide was added (2.5 equiv) before heating the reaction to 95 °C for 4 d. The reaction was checked by LR-MS which was, however, difficult since the product precipitated as red solid. The solid could not be fully redissolved in toluene, dichloromethane, methanol, ethanol, water or ethyl acetate, but nevertheless, the product

mass could still be detected in LR-MS (Scheme IV.15). As this was only a qualitative test, the reaction was not purified or analysed further, yet.



Scheme IV.15: Functionalisation of TESP-NH₂ by a substitution reaction with propargyl bromide in toluene. The product was not purified and no yield was determined. The product **23** formation was followed by LR-MS. Found mass: 260.2 m/z. Theoretical value: 260.17 m/z [M+H]⁺.

In the next step, the CuAAC reaction of L1-N₃ with propargyl bromide was to be tested in solution. As expected, the addition of copper to the ligand immediately results in complex formation which would prevent the click reaction. This was tested in a UV-Vis titration by sequentially adding 0.1 equiv. of copper sulfate to the ligand solution according to the experiment shown in Figure IV.5. In addition, copper sulfate (0.5 equiv.) was added to the formed iron complex C2-LN₃ (Figure IV.5) and iron(II) triflate (0.5 equiv.) was added to the complex formed with copper and L-N₃ to test whether one metal ion might be exchanged by the other due to a clear preference. However, after 60 min the UV-Vis spectra did not display any shifts indicating a metal exchange (spectra can be found in the Appendix, Chapter VII5). Thus, the CuAAC reaction was performed with C2-LN₃ as shown in Scheme IV.16 in order to obtain the click product **24**. Unfortunately, in the longer time frame of the reaction LR-MS revealed that the iron in the C2-LN₃ is exchanged by copper forming **25** and no formation of **24** could be observed.



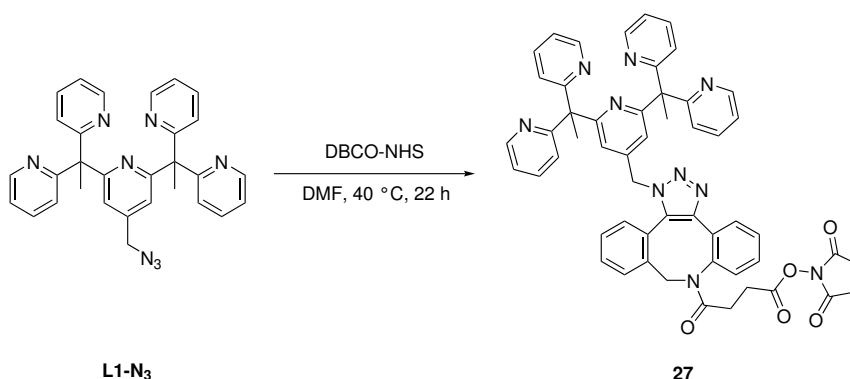
Scheme IV.16: General scheme of the attempted CuAAC reaction of C2-N₃ and propargyl bromide using copper sulfate and sodium ascorbate (**26**) resulting in a metal exchange forming **25** instead of the desired product **24**.

In future experiment, a copper binding ligand should be added to the reaction to prevent the formation of **25** while still allowing for the catalytic activity of the copper ion. This could be done, for example, according to the literature procedures by McDonald *et al.*^[176,177]

Strain Promoted Azide-Alkyne Cycloaddition (SPAAC)

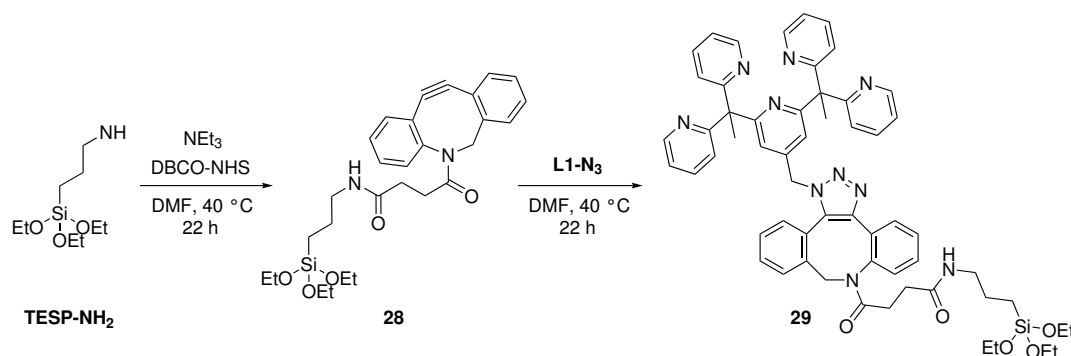
A different option to avoid the formation of copper complexes with our ligand system is the use of SPAAC in which no additional copper is needed as the alkyne is, as the name says, activated by the strain in the ring structure in which the alkyne is embedded. As we need a molecule that is suitable for SPAAC while also having a functionality that can be bound to the silica, we opted for DBCO-NHS. As mentioned, the benefit is the absence of any competing metal ions, but it should be noted that molecules used in SPAAC like DBCO are more expensive and introduce a bigger spacer into the immobilisation setup. It is possible that the additional structure could be attacked by the immobilised iron(IV)-oxido species once it is formed, depending on the flexibility of the linking structure. Nevertheless, this is only a possibility which should be kept in mind.

In a first experiment, the ligand L1-N₃ was reacted with DBCO-NHS in solution to see whether the SPAAC reaction is successful in this combination (Scheme IV.17). The reaction was followed by LR-MS and the expected product mass of **27** was detected after 22 h. It should be mentioned that both starting materials could also still be detected at this point, but as this was a preliminary test reaction, the solvents were removed *in vacuo* and the product was purified by reversed-phase HPLC (Scheme IV.17). The HPLC spectrum showed two partly overlapping peaks (see in the Appendix, Chapter VII5) which in LR-MS displayed identical masses. It is likely that **27** was formed as two different regioisomers, namely the 1,4-triazole or 1,5-triazole adduct. As long as there are no differences in the reactivity, this should not be an issue. However, it should be noted that CuAAC reactions generally only form the pure 1,4-triazole adduct and could be preferable if the formation of a regioisomer mixture on the MCM41 poses difficulties. As a side note, the same reaction was performed with the iron complex C2-N₃ which did not result in the desired click product. Therefore, in future immobilisation experiments, the ligand should be immobilised before forming the iron(II) complex.



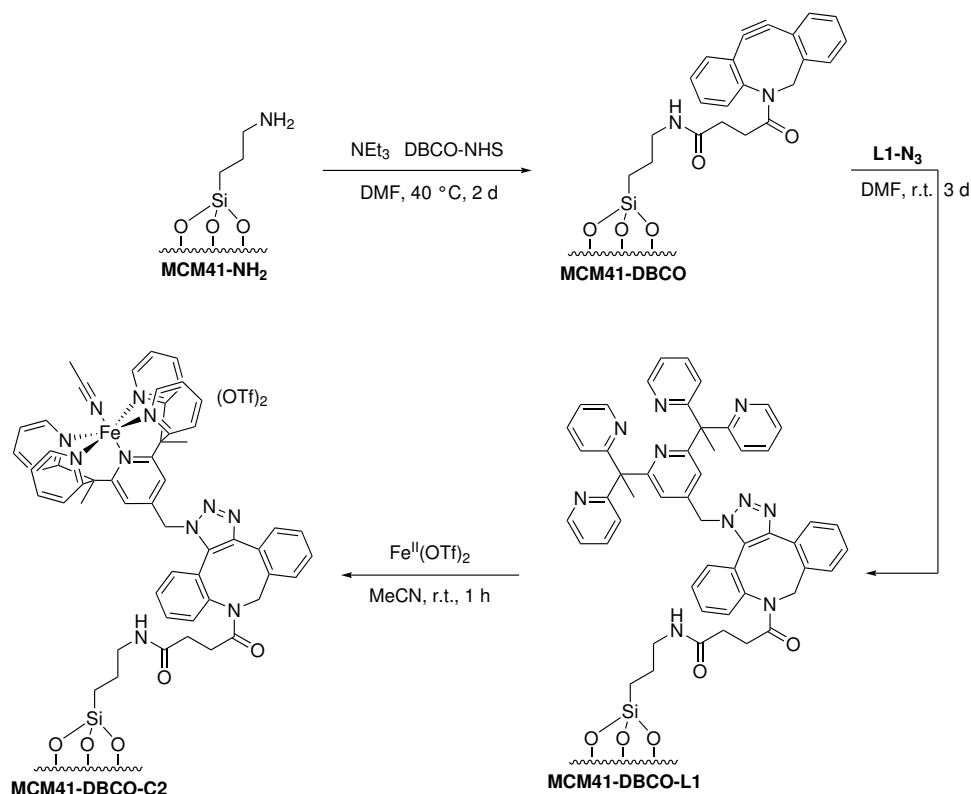
Scheme IV.17: SPAAC reaction of ligand L1-N₃ with DBCO-NHS (1.0 equiv.) forming both regioisomers of **27** (one omitted for clarity). The products were purified by HPLC (Agilent Zorbax SBC18, 250 mm x 30 mm – 5 μ m, 5 % to 95 % acetonitrile in water in 60 min, 0.1 % formic acid, flow 20 mL/min, Detection: 254 nm). The product formation and purification were followed by LR-MS. Found mass: 451.2 m/z, 901.0 m/z. Theoretical value: 451.18 m/z [M+2H]²⁺, 901.36 m/z [M+H]⁺.

As a second step, the reaction of the DBCO-NHS with TESP-NH₂ was performed in solution according to a literature procedure^[258] to confirm that the activated ester of the DBCO-NHS does react with the amino groups on the silica. Thus, both the TESP-NH₂ and DBCO-NHS were dissolved in dimethylformamide separately, the DBCO-NHS solution was added to the TESP-NH₂ and triethylamine was added until pH paper indicated a pH of 9 (see Scheme IV.18). The reaction was stirred at 40 °C for 22 h when LR-MS indicated the formation of **28**. As this product proved poorly soluble once the solvent was removed in a previous attempt, the ligand L1-N₃ was added directly to the mixture and the suspension stirred for additional 22 h. At this point, the product mass was detected by LR-MS indicating a successful SPAAC reaction on compound **28**. Similar to the previous reactions, the poor solubility of the product made purification and further analysis difficult. Nevertheless, the detected masses are a good indication of successful reaction. With these initial results at hand, a first attempt at immobilisation of the ligand L1-N₃ on MCM41 *via* SPAAC was performed.



Scheme IV.18: Reaction of TESP-NH₂ with DBCO-NHS forming **28** and subsequent SPAAC reaction with ligand L1-N₃ forming **29**. The product was not purified and no yield was determined. The product formation was followed by LR-MS. Found mass for **28**: 509.3 m/z. Theoretical value: 509.25 m/z [M+H]⁺. Found mass for **29**: 504.3 m/z. Theoretical value: 504.24 m/z [M+2H]²⁺.

Following the procedures described above, the immobilisation of the iron complex C2-N₃ was performed in three steps (see Scheme IV.19). Initially, the previously synthesized MCM41-NH₂ was reacted with DBCO-NHS in dimethylformamide at 40 °C for 2 d in a 25 mL round bottom flask. The mixture was centrifuged and the solution decanted off. The residue was washed by vortexing the silica in dichloromethane (8x1 mL) and ethyl acetate (2x1 mL) before centrifuging and decanting off the solvent after each step. The MCM41-DBCO was then dried in a vacuum drying cabinet at 40 °C. In the next step, MCM41-DBCO was suspended in dimethylformamide and L1-N₃ was added. As the reaction described earlier (Scheme IV.17) still contained starting materials after 22 h this reaction was stirred for 3 d at ambient temperature. The product was washed and dried according to the procedure applied in the previous step yielding MCM41-DBCO-L1. According to the general procedure for iron(II) complex formation (Chapter IV 3.2), MCM41-DBCO-L1 was suspended in acetonitrile and iron(II) triflate was added. The suspension was stirred for 1 h, washed as described above with acetonitrile (10x1 mL) and



Scheme IV.19: Scheme of the stepwise immobilisation of the complex C2-N₃ on MCM41-NH₂. Sequentially, MCM41-NH₂ is reacted with DBCO-NHS forming MCM41-DBCO. This product is then submerged into a solution of L1-N₃ for 3 d resulting in the SPAAC product MCM41-DBCO-L1 (only one regioisomer shown). Subsequent complex formation upon addition of iron(II) triflate yields the immobilised complex MCM41-DBCO-C2 (only one regioisomer shown). For each step, 1.0 equiv. of reactant (L1-N₃ and iron(II) triflate) was added assuming full conversion in all previous steps.

dried using a rotary evaporator at 40 °C yielding MCM41-DBCO-C2. This last reaction was duplicated with MCM41 and MCM41-NH₂ as references for nonspecifically bound iron. MCM41-DBCO and MCM41-DBCO-L1 were analysed by IR and EA while MCM41-DBCO-C2 and the reference reactions with MCM41 and MCM41-NH₂ were analysed by ICP-OES towards the iron content. The results of these measurements are summarised in Table IV.5. As can be seen, after the reaction of MCM41-NH₂ with DBCO-NHS (1c) the carbon content in the probe increases while the nitrogen and hydrogen content also display a slight increase. Especially the increase of carbon indicates a successful reaction. For the following reaction with the ligand L1-N₃ (2c), a stronger increase in nitrogen content was expected due to the high nitrogen content within the molecule. However, as calculations on the loading on the silica gave no convincing results and an increase in carbon content was observed as well, the product MCM41-DBCO-L1 was further reacted with iron(II) triflate.

The ICP-OES measurements show that the iron content in MCM41-DBCO-C2 (17.5 µg/mg) is significantly higher than in the reference probes MCM41 (3c, 1.15 µg/mg) and MCM41-NH₂ (4c, 1.65 µg/mg), indicating successful immobilisation of the ligand which was then able to form the immobilised complex C2.

Table IV.5.: Overview on the elemental analysis and ICP-OES measurements of the reaction steps during the immobilisation of C2-LN₃ on MCM41-NH₂ using DBCO. The reactions described in this chapter were performed with a different batch of MCM41-NH₂ than in Chapter IV.3.1. The MCM41-NH₂ described here was synthesized by Johanna Großmann.^[260] Therefore, the reference measurement differs from the previous data which are described in the experimental.

	Product	Elemental Analysis			ICP-OES
		C	H	N	Fe [μg/mg]
References					
	MCM41	0.00	0.73	0.15	-
	MCM41-NH ₂	9.76	2.61	3.08	-
1c	MCM41-DBCO	12.5	2.87	3.53	-
2c	MCM41-DBCO-L1	14.0	2.82	3.54	-
After reaction with iron(II) triflate					
3c	MCM41	-	-	-	1.15
4c	MCM41-NH ₂	-	-	-	1.65
5c	MCM41-DBCO-C2	-	-	-	17.5

Although these are only preliminary experiments, the combination of the successful reactions in solution, showing that all bond formations within the immobilisation steps are likely to happen, and the increased iron content in MCM41-DBCO-C2 gives a strong indication that the immobilisation of C2-LN₃ on MCM41-NH₂ using DBCO as a linker was successful and could be a functioning solid support system for the biomimetic iron(IV)-oxido complex C4.

V. Summary and Outlook

Research Data Management

One goal of this thesis was the improvement of the research data management (RDM) within the group. To achieve this, the electronic lab notebook Chemotion was tested and established. To gain deeper insight into the field of RDM and FAIR data, an exemplary synthesis was finished, investigated towards its "FAIRness" and published accordingly. The complete dataset including electronic lab notebook entries and raw data was uploaded to the chemotion repository and attached to the publication, successfully creating a FAIR paper. Additionally, an elaborate network and data storage system was created and set up to accommodate modern RDM requirements and facilitate storage and access of research data while meeting safety requirements.

Biomimetic Oxidation of Synthetic DNA Bases

In this part of the thesis, the reactivity of the biomimetic complex C4 towards synthetic DNA bases was investigated together with Niko Lindlar (né Jonasson), Annika Menke and Fabian Zott. Different synthetic DNA bases like 1-methylcytosine (1mC), 5-methyl-*iso*-cytosine (5m*i*C) and thymine (T/5mU) were synthesized and investigated towards their reactivity upon oxidation by complex C4. Within these investigations, I synthesized 1mC and attempted the synthesis of the expected oxidation products thereof. I also performed oxidation reactions and subsequent product analysis by HPLC-LR-MS and HPLC-HR-MS. The kinetic investigations revealed a significantly faster oxidation of C-methylated compared to the *N*-methylated bases. Together with Fabian Zott, the kinetic results were corroborated by calculated C-H bond dissociation energies (BDEs) identifying BDE calculations as a useful tool in reaction rate prediction. Additionally, based on investigations by HPLC-LR-MS, it was postulated that the oxidation products of 1mC undergo immediate decomposition by deformylation explaining cytosine as the single product of oxidation reactions with 1mC and C4.

Towards the Immobilisation of Py₅-Ligand Systems on a Solid Support

The main focus of this thesis was the immobilisation of the biomimetic complex C4 to facilitate the removal of the complex from solution and suppress side reactions by comproportionation. Previously performed immobilisations on Merrifield or TentaGel resin did not yield the desired applicability. Through the course of this project, two new ligands L1-Cl and L1-N₃ and the corresponding iron(II) complexes C2-Cl and C2-N₃ were successfully synthesized. To accommodate for the physiological conditions generally

applied with the biomimetic reactions performed using C4, the bio-compatible solid support system chitosan was tested. Within this work, the formation of uniform chitosan gel beads was optimized and the subsequent crosslinking and surface modification with glutaraldehyde was investigated. It was attempted to immobilise the amino derivative of the ligand system L1-NH₂ on the gel beads, but initially promising results could not be reproduced or otherwise corroborated. A detailed investigation in the Schiff base reaction between L1-NH₂ and glutaraldehyde could not yield further insight on how immobilisation through this system could be achieved.

The hexagonal mesoporous silica MCM41 was additionally investigated as possible solid support system. The silica was modified according to literature procedure and attempts at immobilisation of the ligand system *via* nucleophilic substitution were performed. However, the analytical data did not indicate successful immobilisation. Following this, reactions towards the immobilisation *via* click reactions were investigated. While copper catalysed azide-alkyne cycloaddition (CuAAC) resulted in complex formation between copper and the ligand system, successful reactions with the strain promoted azide-alkyne cycloaddition (SPAAC) reagent DBCO-NHS were performed. Reference reactions in solution showed successful covalent binding between the silane used for MCM41 modification with the activated NHS ester of the DBCO-NHS while the SPAAC between DBCO and ligand L1-N₃ could also be observed. In initial testing, a modified MCM41 silica was stepwise reacted with DBCO-NHS and the ligand L-N₃. Subsequently, the immobilised ligand was submerged in iron(II) triflate solution and ICP-OES analysis strongly indicates successful formation of the complex C2-N₃ immobilised on MCM41.

In the future, the results obtained with the immobilisation *via* SPAAC should be corroborated by reproducing the experiments and performing additional analysis. As ATR-IR spectroscopy is not able to reveal modifications of the silica within the pores, another method needs to be applied to supplement the EA and ICP-OES data. This could probably be resolved by transmission IR spectroscopy with a higher depth of penetration. In addition, oxidation of the immobilised iron(II) complex needs to be performed to achieve the immobilisation of C4. If the iron(IV)-oxido species shows reactivity to the relatively bulky DBCO linker molecule, the CuAAC should be reinvestigated using copper binding ligands to prevent undesired complex formation. This could also be done for economical reasons, as SPAAC reagents like DBCO-NHS are significantly more expensive.

VI. Experimental

1. General Considerations

Chemical structures, names and properties

Chemical structures were drawn using Chemdraw Professional v19.1.1.2. The names of molecules and general analytical data like chemical formulas, molecular mass, exact mass (of molecules and fragments) and expected elemental analysis were also obtained by using the Chemdraw software.

Literature

For synthetic procedures, relevant citations are given with the title. This includes syntheses which were performed in accordance with literature, inspired by or modified from literature or a general overview of literature procedures regarding that type of reaction.

Reaction Conditions

In regard of this work aiming towards the FAIR data principles (Chapter I2), it was attempted to avoid commonly used, but unspecific terms like *overnight* and *room temperature* (r.t.). However, as this was not implemented at the beginning, but within the time frame of this work, some reactions and experiments were not recorded accordingly. In these cases, a time or temperature range is given in the reaction, which is an estimation based on standard procedures, habits and experience. It should be noted, that the given ranges are most likely, but not necessarily the true conditions of the reaction. Such estimations are marked with a footnote. For some reactions, no proper estimations could be made and thus the unspecific terms were kept.

Experimental Procedures

The expression 'solvents removed *in vacuo*' refers to the solvent of a solution or suspension being removed using a rotary evaporator. Heating baths were set to 40 °C and water cooling at either approx. 20 °C or 4 °C was used. Afterwards, the resulting substance was additionally dried using the Schlenk line for approx. 2-4 h. The expression 'dried *in vacuo*' refers to the substance being dried with the Schlenk line for a considerable longer time ranging from 6-24 h. Reactions which require heating or reflux were performed using Heidolph Heat-On Blocks and Heidolph waterless Findensers for solvent condensation.

Solvent purity

Due to changing offers, prices and university infrastructures, solvents were bought in different purities at different times. In case solvents were bought in technical instead of p.a. quality, dichloromethane, *i*-hexane, diethyl ether and chloroform were distilled *via* rotary evaporation before use. All reactions and washing steps with water described in this work were performed with ultrapure water (type 1, 18.2 M Ω -cm at 25 °C).

2. Methods and Materials

Schlenk Conditions

In this work, reactions under inert atmosphere were performed using a Schlenk line apparatus attached to a RZ6 rotary vane pump by vacuubrand or similar and using a cooling trap submerged into liquid nitrogen. As inert gas, in-house nitrogen which was additionally channelled through a DrieriteTM gas-drying unit was used. Glassware and stirring bars used in these reactions were dried by heating while applying vacuum and subsequently flushing with nitrogen. These steps were repeated three times. All reaction flasks had a glass stopcock with an olive used for the connection to the Schlenk line and a conical ground joint, which was either sealed with a rubber septa or condenser. Liquids were transferred using syringes and cannula, which were flushed with inert nitrogen three times prior to use. Solids were added against a steady stream of nitrogen.

Thin-layer chromatography

Thin-layer chromatography (TLC) was performed on aluminium sheets pre coated with silica gel (pore size = 60 Å) with fluorescent indicator F254 from Merck KGaA. Compound spots were detected using a UV light at $\lambda = 254$ nm and 365 nm. TLC plates were bought as 20x20 cm sheets and cut by hand. TLC was performed on plates with a length (direction of flow) of 6 cm, substances were applied at a distance of 1 cm to the bottom and the chromatography was stopped when the solvent front was approx. 0.5-1 cm from the top edge. Resulting in a travel distance of approx. 4-4.5 cm for the mobile phase.

Flash Column Chromatography

Flash column chromatography was performed on an Interchim PuriFlash PF420 or Interchim PuriFlash XS 520+ system using self-packed columns with silica gel 60 (40-63 μ m) from Merck or Macherey-Nagel. If flash column chromatography was performed by hand, self-packed glass columns and a manual air pump bulb were used. Solvents and gradients are given within the experimental procedure. Fractions were collected in glass tubes and combined according to TLC. Solvents of the collected fractions were removed and the resulting product was dried *in vacuo*.

Infrared Spectroscopy

IR measurements were performed on either a Jasco FT/IR-460Plus or PerkinElmer Spectrum Two FT/IR spectrometer with an ATR Diamond Plate. In case of the Jasco FT/IR-460Plus the software Spectra Manager Version 2 from Jasco was used for data conversion. All spectra shown within this work were processed using Microsoft Excel to open and convert data into a format that can be copied and subsequently processed with Origin 2021b. First, the spectra were corrected by baseline subtraction (mode: 2.derivation, smoothing factor=3, threshold=0.05, points=12, interpolation=Spline;

points were manipulated by hand and an additional baseline subtraction of -100 was used) and subsequently smoothed (mode: Savitzky-Golay, points=25, polynomial order 2). The described method was used for all graphs depicted within this thesis if not mentioned otherwise.

Nuclear Magnetic Resonance Spectroscopy

Nuclear Magnetic Resonance Spectroscopy (NMR) measurements were performed on either a Jeol ECP 270 (400 MHz), Jeol ECX 400 (400 MHz) or Bruker Avance III (400 MHz) at the Department of Chemistry at LMU Munich (^1H at 400 MHz, ^{13}C at 100 MHz) or on either a Bruker Avance III - 300 (300 MHz) and Bruker Avance III - 600 (600 MHz) at the Center for Molecular and Structural Analytics at the HHU Düsseldorf (^1H at 300 MHz or 600 MHz, ^{13}C at 150 MHz). All spectra shown within this work were processed using MestReNova v14.2.0-26256. As a general procedure, the included automatic phase and baseline correction tools were applied first. Then, the spectra were referenced to the according solvent^[262] and NMR shifts given in δ units (ppm) relative to CDCl_3 ($\delta_{\text{H}}=7.26$ (1), $\delta_{\text{C}}=77.16$ (3)), CD_3OD ($\delta_{\text{H}}=3.31$ (5), $\delta_{\text{C}}=49.00$ (7)), DMF-d_7 ($\delta_{\text{H}}=8.03$ (1), $\delta_{\text{C}}=163.15$ (3)), D_2O ($\delta_{\text{H}}=4.79$ (1)), DMSO-d_6 ($\delta_{\text{H}}=2.50$ (5), $\delta_{\text{C}}=39.52$ (7)) or MeCN-d_3 ($\delta_{\text{H}}=1.94$ (5), $\delta_{\text{C}}=118.26$ (1)). After these initial steps, peak picking, integration and multiplett analysis were done by hand to the best of knowledge. Signal multiplicities were characterized as singlet (s), doublet (d), triplet (t), quartet (q), multiplett (m), broad (br) and combinations thereof. For peak assignment of new structures, additional two-dimensional correlation spectroscopy (COSY, 1H-1H), heterobinuclear multiple quantum correlation (HMQC, 1H- ^{13}C) or heterobinuclear multiple bond connectivity (HMBC, 1H- ^{13}C) experiments were performed. Signals were assigned according to the numbering given in the reaction scheme within the experimental procedure for each molecule.

UV-Vis Spectroscopy

UV-Vis spectroscopy was performed on either an Agilent 8453 Diode Array spectrophotometer, an Agilent Cary 300 or an Agilent Cary 3500 Multicell spectrometer using 10 mm quartz Suprasil cuvettes from Hellma. All instruments were equipped with a thermostatted cuvette holder. Spectra were measured at room temperature if not stated otherwise. Data was exported in a csv. file format and processed using Microsoft Excel to open and convert data into a format that can be copied and subsequently processed with Origin 2021b.

Single Crystal X-Ray Diffraction

Single crystal X-ray diffraction at LMU Munich was performed by Dr. Peter Mayer or Jonathan Gutenthaler-Tietze on a Bruker D8 Venture TXS system equipped with a multilayer mirror monochromator and a rotating anode X-ray tube ($\text{Mo K}\alpha$, $\lambda = 0.71073 \text{ \AA}$). The frames were integrated with the Bruker SAINT software package. Data were cor-

rected for absorption effects using the Multi-Scan method (SADABS). The structure was solved and refined using the Bruker SHELXTL Software Package.^[263]

Single crystal X-ray diffraction at HHU Düsseldorf was performed by Jonathan Gutenthaler-Tietze on a Rigaku XtaLAB Synergy S diffractometer equipped with a hybrid pixel array detector and a PhotonJet microfocus sealed X-ray tube (Cu K α , $\lambda = 1.54184 \text{ \AA}$). Data were collected and processed using CrysAlisPro with multi-scan absorption correction. Structure solution was performed with SHELXT (2018/2), refinement with SHELXL (2019/2) in ShelXle, and validation with PLATON.

Thermal ellipsoid plots were generated using ORTEP-3.

High Resolution Mass Spectrometry

High resolution mass spectrometry (HR-MS) used for product identification was performed either on a Thermo Finnigan LTQ FT Ultra Fourier Transform Ionen Cyclotron Resonance (ESI), a Thermo Finnigan LTQ Orbitrap XL spectrometer (ESI), Thermo Q Exactive GC Orbitrap-Mass spectrometer (EI) or Finnigan MAT 95 sector mass spectrometer (EI) at the Department of Chemistry at LMU Munich. Solid samples were dissolved in either acetonitrile or acetone. Data was received as a printout with indicated masses belonging to the target molecule.

Low Resolution Mass Spectrometry

Low-resolution mass spectrometry (LR-MS) was performed on either an Agilent 1100 SL system (G1313A ALS, G1316A COLCOM, G1316A VWD, G1312A Bin Pump) coupled to a Bruker Daltonik HCTultra PTM Discovery system (ESI mode) *via* direct injection using a water/methanol eluent mixture (1:1) with 0.1 % formic acid at LMU Munich or an Agilent 1260 Infinity II HPLC (G7115A DAD, G7116A Column Thermostat, G7167A Multiple Sampler, G7104C Flexible Pump) with an MSD XT Detector *via* direct injection using a water/acetonitrile eluent mixture (1:1) with 0.1 % formic acid. All used solvents were LC-MS grade. Measurements were primarily performed as reaction controls and are not necessarily shown within this thesis. Any data shown in this thesis was processed and analysed with Hystar Data Analysis.

Inductively Coupled Plasma Optical Emission Spectrometry

Inductively Coupled Plasma Optical Emission Spectrometry (ICP-OES) was conducted on an Agilent ICP-OES 5800 by Annette Ricken at HHU Düsseldorf. Probes were digested in a microwave (Temp. 200 °C, Ramp time 45 min, Hold time 45 min, max. Power 1600 W) using an acidic mixture (1.4 mL HNO₃, 0.4 mL HCl, 0.2 mL HBF₄). A silicon standard (2% HNO₃ + 0.05% HF, 1000 mg/L, 'tracecert', Merck Supelco) in different concentrations (0.25 mg/L, 0.50 mg/L and 1.00 mg/L in 2% HNO₃) was used as reference for silicon measurements and an multi element standard (HNO₃, 100 mg/L,

'certipure', Merck Supelco) in different concentrations (0.05 mg/L, 0.10 mg/L, 0.50 mg/L and 1.00 mg/L in 2% HNO₃) was used as a reference for iron measurements.

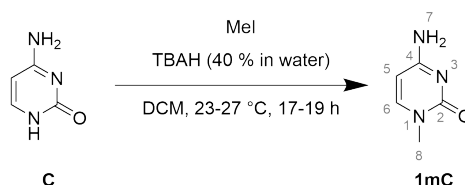
Lyophilisation

Lyophilisation was performed on a Christ Alpha 1-2 LDplus lyophilisator attached to a vacuubrand Vacuu Pure 10C screw pump or a Christ Alpha 3-4 LSCbasic. Samples were frozen in centrifuge tubes which were sealed using lint-free wipes and parafilm prior to lyophilisation.

3. Experimental Procedures

3.1. Epigenetic Substrates

Synthesis of 4-amino-1-methylpyrimidin-2(1*H*)-one (1mC)^[122,123]



Cytosine (**C**) (555 mg, 5.00 mmol, 1.0 equiv.) was suspended in dichloromethane (35 mL). Tetrabutylammonium hydroxide solution (40 % in water, 3.30 mL) was added dropwise to the suspension. Methyl iodide (1.25 mL, 20.0 mmol, 4.0 equiv.) was slowly added to the resulting solution. The mixture was stirred at room temperature (23-27 °C¹) overnight (17-19 h²) forming a white precipitate. Water (20 mL) was added to the suspension, the aqueous phase was separated and washed with dichloromethane (20 mL). The solvent was removed *in vacuo* and the resulting white solid was triturated with hot ethanol, cooled to room temperature (23-27 °C¹), filtered and dried *in vacuo* resulting in 1mC (438 mg, 3.50 mmol, 70 %) as a white solid.

Chemical Formula C₅H₇N₃O (125.13 g/mol⁻¹).

¹H NMR (400 MHz, DMSO-d₆) δ/ppm = 7.55 (d, *J* = 7.1 Hz, 1H, H-6), 6.92 (m, br, 2H, H-7), 5.61 (d, *J* = 7.1 Hz, 1H, H-5), 3.19 (s, 3H, H-8).

¹³C NMR (100 MHz, DMSO-d₆) δ/ppm = 166.1 (C-4), 156.3 (C-2), 146.6 (C-6), 92.9 (C-5), 36.6 (C-8).

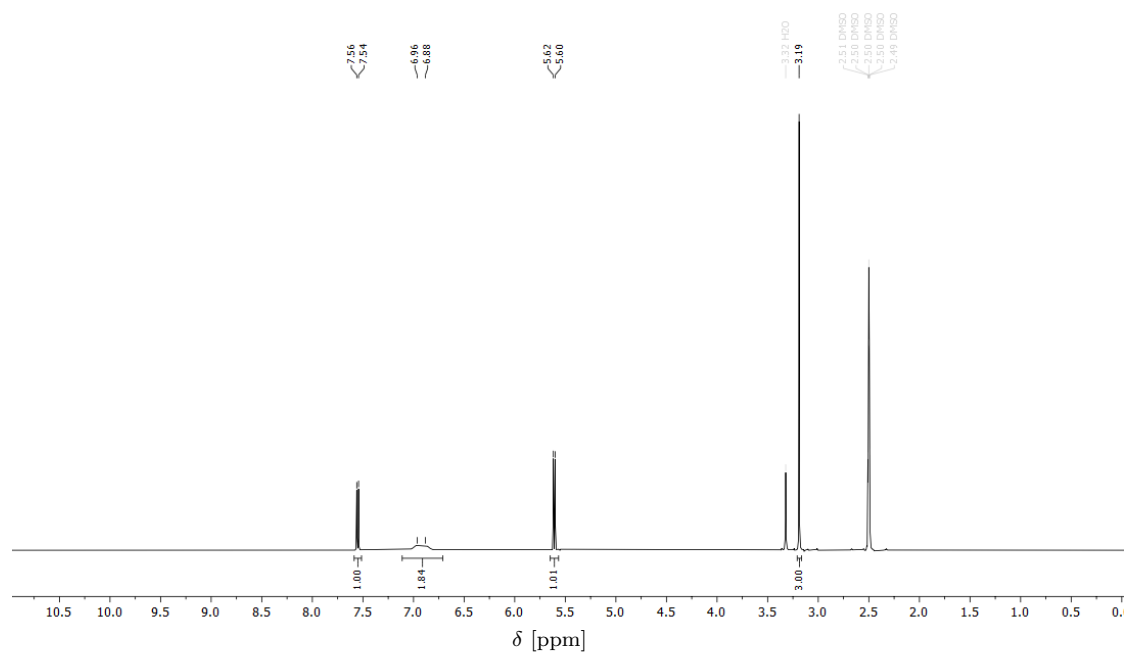
HR-MS (EI) calc. for C₅H₇N₃O⁺: 125.0584 [M]⁺
found: 125.0585 [M]⁺.

Elemental Analysis found (calc.) C 46.73 (47.99), H 5.54 (5.64), N 32.58 (33.58).

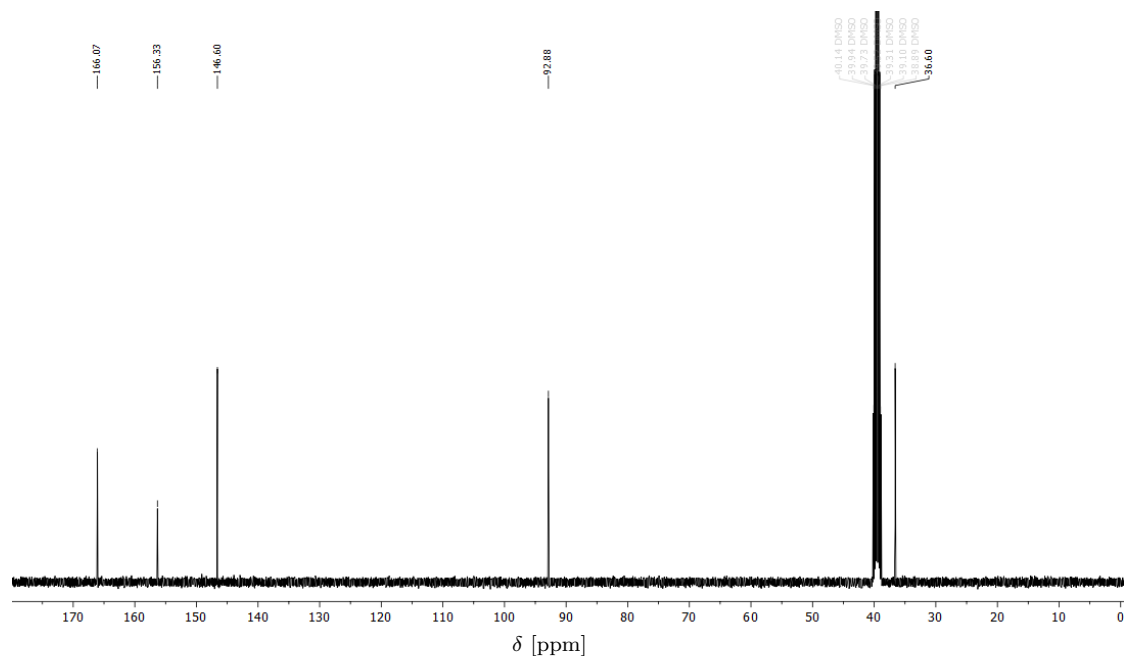
¹Estimated temperature. See Chapter VII-Reaction Conditions.

²Estimated time frame. See Chapter VII-Reaction Conditions.

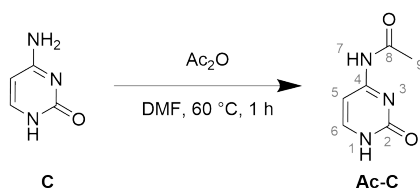
^1H NMR (400 MHz, DMSO- d_6)



^{13}C NMR (100 MHz, DMSO- d_6)



Synthesis of *N*-(2-oxo-1,2-dihydropyrimidin-4-yl)acetamide (Ac-C)³



Cytosine (**C**) (278 mg, 2.50 mmol, 1.0 equiv.) was suspended in dry dimethylformamide. Acetic anhydride (260 μ L, 2.75 mmol, 1.1 equiv.) was added dropwise. The resulting mixture was stirred in a preheated oil bath at 60 °C for 1 h. After cooling to room temperature, the white solid was filtered off and washed with methanol. Drying under high vacuum afforded Ac-C (293 mg, 1.91 mmol, 77 %) as a white solid.

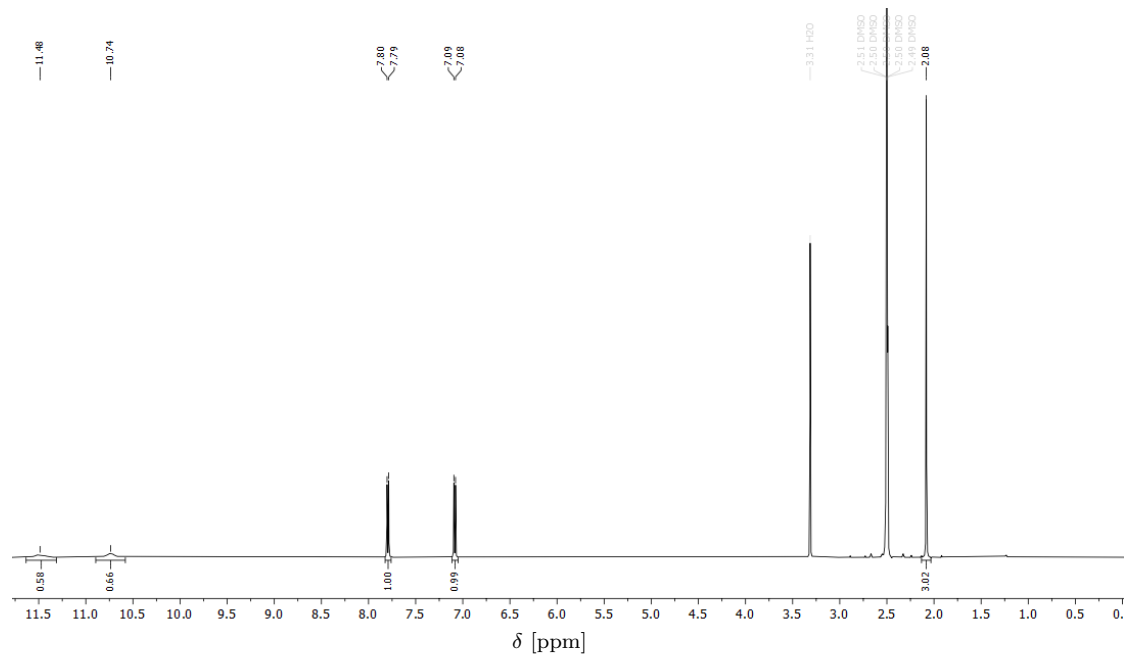
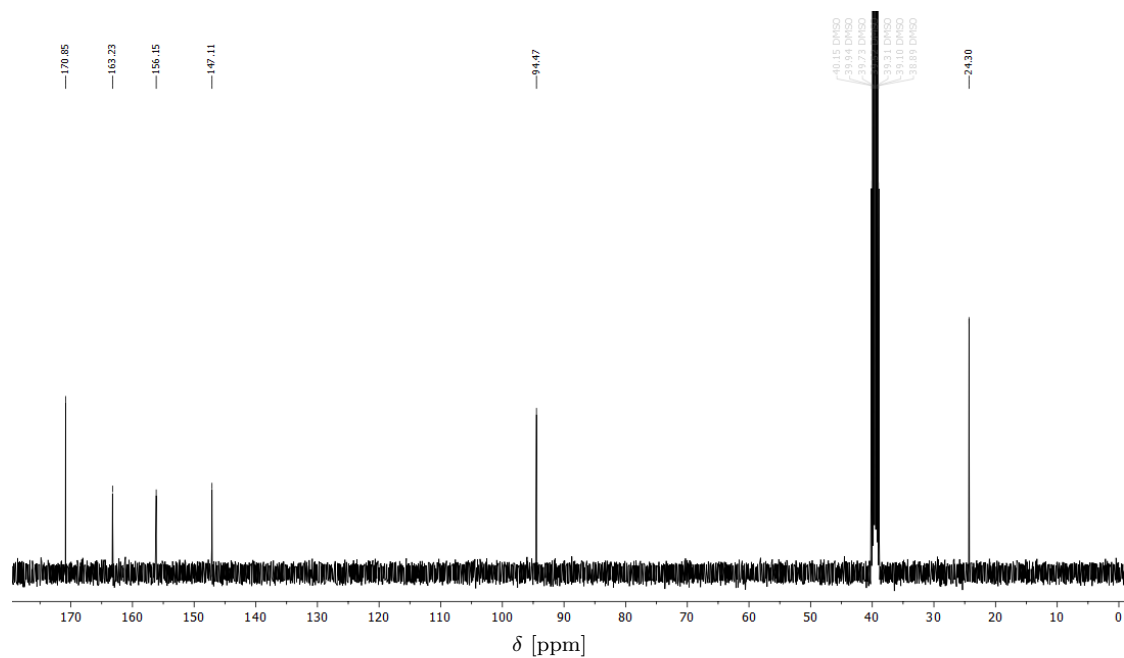
Chemical Formula C₆H₇N₃O₂ (153.14 g/mol⁻¹).

¹H NMR (400 MHz, DMSO-d₆) δ /ppm = 11.48 (s, 1H, H-1/7), 10.73 (s, 1H, H-1/7), 7.79 (d, J = 7.0 Hz, 1H, H-6), 7.09 (d, J = 7.0 Hz, 1H, H-5), 2.08 (s, 3H, H-9).

¹³C NMR (100 MHz, DMSO-d₆) δ /ppm = 170.9 (C-8), 163.2 (C-4), 156.2 (C-2), 147.1 (C-6), 94.5 (C-5), 24.3 (C-9).

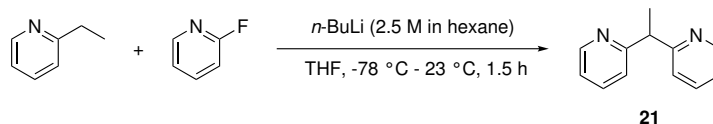
HR-MS (EI) calc. for C₆H₇N₃O₂⁺: 153.0533 [M]⁺
found: 153.0533 [M]⁺.

³This reaction was adapted from a previously performed procedure by Doreen Reuter during an internship under the supervision of Niko Lindlar (né Jonasson).

^1H NMR (400 MHz, DMSO- d_6) ^{13}C NMR (100 MHz, DMSO- d_6)

3.2. Synthesis of Py₅Me₂CH₂X type Ligands (L1-X)

Synthesis of 2,2'-(ethane-1,1-diyl)dipyridine^[124,213,264,265] (**21**)

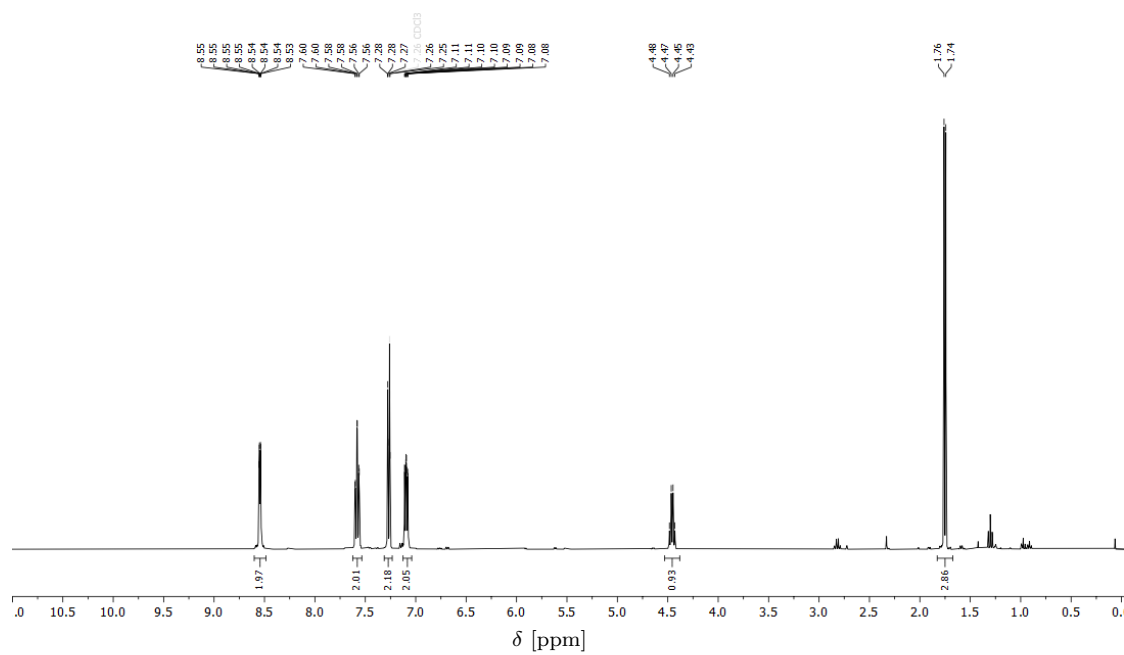


Under Schlenk conditions a flask was charged with 2-ethylpyridine (2.34 g, 2.50 mL, 21.9 mmol, 2.1 equiv.) and absolute tetrahydrofuran (30 mL). The mixture was cooled in an acetone dry-ice bath and a solution of n-butyllithium in hexanes (10.5 mL, 25.3 mmol, 2.5 equiv.) was added dropwise, turning the solution dark red. The mixture was stirred while cooling for 20 min, before 2-fluoropyridine (1.02 g, 0.90 mL, 10.5 mmol, 1.0 equiv.) was added dropwise. After the mixture was stirred for another 10 min, the mixture was allowed to warm to ambient temperature. The mixture was stirred for 1 h, before ~40 g ice were added and the mixture was stirred until the ice was completely melted. The layers were separated and the aqueous layer was extracted with dichloromethane (3x50 mL). The combined organic layers were dried over anhydrous magnesium sulfate. The solvents were removed *in vacuo* and excess 2-ethylpyridine was evaporated using a Schlenk line. **21** (1.60 g, 8.70 mmol, 83 %) was obtained as a viscous brown oil.

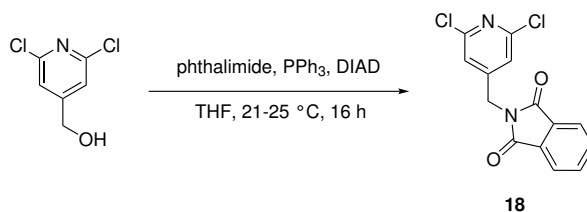
Chemical Formula C₁₂H₁₂N₂ (184.24 g/mol⁻¹).

¹H NMR (400 MHz, CDCl₃) δ/ppm = 8.54 (ddd, *J* = 4.9 Hz, 1.9 Hz, 1.0 Hz, 1H), 7.58 (td, *J* = 7.7 Hz, 1.9 Hz, 1H), 7.30 – 7.23 (m, 1H), 7.09 (ddd, *J* = 7.5 Hz, 4.9 Hz, 1.2 Hz, 1H), 4.46 (q, *J* = 7.2 Hz, 1H), 1.75 (d, *J* = 7.2 Hz, 2H).

^1H NMR (400 MHz, CDCl_3)



Synthesis of 2-((2,6-dichloropyridin-4-yl)methyl)isoindoline-1,3-dione (**30**)^[124]



(2,6-dichloropyridin-4-yl)methanol (1.00 g, 5.62 mmol, 1.0 equiv.), phthalimide (990 mg, 6.74 mmol, 1.2 equiv.) and triphenylphosphine (1.77 g, 6.74 mmol, 1.2 equiv.) were dissolved in tetrahydrofuran (30 mL). After 10 min, diisopropyl azodicarboxylate (1.32 mL, 6.74 mmol, 1.2 equiv.) was added and the reaction mixture was stirred at room temperature (21-25 °C⁴) for 16 h. The precipitate was filtered off, washed with ice cold diethyl ether (3×10 mL) and dried *in vacuo*. **18** (1.43 g, 4.65 mmol, 83 %) was obtained as a colorless solid.

Chemical Formula C₁₄H₈Cl₂N₂O₂ (307.13 g/mol⁻¹).

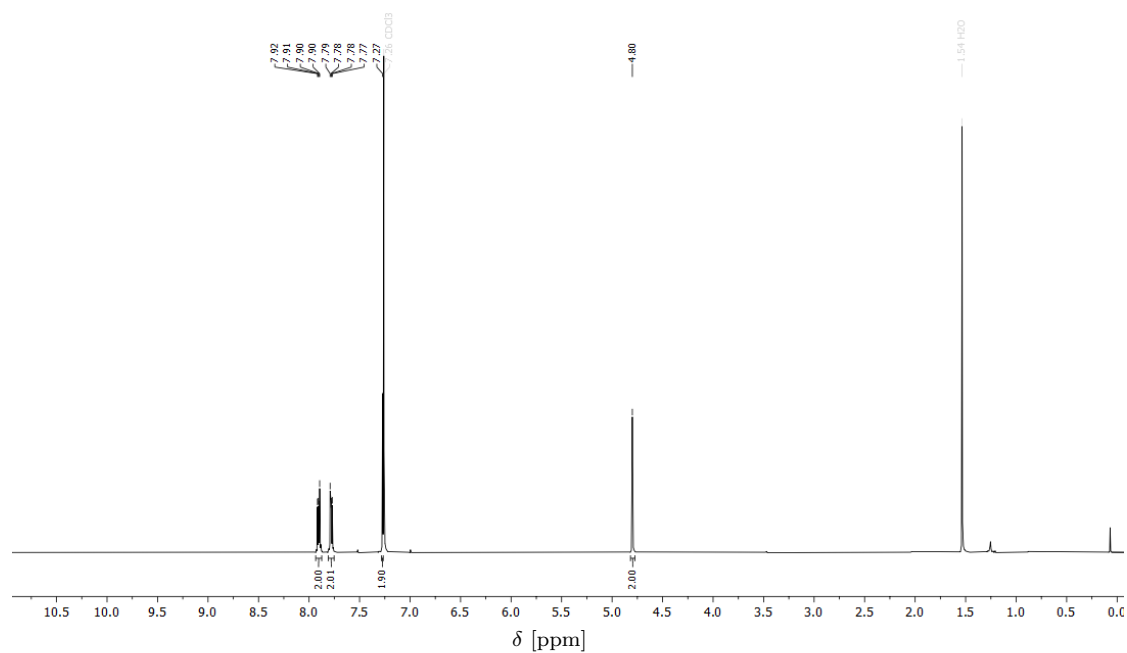
R_f (EtOAc, silica) = 0.89.

¹H NMR (400 MHz, CDCl₃) δ/ppm = 7.91 (dd, *J* = 5.5 Hz, 3.1 Hz, 2H), 7.78 (dd, *J* = 5.5 Hz, 3.1 Hz, 2H), 7.27 (s, 2H), 4.80 (s, 2H).

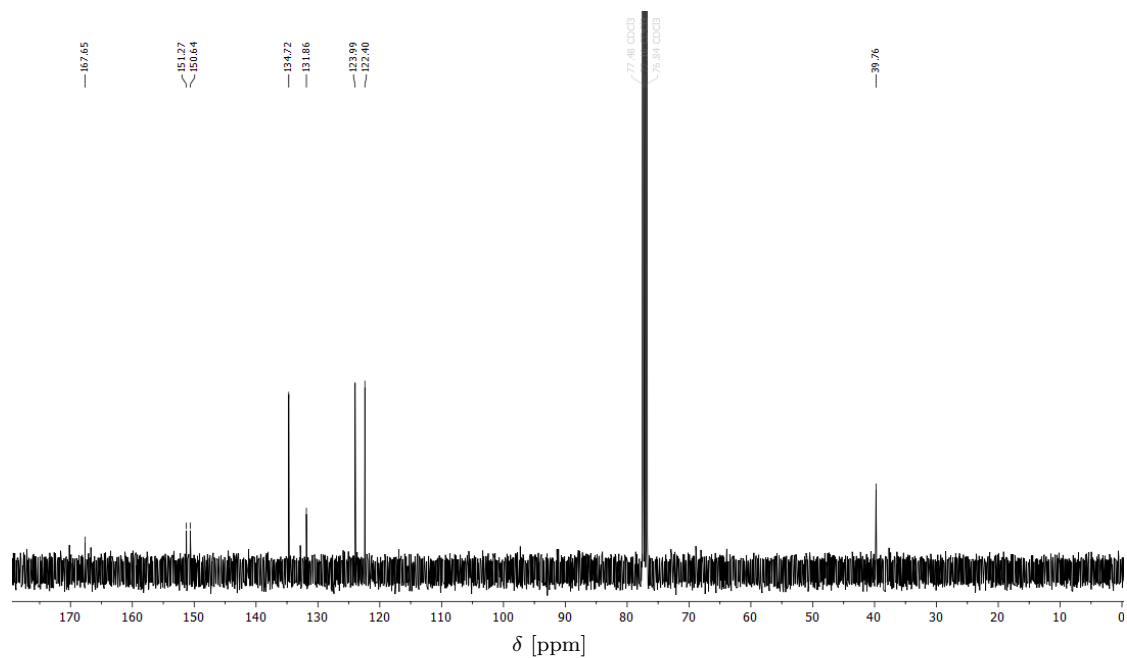
¹³C NMR (100 MHz, CDCl₃) δ/ppm = 167.7, 151.3, 150.6, 134.7, 131.9, 124.0, 122.4, 39.8.

⁴Estimated temperature. See Chapter VII-Reaction Conditions.

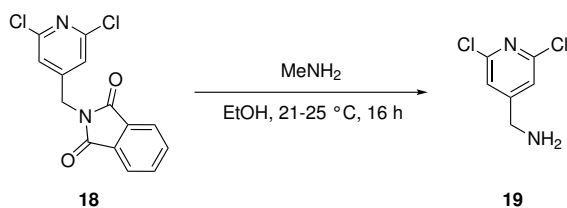
^1H NMR (400 MHz, CDCl_3)



^{13}C NMR (100 MHz, CDCl_3)



Synthesis of (2,6-dichloropyridin-4-yl)methanamine (**19**)^[124]



18 (1.40 g, 4.56 mmol, 1.0 equiv.) was dissolved in a methyl amine solution (33 % in ethanol, 35 mL) and stirred for 16 h at room temperature (21-25 °C⁵). The solvent was removed *in vacuo* leading to a colorless solid which was resolved in 15 % aqueous acetic acid (20 mL) and sonicated for 5 min. Subsequently, the solution was washed with dichloromethane (3×40 mL). The aqueous layer was basified to pH 12 with aqueous sodium hydroxide solution (1 M) and extracted with a mixture of dichloromethane and *iso*-propanol (3:1, 4×50 mL). The organic layer was dried over magnesium sulfate and the solvents were removed *in vacuo*. **19** (670 mg, 3.78 mmol, 83 %) was obtained as a colorless solid.

Chemical Formula C₆H₆Cl₂N₂ (177.03 g/mol⁻¹).

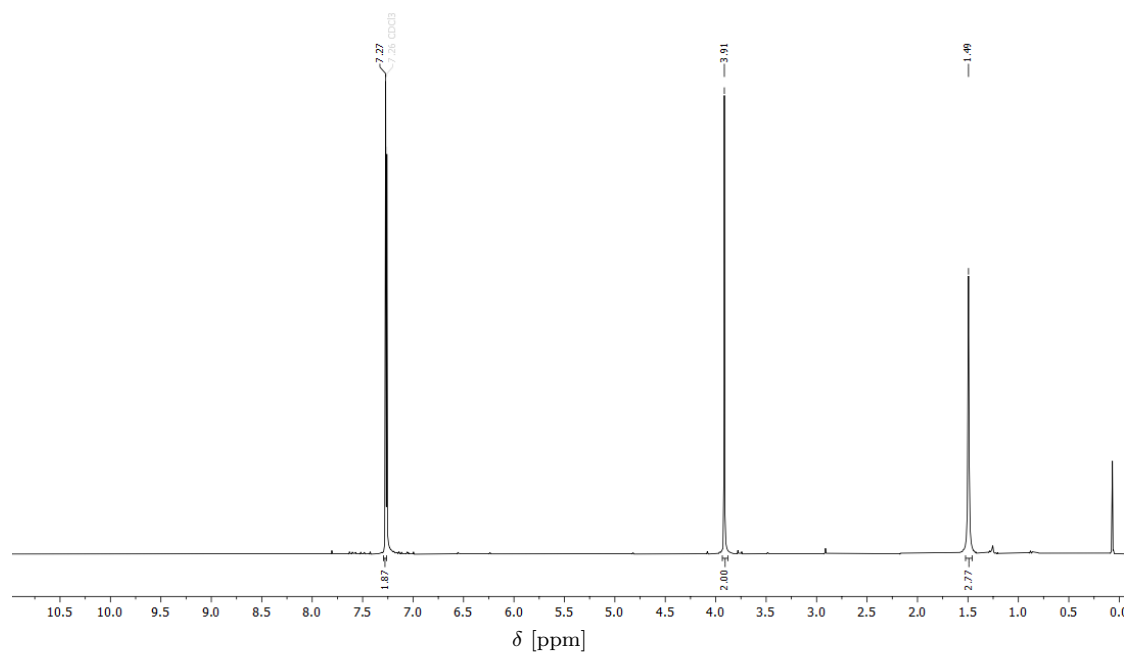
R_f (EtOAc, silica) = 0.09.

¹H NMR (400 MHz, CDCl₃) δ/ppm = 7.27 (s, 2H), 3.91 (s, 2H), 1.41 (s, 2H).

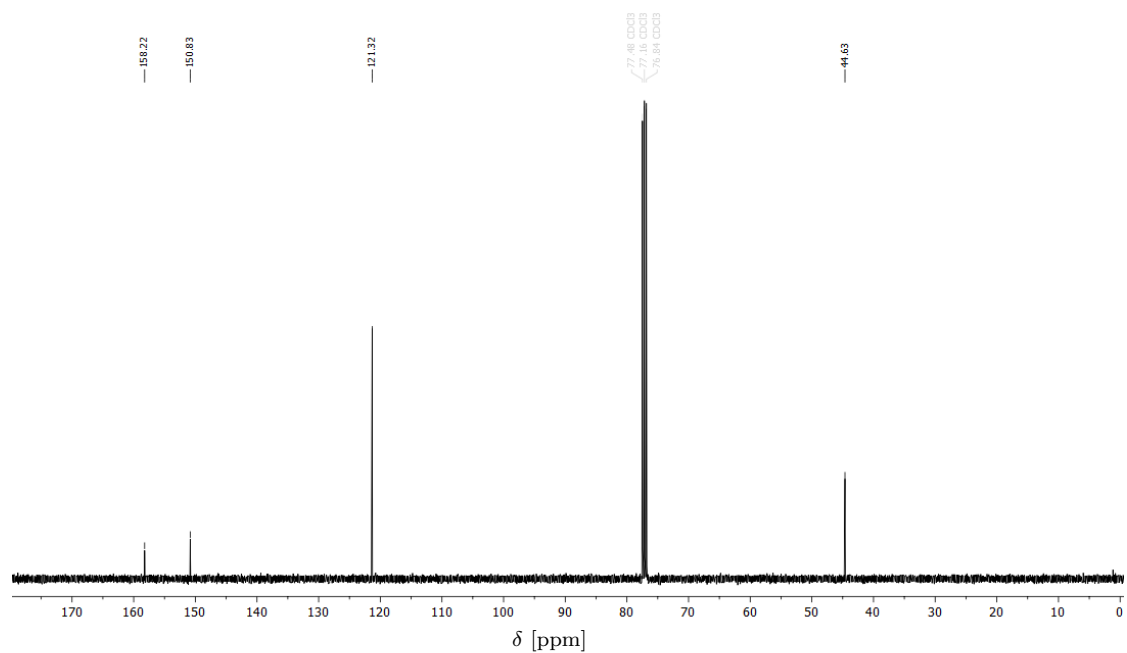
¹³C NMR (100 MHz, CDCl₃) δ/ppm = 158.2, 150.8, 121.3, 44.6.

⁵Estimated temperature. See Chapter VII-Reaction Conditions.

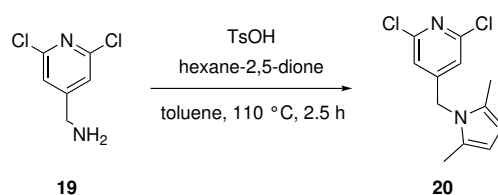
^1H NMR (400 MHz, CDCl_3)



^{13}C NMR (100 MHz, CDCl_3)



Synthesis of 2,6-dichloro-4-((2,5-dimethyl-1*H*-pyrrol-1-yl)methyl)pyridine (**20**)^[89,124]



Under Schlenk conditions a flask was charged with **19** (2.49 g, 14.1 mmol, 1.0 equiv.), *para*-toluenesulfonic acid (242 mg, 1.41 mmol, 0.1 equiv.), powdered molecular sieve (~500 mg) and dry toluene (25 mL). Hexane-2,5-dione (1.95 g, 17.1 mmol, 1.2 equiv.) was added and the solution was heated to 110 °C for 2.5 h. The hot reaction mixture was filtered through a PTFE syringe filter (0.45 µm). The filter was washed with toluene (2 mL) and the solvents were removed *in vacuo*. The solid residue was triturated in a mixture of ethyl acetate and *iso*-propanol (9:1, 15 mL). The filtrate was cooled with an ice-bath for 10 min and the resulting precipitate was filtered off and washed with a mixture of ethyl acetate and propan-2-ol (9:1). The combined solid residues were dried *in vacuo* to give **20** (2.52 g, 9.87 mmol, 70 %) as a white solid.

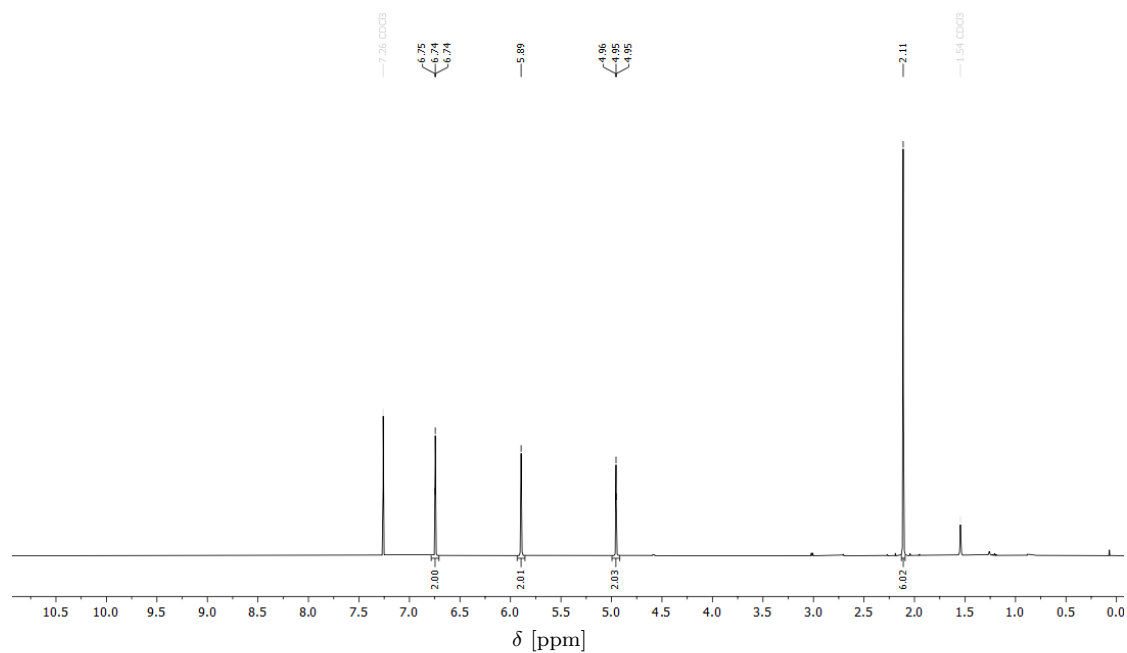
Chemical Formula C₁₂H₁₂Cl₂N₂ (255.14 g/mol⁻¹).

R_f (*i*Hex/EtOAc/NEt₃ 2:2:1, silica) = 0.85.

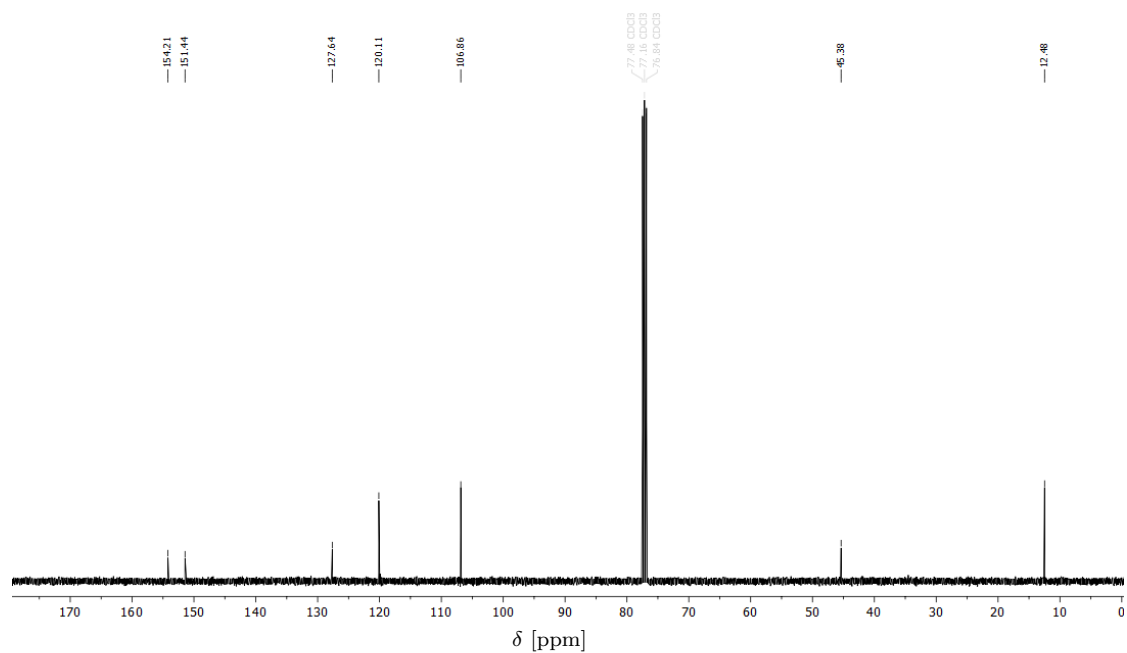
¹H NMR (400 MHz, CDCl₃) δ/ppm = 6.74 (t, *J* = 0.9 Hz, 2H), 5.89 (s, 2H), 4.95 (t, *J* = 0.8 Hz, 2H), 2.11 (s, 6H).

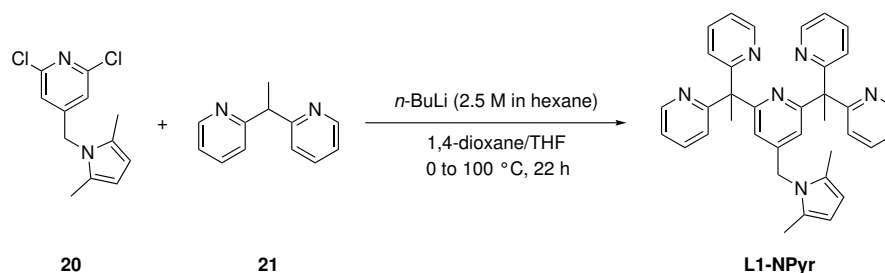
¹³C NMR (100 MHz, CDCl₃) δ/ppm = 154.2, 151.4, 127.6, 120.1, 106.9, 45.4, 12.5.

^1H NMR (400 MHz, CDCl_3)



^{13}C NMR (100 MHz, CDCl_3)



Synthesis of L1-NPyr^[89,124]

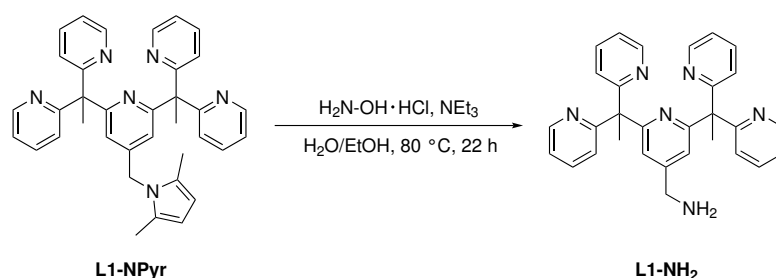
Under Schlenk conditions **21** (1.26 g, 6.82 mmol, 3.0 equiv.) was dissolved in dry 1,4-dioxane (17 mL) and dry tetrahydrofuran (1 mL). The solution was cooled with an ice-bath and *n*-butyl lithium (2.5 M in hexane, 3.2 mL, 7.96 mmol, 3.5 equiv.) was added slowly. After stirring for 45 min, **20** (580 mg, 2.27 mmol, 1.0 equiv.) was dissolved in dry 1,4-dioxane (1 mL) and dry tetrahydrofuran (1 mL) under Schlenk conditions and transferred into the reaction mixture. The deep red mixture was stirred for 5 min and then heated to 105 °C for 22 h under reflux and nitrogen atmosphere. The solution was left to cool to ambient temperature and diluted with ethyl acetate (20 mL). Ice (~5 g), and after stirring for 30 min water (50 mL) was added. The layers were separated and the organic layer was washed with water (20 mL) and brine (10 mL). The aqueous layers were combined and extracted with dichloromethane (3×50 mL). The combined organic layers were dried over magnesium sulfate and the solvents were removed *in vacuo*. The crude product was purified by flash column chromatography (silica, gradient from 0 % NEt₃ and 10 % EtOAc to 10 % NEt₃ and 35 % EtOAc in *i*Hex over 3.5 cv, then isocratic for 3.0 cv) to give L1-NPyr (1.07 g, 1.94 mmol, 85 %) as a yellow, highly viscous oil.

Chemical Formula C₃₆H₃₄N₆ (550.71 g/mol⁻¹).

R_f (*i*Hex/EtOAc/NEt₃ 2:2:1, silica) = 0.79.

¹H NMR (400 MHz, CDCl₃) δ/ppm = 8.50 (ddd, *J* = 4.8 Hz, 1.9 Hz, 0.9 Hz, 4H), 7.39 (ddd, *J* = 8.0 Hz, 7.5 Hz, 1.9 Hz, 4H), 7.04 (ddd, *J* = 7.5 Hz, 4.8 Hz, 1.1 Hz, 4H), 6.78 (dt, *J* = 8.1 Hz, 1.0 Hz, 4H), 6.47 (t, *J* = 0.9 Hz, 2H), 5.67 (s, 2H), 4.84 (t, *J* = 0.9 Hz, 2H), 2.14 (s, 6H), 1.99 (s, 6H).

¹³C NMR (100 MHz, CDCl₃) δ/ppm = 166.2, 164.9, 148.6, 148.3, 135.6, 127.7, 124.0, 121.1, 117.5, 106.0, 60.2, 46.4, 26.8, 12.5.

Synthesis of L1-NH₂ [89,124]

L1-NPyr (665 mg, 1.21 mmol, 1.0 equiv.) was dissolved in ethanol (8 mL) and water (2 mL). Triethylamine (680 μ L, 4.91 mmol, 4.1 equiv.) and hydroxylamine hydrochloride (2.52 g, 36.3 mmol, 30 equiv.) were added subsequently. The reaction mixture was heated to 80 $^\circ$ C for 22 h, cooled to room temperature and diluted with aqueous hydrochloric acid solution (1 M, 48 mL). The aqueous layer was washed with diethyl ether (3 \times 50 mL), basified to pH 12 with aqueous sodium hydroxide solution (6 M) and extracted with dichloromethane (3 \times 50 mL). The combined organic layers were dried over magnesium sulfate and the solvent was removed *in vacuo*. L1-NH₂ (545 mg, 1.15 mmol, 95 %) was obtained as a pale yellow solid.

Chemical Formula C₃₀H₂₈N₆ (472.60 g/mol⁻¹).

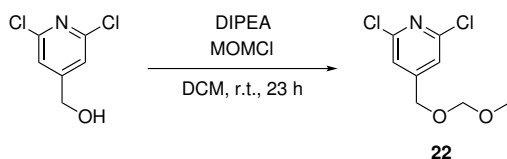
R_f (*i*Hex/EtOAc/NEt₃ 2:2:1, silica) = 0.02.

IR (Diamond-ATR, neat) $\tilde{\nu}$ /cm⁻¹ = 2974, 1599, 1584, 1566, 1562, 1462, 1443, 1431, 1416, 1377, 1357, 1292, 1154, 1107, 1090, 1075, 1046, 992, 925, 879, 837, 807, 773, 759, 745, 681, 668, 649, 637, 616, 559, 546, 532, 513, 405.

¹H NMR (600 MHz, CDCl₃) δ /ppm = 8.50 (ddd, *J* = 4.9, 1.9, 0.9 Hz, 4H), 7.39 (ddd, *J* = 8.0, 7.4, 1.9 Hz, 4H), 7.07 (s, 2H), 7.05 (ddd, *J* = 7.5, 4.8, 1.1 Hz, 4H), 6.83 (dt, *J* = 8.1, 1.0 Hz, 4H), 3.79 (s, 2H), 2.20 (s, 6H).

¹³C NMR (150 MHz, CDCl₃) δ /ppm = 166.3, 164.6, 148.5, 135.7, 124.2, 121.1, 118.5, 60.1, 45.9, 26.9.

Synthesis of 2,6-dichloro-4-((methoxymethoxy)methyl)pyridine (**22**)^[124]



(2,6-dichloropyridin-4-yl)methanol (1.00 g, 5.62 mmol, 1.0 equiv.) was dissolved in dichloromethane (10 mL) and *N,N*-diisopropylethylamine (2.87 mL, 16.9 mmol, 3.0 equiv.) was added. Subsequently, the solution was cooled using an ice-bath and chloromethyl methyl ether (1.07 mL, 14.0 mmol, 2.5 equiv.) was added dropwise. After 1 h the ice bath was removed and the reaction mixture was stirred for additional 23 h. The resulting clear red solution was diluted with dichloromethane (3 mL) and poured into aqueous hydrochloric acid (1.3 M, 30 mL). Stirring for 2 h at room temperature led to a deep yellow mixture. The layers were separated and the aqueous layer was extracted with dichloromethane (3×30 mL). The combined organic layers were dried over magnesium sulfate and the solvent was removed *in vacuo*. The crude product was purified by flash column chromatography (silica, gradient from 5 % to 20 % EtOAc in *i*Hex over 10.0 cv) to give **22** (1.16 g, 5.22 mmol, 93 %) as a colorless oil.

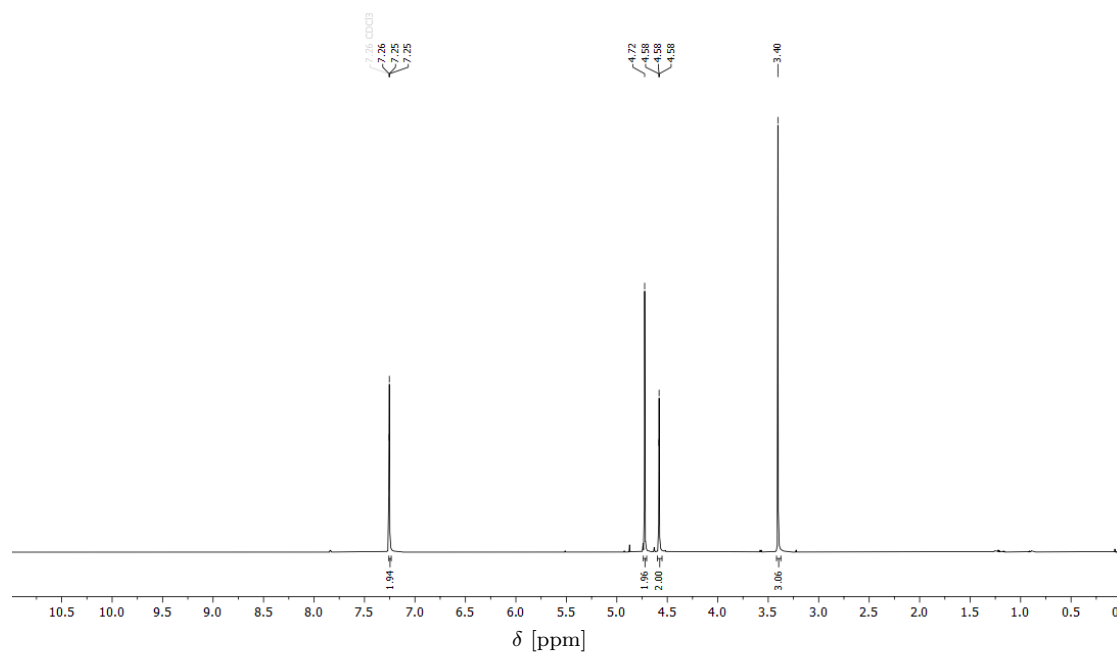
Chemical Formula C₈H₉Cl₂NO₂ (222.07 g/mol⁻¹).

R_f (*i*Hex/EtOAc 1:1, silica) = 0.88.

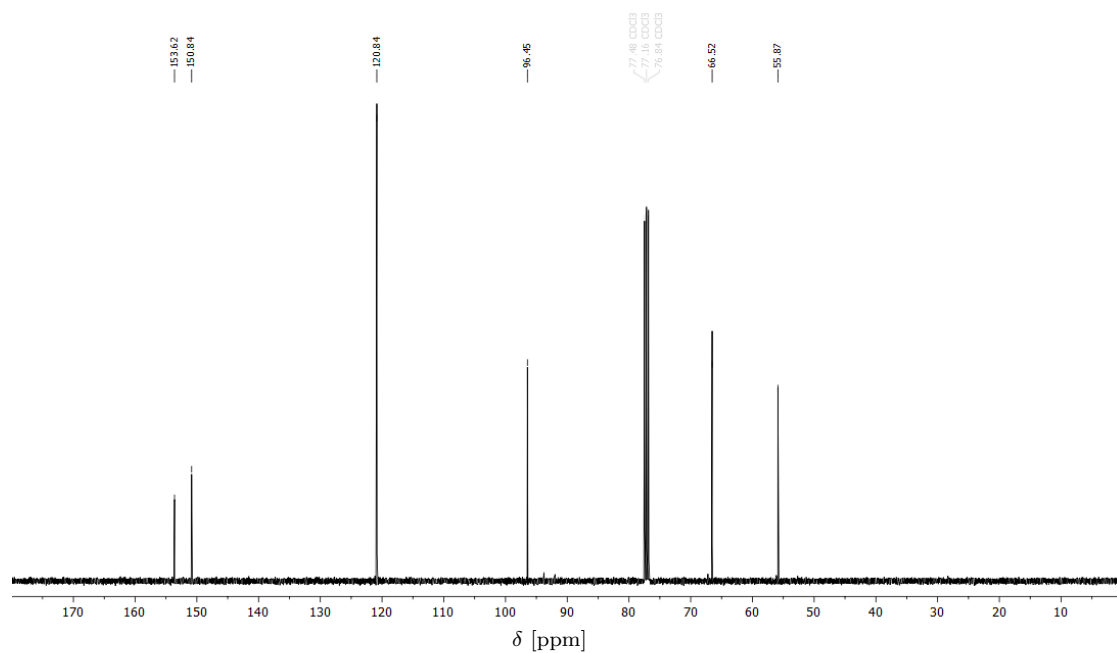
¹H NMR (400 MHz, CDCl₃) δ/ppm = 7.25 (t, *J* = 0.8 Hz, 2H), 4.72 (s, 2H), 4.58 (t, *J* = 0.8 Hz, 2H), 3.40 (s, 3H).

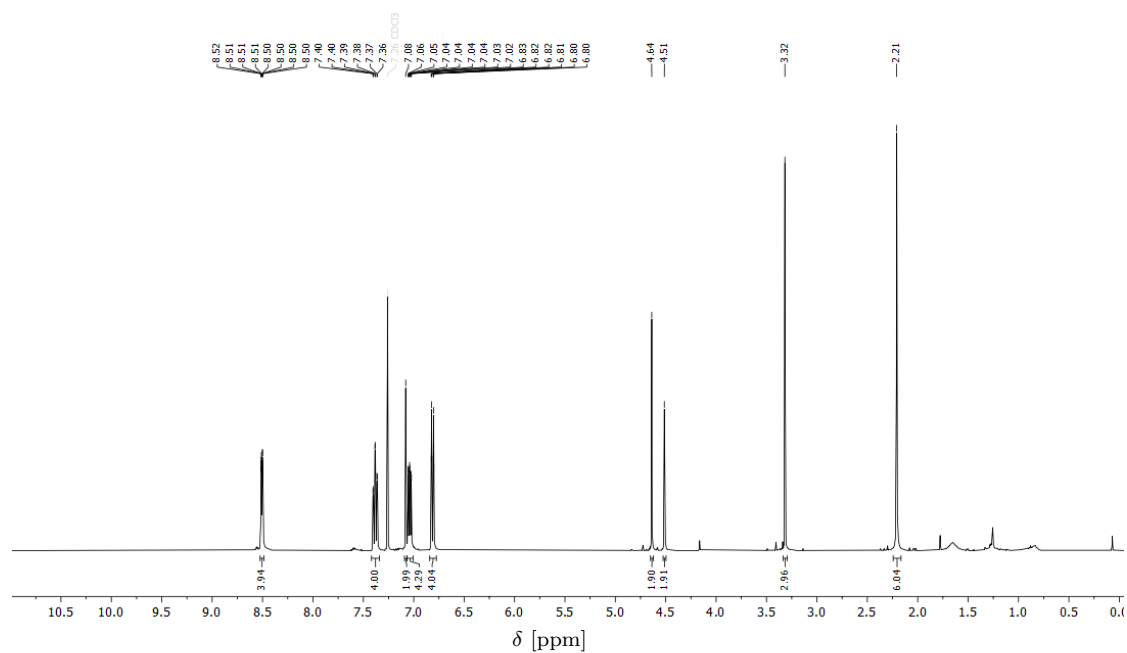
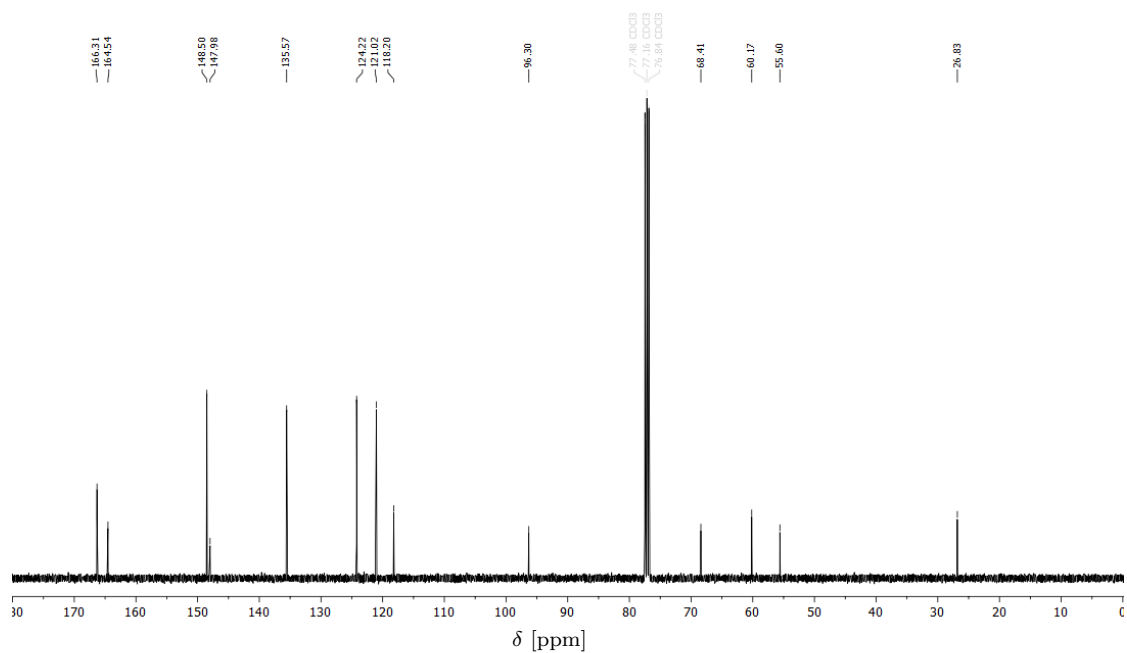
¹³C NMR (100 MHz, CDCl₃) δ/ppm = 153.6, 150.8, 120.8, 96.5, 66.5, 55.9.

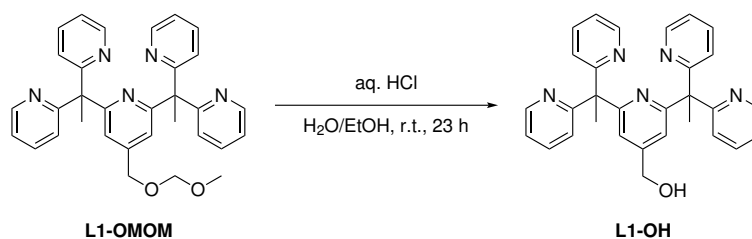
^1H NMR (400 MHz, CDCl_3)



^{13}C NMR (100 MHz, CDCl_3)



^1H NMR (400 MHz, CDCl_3) ^{13}C NMR (100 MHz, CDCl_3)

Synthesis of L1-OH^[124]

L1-OMOM (695 mg, 1.34 mmol, 1.0 equiv.) was dissolved in ethyl acetate (10 mL) and aqueous hydrochloric acid (5 M, 10 mL, 50.0 mmol, 37 equiv.). After stirring for 23 h the solvents were removed *in vacuo*. The crude product was purified by flash column chromatography (silica, gradient from 20 % NEt₃ and 60 % EtOAc to 20 % NEt₃ and 80 % EtOAc in *i*Hex over 10.0 cv) to give L1-OH (381 mg, 805 μmol, 60 %) as a colorless solid.

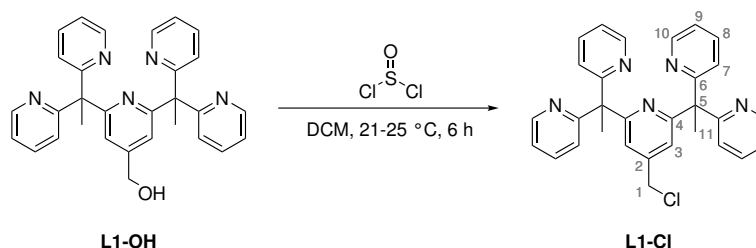
Chemical Formula C₃₀H₂₇N₅O (473.58 g/mol⁻¹).

R_f (*i*Hex/EtOAc/NEt₃ 2:2:1, silica) = 0.22.

IR (Diamond-ATR, neat) $\tilde{\nu}/\text{cm}^{-1}$ = 2995, 2971, 2960, 2928, 2872, 2857, 1729, 1654, 1588, 1566, 1467, 1443, 1427, 1372, 1360, 1350, 1288, 1248, 1152, 1130, 1105, 1089, 1072, 1061, 1047, 1003, 991, 877, 781, 770, 745, 707, 683, 655, 617, 590, 575, 563, 530, 509, 404.

¹H NMR (400 MHz, CD₃OD) δ/ppm = 8.41 (ddd, J = 4.9 Hz, 1.9 Hz, 0.9 Hz, 4H), 7.55 (ddd, J = 8.1 Hz, 7.5 Hz, 1.9 Hz, 4H), 7.19 (ddd, J = 7.5 Hz, 4.9 Hz, 1.1 Hz, 4H), 7.16 (t, J = 0.8 Hz, 2H), 6.82 (dt, J = 8.1 Hz, 1.0 Hz, 4H), 4.56 (s, 2H), 2.17 (s, 6H).

¹³C NMR (100 MHz, CD₃OD) δ/ppm = 167.1, 165.2, 149.1, 137.6, 125.7, 122.7, 118.9, 64.0, 61.1, 27.1.

Synthesis of L1-Cl^[266]

L1-OH (78.0 mg, 165 μmol , 1.0 equiv.) was dissolved in dichloromethane (2.5 mL) and thionyl chloride (50.0 μL , 708 μmol , 4.3 equiv.) was added. The reaction mixture was stirred for 5.5 h at room temperature (21-25 $^\circ\text{C}$ ⁶), washed with saturated aqueous sodium hydrogen carbonate (3 \times 20 mL) and dried over magnesium sulfate. The solvent was removed *in vacuo* and L1-Cl (71.0 mg, 144 μmol , 88 %) was obtained as colorless crystals. The crystals were analyzed by single crystal X-ray crystallography. Details of the crystallographic data can be found in the Appendix (Chapter VII7).

Chemical Formula $\text{C}_{30}\text{H}_{26}\text{ClN}_5$ (492.02 g/mol⁻¹).

R_f (*i*Hex/EtOAc/NEt₃ 2:2:1, silica) = 0.46.

IR (Diamond-ATR, neat) $\tilde{\nu}/\text{cm}^{-1}$ = 3061, 2970, 2936, 2928, 1735, 1588, 1559, 1469, 1446, 1424, 1369, 1312, 1297, 1289, 1277, 1238, 1227, 1205, 1200, 1177, 1152, 1128, 1110, 1101, 1086, 1073, 1046, 1024, 1017, 1009, 992, 961, 946, 914, 823, 783, 763, 744, 714, 699, 692, 680, 668, 658, 653.

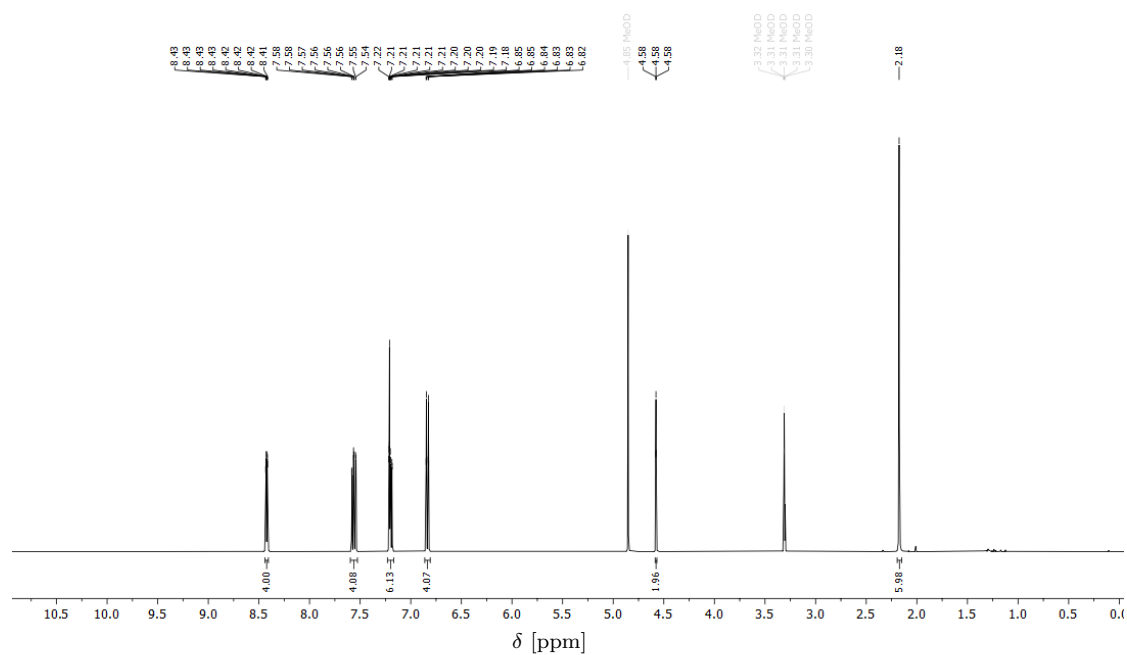
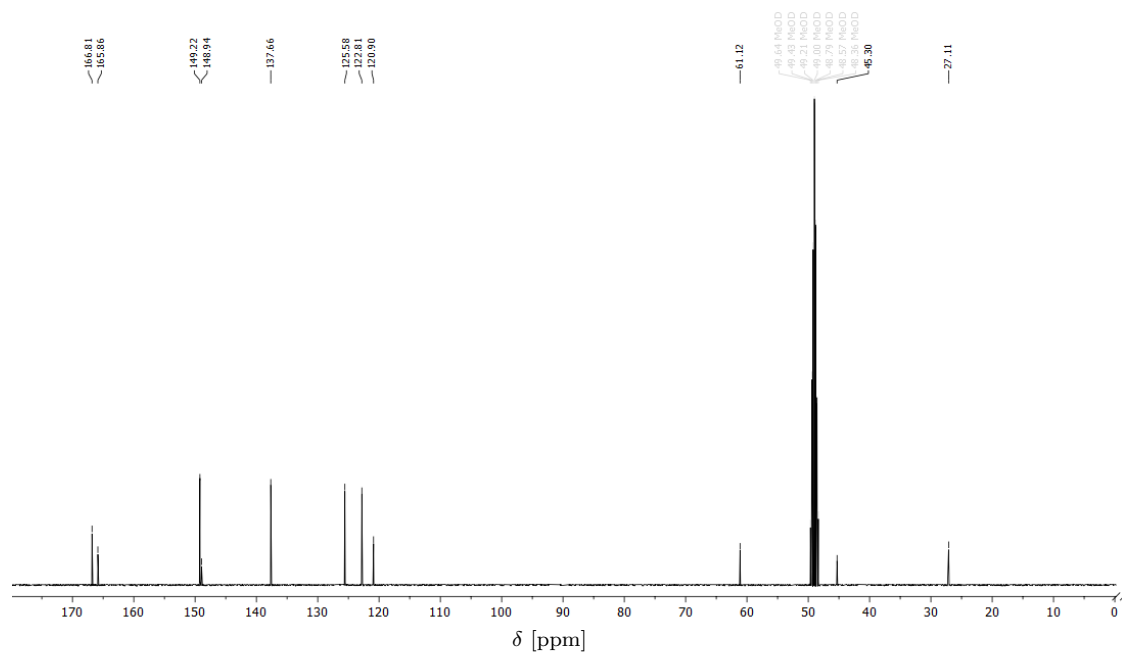
¹H NMR (400 MHz, CD₃OD) δ/ppm = 8.42 (ddd, J = 4.9 Hz, 1.9 Hz, 0.9 Hz, 4H, H-10), 7.56 (ddd, J = 8.1 Hz, 7.5 Hz, 1.9 Hz, 4H, H-8), 7.21 (t, J = 0.5 Hz, 2H, H-3), 7.20 (ddd, J = 7.5 Hz, 4.9 Hz, 1.1 Hz, 4H, H-9), 6.84 (dt, J = 8.1 Hz, 1.0 Hz, 4H, H-7), 4.58 (t, J = 0.6 Hz, 2H, H-1), 2.18 (s, 6H, H-11).

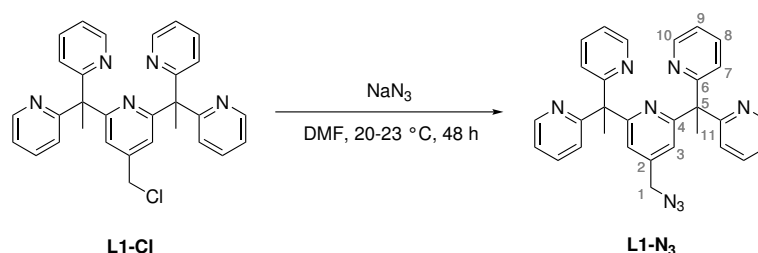
¹³C NMR (100 MHz, CD₃OD) δ/ppm = 166.8 (C-6), 165.9 (C-4), 149.2 (C-10), 148.9 (C-2), 137.7 (C-8), 125.6 (C-7), 122.8 (C-9), 120.9 (C-3), 61.1 (C-5), 45.3 (C-1), 27.1 (C-11).

HR-MS (EI) calc. for $\text{C}_{29}\text{H}_{23}\text{ClN}_5$ ⁺: 476.1637 [M-CH₃]⁺
found: 476.1630 [M-CH₃]⁺.

Elemental Analysis found (calc.) C 72.88 (73.23), H 5.49 (5.33), N 13.31 (14.23).

⁶Estimated temperature. See Chapter VII-Reaction Conditions.

^1H NMR (400 MHz, CD_3OD) ^{13}C NMR (100 MHz, CD_3OD)

Synthesis of L1-N₃

This procedure was part of the Master thesis of Johanna Großmann.

In a 250 mL round bottom flask, L1-Cl (515 mg, 1.04 mmol, 1.0 equiv.) was dissolved in dimethylformamide (45 mL) and sodium azide (136.6 mg, 2.10 mmol, 2.0 equiv.) was added. The reaction mixture was stirred for 48 h at room temperature (20-23 °C⁷). Excess sodium azide was quenched with a solution of sodium nitrite (155 mg) in water (10 mL) and sulfuric acid (1 mL). The mixture was stirred for 4 h in a closed fume hood and then the solvent was removed *in vacuo*. The resulting oil was taken up in ethyl acetate (50 mL) and washed with a mixture of water (50 mL) and aqueous sodium hydrogen carbonate solution (15 mL). The aqueous phase was separated and extracted with ethyl acetate (3x30 mL). The combined organic layers were washed with water (20 mL) and brine (30 mL), dried using a phase separation filter and the solvent was removed *in vacuo*. The solid was dissolved in acetone for recrystallization. After no crystal formation was observed, the solvent was removed *in vacuo* and the resulting oil recrystallized in diethyl ether affording L1-N₃ (505 mg, 1.01 mmol, 97 %) as colorless crystals.

The crystals were analysed by single crystal X-ray crystallography. Details of the crystallographic data can be found in the Appendix (Chapter VII7).

Chemical Formula C₃₀H₂₆N₈ (498.56 g/mol⁻¹).

R_f (*i*Hex/EtOAc/NEt₃ 60:35:5, silica) = 0.46.

IR (Diamond-ATR, neat) $\tilde{\nu}$ /cm⁻¹ = 3055, 3001, 2934, 2872, 2097, 1585, 1564, 1467, 1428, 1366, 1357, 1343, 1290, 1273, 1152, 1128, 1104, 1093, 1084, 1074, 1047, 992, 872, 798, 786, 765, 745, 657, 651, 641, 619, 600, 593, 577, 522.

¹H NMR (600 MHz, CD₃CN) δ /ppm = 8.43 (ddd, *J* = 4.8 Hz, 1.9 Hz, 0.9 Hz, 4H), 7.51 (dddd, *J* = 8.2 Hz, 7.4 Hz, 1.9 Hz, 0.9 Hz, 4H), 7.17 – 7.10 (m, 4H), 7.02 (s, 2H), 6.89 (dd, *J* = 8.0 Hz, 1.3 Hz 4H), 4.33 (s, 2H), 2.11 (s, 6H).

¹³C NMR (150 MHz, CD₃CN) δ /ppm = 166.9, 166.0, 149.1, 146.1, 136.6, 124.7,

⁷Estimated temperature. See Chapter VII-Reaction Conditions.

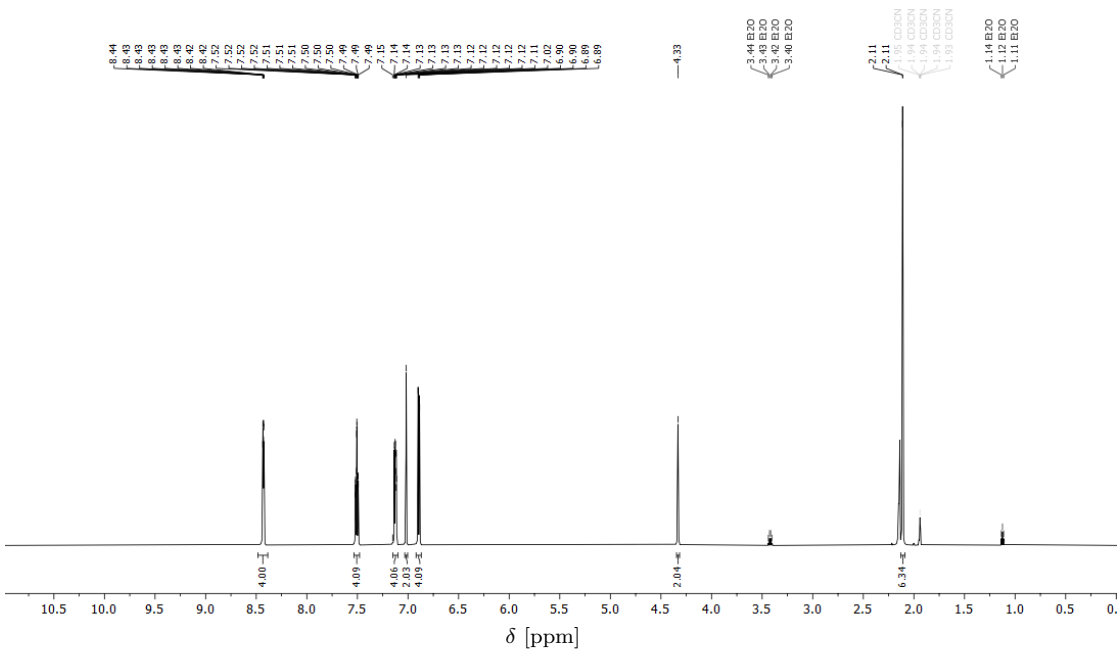
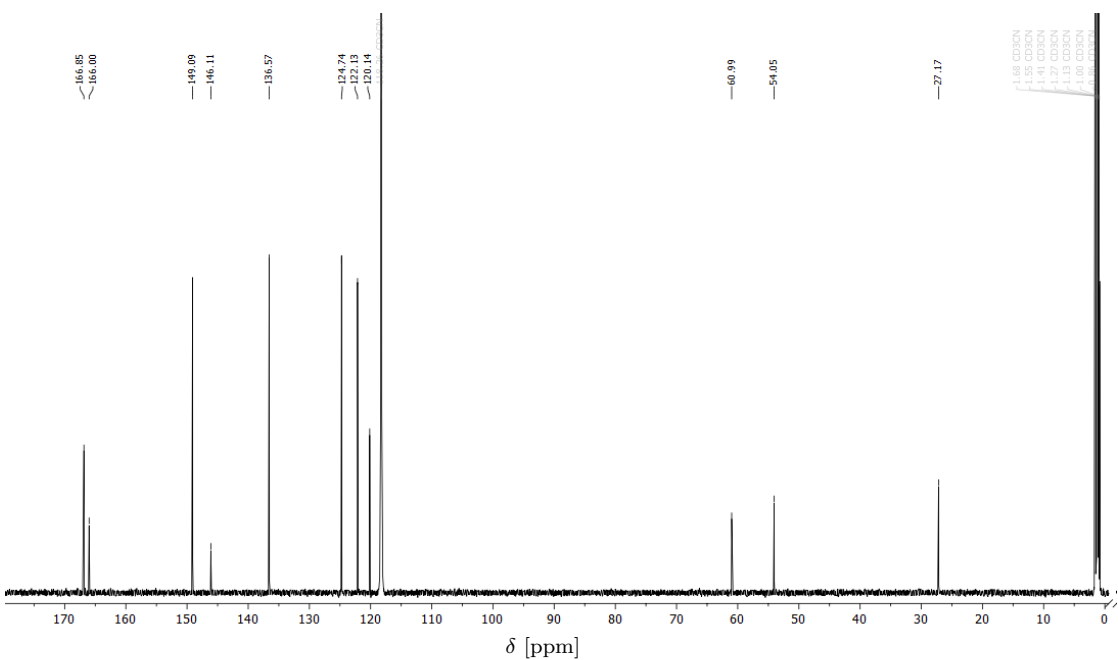
122.1, 120.1, 61.0, 54.1, 27.2.

^1H NMR (600 MHz, CDCl_3)⁸ δ/ppm = 8.51 (ddd, J = 4.8 Hz, 1.9 Hz, 0.9 Hz, 4H, H-10), 7.42 (ddd, J = 7.9 Hz, 7.5 Hz, 1.9 Hz, 4H, H-8), 7.06 (ddd, J = 7.4 Hz, 4.8 Hz, 1.1 Hz, 4H, H-9), 7.01 (t, J = 0.7 Hz, 2H, H-3), 6.85 (dt, J = 8.0 Hz, 1.0 Hz, 4H, H-7), 4.29 (s, 2H, H-1), 2.20 (s, 6H, H-11).

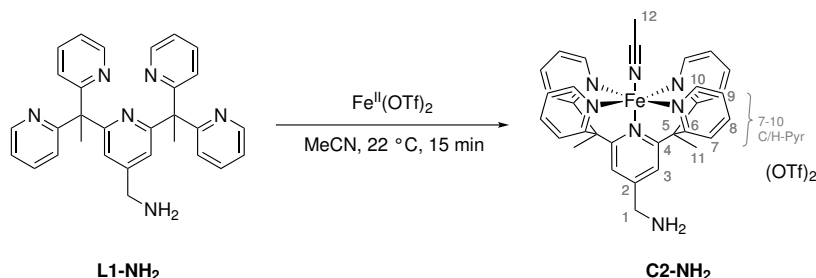
^{13}C NMR (150 MHz, CDCl_3)⁸ δ/ppm = 166.0 (C-6), 165.1 (C-4), 148.6 (C-10), 145.0 (C-2), 135.7 (C-8), 124.0 (C-7), 121.2 (C-9), 118.9 (C-3), 60.2 (C-5), 54.0 (C-1), 26.9 (C-11).

HR-MS (ESI) calc. for $\text{C}_{30}\text{H}_{27}\text{N}_8^+$: 499.2354 $[\text{M}+\text{H}]^+$
found: 499.2359 $[\text{M}+\text{H}]^+$.

⁸Measured with a different reaction batch.

¹H NMR (600 MHz, CD₃CN) ^{13}C NMR (150 MHz, CD_3CN)

3.3. Synthesis of Iron Complexes

Synthesis of C2-NH₂ [89,124]

L1-NH₂ (80.0 mg, 0.17 mmol, 1.0 equiv.) was suspended in acetonitrile (15 mL) at ambient temperature. Iron(II) triflate (60.3 mg, 0.17 mmol, 1.0 equiv.) was added and the mixture stirred for 15 min. The deep red solution was poured through a paper filter and cold diethyl ether (4 °C, 60 mL) was added to the filtered solution until precipitation occurred. The mixture was stirred for 5 min and filtered through a sintered glass frit. The solid was washed with cold diethyl ether and dried *in vacuo* affording C2-NH₂ (96.8 mg, 0.11 mmol, 66 %) as a red-orange powder.

Chemical Formula C₃₄H₃₁F₆FeN₇O₆S₂ (867.62 g/mol⁻¹).

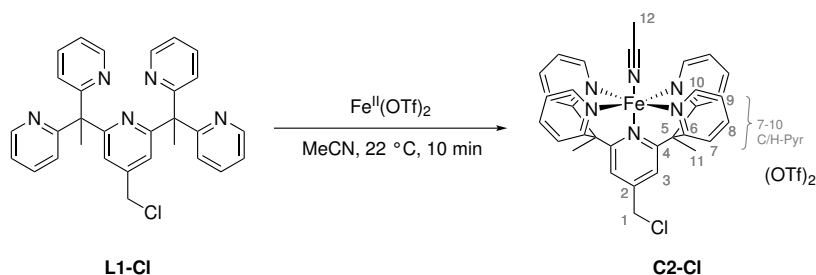
IR (Diamond-ATR, neat) $\tilde{\nu}/\text{cm}^{-1}$ = 1468, 1442, 1255, 1224, 1156, 1030, 767, 638, 574, 517.

¹H NMR (600 MHz, CD₃CN) δ/ppm = 9.80 (d, J = 5.9 Hz, 4H, H-Pyr), 8.04 (s, 2H, H3), 7.94 (s, 4H, H-Pyr), 7.93 (s, 4H, H-Pyr), 7.54 (td, J = 5.6, 3.4 Hz, 4H, H-Pyr), 4.09 (s, 2H, H1), 2.76 (s, 6H, H11), 1.96 (s, 3H, H12).

¹³C NMR (150 MHz, CD₃CN) δ/ppm = 164.5 (C4), 163.0 (C6), 158.1 (C-Pyr), 139.7 (C-Pyr), 124.3 (C-Pyr), 123.7 (C-Pyr), 121.2 (C3), 55.6 (C5), 44.5 (C1), 24.1 (C11).

HR-MS (ESI) calc. for C₃₀H₂₈FeN₆²⁺: 264.0857 [M-MeCN-2OTf]²⁺
found: 264.0857 [M-MeCN-2OTf]²⁺.

Elemental Analysis found (calc.) C 43.71 (47.07), H 5.76 (3.60), N 10.44 (11.30), S 7.39 (8.61).

Synthesis of C2-Cl^[89,124]

L1-Cl (58.8 mg, 0.12 mmol, 1.0 equiv.) was dissolved in acetonitrile (10 mL) at ambient temperature. Iron(II) triflate (42.6 mg, 0.12 mmol, 1.0 equiv.) was added and the mixture stirred for 10 min. Cold diethyl ether (4 °C, 40 mL) was added to the deep red solution until precipitation occurred. The mixture was stirred for 5 min and filtered through a sintered glass frit. The solid was washed with cold diethyl ether and dried *in vacuo* affording C2-Cl (72.6 mg, 0.08 mmol, 68 %) as red-orange powder.

The complex was crystallised from a solution in acetonitrile by slow evaporation of the solvent. The crystals were analysed by single crystal X-ray crystallography. Details of the crystallographic data can be found in the Appendix (Chapter VII7).

Chemical Formula $\text{C}_{34}\text{H}_{29}\text{ClF}_6\text{FeN}_6\text{O}_6\text{S}_2$ (886.05 g/mol⁻¹).

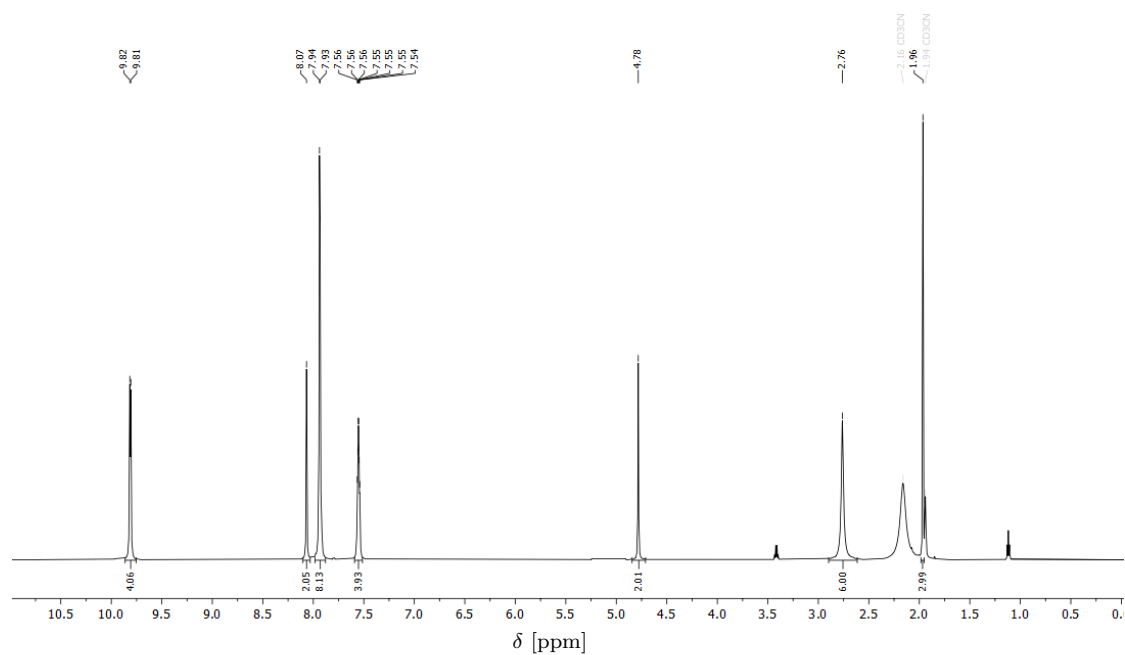
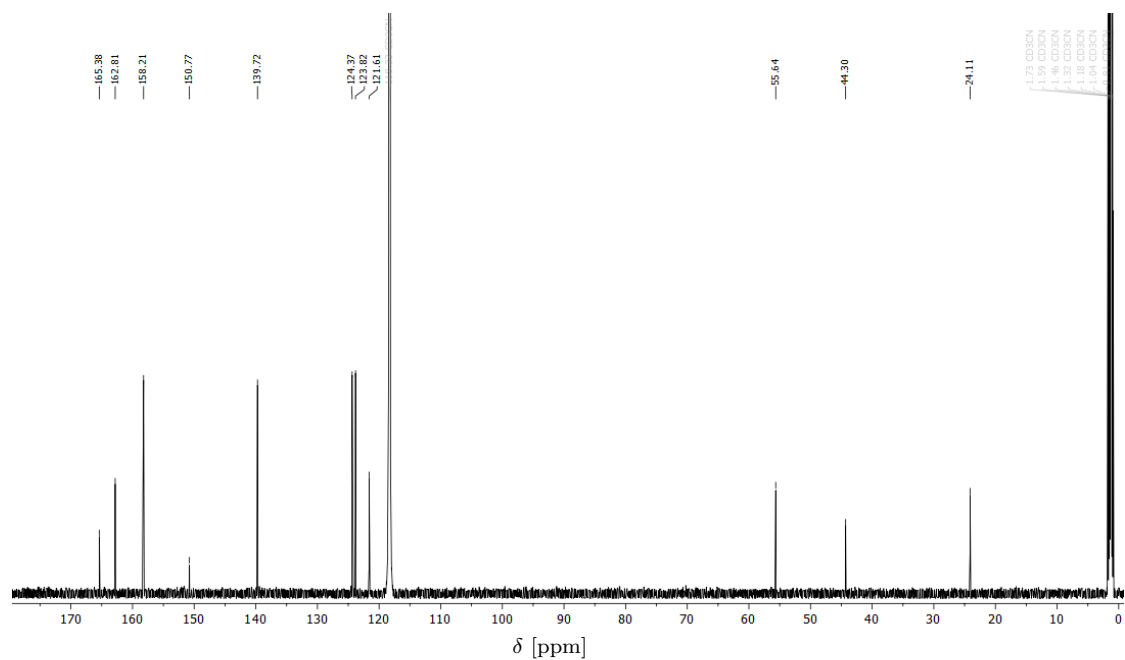
IR (Diamond-ATR, neat) $\tilde{\nu}/\text{cm}^{-1}$ = 1468, 1442, 1272, 1257, 1224, 1149, 1107, 1031, 771, 728, 638, 611, 573, 531, 517.

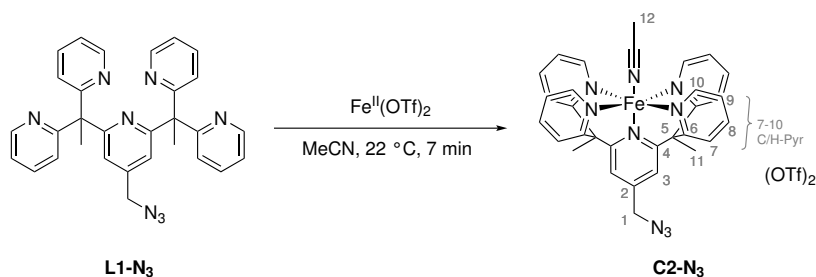
¹H NMR (600 MHz, CD₃CN) δ/ppm = 9.81 (d, J = 5.9 Hz, 4H, H-Pyr), 8.04 (s, 2H, H3), 7.94 (s, 4H, H-Pyr), 7.93 (s, 4H, H-Pyr), 7.55 (td, J = 5.5, 3.4 Hz, 4H, H-Pyr), 4.78 (s, 2H, H1), 2.76 (s, 6H, H11), 1.96 (s, 3H, H12).

¹³C NMR (150 MHz, CD₃CN) δ/ppm = 165.4 (C4), 162.8 (C6), 158.2 (C-Pyr), 139.7 (C-Pyr), 124.3 (C-Pyr), 123.8 (C-Pyr), 121.6 (C3), 55.6 (C5), 44.3 (C1), 24.1 (C11).

HR-MS (ESI) calc. for $\text{C}_{30}\text{H}_{26}\text{ClFeN}_5$ ²⁺: 273.5608 [M-MeCN-2OTf]²⁺
found: 273.5609 [M-MeCN-2OTf]²⁺.

Elemental Analysis found (calc.) C 44.68 (46.04), H 3.62 (3.30), N 8.94 (9.47), S 7.38 (7.23).

^1H NMR (600 MHz, CD_3CN) ^{13}C NMR (150 MHz, CD_3CN)

Synthesis of C2-N₃

This procedure was part of the Master thesis of Johanna Großmann.

In a 100 mL round-bottom flask, L1-N₃ (307 mg, 0.616 mmol, 1.0 equiv.) was dissolved in acetonitrile (25 mL) at ambient temperature. Iron(II) triflate (231 mg, 0.653 mmol, 1.1 equiv.) was added and the mixture stirred for 7 min. Cold diethyl ether (4 °C, 60 mL) was added to the deep red solution until precipitation occurred. The suspension was filtered through a sintered glass frit. The solid was washed with cold diethyl ether and dried *in vacuo* affording C2-N₃ (500 mg, 0.556 mmol, 90 %) as a red-orange powder.

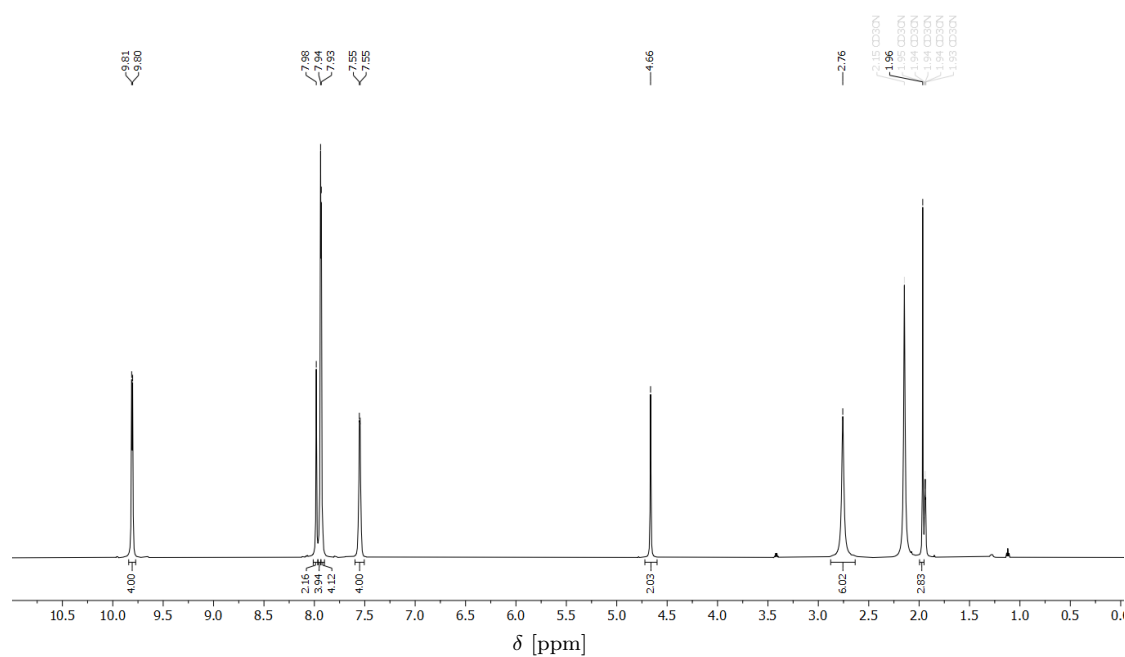
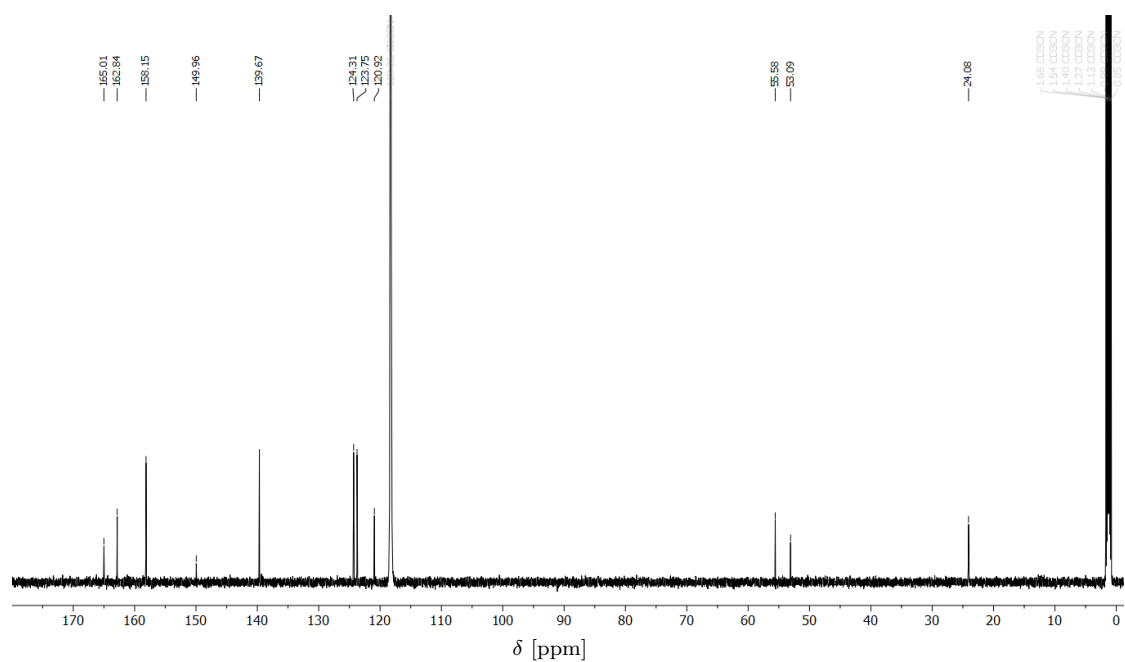
Chemical Formula C₃₄H₂₉F₆FeN₉O₆S₂ (893.62 g/mol⁻¹).

IR (Diamond-ATR, neat) $\tilde{\nu}/\text{cm}^{-1}$ = 3139, 3117, 3068, 3003, 2981, 2164, 2113, 2088, 1619, 1598, 1575, 1563, 1468, 1441, 1394, 1384, 1351, 1274, 1257, 1224, 1151, 1107, 1067, 1031, 898, 874, 828, 797, 772, 758, 728.5, 665, 637, 572, 531, 516, 462, 434.

¹H NMR (600 MHz, CD₃CN) δ/ppm = 9.81 (d, J = 5.9 Hz, 4H, H-Pyr), 7.98 (s, 2H, H-3), 7.94 (s, 4H, H-Pyr), 7.93 (s, 4H, H-Pyr), 7.55 (q, J = 5.0 Hz, 4H, H-Pyr), 4.66 (s, 2H, H-1), 2.76 (s, 6H, H-11), 1.96 (s, 3H, H-12).

¹³C NMR (150 MHz, CD₃CN) δ/ppm = 165.0 (C-4), 162.8 (C-6), 158.1 (C-Pyr), 150.0 (C-2), 139.7 (C-Pyr), 124.3 (C-Pyr), 123.8 (C-Pyr), 120.9 (C-Pyr), 55.6 (C-5), 53.1 (C-1), 24.1 (C-11).

HR-MS (ESI) calc. for C₃₀H₂₆FeN₈²⁺: 277.0810 [M-MeCN-2OTf]²⁺
found: 277.0809 [M-MeCN-2OTf]²⁺.

^1H NMR (600 MHz, CD_3CN) ^{13}C NMR (150 MHz, CD_3CN)

3.4. Synthesis of Chitosan Beads and Modifications

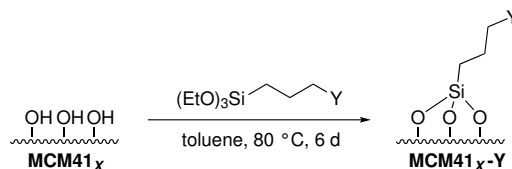
Chitosan Bead Formation^[225]

A beaker was charged with 1.5 % (v/v) aqueous acetic acid solution (20 mL). Under vigorous stirring, chitosan (300 mg, ≥ 75 % deacetylated) was dissolved very slowly in small portions leading to a clear, highly viscous solution containing 1.5 % (w/v) chitosan. The mixture was centrifuged (4500 rpm, 15 min) and transferred into a syringe which was then clamped into a syringe pump and equipped with a syringe-needle (Luer-Lock, $\varnothing = 0.40$ mm). The tip of the needle was placed 1-1.5 cm above the surface of a 1 M potassium hydroxide solution (25 % ethanol in water). The beaker containing the hydroxide solution was placed in a wider beaker and filled to the top so that the solution will overflow when the surface level rises. This is done to keep the falling height of the drops consistent, since it affects the resulting shape⁹. While stirring, the pump was started (20 mL/h), leading to a slow, controlled dripping of the chitosan gel. The obtained uniform, colorless chitosan beads were allowed to ripen for 2-3 h in the potassium hydroxide solution while gently stirring. The beads were filtered off with a perforated 50 mL centrifuge tube and washed by filling the tube with water and letting it flow through (3x40 mL). The beads were filled in a glass bottle, submerged in water and put on a laboratory shaker for at least 15 min, filtered off and the process repeated once. The beads were then filtered, washed with water (3x40 mL) and stored in water.

⁹A higher distance results in flat disks, while a short falling distance will give tear-drop shaped beads.

3.5. Synthesis of modified MCM41 Silica

General Procedure



MCM41_X silica (2.00 g, 33.3 mmol, 1.0 equiv.) was suspended in toluene (65 mL). Either (3-chloropropyl)triethoxysilane or 3-(triethoxysilyl)propan-1-amine (8 mL, approx. 1.0 equiv.) were added. The suspension was heated to 80 °C for 6 d. The suspension was left to cool to ambient temperature, filtered through a soxhlet extraction thimble and the residue washed with dichloromethane (30 mL). The extraction thimble was transferred into a soxhlet apparatus. The apparatus was filled with dichloromethane (85 mL) and heated to 55 °C for 2 d to thoroughly wash the silica. The extraction thimble was removed, washed with fresh dichloromethane (30 mL) and the MCM41_X-Y silica was dried in a vacuum drying cabinet at 40 °C for 4 d.

Two different types of MCM41 silica were used: a powdered silica¹⁰ and a pelleted silica¹¹ form. Both MCM41_X silica types were treated, washed and dried as described above without adding a silane for modification. These were then used as references MCM41_{pow} and MCM41_{pel} in analytical methods to accommodate for changes in the silica structure due to heat or solvent treatment.

Elemental analysis was used for carbon (C), hydrogen (H) and nitrogen (N) values while the silica (Si) content was measured *via* ICP-OES. All values are an average of two measurements of each sample. Values in grey showed strong variation between two measurements and should be interpreted carefully.

Product	C	H	N	Si	Yield
MCM41 _{pow}	0.01	0.85	0.00	49.3	-
MCM41 _{pow} -Cl	4.63	1.42	0.00	40.8	1.98 g
MCM41 _{pow} -NH ₂	6.78	1.93	1.81	55.5	2.00 g
MCM41 _{pel}	0.07	1.22	0.00	39.3	-
MCM41 _{pel} -Cl	4.89	1.80	0.00	35.5	1.82 g
MCM41 _{pel} -NH ₂	8.59	2.38	2.91	35.4	1.87 g

¹⁰Silica, mesostructured, MCM-41 type (hexagonal), Aldrich, 6463645-5G, BCCD5791.

¹¹Silica, MCM-41, pellet (2x5 mm), Merck, 900773-5G, MKCQ8422.

VII. Appendix

1. Supporting Information: Modular Synthesis of New Pyrroloquinoline Quinone Derivatives

1.1. Materials and Methods

Solvents and Chemicals

Reagents available commercially or from the LMU Munich chemical supply were used without further purification except for dichloromethane, diethyl ether, and hexanes. These were purchased from the LMU Munich chemical supply in technical grade and were distilled once under reduced pressure prior to use.

Autoclave

Autoclave reactions were performed in a Parr 5500 Series reactor.

Liquid Chromatography

Flash column chromatography was performed with an Interchim PuriFlash PF420 instrument by using self-packed columns with silica gel 60 (40-63 μm) from Merck as the stationary phase. Thin-layer chromatography was performed by using precoated aluminum sheets (silica gel 60, F-254, Merck). Samples were visualized by ultraviolet light ($\lambda = 254\text{ nm}$).

NMR Spectroscopy

^1H NMR and ^{13}C NMR spectra were recorded at room temperature with a Bruker Avance III (400 MHz) spectrometer operating at 400 MHz for proton nuclei and 101 MHz for carbon nuclei at the Department of Chemistry at the LMU Munich. ^1H chemical shifts are reported in ppm relative to CDCl_3 ($\delta\text{H} = 7.26$), CD_3CN ($\delta\text{H} = 1.94$), D_2O ($\delta\text{H} = 4.79$), or DMSO-d_6 ($\delta\text{H} = 2.50$). ^{13}C chemical shifts are given in ppm relative to CDCl_3 ($\delta\text{C} = 77.16$), CD_3CN ($\delta\text{C} = 1.32$), or DMSO-d_6 ($\delta\text{C} = 39.52$). The following abbreviations are used: s = singlet, d = doublet, t = triplet, dd = doublet of doublets, dt = doublet of triplets, m = multiplet, br = broad.

Elemental Analysis

Elemental analyses (C,H,N) were recorded on an Elementar vario EL instrument at the Department of Chemistry at the LMU Munich.

Mass Spectrometry

Mass spectrometry was carried out at the Department of Chemistry at the LMU Munich. EI spectra were recorded with Thermo Q Exactive GC, Thermo Finnigan MAT 95, or Jeol MStation mass spectrometers. ESI spectra were recorded with a Thermo Finnigan

LTQ FT Ultra Fourier Transform Ion Cyclotron Resonance mass spectrometer. Solid samples were dissolved in acetone.

IR Spectroscopy

FT-IR spectroscopy was carried out with a Jasco FT/IR-460Plus instrument with an ATR diamond plate.

1.2. Synthetic Procedures

N-(2-Methoxy-5-nitrophenyl)formamide (**2**)

Adapted from a literature procedure.^[51]

In a two-necked round-bottomed flask (250 mL) equipped with a KPG stirrer, acetic anhydride (35.0 mL, 370 mmol, 1.6 equiv.) was cooled to 0 °C. Formic acid (35.0 mL, 928 mmol, 3.9 equiv.) was slowly added, and the mixture was stirred at 0 °C for 1.5 h. 2-Methoxy-5-nitroaniline (**31**) (40.0 g, 238 mmol, 1.0 equiv.) was added in four equal portions over 1 h at 0 °C. The reaction mixture was allowed to warm to room temperature and stirred overnight. The resulting thick yellow paste was diluted with water (850 mL) and stirred until the solid was evenly suspended. The solid was filtered through a glass frit, washed with water, and dried at 60 °C for 3 h and subsequently under high vacuum at room temperature affording **2** (46.3 g, 236 mmol, 99 %) as a yellow solid; mp 194-202 °C.

IR (Diamond-ATR, neat): 3322, 1694, 1613, 1593, 1532, 1505, 1331, 1141, 819 cm⁻¹.

¹H NMR (400 MHz, DMSO-d₆): δ = 10.10 (s, 1 H), 9.13 (d, J = 2.9 Hz, 1 H), 8.38 (d, J = 1.8 Hz, 1 H), 8.03 (dd, J = 9.1, 2.9 Hz, 1 H), 7.27 (d, J = 9.1 Hz, 1 H), 4.00 (s, 3 H).

¹³C NMR (101 MHz, DMSO-d₆): δ = 160.8, 153.5, 140.3, 127.2, 120.3, 114.5, 111.0, 56.8.

HR-MS (EI): m/z [M]⁺ calcd for C₈H₈N-2O⁺: 196.0479; found: 196.0478.

N-(5-Amino-2-methoxyphenyl)formamide (**3**)

Adapted from a literature procedure.^[51]

Pd/C (447 mg, 10 wt%, 0.5 mol%) was suspended in ethanol (80 mL) and combined with **2** (15.0 g, 76.5 mmol, 1.0 equiv.) in an autoclave (300 mL volume). The autoclave reactor was flushed with H₂ three times and then filled with hydrogen gas (7 bar). The reaction mixture was slowly heated to 65 °C and was stirred at this temperature for 3 h. After cooling to room temperature, the suspension was filtered through a pad of Celite under a nitrogen stream. The filter pad was washed with dimethylformamide. The solvent was removed *in vacuo*, and the crude product was triturated with chloroform to yield **3** (11.0 g, 66.5 mmol, 87 %) as a beige solid; mp 150-153 °C.

IR (Diamond-ATR, neat): 3391, 3269, 1673, 1530, 1487, 1457, 1436, 1294, 1217, 1175, 1153, 863, 795 cm^{-1} .

^1H NMR (400 MHz, DMSO- d_6): δ = 9.38 (s, 1 H), 8.24 (s, 1 H), 7.54 (d, J = 2.7 Hz, 1 H), 6.73 (d, J = 8.6 Hz, 1 H), 6.25 (dd, J = 8.6, 2.7 Hz, 1 H), 4.68 (s, 2 H), 3.70 (s, 3 H).

^{13}C NMR (101 MHz, DMSO- d_6): δ = 159.8, 142.5, 139.9, 127.5, 112.7, 108.9, 107.1, 56.5.

HR-MS (EI): m/z $[\text{M}]^+$ calcd for $\text{C}_8\text{H}_{10}\text{N}_2\text{O}_2^+$: 166.0737; found: 166.0736.

Methyl 2-methyl-3-oxobutanoate (**4**)

Adapted from a literature procedure.^[63]

Methyl iodide (12.2 g, 86.1 mmol, 1.0 equiv.) was added to methyl 3-oxobutanoate (10.0 g, 86.1 mmol, 1.0 equiv.) in a round-bottomed flask, and the mixture was cooled to 0 °C. Potassium carbonate (17.9 g, 129 mmol, 1.5 equiv.) was added in portions over 1 h. The reaction mixture was allowed to warm to room temperature and stirred overnight. The thick suspension was diluted with diethyl ether (15 mL) and stirred for 2 h. The reaction mixture was filtered and concentrated *in vacuo*. Subsequent distillation (10.0 mbar, 54 °C) afforded **4** (7.33 g, 56.3 mmol, 65 %) as a colorless liquid.

IR (Diamond-ATR, neat): 2993, 2955, 1742, 1713, 1206, 1152 cm^{-1} .

^1H NMR (400 MHz, CDCl_3): δ = 3.74 (s, 3 H), 3.52 (q, J = 7.2 Hz, 1 H), 2.24 (s, 3 H), 1.35 (d, J = 7.2 Hz, 3 H).

^{13}C NMR (101 MHz, CDCl_3): δ = 203.7, 171.1, 53.6, 52.6, 28.6, 12.9.

HR-MS (EI): m/z $[\text{M-OMe}]^+$ calcd for $\text{C}_5\text{H}_7\text{O}_2^+$: 99.0411; found: 99.0411.

Methyl (E)-2-(2-(3-formamido-4-methoxyphenyl)hydrazinylidene) propanoate (**5**)

Adapted from a literature procedure.^[51]

A solution of **4** (312 mg, 2.40 mmol, 1.2 equiv.) in methanol/water (1:1, 27 mL) was prepared in a round-bottomed flask and cooled to 0 °C. Potassium hydroxide (135 mg, 2.40 mmol, 1.2 equiv.) was added. Compound **3** (332 mg, 2.00 mmol, 1.0 equiv.) was dissolved in 0.3 M hydrochloric acid (13 mL) and cooled to 0 °C. Sodium nitrite (138 mg, 2.00 mmol, 1.0 equiv.) was added, and the reaction mixture was briefly stirred and subsequently added to the solution of **4** *via* a transfer cannula. The red reaction mixture

was allowed to warm to room temperature and stirred overnight. The precipitate was filtered off, washed with ice-cold ethanol/water (1:1), and dried under high vacuum to afford **5** (392 mg, 1.48 mmol, 74 %) as a red solid; mp 170-179 °C.

IR (Diamond-ATR, neat): 3371, 3256, 1677, 1531, 1213, 1199, 1140, 801, 755 cm⁻¹.

¹H NMR (400 MHz, DMSO-d₆): δ = 9.77 (s, 1 H), 9.60 (s, 1 H), 8.30 (d, J = 2.0 Hz, 1 H), 8.19 (t, J = 1.4 Hz, 1 H), 7.01 (s, 1 H), 6.99 (s, 1 H), 3.80 (s, 3 H), 3.71 (s, 3 H), 2.03 (s, 3 H).

¹³C NMR (101 MHz, DMSO-d₆): δ = 165.5, 159.9, 143.3, 138.0, 130.3, 127.2, 111.9, 108.7, 107.1, 56.1, 51.6, 11.8.

HR-MS (ESI): m/z [M-H]⁻ calcd for C₁₂H₁₄N₃O₄⁻: 264.0990; found: 264.0989.

(E)-N-(2-Methoxy-5-(2-(3-oxobutan-2-ylidene)hydrazinyl)phenyl) formamide (6)

Adapted from a literature procedure.^[51]

Keto ester derivative **4** (312 mg, 2.40 mmol, 1.2 equiv.) was dissolved in a mixture of methanol/water (1:1, 15 mL) and cooled to 0 °C in a round-bottomed flask. Potassium hydroxide (135 mg, 2.40 mmol, 1.2 equiv.) was added. The colorless solution was stirred at 0 °C for 6 h and kept in a fridge at 4 °C for 14 h. Aniline derivative **3** (332 mg, 2.00 mmol, 1.0 equiv.) was suspended in 0.3 M hydrochloric acid (13 mL) and cooled to 0 °C. Sodium nitrite (138 mg, 2.00 mmol, 1.0 equiv.) was added to the acidic suspension, and the resulting mixture was added to the alkalic solution *via* a transfer cannula. The red reaction mixture was slowly allowed to warm to room temperature and stirred overnight. The precipitate was filtered off, washed with ice-cold ethanol/water (1:1), and dried under high vacuum to afford **6** (357 mg, 1.43 mmol, 72 %) as a red solid; mp 206-214 °C.

IR (Diamond-ATR, neat): 3307, 3234, 1682, 1662, 1539, 1215, 1169, 1032, 797 cm⁻¹.

¹H NMR (400 MHz, DMSO-d₆): δ = 9.95 (s, 1 H), 9.63 (s, 1 H), 8.34 (d, J = 2.5 Hz, 1 H), 8.31 (d, J = 1.9 Hz, 1 H), 7.05 (dd, J = 8.8, 2.5 Hz, 1 H), 7.00 (d, J = 8.9 Hz, 1 H), 3.81 (s, 3 H), 2.34 (s, 3 H), 1.92 (s, 3 H).

¹³C NMR (101 MHz, DMSO-d₆): δ = 195.8, 160.1, 143.4, 139.6, 137.8, 127.5, 111.9, 108.7, 107.0, 56.1, 23.8, 8.8.

HR-MS (ESI): m/z [M-H]⁻ calcd for C₁₂H₁₄N₃O₃⁻: 248.1041; found: 248.1042.

Methyl 6-formamido-5-methoxy-1H-indole-2-carboxylate (7)

Adapted from a literature procedure.^[51]

Hydrazone **5** (591 mg, 2.23 mmol, 1.0 equiv.) was dissolved in formic acid (5 mL) in a round-bottomed flask and stirred at 70 °C overnight. The reaction mixture was allowed to cool to room temperature, and the formic acid was removed *in vacuo*. The residue was repeatedly suspended in water (10 mL) and concentrated *in vacuo* (3x). The crude product was triturated with methanol and cooled in the fridge overnight. The solid was filtered off, washed with cold methanol, and dried under high vacuum to afford **7** (334 mg, 1.35 mmol, 60 %) as an orange solid; mp 209-213 °C.

IR (Diamond-ATR, neat): 3314, 1670, 1537, 1353, 1288, 1215, 1161, 1020, 794 cm⁻¹.

¹H NMR (400 MHz, DMSO-d₆): δ = 11.72 (s, 1 H), 9.71 (s, 1 H), 8.41 (s, 1 H), 8.36 (s, 1 H), 7.18 (s, 1 H), 7.04 (dd, J = 2.1, 0.7 Hz, 1 H), 3.87 (s, 3 H), 3.84 (s, 3 H).

¹³C NMR (101 MHz, DMSO-d₆): δ = 161.5, 160.1, 144.6, 132.2, 126.5, 126.4, 122.1, 107.7, 103.3, 101.6, 55.9, 51.6.

HR-MS (ESI): m/z [M-H]⁻ calcd for C₁₂H₁₁N₂O₄⁻: 247.0724; found: 247.0724.

N-(2-Acetyl-5-methoxy-1H-indol-6-yl)formamide (8)

Adapted from a literature procedure.^[51]

Hydrazone **6** (470 mg, 1.88 mmol, 1.0 equiv.) was dissolved in formic acid (7 mL) in a round-bottomed flask and stirred at 70 °C overnight. The reaction mixture was allowed to cool to room temperature, and the formic acid was removed *in vacuo*. The residue was repeatedly suspended in water (15 mL) and concentrated *in vacuo* (3x). The crude product was triturated with hot methanol (approx. 2 mL) and cooled in an ice-bath. The solid was filtered off, washed with cold methanol, and dried under high vacuum to afford **8** (245 mg, 1.05 mmol, 56 %) as a beige solid; mp 253-255 °C.

IR (Diamond-ATR, neat): 3201, 1670, 1632, 1523, 1361, 1280, 1228, 1206, 1155, 1021, 842 cm⁻¹.

¹H NMR 400 MHz, DMSO-d₆): δ = 11.54 (s, 1 H), 9.74 (s, 1 H), 8.40 (s, 1 H), 8.36 (s, 1 H), 7.21 (dd, J = 2.1, 0.7 Hz, 1 H), 7.19 (s, 1 H), 3.88 (s, 3 H), 2.49 (s, 3 H).

¹³C NMR (101 MHz, DMSO-d₆): δ = 189.1, 160.1, 144.6, 135.6, 132.3, 127.1, 122.3, 109.4, 103.3, 101.9, 56.0, 25.9.

HR-MS (ESI): m/z [M-H]⁻ calcd for C₁₂H₁₁N₂O₃⁻: 231.0775; found: 231.0774.

Methyl 6-amino-5-methoxy-1H-indole-2-carboxylate (9)

Adapted from a literature procedure.^[51]

Concentrated hydrochloric acid (2.67 mL, 32.0 mmol, 3.0 equiv.) was added to a stirred solution of acetone/water (66.7 mL, 96:4) in a round-bottomed flask. Compound **7** (2.65 g, 10.7 mmol, 1.0 equiv.) was added, and the reaction mixture was heated to 70 °C and stirred for 2 h. The precipitate was filtered off and washed with acetone. The solid was taken up in chloroform (120 mL) and aqueous sodium hydroxide (2 M, 120 mL). The aqueous phase was extracted with chloroform (2x100 mL), and the combined organic layers were washed with brine and dried over sodium sulfate. The solvent was removed *in vacuo* to afford **9** (1.98 g, 9.00 mmol, 84 %) as a light-brown solid; mp 160-162 °C.

IR (Diamond-ATR, neat): 3333, 1683, 1522, 1504, 1297, 1273, 1211, 1195, 1150, 1028, 839, 760 cm⁻¹.

¹H NMR (400 MHz, DMSO-d₆): δ = 11.17 (s, 1 H), 6.92 (dd, J = 2.2, 0.9 Hz, 1 H), 6.90 (s, 1 H), 6.62 (d, J = 0.7 Hz, 1 H), 4.96 (s, 2 H), 3.79 (s, 3 H), 3.78 (s, 3 H).

¹³C NMR (101 MHz, DMSO-d₆): δ = 161.7, 144.5, 138.4, 134.3, 123.1, 117.8, 108.5, 100.8, 94.1, 55.4, 51.1.

HR-MS (ESI): m/z [M+H]⁺ calcd for C₁₁H₁₃N₂O₃⁺: 221.0921; found: 221.0921.

1-(6-Amino-5-methoxy-1H-indol-2-yl)ethan-1-one (10)

Adapted from a literature procedure.^[51]

Concentrated hydrochloric acid (0.22 mL, 2.58 mmol, 3.0 equiv.) was added to a stirred solution of acetone/water (5.38 mL, 96:4) in a round-bottomed flask. Compound **8** (200 mg, 0.86 mmol, 1.0 equiv.) was added, and the reaction mixture was heated to 70 °C and stirred for 90 min. After cooling to room temperature, the solvent was evaporated and the residue was suspended in aqueous sodium hydroxide (2 M, 10 mL) and dichloromethane (10 mL). The biphasic mixture was filtered, and the aqueous phase was extracted with dichloromethane (2x10 mL). The combined organic layers were washed with brine and dried over sodium sulfate, and the solvent was removed *in vacuo* to afford **10** (139 mg, 0.68 mmol, 79 %) as a light-brown solid; mp 205-206 °C.

IR (Diamond-ATR, neat): 3459, 3361, 1609, 1520, 1353, 1296, 1271, 1209, 1149, 1021, 848 cm⁻¹.

¹H NMR (400 MHz, DMSO-d₆): δ = 11.02 (s, 1 H), 7.08 (dd, J = 2.3, 0.8 Hz, 1 H), 6.91 (s, 1 H), 6.59 (d, J = 0.6 Hz, 1 H), 5.07 (s, 2 H), 3.78 (s, 3 H), 2.40 (s, 3 H).

^{13}C NMR (101 MHz, DMSO- d_6): δ = 187.4, 144.6, 139.3, 135.2, 133.0, 118.0, 110.6, 101.1, 93.8, 55.4, 25.4.

HR-MS (ESI): m/z $[\text{M}+\text{H}]^+$ calcd for $\text{C}_{11}\text{H}_{13}\text{N}_2\text{O}_2^+$: 205.0972; found: 205.0971.

Methyl (E)-4-oxopent-2-enoate (**12**)

Adapted from a literature procedure^[51] and performed under an inert atmosphere using Schlenk techniques. Methyl levulinate (**11**) (3.99 g, 30.7 mmol, 1.0 equiv.) was dissolved in dry chloroform (10 mL) in a two-necked round-bottomed flask (100 mL) and cooled to 0 °C. A solution of bromine (1.80 mL, 35.1 mmol, 1.1 equiv.) in dry chloroform (6 mL) was added dropwise. The mixture was stirred 0 °C for 1 h, allowed to warm to room temperature, and stirred for 30 min until the solution turned from brown to light yellow. Excess hydrogen bromide was removed under nitrogen flow. A solution of triethylamine (14.0 mL, 100 mmol, 3.3 equiv.) in dry chloroform (20 mL) was slowly added, and the reaction mixture was stirred for 30 min. The reaction mixture was washed with water (2x40 mL), hydrochloric acid (2 M, 2x40 mL), saturated sodium carbonate solution (2x40 mL), and brine (40 mL). The organic phase was carefully concentrated *in vacuo* (not less than 300 mbar). The resulting brown liquid was distilled by slow heating from 50-130 °C in 10 °C steps under vacuum (8-11 mbar), and the product was collected in a cold trap to afford **12** (1.72 g, 13.4 mmol, 44 %) as colorless crystals; mp 57-60 °C.¹

IR (Diamond-ATR, neat): 3061, 3008, 2957, 1719, 1675, 1644, 1264, 1253, 1197, 1180, 1023 cm^{-1} .

^1H NMR (400 MHz, CDCl_3): δ = 7.01 (d, J = 16.1 Hz, 1 H), 6.64 (d, J = 16.1 Hz, 1 H), 3.81 (s, 3 H), 2.35 (s, 3 H).

^{13}C NMR (101 MHz, CDCl_3): δ = 197.6, 166.0, 140.2, 131.2, 52.5, 28.3.

HR-MS (EI): m/z $[\text{M}-\text{CH}_3]^+$ calcd for $\text{C}_5\text{H}_5\text{O}_3^+$: 113.0233; found: 113.0233.

5-Methoxy-2,7-bis(methoxycarbonyl)-9-methylpyrrolo[2,3-f]quinolin-1-ide (**13**)

Adapted from a literature procedure.^[51]

Compounds **9** (552 mg, 2.5 mmol, 1.0 equiv.) and **12** (353 mg, 2.75 mmol, 1.1 equiv.) were suspended in chloroform (50 mL) in a round-bottomed flask, and the mixture was stirred at 60 °C for 6 d. After the reaction mixture had cooled to room temperature, hydrogen chloride generated *in situ* in a second reaction vessel (by dropping concentrated sulfuric acid on sodium chloride) was bubbled through the reaction mixture for 1 h. The

¹For a detailed description of the distillation, please refer to the repository https://dx.doi.org/10.14272/collection/RAJ_2022-08-25.

reaction was stirred for 1 h at room temperature and then quenched with saturated sodium carbonate solution (30 mL). The layers were separated, and the aqueous layer was extracted with chloroform (2x30 mL). The combined organic layers were dried over sodium sulfate. The solvent was removed *in vacuo*, and the residue was purified by flash column chromatography (5 % methanol in dichloromethane, $R_f = 0.56$) to afford **13** (585 mg, 1.78 mmol, 71 %) as a light-brown solid; mp 182-192 °C.

IR (Diamond-ATR, neat): 3480, 2953, 1711, 1694, 1276, 1256, 1205, 994, 763 cm^{-1} .

^1H NMR (400 MHz, DMSO- d_6): $\delta = 10.88$ (s, 1 H), 8.09 (d, $J = 0.7$ Hz, 1 H), 7.47 (s, 1 H), 7.38 (d, $J = 1.9$ Hz, 1 H), 3.99 (s, 3 H), 3.95 (s, 3 H), 3.92 (s, 3 H), 3.13 (s, 3 H).

^{13}C NMR (101 MHz, DMSO- d_6): $\delta = 165.6, 161.0, 150.9, 144.0, 143.6, 140.1, 128.1, 126.2, 125.3, 122.9, 119.9, 109.7, 102.6, 55.7, 52.4, 52.0, 22.0$.

HR-MS (ESI): m/z $[\text{M}-\text{H}]^-$ calcd for $\text{C}_{17}\text{H}_{15}\text{N}_2\text{O}_5^-$: 327.0986; found: 327.0988.

Methyl 2-acetyl-5-methoxy-9-methyl-1H-pyrrolo[2,3-f]quinoline-7-carboxylate (14)

Adapted from a literature procedure.^[51]

Compounds **10** (316 mg, 1.55 mmol, 1.0 equiv.) and **12** (218 mg, 1.70 mmol, 1.1 equiv.) were suspended in chloroform (40 mL) in a round-bottomed flask and stirred at 60 °C for 6 d. After the reaction mixture had cooled to room temperature, hydrogen chloride generated *in situ* (by dropping concentrated sulfuric acid on sodium chloride) was bubbled through the reaction mixture for 1 h. The reaction was stirred for 1 h at room temperature and then quenched with saturated sodium carbonate solution (30 mL). The layers were separated, and the aqueous layer was extracted with chloroform (2 x 30 mL). The combined organic layers were dried over sodium sulfate. The solvent was removed *in vacuo*, and the residue was purified by flash column chromatography (2 % methanol in dichloromethane, $R_f = 0.29$) to afford **14** (332 mg, 1.06 mmol, 69 %) as a light-brown solid; mp 236-236 °C.

IR (Diamond-ATR, neat): 3406, 2947, 1707, 1639, 1257, 1208, 1156, 1130, 1040, 852 cm^{-1} .

^1H NMR (400 MHz, DMSO- d_6): $\delta = 10.60$ (s, 1 H), 8.09 (d, $J = 0.7$ Hz, 1 H), 7.56 (d, $J = 1.9$ Hz, 1 H), 7.46 (s, 1 H), 4.00 (s, 3 H), 3.95 (s, 3 H), 3.11 (s, 3 H), 2.61 (s, 3 H).

^{13}C NMR (101 MHz, DMSO- d_6): $\delta = 189.0, 165.6, 150.9, 144.3, 143.9, 140.5, 136.3, 126.8, 125.5, 123.0, 119.9, 110.9, 102.7, 55.8, 52.5, 26.3, 21.9$.

HR-MS (ESI): m/z $[M-H]^-$ calcd for $C_{17}H_{15}N_2O_4^-$: 311.1037; found: 311.1039.

Dimethyl 9-methyl-4,5-dioxo-4,5-dihydro-1H-pyrrolo[2,3-f]quinoline-2,7-dicarboxylate ($P_{ME}QQ_{MEM}$)

Adapted from a literature procedure.^[51]

Compound **13** (200 mg, 0.61 mmol, 1.0 equiv.) was suspended in acetonitrile/water (4:1, 6 mL), and the mixture was cooled to 0 °C. A solution of ceric ammonium nitrate (1.34 g, 2.44 mmol, 4.0 equiv.) in acetonitrile/water (4:1, 8 mL) was added, and the reaction mixture was stirred at 0 °C for 30 min. The precipitate was filtered off and washed with water and toluene/ethyl acetate (1:1). The solid was dried at 100 °C for 20 min and subsequently under high vacuum at room temperature to afford $P_{ME}QQ_{MEM}$ (61.2 mg, 0.19 mmol, 31 %) as a red solid; R_f = 0.23 (2 % methanol in dichloromethane); mp 253-256 °C. Crystals suitable for X-ray analysis were grown from dimethylformamide by slow vapor diffusion of diethyl ether.²

IR (Diamond-ATR, neat): 3599, 3515, 3080, 1713, 1674, 1497, 1437, 1316, 1237, 982, 763 cm^{-1} .

1H NMR (400 MHz, DMSO- d_6): δ = 11.44 (s, 1 H), 8.15 (s, 1 H), 7.30 (d, J = 1.5 Hz, 1 H), 3.92 (s, 3 H), 3.88 (s, 3 H), 2.91 (s, 3 H).

^{13}C NMR (101 MHz, DMSO- d_6): δ = 178.5, 173.7, 164.6, 160.0, 147.1, 145.6, 144.8, 137.2, 130.5, 128.1, 127.4, 123.8, 114.4, 52.7, 52.2, 20.8.

HR-MS (ESI): m/z $[M-H]^-$ calcd for $C_{16}H_{11}N_2O_6^-$: 327.0623; found: 327.0624.

Methyl 2-acetyl-9-methyl-4,5-dioxo-4,5-dihydro-1H-pyrrolo[2,3-f]-quinoline-7-carboxylate (P_KQQ_{MEM})

Adapted from a literature procedure.^[51]

Compound **14** (200 mg, 0.64 mmol, 1.0 equiv.) was suspended in acetonitrile/water (3:1, 5 mL) in a round-bottomed flask, and the mixture was cooled to 0 °C. A solution of ceric ammonium nitrate (1.42 g, 2.56 mmol, 4.0 equiv.) in acetonitrile/water (3:1, 6 mL) was added, and the reaction mixture was stirred at 0 °C for 40 min. The precipitate was filtered off and washed with acetonitrile/water (3:1). The solid was dried at 100 °C for 1 h and subsequently under high vacuum at room temperature to afford P_KQQ_{MEM} (91.7 mg, 0.29 mmol, 46 %) as a red solid; R_f = 0.21 (2 % methanol in dichloromethane); mp 281-285 °C.

²CCDC 2193479 contains the supplementary crystallographic data for this paper. The data can be obtained free of charge from The Cambridge Crystallographic Data Centre *via* www.ccdc.cam.ac.uk/structures.

IR (Diamond-ATR, neat): 3362, 3114, 3068, 2852, 1705, 1658, 1493, 1425, 1379, 1308, 1236, 1221, 993, 760 cm^{-1} .

^1H NMR (400 MHz, DMSO- d_6): δ = 11.13 (s, 1 H), 8.15 (s, 1 H), 7.67 (d, J = 1.9 Hz, 1 H), 3.93 (s, 3 H), 2.91 (s, 3 H), 2.53 (s, 3 H).

^{13}C NMR (101 MHz, DMSO- d_6): δ = 188.3, 178.6, 173.9, 164.5, 147.3, 145.8, 145.0, 137.7, 135.5, 130.5, 128.0, 123.9, 116.0, 52.7, 26.1, 20.7.

HR-MS (ESI): m/z $[\text{M-H}]^-$ calcd for $\text{C}_{16}\text{H}_{11}\text{N}_2\text{O}_5^-$: 311.0673; found: 311.0674.

2. Additional Spectra Chapter III3

LC UV-Vis traces of the experiment described in Chapter III3.3 (see Figure III.5).

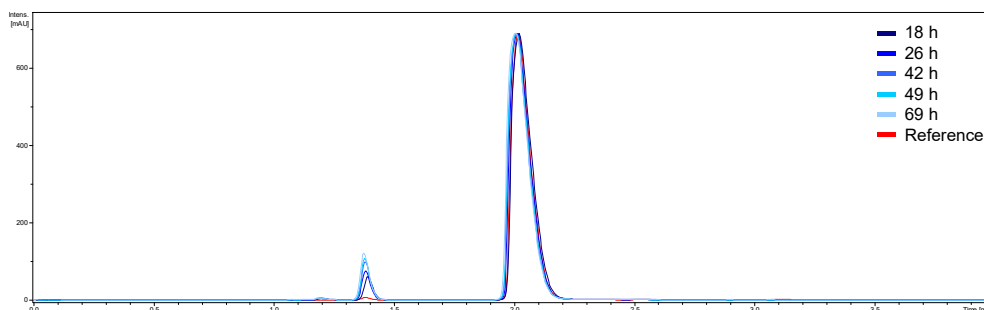


Figure VII.1.: A reaction of 1mC with the iron(IV)-oxido complex C4 was performed. UV-Vis traces (280 nm) of reaction aliquots taken after 18 h, 26 h, 42 h, 49 h and 69 h of the first triplicate. Measured on LC-MS using a C-18-PFP column (ACE, 150x4.6 mm) and a solvent gradient from 100 % A to 99.7 % A and 0.3 % B over 5 min (A = H₂O + 0.1 % formic acid (FA), B = MeOH + 0.1 % FA). Conditions [1mC] = 1 mM, [C4] = 1 mM, 27 °C. Reference conditions [1mC] = 1 mM, 27 °C, 66 h.

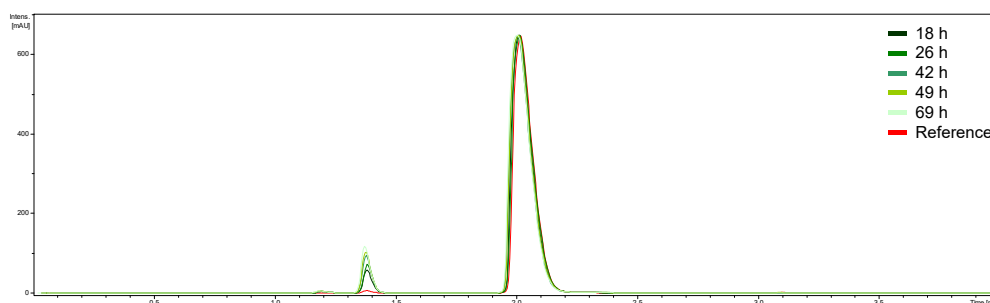


Figure VII.2.: A reaction of 1mC with the iron(IV)-oxido complex C4 was performed. UV-Vis traces (280 nm) of reaction aliquots taken after 18 h, 26 h, 42 h, 49 h and 69 h of the second triplicate. Measured on LC-MS using a C-18-PFP column (ACE, 150x4.6 mm) and a solvent gradient from 100 % A to 99.7 % A and 0.3 % B over 5 min (A = H₂O + 0.1 % formic acid (FA), B = MeOH + 0.1 % FA). Conditions [1mC] = 1 mM, [C4] = 1 mM, 27 °C. Reference conditions [1mC] = 1 mM, 27 °C, 66 h.

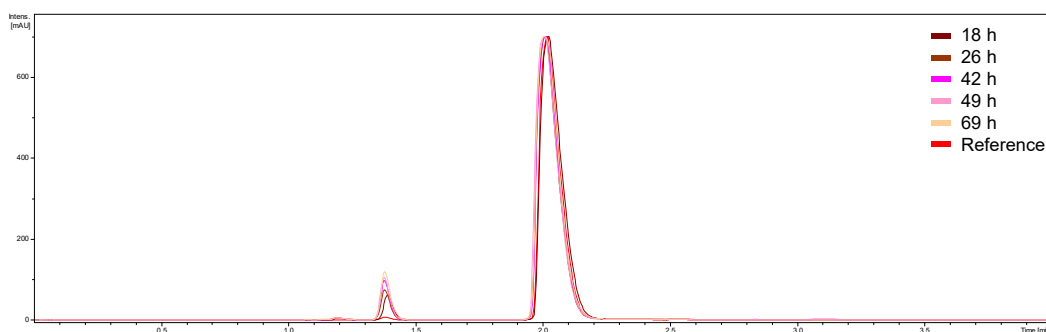


Figure VII.3.: A reaction of 1mC with the iron(IV)-oxido complex C4 was performed. UV-Vis traces (280 nm) of reaction aliquots taken after 18 h, 26 h, 42 h, 49 h and 69 h of the third triplicate. Measured on LC-MS using a C-18-PFP column (ACE, 150x4.6 mm) and a solvent gradient from 100 % A to 99.7 % A and 0.3 % B over 5 min (A = H₂O + 0.1 % formic acid (FA), B = MeOH + 0.1 % FA). Conditions [1mC] = 1 mM, [C4] = 1 mM, 27 °C. Reference conditions [1mC] = 1 mM, 27 °C, 66 h.

3. Supporting Information: Biomimetic Oxidation of 1-Methylcytosine and Other Synthetic DNA Bases

3.1. Materials and Methods

Solvents and Chemicals

Chemicals were purchased from commercial sources (Sigma Aldrich, ABCR, Acros Organics, Alfa Aesar, TCI Chemicals, Oakwood Chemicals) or the LMU Munich chemical supply and used without further purification except for dichloromethane, diethyl ether, and hexanes. These were purchased from the LMU Munich chemical supply and were distilled once under reduced pressure prior to use.

Methods and Manipulations

All manipulations were carried out under ambient conditions if not stated otherwise. Air- and moisture-sensitive chemicals and absolute solvents were transferred *via* stainless-steel cannula or syringe. Organic solutions were concentrated by rotary evaporation at 40 °C. Analytical thin layer chromatography (TLC) was performed on pre-coated (silica gel, 0.25 mm, 60 Å pore-size, 230-400 mesh, Merck KGA) aluminum plates or which were impregnated with a fluorescent indicator (254 nm). TLC plates were visualized by exposure to ultraviolet light.

Unless otherwise indicated, a new batch of C4 was prepared freshly for each set of experiments according to the procedure described by Daumann and Jonasson,^[90] stored at −20 °C and it was not used longer than for three days. The anion exchange step was performed *in situ* only a few minutes before reaction start. OriginPro 2018G was used for data evaluation.

NMR spectroscopy

¹H NMR, ²H NMR and ¹³C NMR spectra were recorded at room temperature on Bruker Avance III (400 MHz) operating at 400 MHz for proton nuclei and 100 MHz for carbon nuclei. ¹H chemical shifts are reported in ppm units relative to CDCl₃ (δ H = 7.26), CD₃CN (δ H = 1.94), D₂O (δ H = 4.79) or DMSO-d₆ (δ H = 2.50). ¹³C chemical shifts are given in ppm units relative to CDCl₃ (δ C = 77.16), CD₃CN (δ C = 1.32) or DMSO-d₆ (δ C = 39.52).^[262] The following abbreviations were used: s = singlet, d = doublet, t = triplet, dd = doublet of doublets, dt = doublet of triplets, m = multiplet, br = broad. Coupling constants (J) are given in Hertz.

Elemental Analysis

Elemental analyses were determined with an Elementar vario micro.

UV-Vis Kinetics

Instruments

UV-Vis full spectra including full spectra kinetics were recorded on an Agilent 8453 Diode

Array Spectrophotometer with a thermostatted cuvette holder at room temperature. 10 mM quartz Suprasil cuvettes from Hellma® were used in these experiments. Initial rate kinetics of the reaction of the substrates with C4 were recorded on an Epoch2 Plate reader from Biotek using 96-well plates at 30 °C.

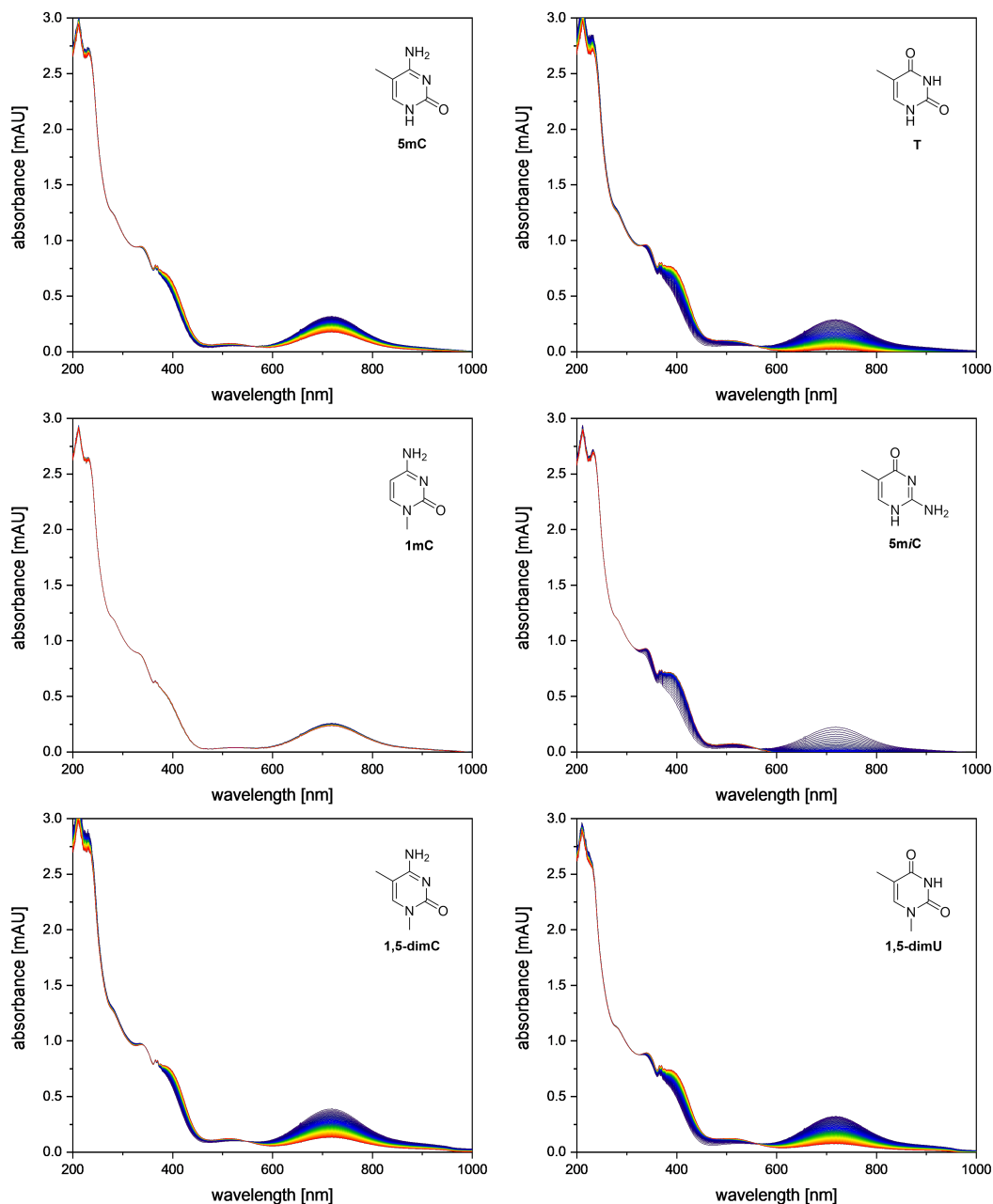


Figure VII.4.: Kinetics of different substrates with C4 followed over 1 h recording full UV-Vis spectra. Conditions: [C4] = 1 mM; [S] = 1 mM, H₂O, T = 23 °C.

General Procedure for UV-Vis kinetics

For initial rate kinetics, the absorption values at 718 nm were collected every 7 s on an Epoch2 Plate reader and all experiments were performed twice. For data evaluation

the absorption values from 63 s to 119 s were used for slope determination and linear regression was performed within a plot of the averaged slope against the respective equivalents of C4. Full UV-Vis spectra were collected every 60 s over a period of 1 h on an Agilent 8453 Diode Array Spectrophotometer.

Results and Additional Spectra

In addition to the initial rate kinetics described in the manuscript, also full UV-Vis spectra were recorded to gain information about the iron species that is formed within the reaction. The characteristic absorption band of the iron(IV)-oxido moiety at 718 nm disappears within reaction whereas the appearance of a typical feature of the corresponding iron(III) species that is formed upon reaction can be observed.

Additionally, only the iron(IV)-oxido complex C4 without substrate was followed under the same conditions with UV-Vis spectroscopy as control reaction. The observed decrease of the iron(IV)-oxido absorption band at 718 nm is not caused by decomposition of the iron(IV)-oxido complex by itself but within a reaction with different substrates. With 1mC the reaction is marginally faster, showing some, albeit very slow, oxidation of this substrate.

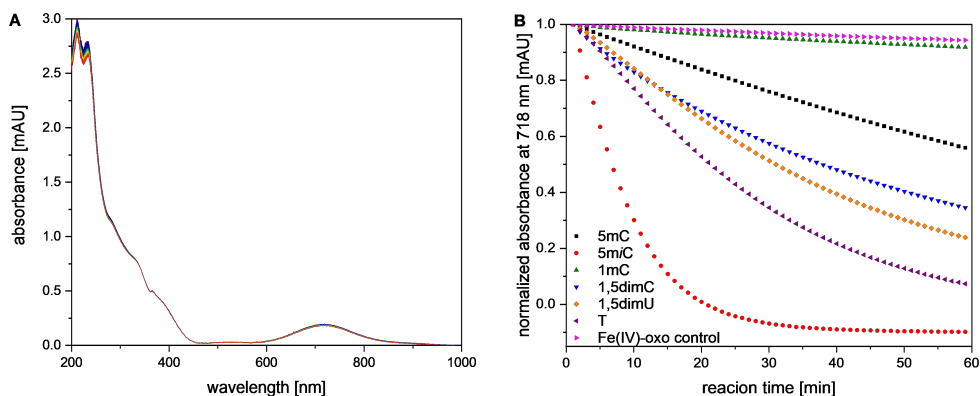


Figure VII.5.: A) control reaction of C4 without substrate over 1 h. Conditions: $[C4] = 1 \text{ mM}$; H_2O , $T = 23^\circ\text{C}$. B) Plot of the development of the absorbance of a series of reactions including the iron(IV)-oxido control reaction. Conditions: $[C4] = 1 \text{ mM}$; $[S] = 1 \text{ mM}$, H_2O , $T = 23^\circ\text{C}$.

In addition to the data shown in the manuscript, we performed an additional set of UV-Vis measurements at the same conditions to show the robustness of the system and look for signs of decomposition of C4. The obtained reaction rates (Figure VII.6) are lower than those shown in the manuscript, indicating that C4 suffers some small amount of decomposition, however, the same trends can be observed. The batch of iron(IV)-oxido complex C4 used for these experiments had been stored for 5 days at -20°C with several thaw-freeze cycles which is probably the cause for the observed decrease in reaction rates. This shows that C4 should always be made fresh for each measurement.

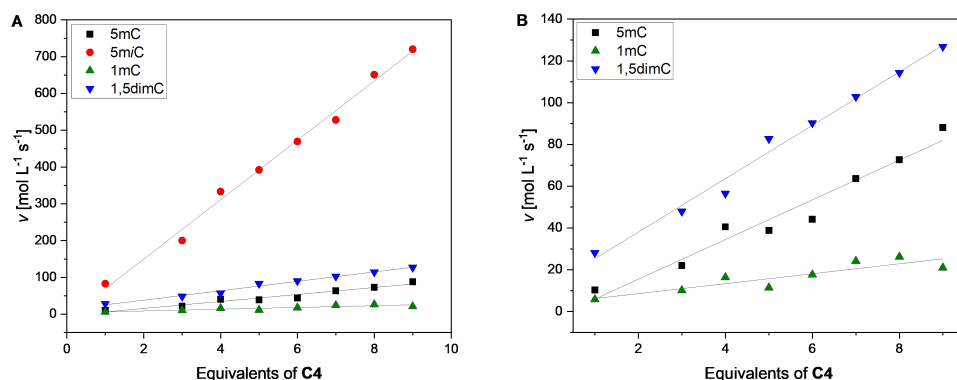


Figure VII.6.: A) Second set of UV-Vis kinetic measurements of reaction rates at 1-9 equiv. of C4 towards 5mC, 5mzC, 1mC, and 1,5dimC including linear fits. B) Zoomed in excerpt of the data presented in A. Conditions: $[C4] = 1\text{--}9 \text{ mM}$; $[S] = 1 \text{ mM}$, H_2O , $T = 23^\circ\text{C}$.

3.2. Product Analysis by HPLC-MS and GC-MS

General Procedure

To an aqueous solution of the corresponding substrate (2.0 mM, 50.0 μL , 1.0 equiv.) a freshly prepared aqueous solution of C4(1) (10 mM, 100 μL , 1.0 equiv. or 500 μL , 5.0 equiv.) was added to give a total volume of 1.0 mL. The reaction mixture was shaken at 30°C and after 1 h as well as 24 h of reaction time, a sample (200 μL) of the reaction solution was taken, filtered through silica and washed with water (6.0 mL).

High Performance Liquid Chromatography – Mass Spectrometry

Reaction samples were dried by lyophilisation. The entire amount of the obtained sample was suspended in 2.0 mL of water. Of the solution, 100 μL were diluted with 300 μL water, filtered and injected (10 μL) onto an Agilent® UHPLC 1260 InfinityII (G7115A 1260 DAD WR, G7116A 1260 MCT, G7167A 1260 Multisampler, G7104C1260 Flexible Pump) equipped with an ACE 5 C18-PFP (150 x 4.6 mm, ACE-1210-1546) column and coupled to an Agilent® 6530 C QTOF LC-MS (G1958-65171) system. Measurements were performed at 30°C eluent temperature. As eluent system a water/methanol mixture with 0.1% formic acid was used with a gradient of 0-15% methanol with 0.1% formic acid over 15 min which was then kept at 15% methanol with 0.1% formic acid for 5 min. All used solvents were LC-MS grade. ESI-Mass spectra were recorded in scan mode between 50-250 m/z .

Liquid Chromatography – Mass Spectrometry

Oxidation products of 1mC were detected by injecting untreated reaction solution onto an Agilent® 1100 SL system (G1313A ALS, G1316A COLCOM, G1316A VWD, G1312A Bin Pump) equipped with an ACE 5 C18-PFP (150 x 4.6 mm, ACE-1210-1546) column and coupled to a Bruker Daltonik HCTultra PTM Discovery system (ESI mode). As eluent system a water/methanol mixture with 0.1% formic acid was used with a gradient of 0-10% methanol with 0.1% formic acid over 10 min which was then kept at 15% methanol

with 0.1% formic acid for 5 min. All used solvents were LC-MS grade. ESI-Mass spectra were recorded in scan mode between 100-1000 m/z.

Gas Chromatography – Mass Spectrometry

Reaction samples were dried by lyophilisation prior to derivatization. The entire amount of the obtained sample was suspended in 400 μ L acetonitrile, 100 μ L BSTFA were added and the mixture heated to 70 °C for 30 min. The samples were filtered and injected (1 μ L, split depending on substrate concentration) onto an Agilent® 7920 GC equipped with a 30 m HP5-MS column (Agilent® 19091S-433UI) coupled to an Agilent® 5970 EI mass spectrometer. The injector temperature was set to 280 °C and the temperature of the ion source 230 °C. The initial oven temperature was 80 °C, held there for 2 min, ramped to 240 °C at 5 K/min and then held there for 20 min. Mass spectra were recorded in scan mode between 70-400 m/z.

Lyophilisation

Samples were lyophilised on a Christ Alpha 1-2 LDplus lyophilisator attached to a vacuubrand VACUU PURE® 10C screw pump.

HPLC-HR-MS Traces

Signals at 3.5 min occurring in all measurements are considered an impurity resulting from the removal of C4 and reacted product thereof using silica.

Table VII.1.: Detected substrates and their respective products using UHPLC-MS including exact masses and retention times. Samples were prepared and measurements were performed as described above. Conditions: [C4] = 1 mM or 5 mM; [S] = 1 mM, H₂O, T = 30 °C.

c	Products	Exact Mass [m/z]	Retention Time [min]
5mC		126.0662	7.0
	5hmC	142.0611	5.0
	5fC	140.0455	8.2
	5caC	156.0404	6.0

5mC		126.0662	9.8
	5hmC	142.0611	5.7
	5fC	140.0455	11.5
	5caC	156.0404	13.8

1mC		126.0662	7.7
	C	112.0505	5.1

Substrate	Products	Exact Mass [m/z]	Retention Time [min]
1,5-dimC		140.0818	10.8
	1m-5hmC	156.0768	7.3
	1m-5fC	154.0611	11.7
	1m-5caC	170.0560	9.2
	5mC	126.0662	7.0
	5caC	156.0404	6.0

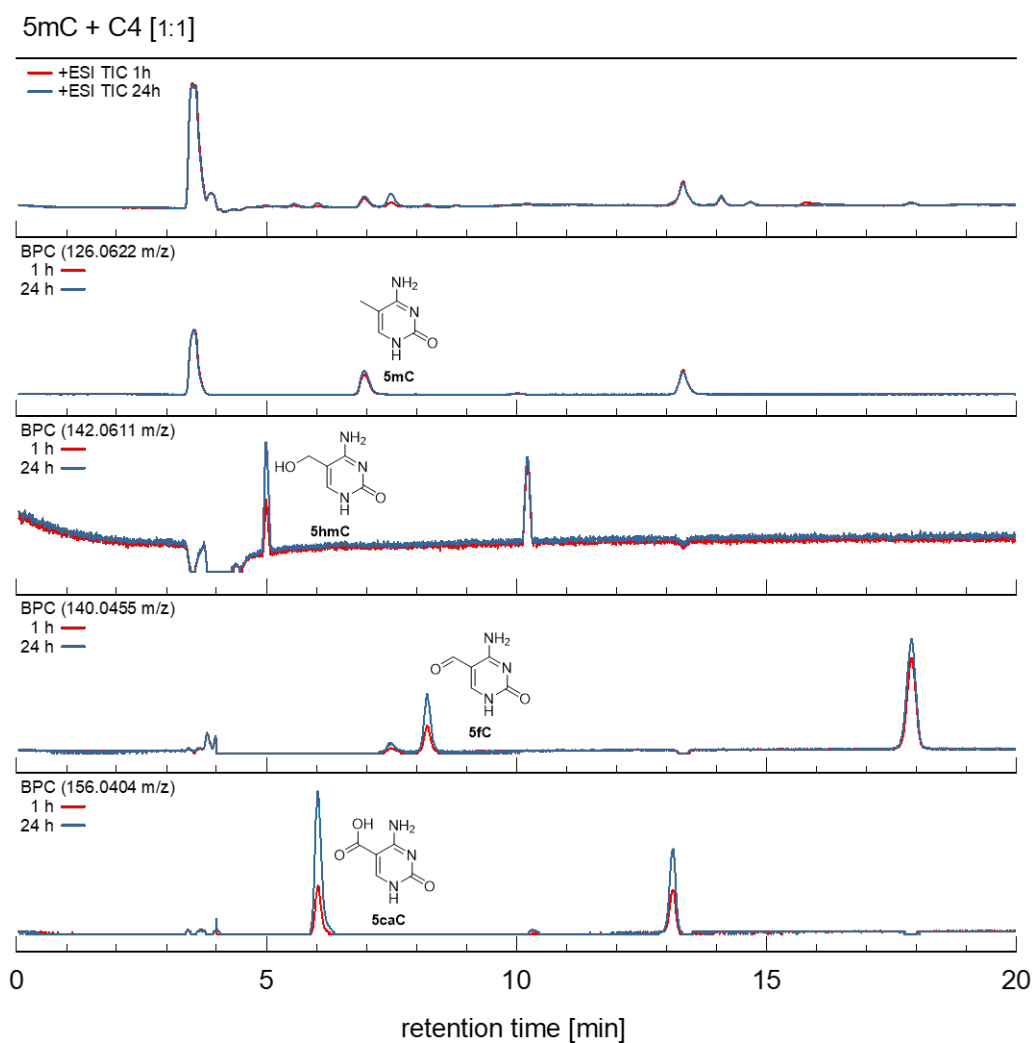


Figure VII.7.: Excerpt of the HPLC-MS traces of the reaction of C4 with 5mC. Conditions: [C4] = 1 mM; [S] = 1 mM, H₂O, T = 30 °C. Displayed are the total ion chromatogram (TIC) and extracted base peak chromatograms (BPC) for 5mC (126.0662 m/z), 5hmC (142.0611 m/z), 5fC (140.0455 m/z) and 5caC (156.0404 m/z) after 1 h and 24 h.

3. Supporting Information: Biomimetic Oxidation of 1-Methylcytosine and Other Synthetic DNA Bases

5mC + C4 [1:5]

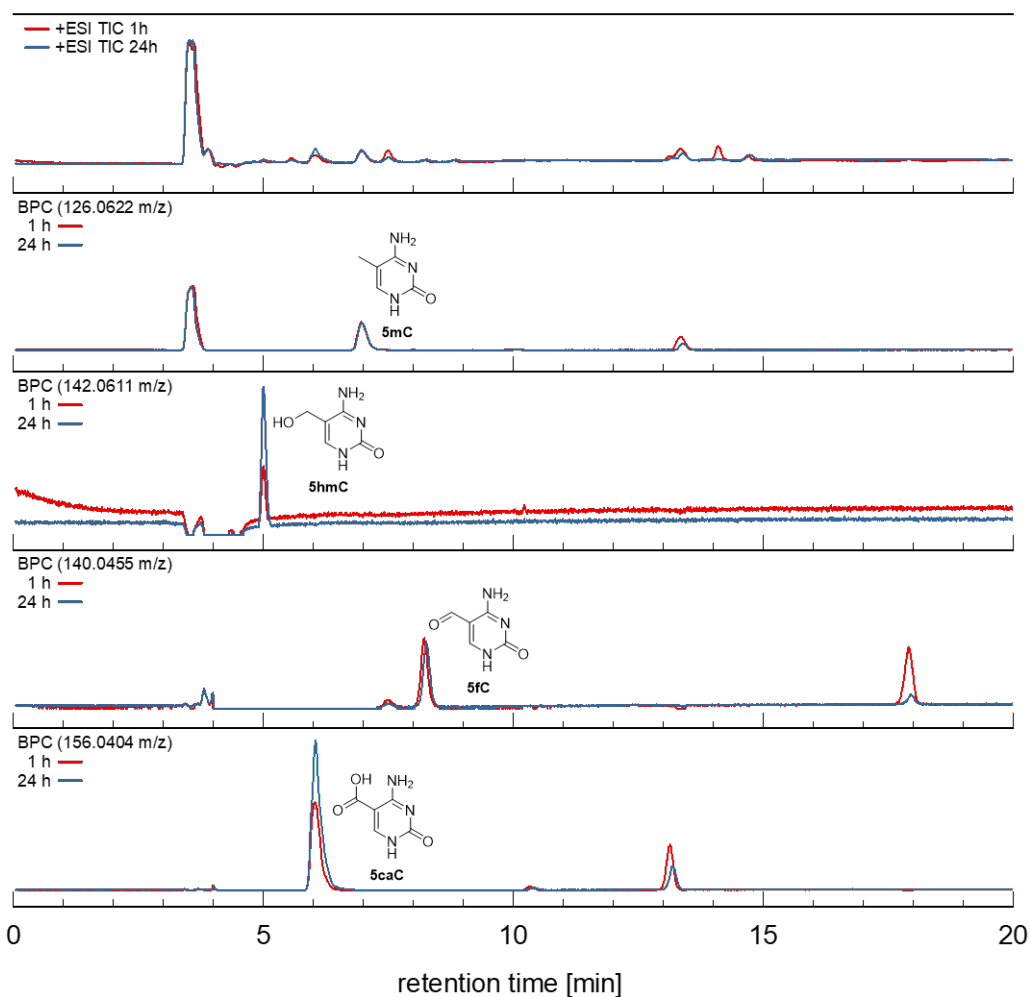


Figure VII.8.: Excerpt of the HPLC-MS traces of the reaction of C4 with 5mC. Conditions: [C4] = 5 mM; [S] = 1 mM, H₂O, T = 30 °C. Displayed are the total ion chromatogram (TIC) and extracted base peak chromatograms (BPC) for 5mC (126.0662 m/z), 5hmC (142.0611 m/z), 5fC (140.0455 m/z) and 5caC (156.0404 m/z) after 1 h and 24 h.

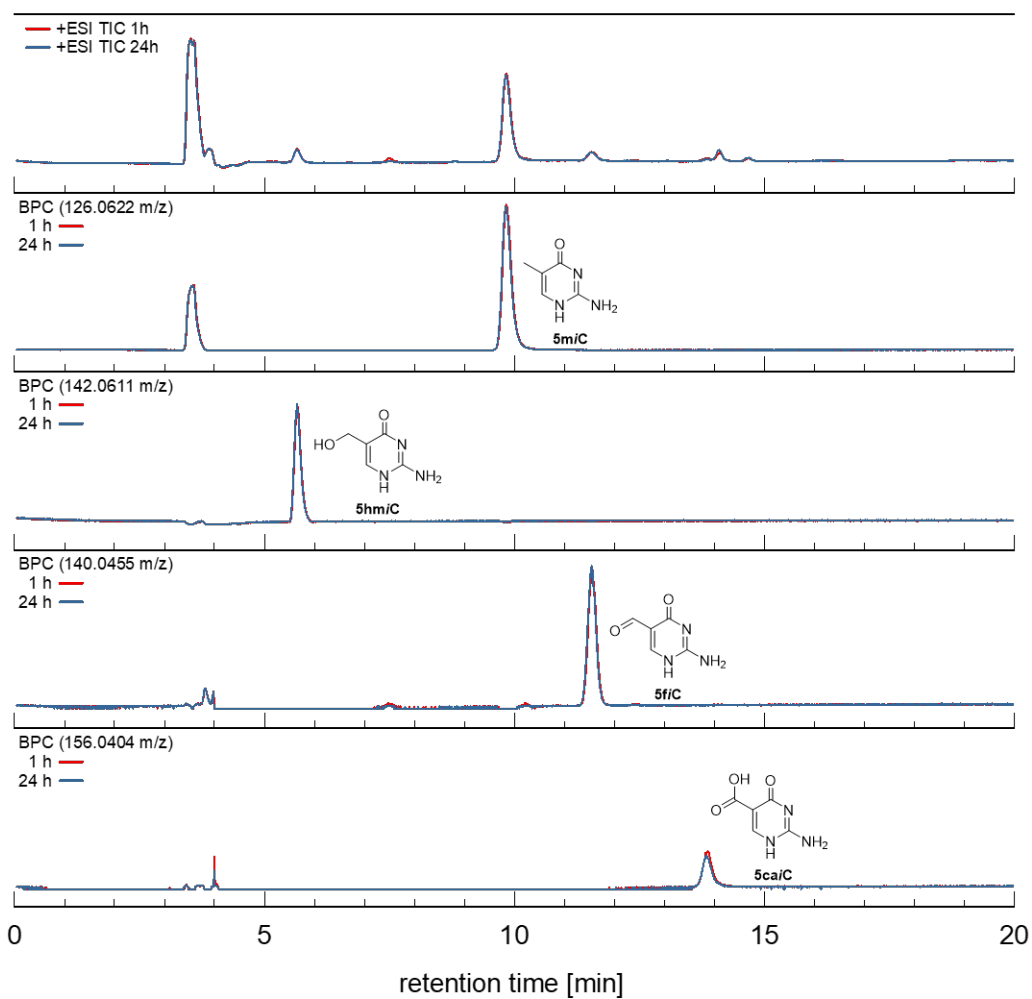
5*mi*C + C4 [1:1]

Figure VII.9.: Excerpt of the HPLC-MS traces of the reaction of C4 with 5*mi*C. Conditions: [C4] = 1 mM; [S] = 1 mM, H₂O, T = 30 °C. Displayed are the total ion chromatogram (TIC) and extracted base peak chromatograms (BPC) for 5*mi*C (126.0662 m/z), 5*hmi*C (142.0611 m/z), 5*fi*C (140.0455 m/z) and 5*cai*C (156.0404 m/z) after 1 h and 24 h.

3. Supporting Information: Biomimetic Oxidation of 1-Methylcytosine and Other Synthetic DNA Bases

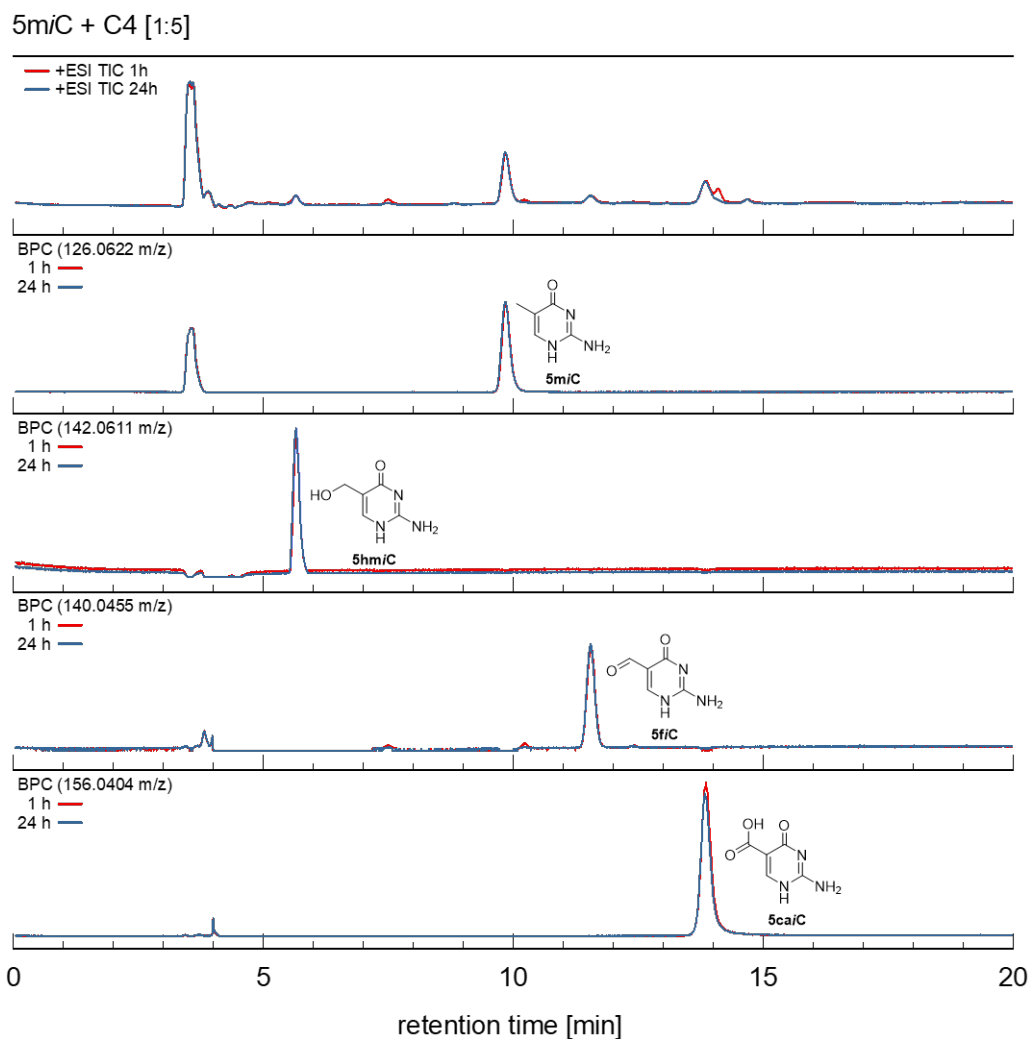


Figure VII.10.: Excerpt of the HPLC-MS traces of the reaction of C4 with 5m/C. Conditions: [C4] = 5 mM; [S] = 1 mM, H₂O, T = 30 °C. Displayed are the total ion chromatogram (TIC) and extracted base peak chromatograms (BPC) for 5m/C (126.0662 m/z), 5hm/C (142.0611 m/z), 5fi/C (140.0455 m/z) and 5cai/C (156.0404 m/z) after 1 h and 24 h.

1mC + C4 [1:1]

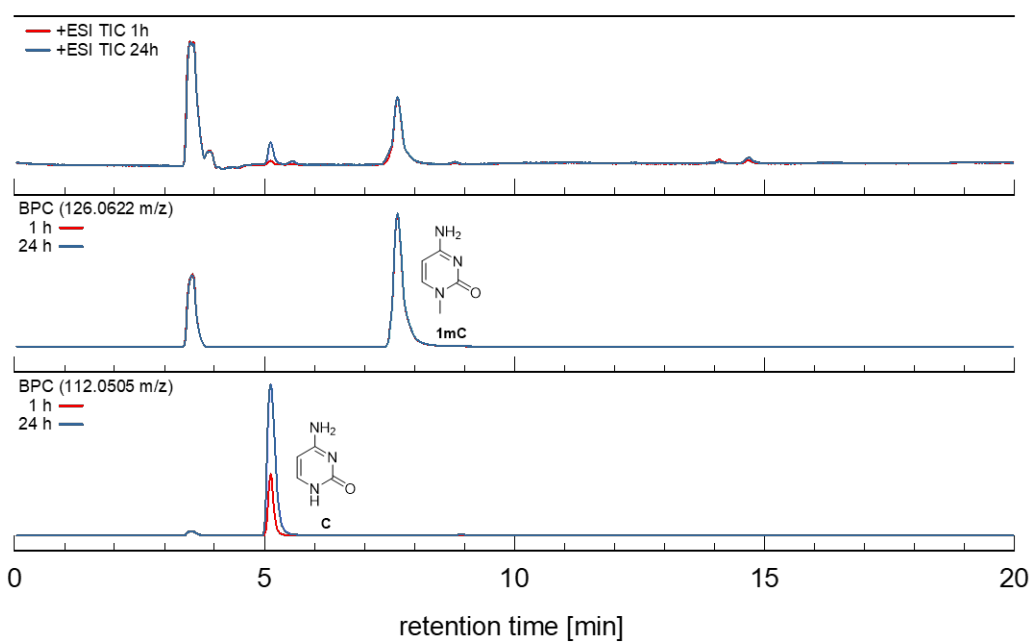


Figure VII.11.: Excerpt of the HPLC-MS traces of the reaction of C4 with 1mC. Conditions: [C4] = 1 mM; [S] = 1 mM, H₂O, T = 30 °C. Displayed are the total ion chromatogram (TIC) and extracted base peak chromatograms (BPC) for 1mC (126.0662 m/z) and C (112.0505 m/z) after 1 h and 24 h.

1mC + C4 [1:5]

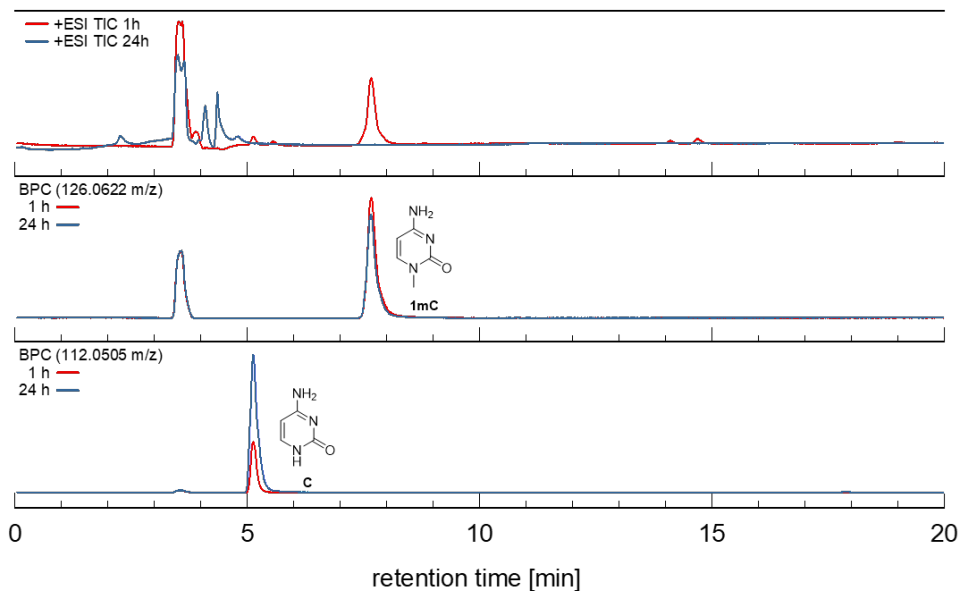


Figure VII.12.: Excerpt of the HPLC-MS traces of the reaction of C4 with 1mC. Conditions: [C4] = 5 mM; [S] = 1 mM, H₂O, T = 30 °C. Displayed are the total ion chromatogram (TIC) and extracted base peak chromatograms (BPC) for 1mC (126.0662 m/z) and C (112.0505 m/z) after 1 h and 24 h.

3. Supporting Information: Biomimetic Oxidation of 1-Methylcytosine and Other Synthetic DNA Bases

1,5-dimC + C4 [1:1]

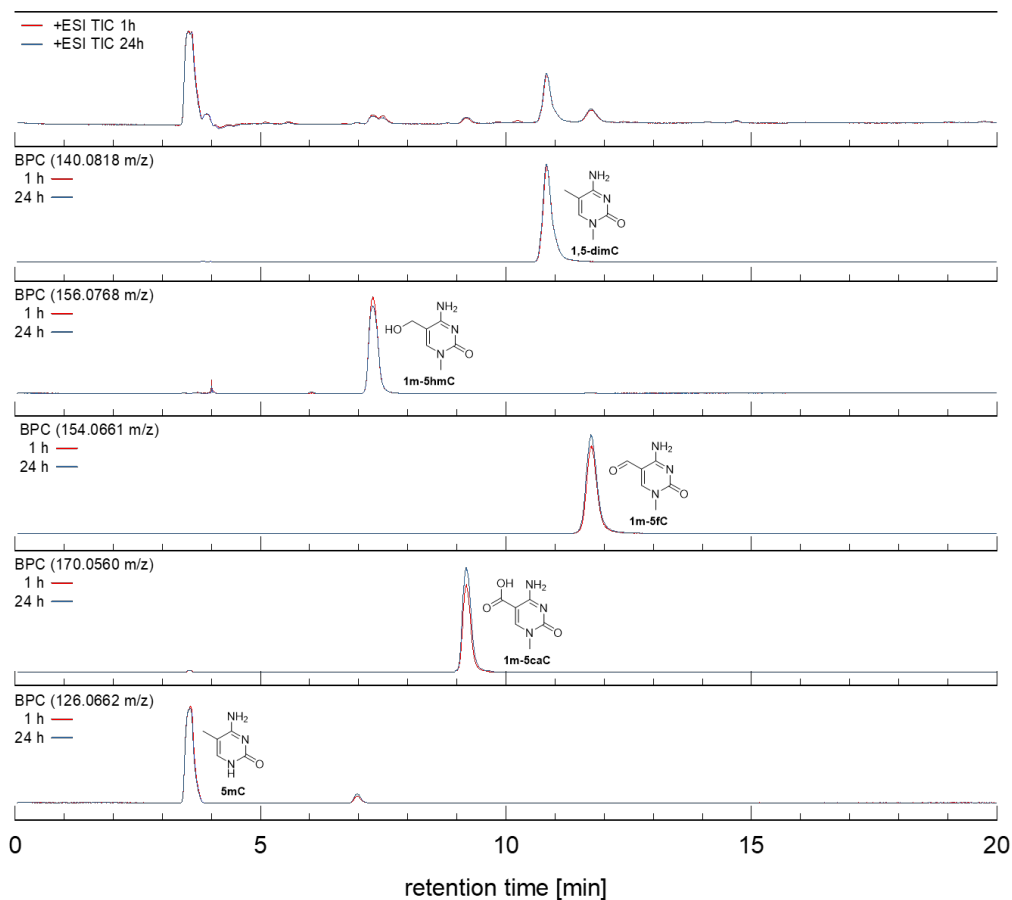


Figure VII.13.: Excerpt of the HPLC-MS traces of the reaction of C4 with 1,5-dimC. Conditions: [C4] = 1 mM; [S] = 1 mM, H₂O, T = 30 °C. Displayed are the total ion chromatogram (TIC) and extracted base peak chromatograms (BPC) for 1,5-dimC (140.0818 m/z), 1m-5hmC (156.0768 m/z), 1m-5fC (154.0661), 1m-5caC (170.0560 m/z), 5mC (126.0662 m/z) after 1 h and 24 h.

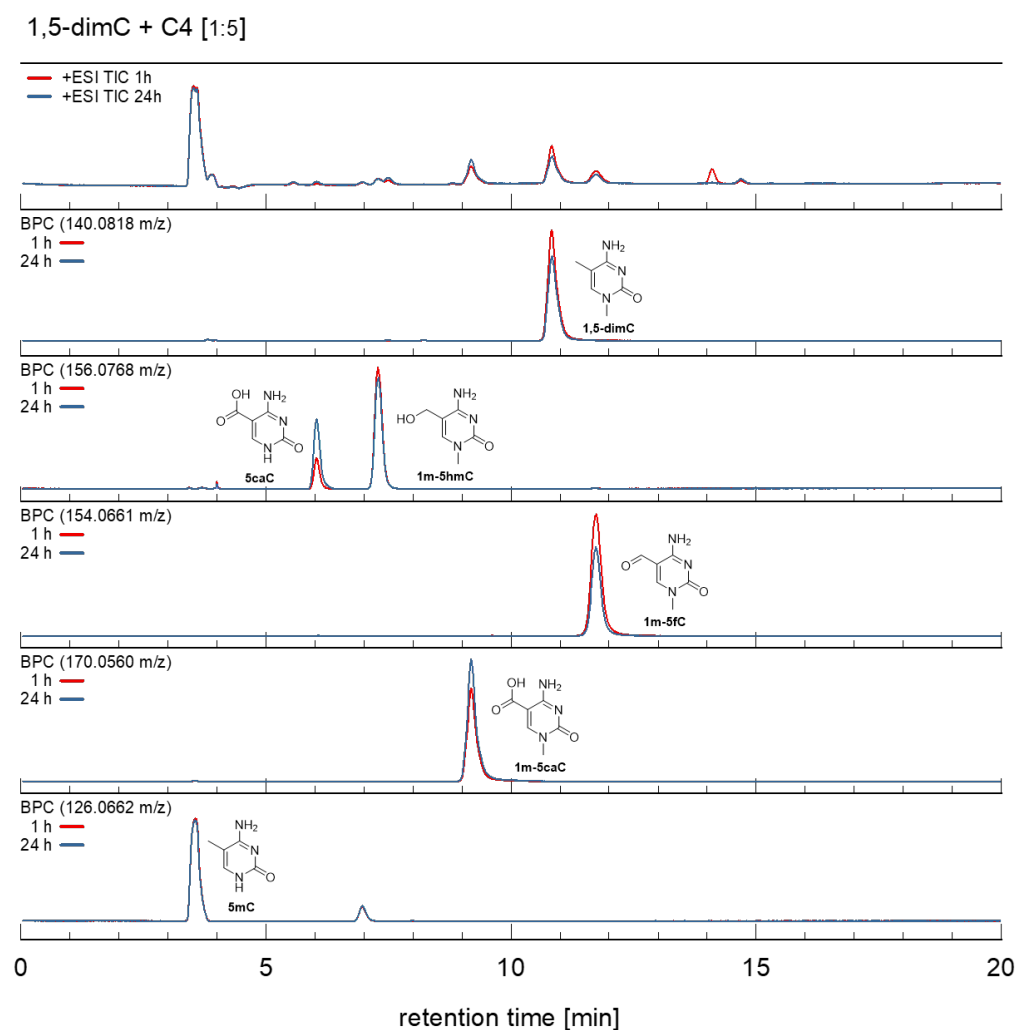


Figure VII.14.: Excerpt of the HPLC-MS traces of the reaction of C4 with 1,5-dimC. Conditions: [C4] = 5 mM; [S] = 1 mM, H₂O, T = 30 °C. Displayed are the total ion chromatogram (TIC) and extracted base peak chromatograms (BPC) for 1,5-dimC (140.0818 m/z), 1m-5hmC (156.0768 m/z) + 5caC (156.0404 m/z), 1m-5fC (154.0661), 1m-5caC (170.0560 m/z), 5mC (126.0662 m/z) after 1 h and 24 h.

3. Supporting Information: Biomimetic Oxidation of 1-Methylcytosine and Other Synthetic DNA Bases

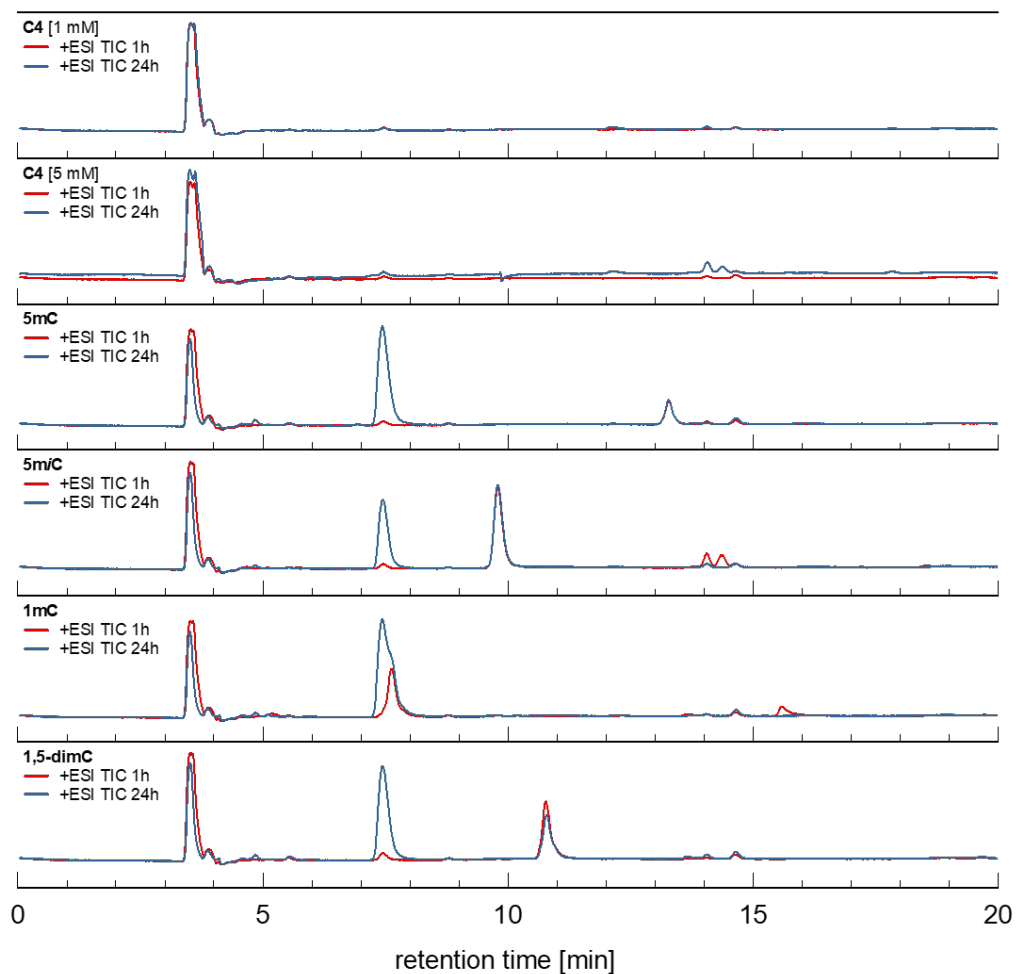


Figure VII.15.: Displayed are the total ion chromatograms (TIC) of control reactions of 5mC, 5mC, 1mC, 1,5-dimC and C4 after 1 h and 24 h. Conditions: $[S] = 1 \text{ mM}$, H_2O , $T = 30^\circ\text{C}$. No significant changes were observed. The signal at 7.4 min occurs independent of the substrate and is therefore considered an impurity originating from the column.

LC-LR-MS Traces

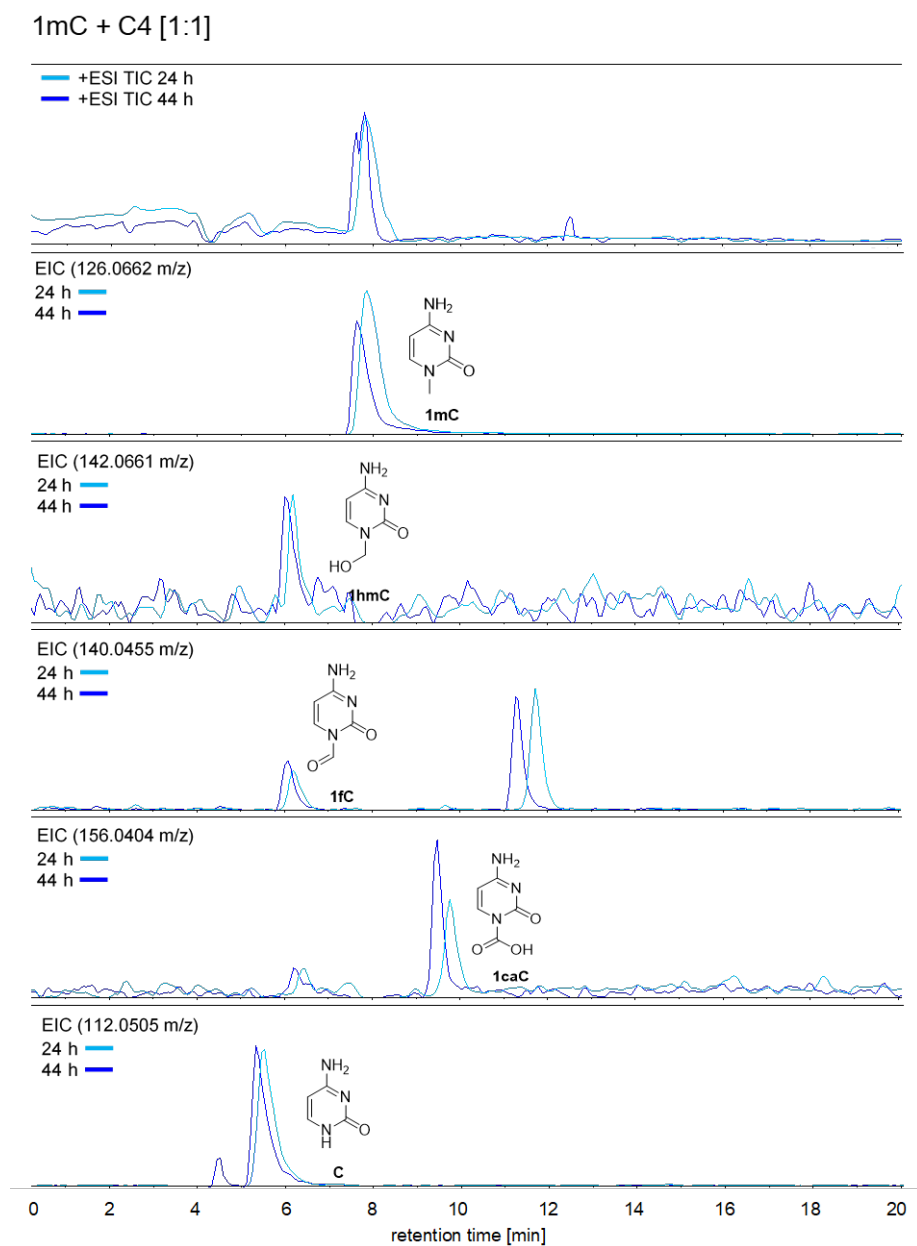


Figure VII.16.: Excerpt of the LC-MS traces of the reaction of C4 with 1mC. Conditions: [C4] = 1 mM; [S] = 1 mM, H₂O, T = 30 °C. Displayed are the total ion chromatogram (TIC) and extracted ion chromatograms (EIC) for 1mC (126.0662 m/z), 1hmC (142.0661 m/z), 1fC (140.0455 m/z), 1caC (156.0404 m/z) and C (112.0505 m/z) after 24 h and 44 h. The additional signal in the EIC of 140.0455 m/z was also found in control reactions (Figure VII.17) and is therefore not originated from reaction with 1.

3. Supporting Information: Biomimetic Oxidation of 1-Methylcytosine and Other Synthetic DNA Bases

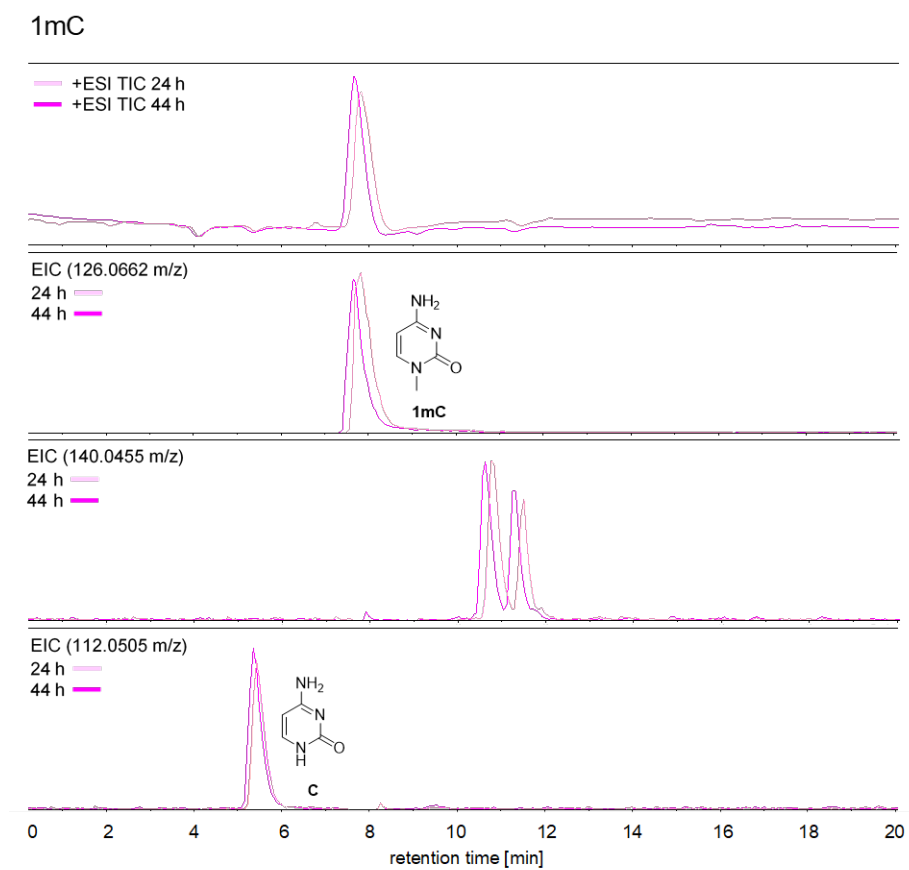


Figure VII.17.: Displayed are the total ion chromatograms (TIC) of a control reaction of 1mC without C4 after 24 h and 44 h. Conditions: $[S] = 1 \text{ mM}$, H_2O , $T = 30^\circ\text{C}$. Additionally, extracted ion chromatograms (EIC) of 1mC (126.0662 m/z), cytosine (112.0505 m/z) and 140.0455 m/z are shown. Cytosine was found as a minor impurity stemming from synthesis of 1mC, but no significant changes in intensity were observed. The EIC of 140.0455 m/z shows an impurity also observed in reaction with C4 (Figure VII.16) which is considered an impurity originating from the starting material.

GC-MS Traces

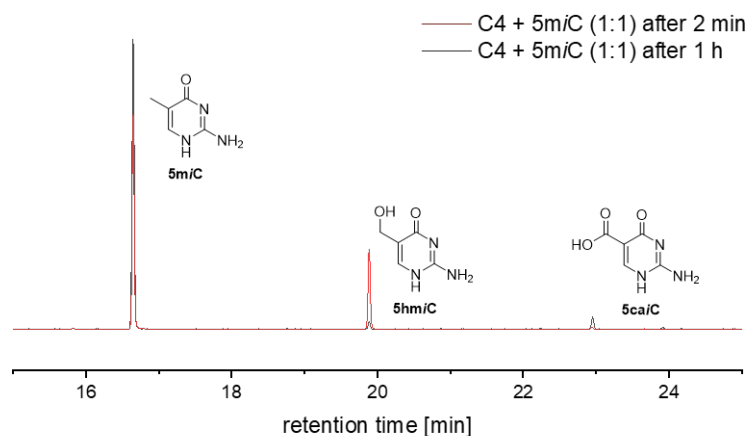


Figure VII.18.: Excerpt of the GC-MS traces of reactions of C4 with 5m*i*C after 1 h or 2 min. 5hm*i*C and 5ca*i*C were observed in addition to the starting material. Conditions: [C4] = 1 mM; [5m*i*C] = 1 mM, H₂O, T = 30 °C.

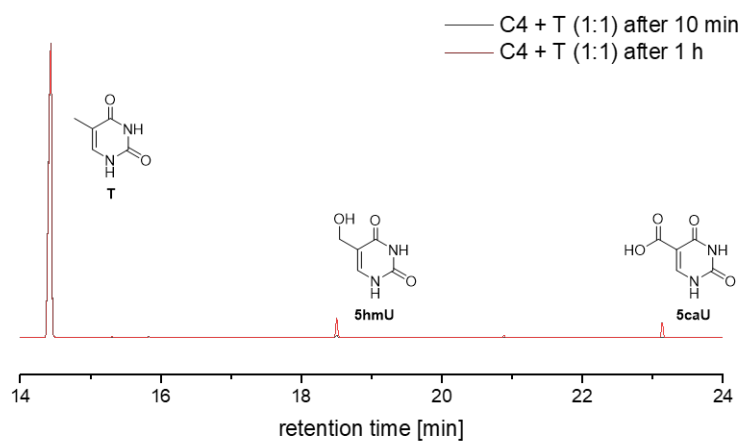


Figure VII.19.: Excerpt of the GC-MS traces of reactions of C4 with T after 10 min or 1 h. 5hmU and 5caU were observed in addition to the starting material. Conditions: [C4] = 1 mM; [T] = 1 mM, H₂O, T = 30 °C.

3.3. Bond Dissociation Energy Calculations

For this chapter please check the supporting information of the publication,^[122] which is available online. Since the bond dissociation energy calculations were performed by Fabian Zott and not part of my research, they are not included in this thesis.

3.4. Synthetic Procedures

5-methylisocytosine (5mC)

According to a modified literature procedure.^[267] Ethyl propionate (4.50 mL, 3.98 g, 39.0 mmol, 1.5 equiv.) was added to a solution of sodium methoxide (2.82 g, 52.2 mmol, 2.0 equiv.) and dimethylformamide (4 mL) under nitrogen atmosphere. Methyl formate (1.60 mL, 1.57 g, 26.1 mmol, 1.0 equiv.) was added to the mixture over a period of one hour, resulting in a slight foaming. The solution was stirred for 30 min at room temperature. A solution of guanidine hydrochloride (2.49 g, 26.1 mmol, 1.0 equiv.) in methanol (9.2 mL) was added rapidly and the mixture was refluxed (bath temperature 95 °C) for 2 h. The suspension was allowed to cool and when it reached 30 °C it was filtered through a sintered glass frit. The filter cake was discarded, and the pH of the filtrate was adjusted to 6 with concentrated hydrochloric acid, resulting in a colorless precipitate. The mixture was kept at 4 °C for 30 min, filtered off through a sintered glass frit, washed with methanol and recrystallized in water. The precipitate was filtered, washed with water and dried *in vacuo* to yield 5-methylisocytosine as a colorless solid (684.4 mg, 5.47 mmol, 21 %).

¹H NMR (400 MHz, DMSO-d₆): δ [ppm] = 10.90 (br. s, 1H), 7.39 (q, J = 1.4 Hz, 1H), 6.33 (s, 2H), 1.74 (d, J = 1.1 Hz, 3H).

Elemental Analysis: calc. for C₅H₇N₃O: C, 47.99; H, 5.64; N, 33.58. Found: C, 47.93; H, 5.86; N, 33.48.

HR-MS (ESI): calc. for C₅H₉N₃O⁺ [M+H⁺]⁺ 126.06619; found 126.06631 m/z.

1-methyluracil (1mU)

According to a modified literature procedure.^[268] Uracil (5.00 g, 44.6 mmol, 1.0 equiv.) was placed in a flame dried flask and suspended in hexamethyldisilazide (HMDS, 25.2 g, 32.0 mL, 156 mmol, 3.5 equiv.). TMSCl (2.70 g, 3.14 mL, 25.0 mmol, 0.56 equiv.) was added and the mixture was refluxed under nitrogen atmosphere at an oil bath temperature of 130 °C until the suspension turned clear, about 2 h. After cooling to room temperature, the solution was concentrated to a volume of about 10 mL. After addition of iodomethane (27.2 g, 11.9 mL, 194 mmol, 4.34 equiv.) the mixture was refluxed for a further 18 h at an oil bath temperature of 60 °C. Volatile reagents were evaporated and the residue was suspended in *iso*-propanol (25 mL). It was then filtered off, washed with isopropanol and recrystallized in water to yield 1-methyluracil (4.03 g, 31.9 mmol, 73 %) as colorless crystals.

^1H NMR (400 MHz, DMSO- d_6): δ [ppm] = 11.22 (s, 1H), 7.61 (d, J = 7.8 Hz, 1H), 5.51 (d, J = 7.8 Hz, 1H), 3.21 (s, 3H).

^{13}C NMR (100 MHz, DMSO- d_6): δ [ppm] = 164.0, 151.3, 146.5, 100.5, 35.2.

Elemental Analysis: calc. for $\text{C}_5\text{H}_6\text{N}_2\text{O}_2$: C, 47.62; H, 4.80; N, 22.21. Found: C, 46.69; H, 4.68; N, 22.16.

HR-MS (EI): calc. for $\text{C}_5\text{H}_7\text{N}_2\text{O}_2^+ [\text{M}+\text{H}^+]^+$ 126.0429; found 126.0423 m/z.

1,5-dimethyluracil (1,5dimU)

According to a modified literature procedure.^[269] In an oven dried Schlenk flask under nitrogen, a suspension of thymine (1.90 g, 15.0 mmol), HMDS (35 mL) and Me_3SiCl (0.75 mL) was refluxed for 5 h. After cooling down to 40 °C iodomethane (15 mL) was added to the reaction mixture and the suspension was refluxed overnight. All volatile compounds were removed under high vacuum with the addition of a cooling trap, to yield a brown solid. Now 35 mL of 6 N acetic acid were added, the reaction mixture was stirred for 20 min at room temperature and the solvent was removed under reduced pressure. The crude product was recrystallized in water to yield 1,5-dimethyluracil (1.47 g, 10.5 mmol, 70 %) as a slightly brown solid.

^1H NMR (400 MHz, DMSO- d_6): δ [ppm] = 12.21 (br. s, 1H), 7.50 (s, 1H), 3.19 (s, 3H), 1.73 (s, 3H).

^{13}C NMR (100 MHz, DMSO- d_6): δ [ppm] = 164.5, 151.2, 142.4, 108.1, 35.0, 11.9.

Synthesis of 1-methylcytosine (1mC)

According to literature procedure.^[123]

^1H NMR (400 MHz, DMSO- d_6): δ [ppm] = 7.55 (d, 3J = 7.1 Hz, 1H), 6.91 (s, 2H), 5.60 (d, 3J = 7.1 Hz, 1H), 3.19 (s, 3H).

^{13}C NMR (100 MHz, DMSO- d_6): δ [ppm] = 166.1, 156.3, 146.6, 92.9, 36.6.

Elemental Analysis: calc. for $\text{C}_5\text{H}_7\text{N}_3\text{O}$: C, 47.99; H, 5.64; N, 33.58. Found: C, 47.73; H, 5.64; N, 32.58.

HR-MS (EI): calc. for $\text{C}_5\text{H}_7\text{N}_3\text{O}^+ [\text{M}]^+$ 125.0584; found 125.0585 m/z.

4. Additional Experimental Information Chapter IV3

Reaction Conditions for Attempted Synthesis of 16

Table VII.2.: Reaction conditions tested for the formation of **17** (see IV.1). Different reaction scales, equivalents and orders of addition were tested. The Educt was mixed with the given amounts of sulfuric acid and methanol. Then, a saturated solution of ferrous sulfate and hydrogen peroxide were added in succession. The solution which was added first is indicated by a star (*). The temperature was measured in solution and kept by cooling with an ice-water mixture. None of the given reactions could be reproduced in similar yields. The Educt could be recovered in good amounts after flash column chromatography.

	Flask		Educt		H ₂ SO ₄		MeOH		FeSO ₄ · 7 H ₂ O		H ₂ O ₂ (30 %)		Temp.	Time	Yield
	V [mL]	m [g]	n [mol]	V [mL]	equiv.	V [mL]	V [mL]	equiv.	V [mL]	equiv.	V [mL]	equiv.	[°C]	[min]	[%]
1	50	0.98	5.00	5.00	19	5.00	5.00	1.4	3.54*	7.0*	20-25	20	12		
2	50	1.00	5.12	5.00	18	5.00	5.00*	1.4*	4.31	8.3	20-25	o.n. ^a	n.d. ^b		
3	100	1.95	10.0	10.0	19	10.0	10.0	1.4	7.09*	7.0*	20-25	20	11		
4	250	3.00	15.4	30.0	36	30.0	16.0*	1.5*	12.9	8.3	20-25	25	10		
5	250	3.11	15.9	34.2	40	30.0	29.0*	2.6*	12.9	8.0	25-40	15	15		

^aReaction performed overnight, approximately 18 h.

^bYield was not determined as TLC showed no product formation.

5. Additional Spectra Chapter IV4

SEM-EDX Data of CB

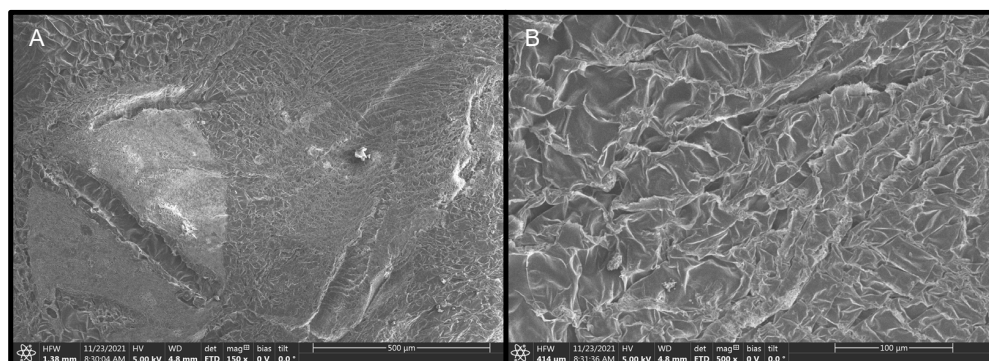


Figure VII.20.: Scanning electron microscope (SEM) images of a lyophilised chitosan gel bead's (CB) surface in different magnifications (A: 150x, B: 500x). SEM-EDX measurements were performed by Christian Minke on a FEI Helios G3 UC at LMU Munich.

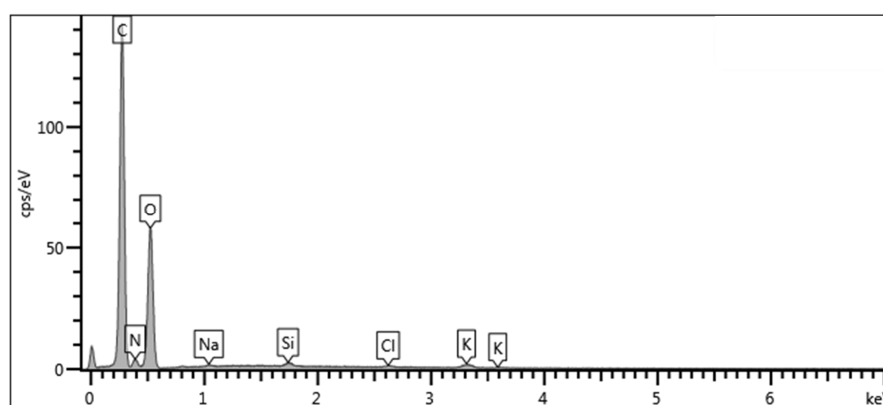


Figure VII.21.: EDX spectrum of a lyophilised chitosan gel bead's (CB) surface. Carbon content could not be determined due to the fixation of the beads on a carbon surface for measurement.

Table VII.3.: Data from the EDX measurement of a lyophilised chitosan gel bead's (CB) surface. Carbon content is excluded from Atom% calculations due to the fixation of the beads on a carbon surface for measurement.

Element	Atom%
N	10.3
O	86.5
Na	0.75
Si	0.86
Cl	0.40
K	1.16
Total:	100.00

SEM-EDX Data of CB-GA

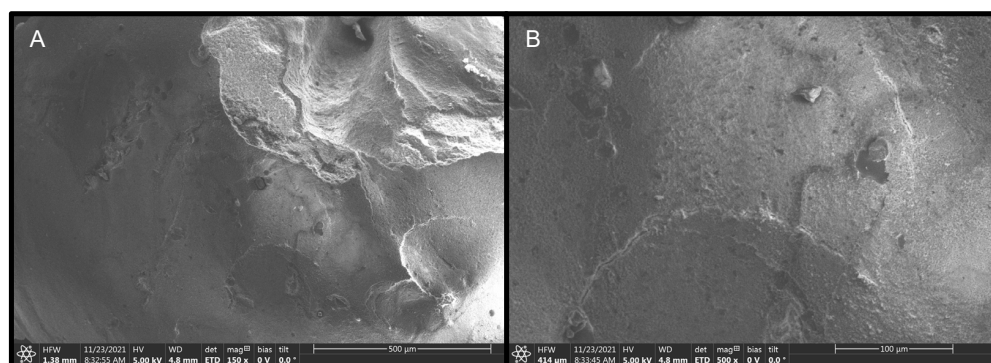


Figure VII.22.: Scanning electron microscope (SEM) images of a lyophilised chitosan gel bead's surface functionalised with glutaraldehyde (CB-GA) in different magnifications (A: 150x, B: 500x). *SEM-EDX measurements were performed by Christian Minke on FEI Helios G3 UC at LMU Munich.*

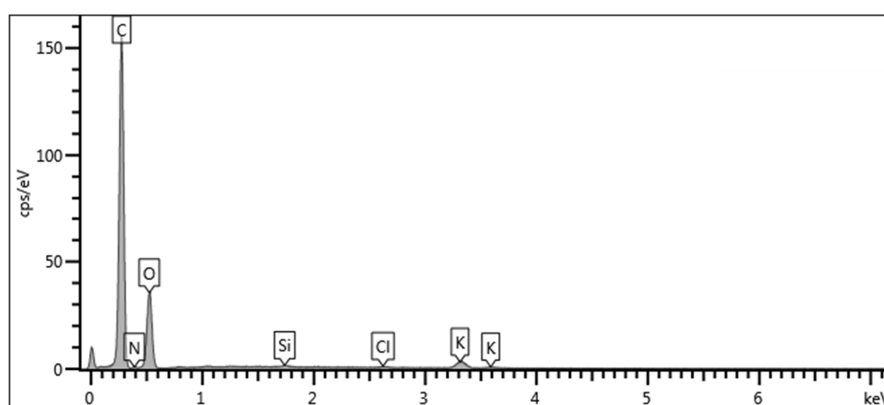


Figure VII.23.: EDX spectrum of a lyophilised chitosan gel bead's surface functionalised with glutaraldehyde (CB-GA). Carbon content could not be determined due to the fixation of the beads on a carbon surface for measurement.

Table VII.4.: Data from the EDX measurement of a lyophilised chitosan gel bead's surface functionalised with glutaraldehyde (CB-GA). Carbon content is excluded from Atom% calculations due to the fixation of the beads on a carbon surface for measurement.

Element	Atom%
N	1.88
O	92.5
Si	0.52
Cl	0.48
K	4.63
Total:	100.00

SEM-EDX Data of CB-GA-L1

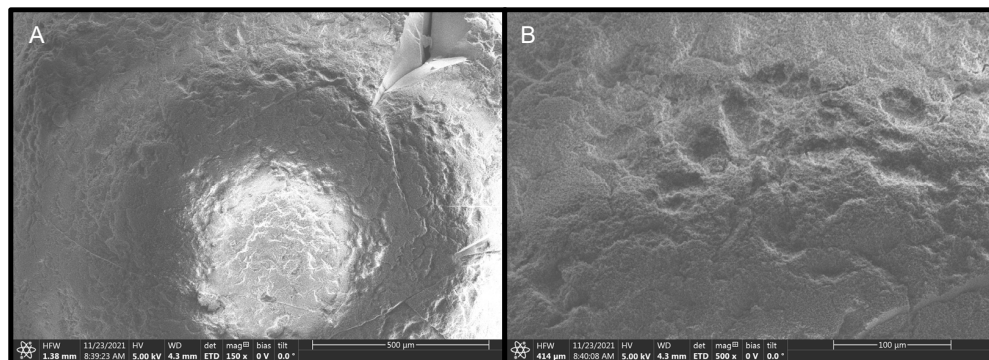


Figure VII.24.: Scanning electron microscope (SEM) images of a lyophilised chitosan gel bead's surface functionalised with glutaraldehyde and ligand L1 (CB-GA-L1) in different magnifications (A: 150x, B: 500x). SEM-EDX measurements were performed by Christian Minke on a FEI Helios G3 UC at LMU Munich.

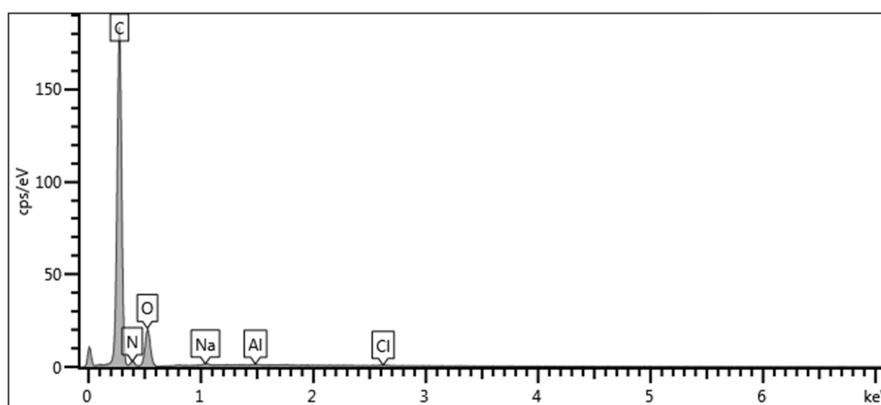


Figure VII.25.: EDX spectrum of a lyophilised chitosan gel bead's surface functionalised with glutaraldehyde and ligand L1 (CB-GA-L1). Carbon content could not be determined due to the fixation of the beads on a carbon surface for measurement.

Table VII.5.: Data from the EDX measurement of a lyophilised chitosan gel bead's surface functionalised with glutaraldehyde and ligand L1 (CB-GA-L1). Carbon content is excluded from Atom% calculations due to the fixation of the beads on a carbon surface for measurement.

Element	Atom%
N	15.2
O	81.5
Na	2.13
Al	0.61
Cl	0.53
Total:	100.00

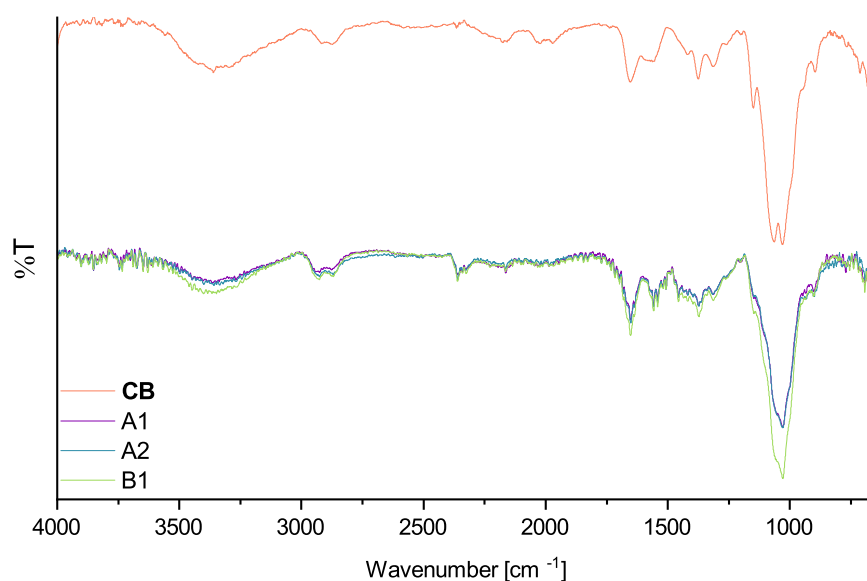
IR spectra of experiments described in Chapter IV.2 (see Figure IV.16)

Figure VII.26.: IR spectra of the functionalisation of CBs with GA with a spectrum of pure CB as a reference. Numbering and reaction conditions according to Figure IV.16. CBs of fraction A were reacted with GA either 30 min (A1) or 15 min (A2). CBs of fraction B were reacted with GA for 5 min. All reactions were performed under ambient temperature in ultrapure water. Beads were washed according to general procedure and lyophilised before measurement.

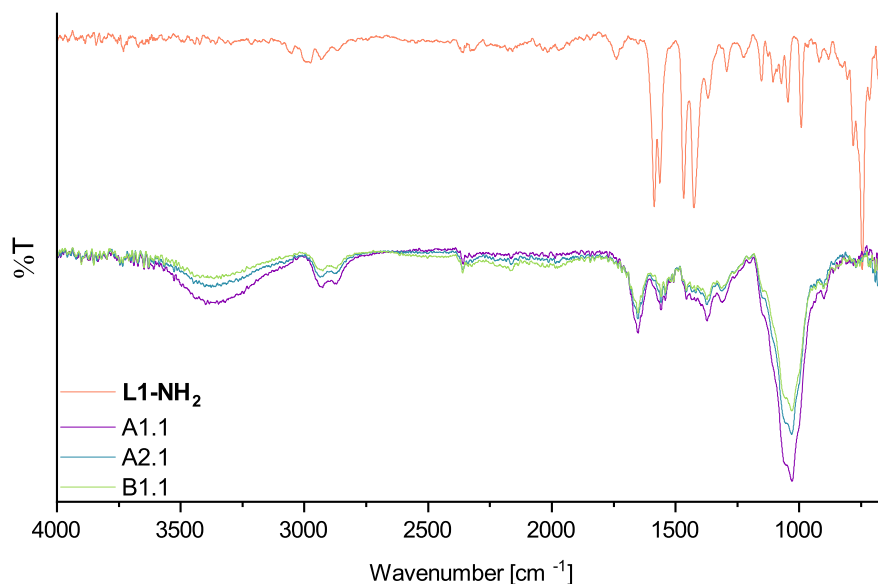


Figure VII.27.: IR spectra of the functionalisation of CB-GAs with L1 with a spectrum of pure L1 as a reference. Numbering and reaction conditions according to Figure IV.16. CB-GAs of fraction A1, A2 and B1 were each reacted with L1 (2 mM, methanol) for 16 h resulting in A1.1, A2.1 and B1.1. All reactions were performed under ambient temperature in ultrapure water. Beads were washed according to general procedure and lyophilised before measurement.

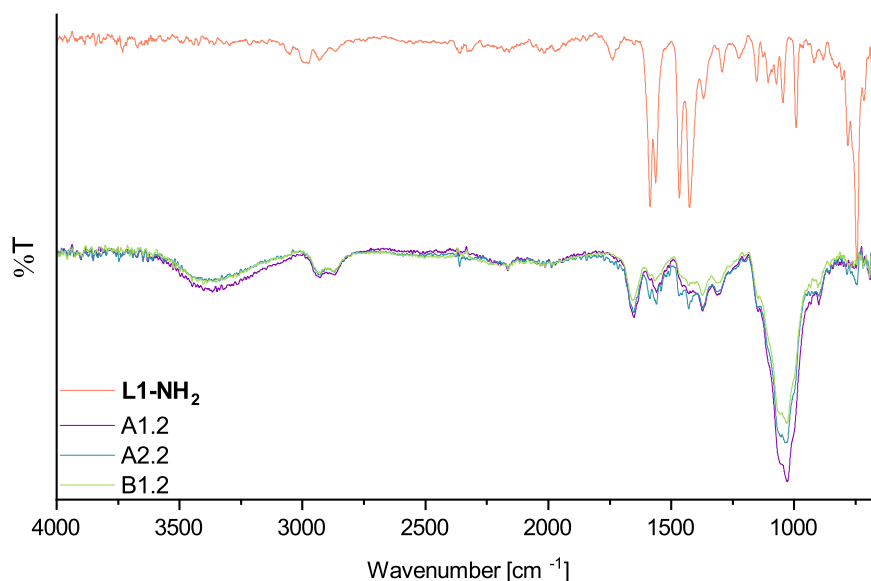


Figure VII.28.: IR spectra of the functionalisation of CB-GAs with L1 with a spectrum of pure L1 as a reference. Numbering and reaction conditions according to Figure IV.16. CB-GAs of fraction A1, A2 and B1 were each reacted with L1 (2 mM, methanol) for 20 h resulting in A1.2, A2.2 and B1.2. All reactions were performed under ambient temperature in ultrapure water. Beads were washed according to general procedure and lyophilised before measurement.

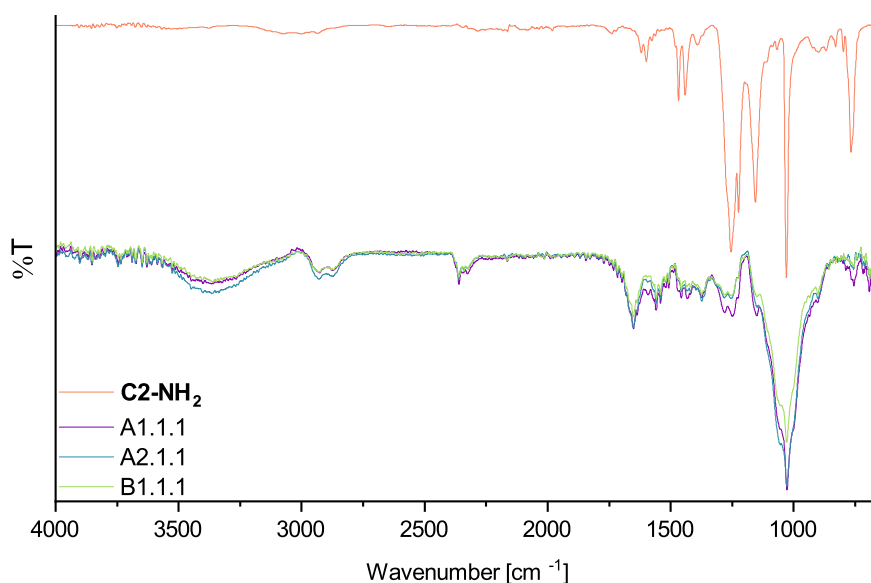


Figure VII.29.: IR spectra of the reaction of CB-GA-L1s with iron(II) triflate with a spectrum of pure C2-NH₂ as a reference. Numbering and reaction conditions according to Figure IV.16. CB-GA-L1s of fraction A1.1, A2.1 and B1.1 were each reacted with iron(II) triflate (1.0 equiv.) for 5 h without prior washing procedure resulting in A1.1.1, A2.1.1 and B1.1.1. All reactions were performed under ambient temperature in ultrapure water. Beads were washed according to general procedure and lyophilised before measurement.

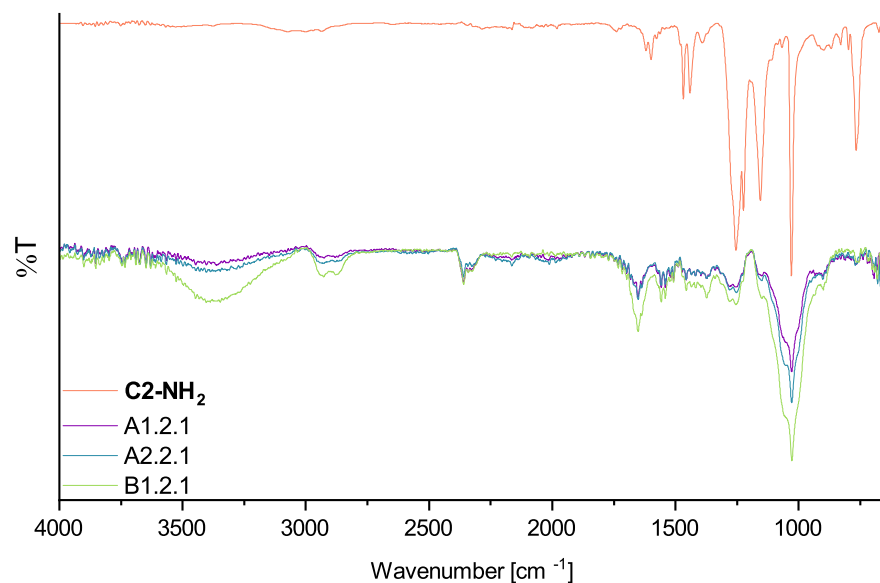


Figure VII.30.: IR spectra of the reaction of CB-GA-L1s with iron(II) triflate with a spectrum of pure C2-NH₂ as a reference. Numbering and reaction conditions according to Figure IV.16. CB-GA-L1s of fraction A1.2, A2.2 and B1.2 were each reacted with iron(II) triflate (2.5 M, water) for 20 h resulting in A1.2.1, A2.2.1 and B1.2.1. All reactions were performed under ambient temperature in ultrapure water. Beads were washed according to general procedure and lyophilised before measurement.

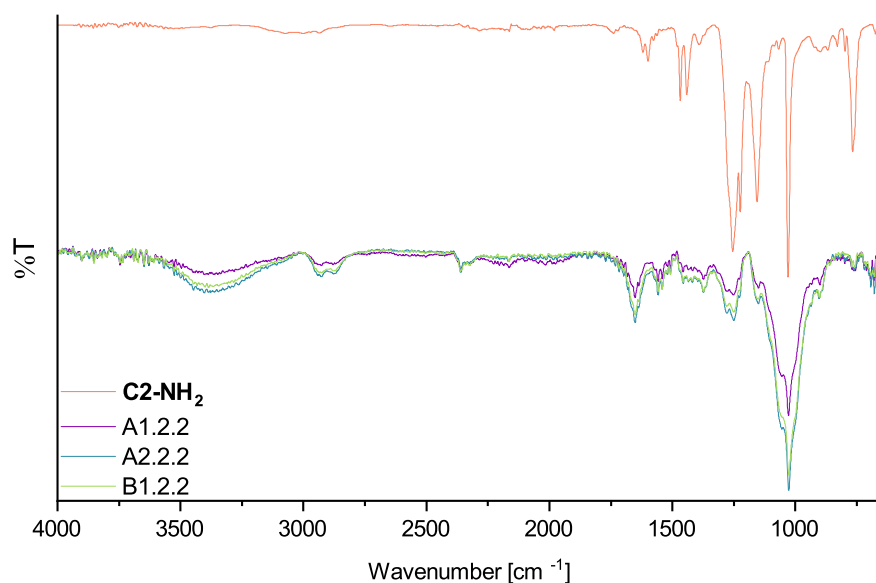


Figure VII.31.: IR spectra of the reaction of CB-GA-L1s with iron(II) triflate with a spectrum of pure C2-NH₂ as a reference. Numbering and reaction conditions according to Figure IV.16. CB-GA-L1s of fraction A1.2, A2.2 and B1.2 were each reacted with iron(II) triflate (2.5 M, water) for 20 h resulting in A1.2.2, A2.2.2 and B1.2.2. All reactions were performed under ambient temperature in ultrapure water. Beads were rinsed and lyophilised before measurement.

NMR and GC-MS spectra of glutaraldehyde at different pH values

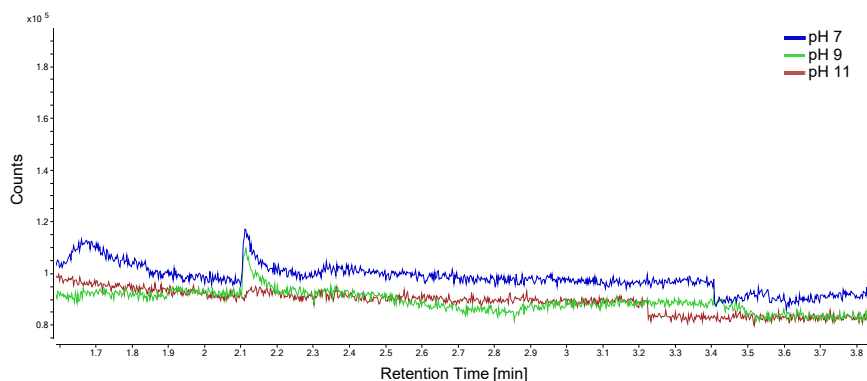


Figure VII.32.: GC spectra of a glutaraldehyde solution at different pH values. Conditions: pH 7 (0.01 mL 0.1 M NaOH, 2.00 mL water, 1.00 mL 0.1 M GA solution, 9.45 mL acetonitrile), pH 9 (0.04 mL 0.1 M NaOH, 1.95 mL water, 1.00 mL 0.1 M GA solution, 9.45 mL acetonitrile), pH11 (0.22 mL 0.1 M NaOH, 1.80 mL water, 1.00 mL 0.1 M GA solution, 9.45 mL acetonitrile). Solution were stirred for 2 h at ambient temperature. Reactions were filtered (syringe filter, 0.25 μ m) prior to GC-MS measurements. Column: HP-5ms Ultra Inert, Injection Temp.: 150 $^{\circ}$ C, Split: 1:100, Oven Temp.: 100 $^{\circ}$ C (constant-temperature), Runtime: 5 min.

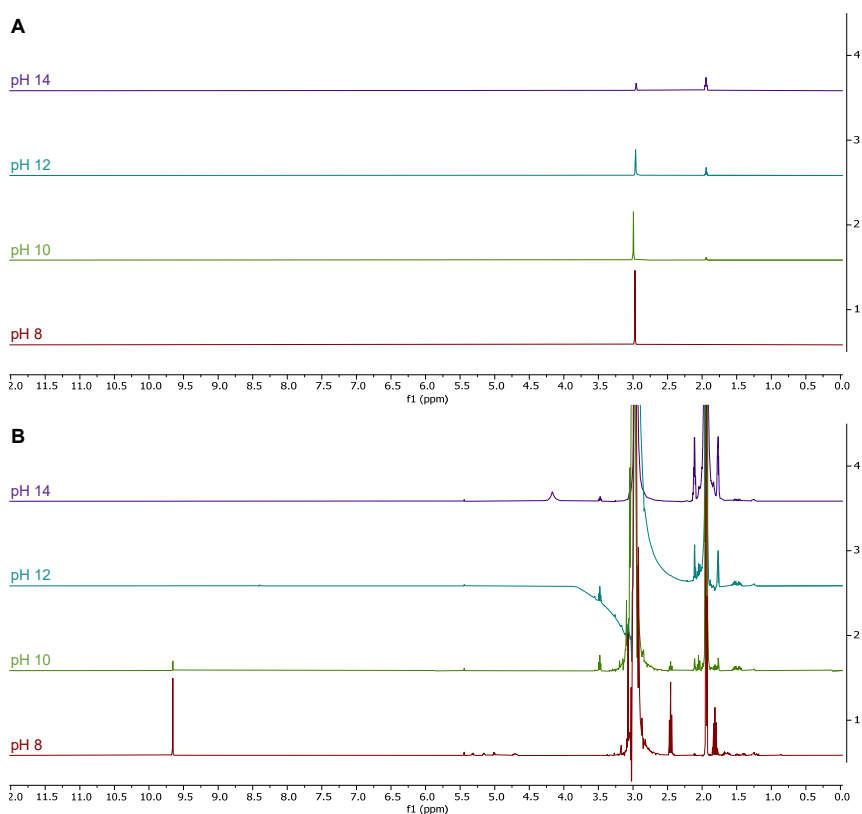


Figure VII.33.: NMR spectra of a glutaraldehyde solution at different pH values. Conditions: pH 8 (0.10 μ L NaOD, 40.0 μ L 0.1 M GA solution, 460 μ L acetonitrile- d_3), pH 10 (0.50 μ L NaOD, 40.0 μ L 0.1 M GA solution, 0.46 mL acetonitrile- d_3), pH 12 (1.00 μ L NaOD, 0.04 mL 0.1 M GA solution, 459 μ L acetonitrile- d_3), pH 14 (5.00 μ L NaOD, 0.04 mL 0.1 M GA solution, 455 μ L acetonitrile- d_3). Solutions were prepared in 1.5 mL centrifuge tubes and 450 μ L were transferred into NMR tubes for measurement. A) Zoom out showing full solvent peaks. B) Zoom in to show traces of glutaraldehyde (pH 8) and the loss of signals at higher pH values.

NMR spectra of 2L1-2GA

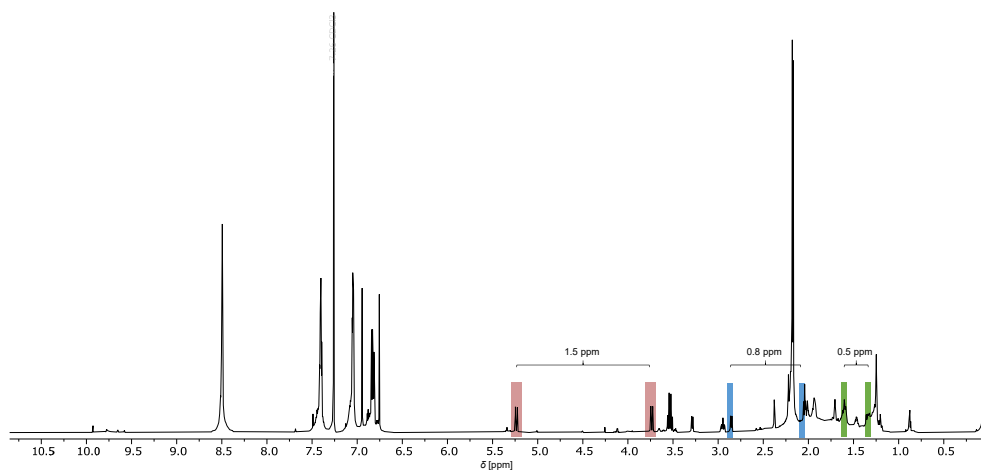


Figure VII.34.: ^1H NMR (800 MHz) of 2L1-2GA in CDCl_3 . Signal that possibly stem from diastereotopic protons are marked in rose, blue and green and the respective splitting $\Delta\delta$ is given in ppm.

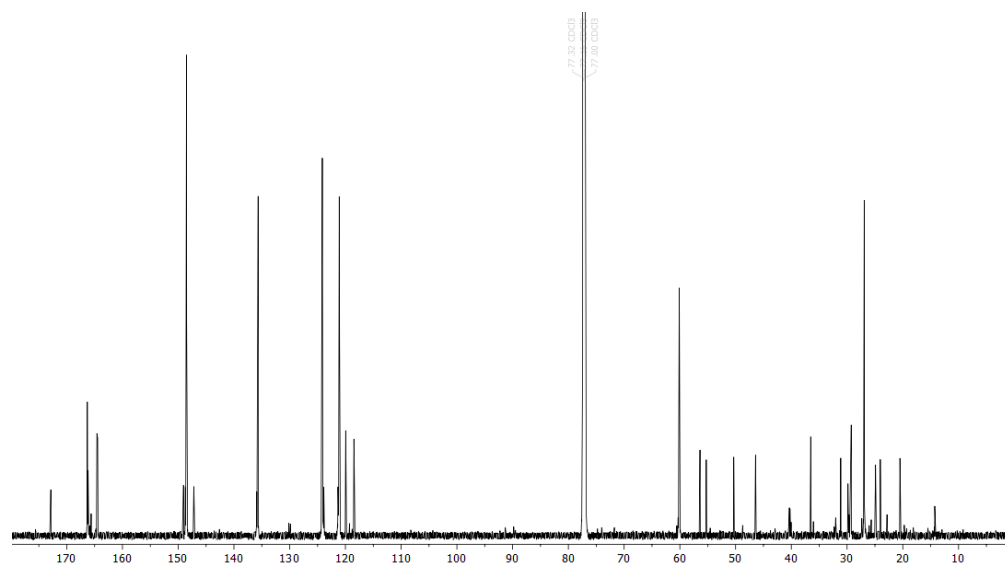
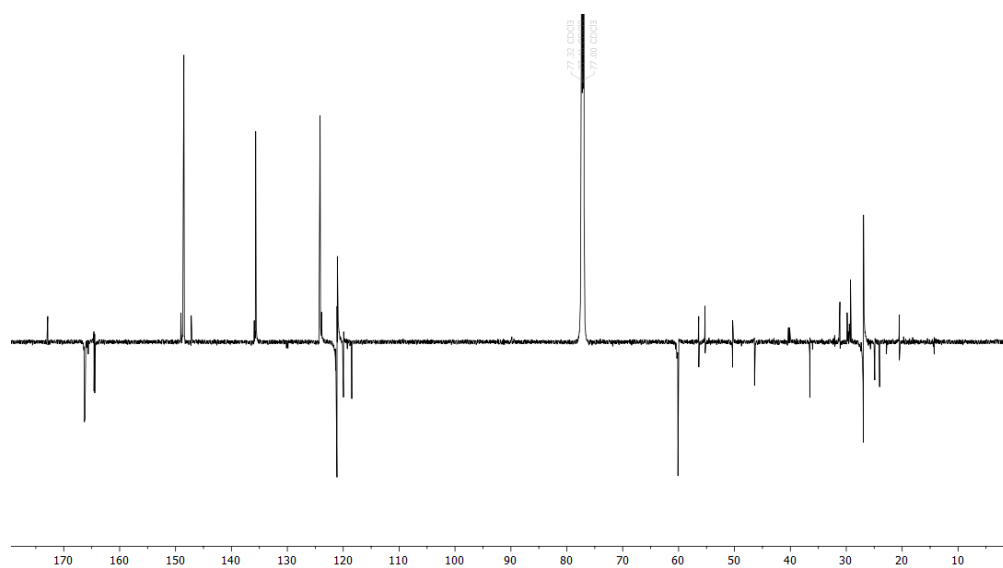
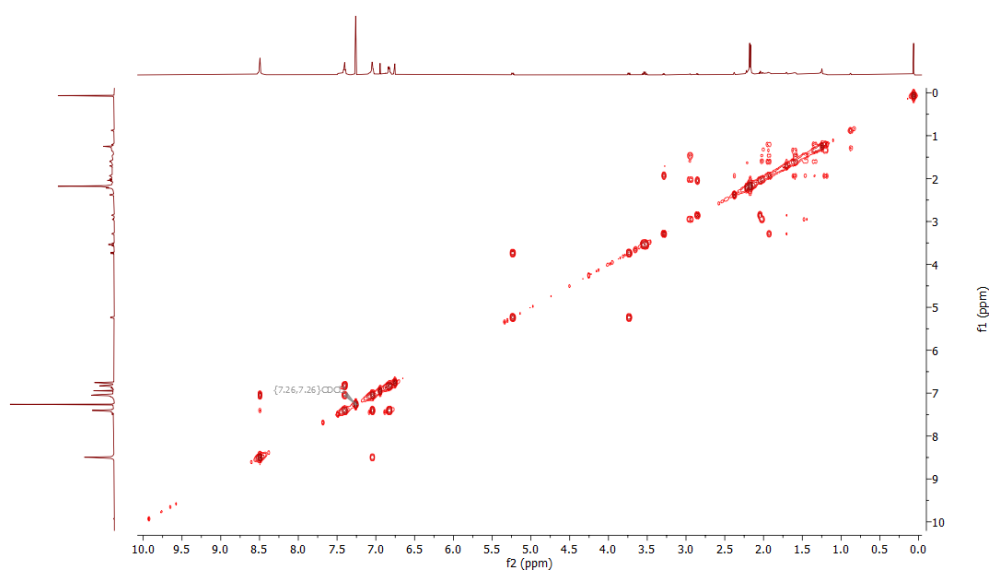


Figure VII.35.: ^{13}C NMR (200 MHz) of 2L1-2GA in CDCl_3 .

Figure VII.36.: DEPT135 NMR (200 MHz) of 2L1-2GA in CDCl₃.Figure VII.37.: 2D COSY (1H-1H) NMR (800 MHz, 298 K) of 2L1-2GA in CDCl₃.

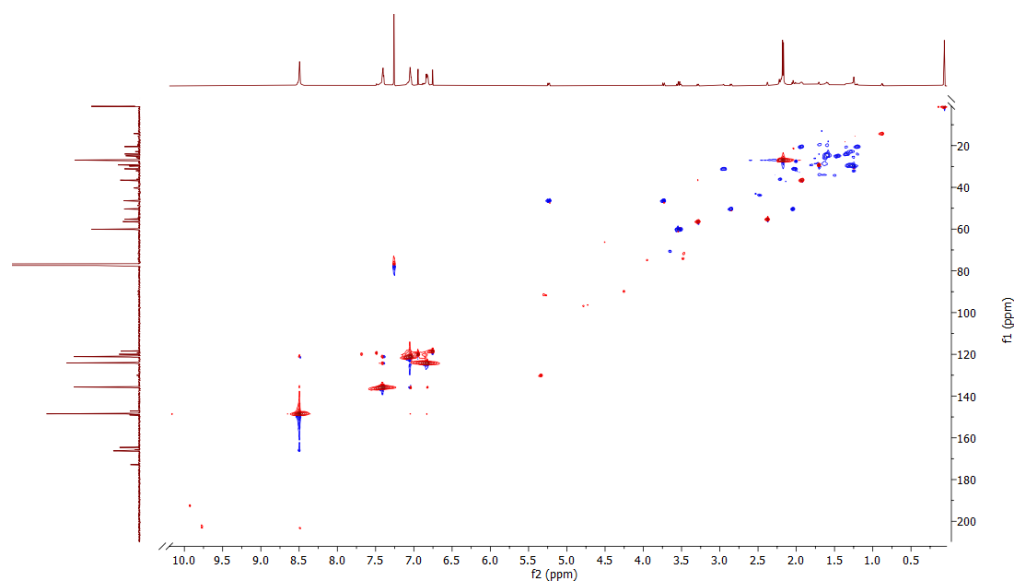


Figure VII.38.: 2D HMQC (^1H - ^{13}C) NMR (800 MHz, 200 MHz, 298 K) of 2L1-2GA in CDCl_3 .

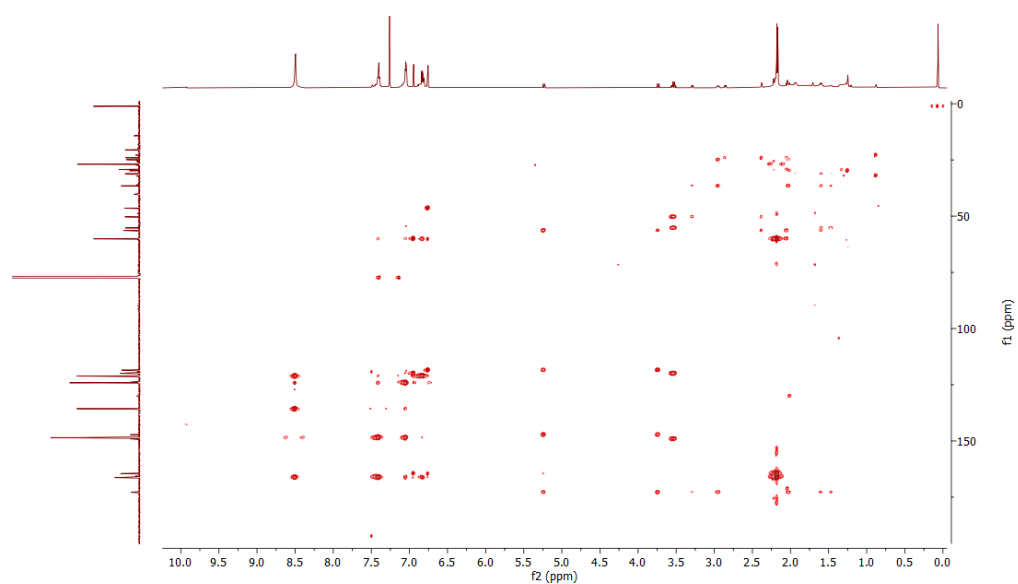


Figure VII.39.: 2D HMBC (^1H - ^{13}C) NMR (800 MHz, 200 MHz, 298 K) of 2L1-2GA in CDCl_3 .

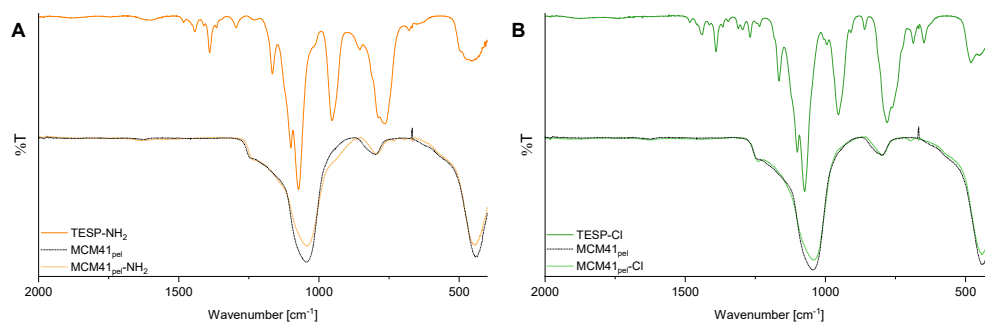
IR spectra of the functionalisation of MCM41_X with TESP-X

Figure VII.40.: A) IR spectrum of the functionalised MCM41_{pel}-NH₂ in comparison to MCM41_{pel} and TESP-NH₂. B) IR spectrum of the functionalised MCM41_{pel}-Cl in comparison to MCM41_{pel} and TESP-Cl. See Figure IV.18

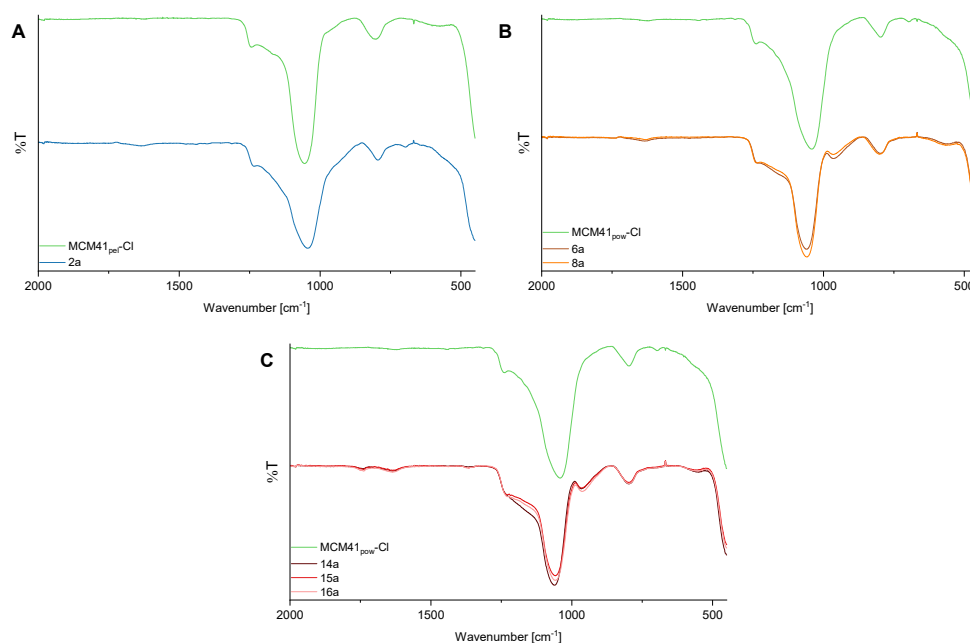


Figure VII.41.: IR spectra of tested reactions of L1-NH₂ with MCM41_X-Cl. A) 2a (MCM41_{pel}-Cl with L1-NH₂ in H₂O with NEt₃). B) 6a (MCM41_{pow}-Cl with L1-NH₂ in H₂O with NEt₃), 8a (MCM41_{pow}-Cl without L1-NH₂ in MeOH with NEt₃). C) 14a (MCM41_{pow}-Cl with L1-NH₂ in H₂O with K₂CO₃), 15a (MCM41_{pow}-Cl with L1-NH₂ in DCM/MeOH with K₂CO₃), 16a (MCM41_{pow}-Cl without L1-NH₂ in MeOH with K₂CO₃). See Table IV.3.

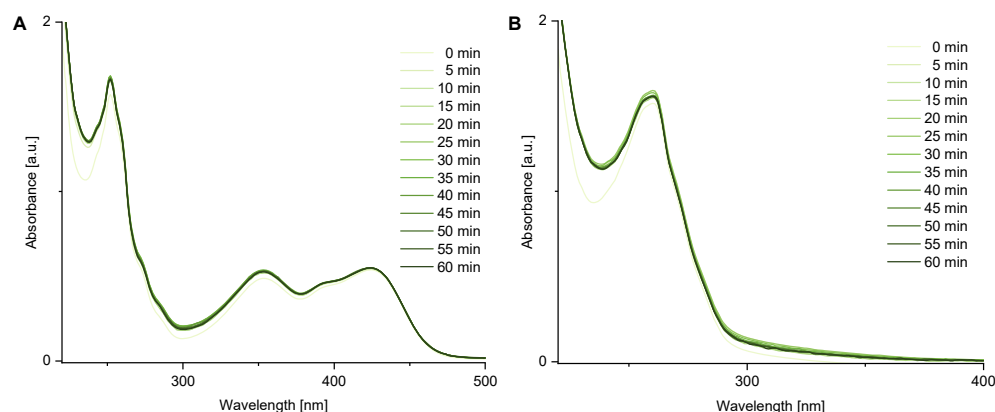
UV-Vis spectra of C2-N₃ and copper complex **25**

Figure VII.42.: A) UV-Vis spectra of iron(II) complex C2-N₃ (formed by metal titration from L1-N₃ and 1.3 equiv. iron(II) triflate, see Figure IV.5) over time after addition of 0.5 equiv. copper(II) sulfate (20 mM in MeCN). B) UV-Vis spectra of copper(II) complex **25** (formed by metal titration from L1-N₃ and 1.3 equiv. copper(II) sulfate, according to Figure IV.5) over time after addition of 0.5 equiv. iron(II) triflate (20 mM in MeCN).

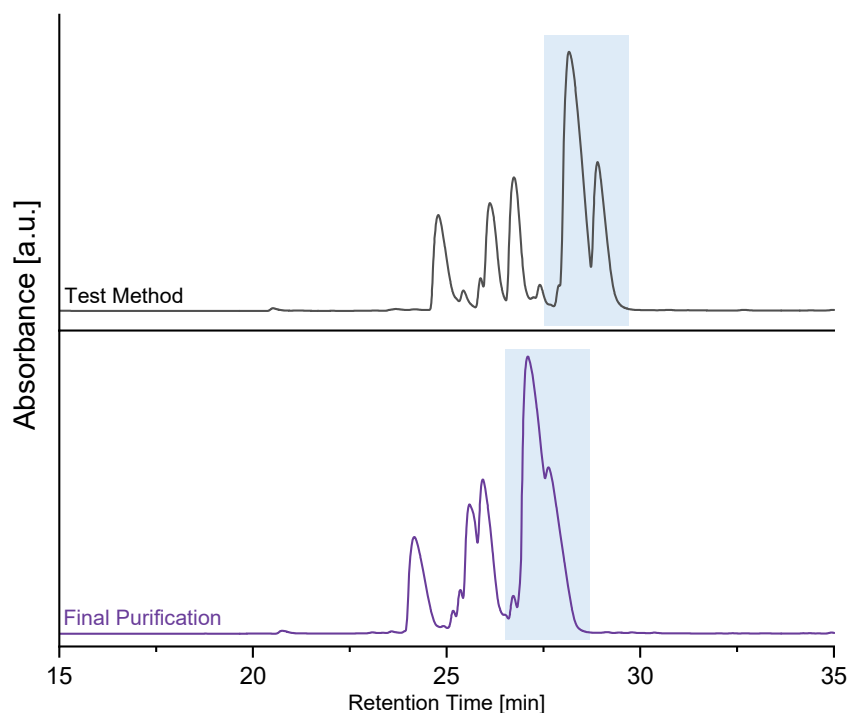
HPLC Purification of **27**

Figure VII.43.: HPLC purification of both regioisomers of **27** (see Scheme IV.17). The upper HPLC trace (254 nm) shows a test method for the purification of the compound (Agilent Zorbax SBC18, 250 mm x 30 mm – 5 μ m, 5 % to 95 % acetonitrile in water in 60 min, 0.1 % formic acid, flow 20 mL/min, Injection volume 0.3 mL, 2.5 mg/mL). The peaks marked in light blue correspond to the regioisomers of **27**, which were identified by LR-MS. Found mass: 451.2 m/z, 901.0 m/z. Theoretical value: 451.18 m/z [M+2H]²⁺, 901.36 m/z [M+H]⁺. As the separation of both isomers is not needed in this case, the same method with a higher injection volume and concentration (displayed in the lower trace, 254 nm) was used for further purification (Injection volume 1 mL, 5 mg/mL).

6. IR Spectra

IR spectrum of L1-NH₂

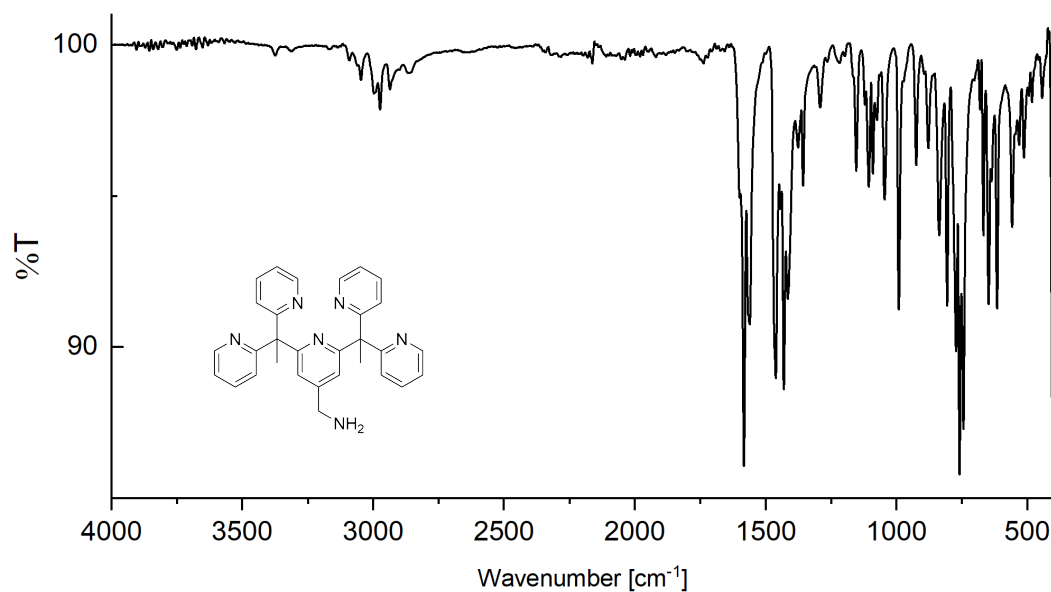


Figure VII.44.: IR spectrum of ligand L1-NH₂ measured on a PerkinElmer Spectrum Two FT/IR spectrometer and processed with Origin 2021b as described in Chapter VI.2.

IR spectrum of L1-OH

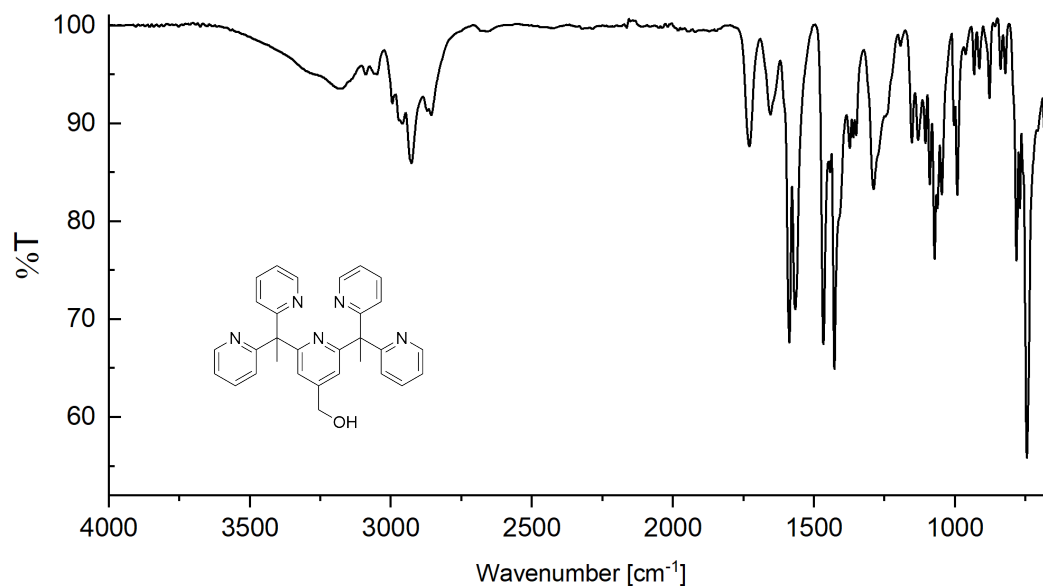


Figure VII.45.: IR spectrum of ligand L1-OH measured on a Jasco FT/IR-460Plus spectrometer and processed with Origin 2021b as described in Chapter VI.2.

IR spectrum of L1-Cl

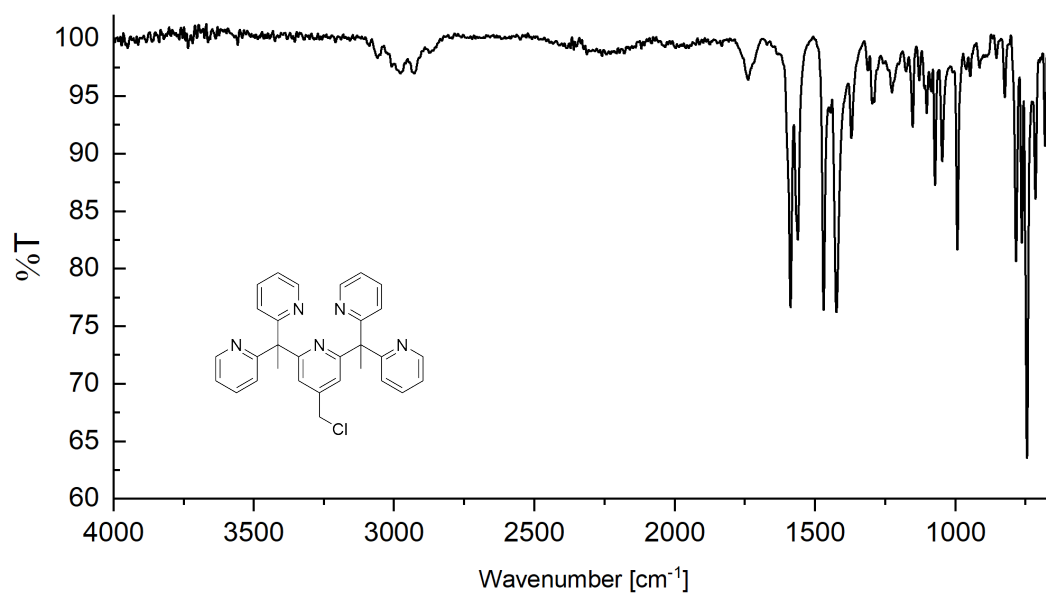


Figure VII.46.: IR spectrum of ligand L1-Cl measured on a Jasco FT/IR-460Plus spectrometer and processed with Origin 2021b as described in Chapter VI.2.

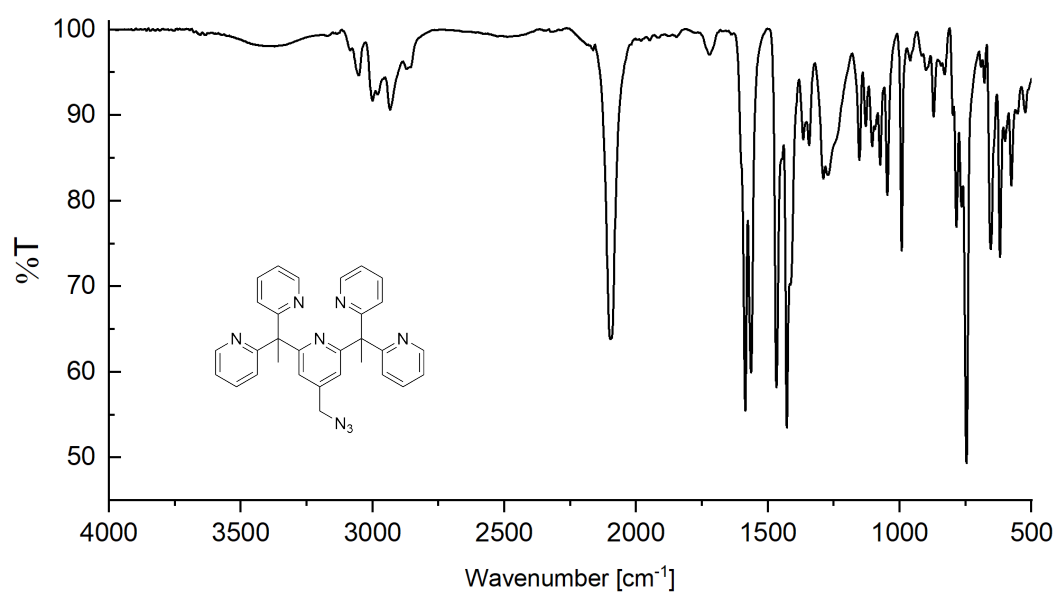
IR spectrum of L1-N₃

Figure VII.47.: IR spectrum of ligand L1-N₃ measured on a PerkinElmer Spectrum Two FT/IR spectrometer and processed with Origin 2021b as described in Chapter VI.2.

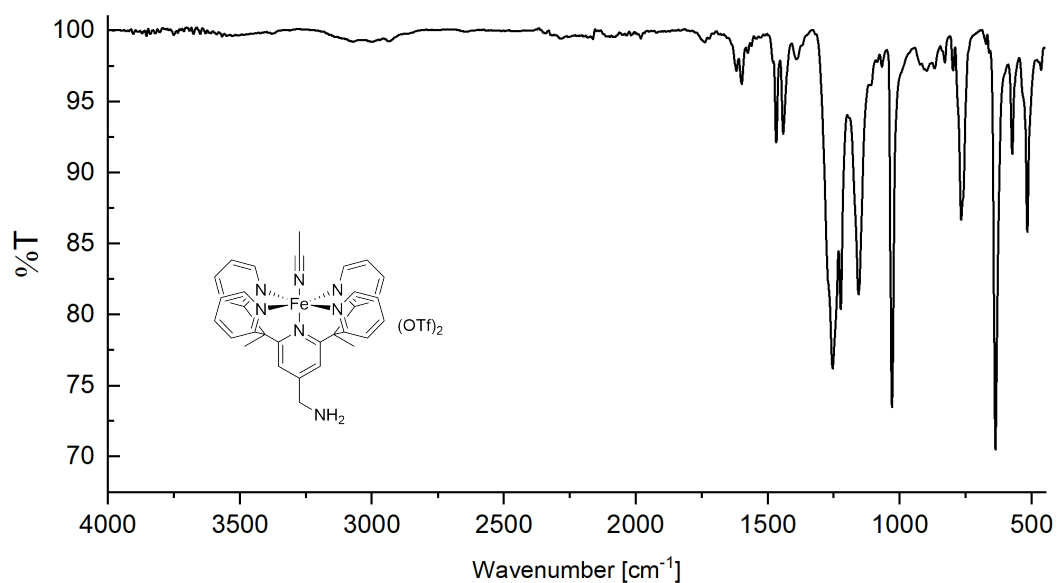
IR spectrum of C2-N₂

Figure VII.48.: IR spectrum of ligand C2-N₂ measured on a PerkinElmer Spectrum Two FT/IR spectrometer and processed with Origin 2021b as described in Chapter VI.2.

IR spectrum of C2-Cl

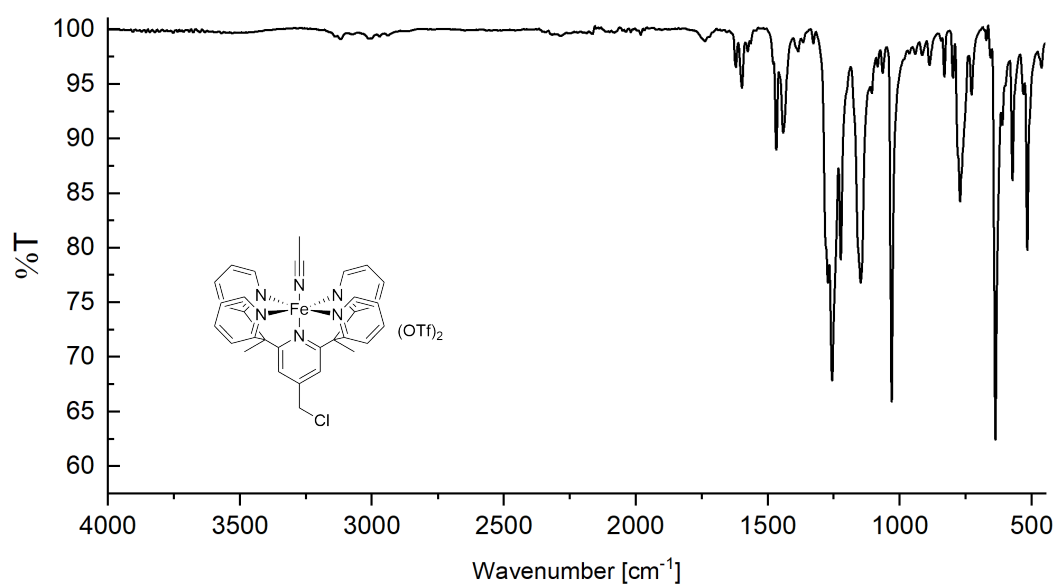


Figure VII.49.: IR spectrum of ligand C2-Cl measured on a PerkinElmer Spectrum Two FT/IR spectrometer and processed with Origin 2021b as described in Chapter VI.2.

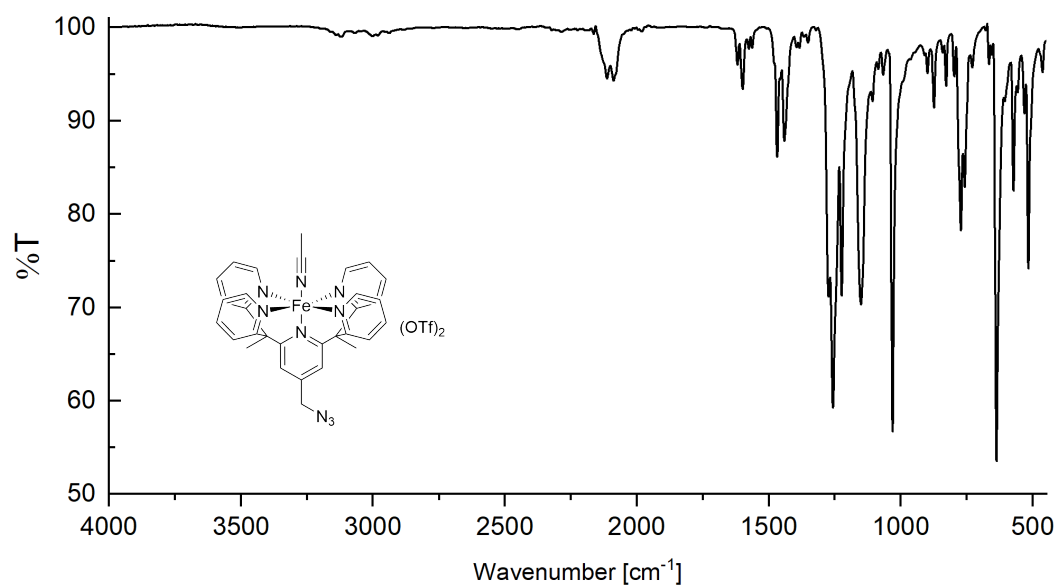








IR spectrum of C2-N₃

Figure VII.50.: IR spectrum of ligand C2-N₃ measured on a PerkinElmer Spectrum Two FT/IR spectrometer and processed with Origin 2021b as described in Chapter VI.2.

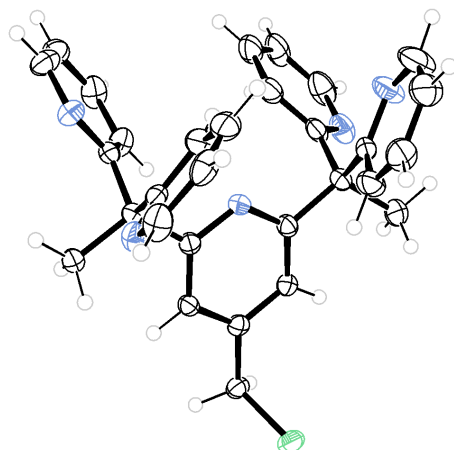
7. Crystallographic Data

All shown crystallographic data was measured and processed according to Chapter VI2. All graphical representations were created using Ortep3. Atom colours are given in Table VII.6.

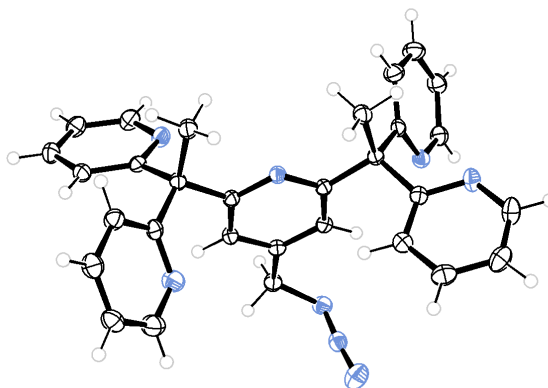
Table VII.6.: Colours used for graphical representations of different atoms in crystal structures. Colour names are given according to their name used in Ortep3.

Atom		Colour
Carbon	black	
Hydrogen	light grey	
Nitrogen	dark turquoise	
Oxygen	scarlet	
Fluorine	yellow green	
Chlorine	forest green	
Sulfur	bright gold	
Iron	orange	

Crystallographic Data of L1-Cl

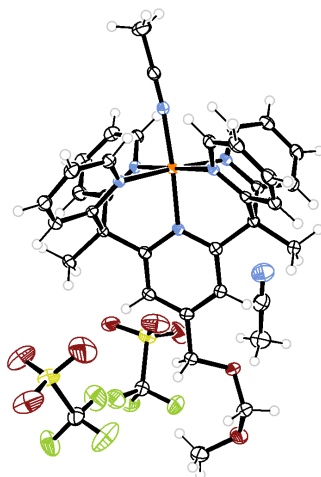


Formula	C ₃₀ H ₂₆ ClN ₅
M_r [g mol ⁻¹]	429.01
Calc. density [g/cm ³]	1.276
Crystal size [mm]	0.40 x 0.20 x 0.18
μ [mm ⁻¹]	0.176
Crystal system	orthorhombic
Space group	'P c a 21'
Z	4
a [Å]	16.9571(5)
b [Å]	9.2118(3)
c [Å]	16.5092(5)
α [°]	90
β [°]	90
γ [°]	90
V [Å ³]	2578.83(14)
Diffractometer	'Bruker D8 Venture TXS' (LMU)
Radiation	MoK α
T [K]	101
Θ range [°]	2.2150-26.8240
Absorption correction	Multi-Scan
Transmission factor range	0.913-1.000
Observed reflexes	6392
Reflexes in refinement	5602
R_{int}	0.0439
x, y (weighting scheme)	0.0435, 0.6723
Hydrogen refinement	H(C) constr
Parameters	327
Restraints	1
$R(F_{obs})$	0.0421
$R_w(F^2)$	0.0953
S	1.036
$shift/error_{max}$	0.000
max. electron density [e ²]	0.253
min. electron density [e ²]	-0.186

Crystallographic Data of L1-N₃

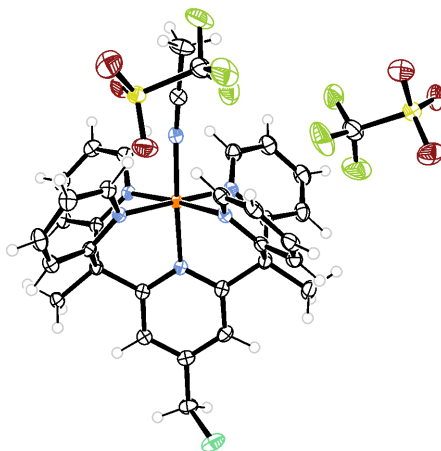
Formula	C ₃₀ H ₂₆ N ₈
<i>M_r</i> [g mol ⁻¹]	498.59
Calc. density [g/cm ³]	1.359
Crystal size [mm]	0.309 x 0.190 x 0.035
μ [mm ⁻¹]	0.673
Crystal system	triclinic
Space group	'P -1'
Z	2
<i>a</i> [Å]	8.93930(10)
<i>b</i> [Å]	9.7409(2)
<i>c</i> [Å]	15.3520(2)
α [°]	85.5040(10)
β [°]	85.4100(10)
γ [°]	66.242(2)
<i>V</i> [Å ³]	1218.03(4)
Diffractometer	'Rigaku XtaLAB Synergy S' (HHU)
Radiation	CuK α
Wavelength	1.54184 Å
T [K]	150
Θ range [°]	2.891-78.718
Absorption correction	Multi-Scan
Transmission factor range	0.95931-1.00000
Observed reflexes	4793
Reflexes in refinement	4526
<i>R_{int}</i>	0.0212
<i>x</i> , <i>y</i> (weighting scheme)	0.0552, 0.3931
Hydrogen refinement	H(C) constr
Parameters	345
Restraints	0
<i>R</i> (<i>F_{obs}</i>)	0.0366
<i>R_w</i> (<i>F</i> ²)	0.0996
<i>S</i>	1.049
<i>shift/error_{max}</i>	0.045
max. electron density [e ²]	0.360
min. electron density [e ²]	-0.234

Crystallographic Data of C2-OMOM



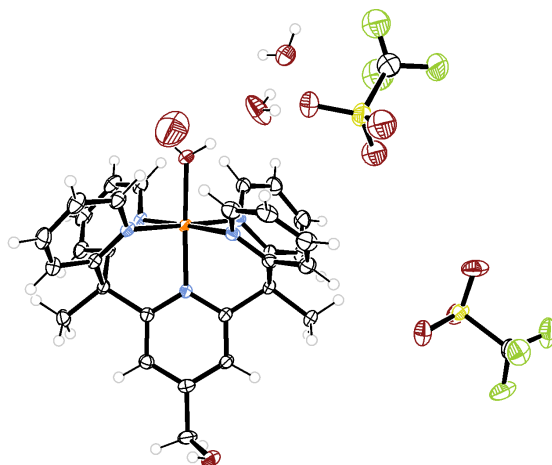
Formula	C ₃₄ H ₃₄ FeN ₆ O ₂ , 2 (CF ₃ O ₃ S), C ₂ H ₃ N
M_r [g mol ⁻¹]	935.72
Calc. density [g/cm ³]	1.602
Crystal size [mm]	0.38 x 0.37 x 0.08
μ [mm ⁻¹]	0.579
Crystal system	monoclinic
Space group	'P 21/c'
Z	4
a [Å]	12.0859(5)
b [Å]	14.5426(5)
c [Å]	22.5185(8)
α [°]	90
β [°]	92.535(3)
γ [°]	90
V [Å ³]	3954.0(3)
Diffractometer	'Bruker D8 Venture TXS' (LMU)
Radiation	MoK α
Wavelength	0.71073 Å
T [K]	102
Θ range [°]	1.784-29.707
Absorption correction	Multi-Scan
Transmission factor range	0.87321-1.00000
Observed reflexes	9801
Reflexes in refinement	7250
R_{int}	0.0584
x, y (weighting scheme)	0.0541, 3.5555
Hydrogen refinement	H(C) constr
Parameters	564
Restraints	0
$R(F_{obs})$	0.0472
$R_w(F^2)$	0.1103
S	1.036
$shift/error_{max}$	0.087
max. electron density [e ²]	0.654
min. electron density [e ²]	-0.433

Crystallographic Data of C2-Cl



Formula	C ₃₂ H ₂₉ ClFeN ₆ , 2 (CF ₃ O ₃ S)
<i>M_r</i> [g mol ⁻¹]	887.05
Calc. density [g/cm ³]	1.660
Crystal size [mm]	0.160 x 0.093 x 0.065
μ [mm ⁻¹]	5.983
Crystal system	triclinic
Space group	'P 21/c'
<i>Z</i>	4
<i>a</i> [Å]	9.59840(10)
<i>b</i> [Å]	21.36250(10)
<i>c</i> [Å]	17.32430(10)
α [°]	90
β [°]	91.9680(10)
γ [°]	90
<i>V</i> [Å ³]	3550.18(5)
Diffractometer	'Rigaku XtaLAB Synergy-S' (HHU)
Radiation	CuK α
Wavelength	1.54184 Å
<i>T</i> [K]	150
Θ range [°]	3.286-74.624
Absorption correction	Multi-Scan
Transmission factor range	0.55277-1.00000
Observed reflexes	7090
Reflexes in refinement	6864
<i>R_{int}</i>	0.0342
<i>x</i> , <i>y</i> (weighting scheme)	0.0281, 2.8226
Hydrogen refinement	H(C) constr
Parameters	508
Restraints	0
<i>R</i> (<i>F_{obs}</i>)	0.0314
<i>R_w</i> (<i>F</i> ²)	0.726
<i>S</i>	1.087
<i>shift/error_{max}</i>	0.001
max. electron density [e ²]	0.335
min. electron density [e ²]	-0.301

Crystallographic Data of C3-OH



Formula	C ₃₀ H ₂₉ FeN ₅ O ₂ , 2 (CF ₃ O ₃ S), 3 H ₂ O
<i>M_r</i> [g mol ⁻¹]	899.62
Calc. density [g/cm ³]	1.683
Crystal size [mm]	0.12 x 0.04 x 0.03
μ [mm ⁻¹]	0.643
Crystal system	triclinic
Space group	'P -1'
Z	2
<i>a</i> [Å]	11.0078(4)
<i>b</i> [Å]	13.1643(6)
<i>c</i> [Å]	13.3562(5)
α [°]	73.0310(10)
β [°]	89.2180(10)
γ [°]	74.0760(10)
<i>V</i> [Å ³]	1775.50(12)
Diffractometer	'Bruker D8 Venture TXS' (LMU)
Radiation	MoKα
T [K]	173
Θ range [°]	2.899-27.102
Absorption correction	Multi-Scan
Transmission factor range	0.91-0.98
Observed reflexes	6225
Reflexes in refinement	7772
<i>R_{int}</i>	0.0383
<i>x</i> , <i>y</i> (weighting scheme)	0.0599, 5.0976
Hydrogen refinement	mixed
Parameters	541
Restraints	27
R(<i>F_{obs}</i>)	0.0575
R _w (<i>F</i> ²)	0.1496
<i>S</i>	1.024
<i>shift/error_{max}</i>	0.001
max. electron density [e ²]	1.522
min. electron density [e ²]	-0.987

8. List of Abbreviations

%T percent transmittance

Ac acetate

α -KG α -ketoglutarate

approx. approximately

ATR attenuated total reflection

BDE bond dissociation energy

Bu butyl

calc. calculated

CAN ceric ammonium nitrate

CB chitosan gel bead

CNT carbon nanotube

COSY homonuclear correlation spectroscopy

COVID coronavirus disease

CuAAC copper catalysed azide-alkyne cycloaddition

cv column volumes

δ chemical shift (NMR)

d doublet

DBCO dibenzocyclooctyne

DBU 1,8-diazabicyclo[5.4.0]undec-7-ene

DCM dichloromethane

DEPT distortionless enhancement by polarization transfer

DFG Deutsche Forschungsgemeinschaft

DFT density functional theory

DIAD diisopropyl azodicarboxylate

DIPEA *N,N*-diisopropylethylamine

DMF dimethylformamide

DMP data management plan

DMSO dimethyl sulfoxide

DNA deoxyribonucleic acid

DNMT DNA methyltransferase

DOI digital object identifier

EA elemental analysis

EDX energy-dispersive X-ray spectroscopy

EI electron ionization

ELN electronic laboratory notebook

equiv. equivalents

ERC European Research Council

ESI electrospray ionization

Et ethyl

FA formic acid

FAIR findable accessible interoperable reusable

FT fourier transformation

GA glutaraldehyde

GC gas chromatography

HAT hydrogen atom transfer

Hex hexane

HHU Heinrich Heine University

HMBC heterobinuclear multiple bond connectivity

HMQC heterobinuclear multiple quantum correlation

HPLC high-performance liquid chromatography

HR high resolution

i iso

ICP-OES inductively coupled plasma optical emission spectroscopy

ID identification

IR Infrared

IUPAC International Union of Pure and Applied Chemistry

J coupling constant

LMU Ludwig-Maximilians University

LR low resolution

m multiplet

MCM41 mobil composition of matter number 41

MDH methanol dehydrogenase

Me methyl

MNP magnetic nanoparticle

MOF metal-organic framework

MOMCl chloromethyl methyl ether

MS mass spectrometry

NHS *N*-hydroxysuccinimide

NMR nuclear magnetic resonance

p.a. pro analysi

PCR polymerase chain reaction

pel pellet

PFP	pentafluorophenyl
PhD	doctor of philosophy
pow	powder
PQQ	pyrroloquinoline quinone
q	quartet
QM	quantum mechanics
R_f	retardation factor
r.t.	room temperature
RDM	research data management
RNA	ribonucleic acid
s	singlet
SEM	scanning electron microscope
SPAAC	strain promoted azide-alkyne cycloaddition
t	triplet
TA	triazole
TauD	taurine- α -ketoglutarate dioxygenase
TBAH	tetrabutylammonium hydroxide
Temp.	temperature
TESP	tri-ethoxy-silyl-propyl
TET	ten-eleven-translocation
THF	tetrahydrofuran
TLC	thin-layer chromatography
TOF	turnover frequency
UV	ultraviolet
VHS	video home system
VPN	virtual private network
ZIM	center for information and media technology

9. Bibliography

- [1] EUROPEAN COMMISSION, *A European strategy for data*, COM(2020) 66 final, **2020**, <https://eur-lex.europa.eu/legal-content/EN/TXT/?qid=1593073685620&uri=CELEX%3A52020DC0066>, Accessed: 03.02.2025.
- [2] Tommaso Boccali, Anne Elisabeth Søltnes, Mark Thorley, Stefan Winkler-Nees, Marie Timmermann, *Sci. Eur.* **2021**.
- [3] Deutsche Forschungsgemeinschaft DFG, *DFG Guidelines on the Handling of Research Data*, **2015**, <https://www.dfg.de/resource/blob/172098/b08fcad16f1ff5ddca967f1ebde3a8c3/guidelines-research-data-data.pdf>, Accessed: 03.02.2025.
- [4] Deutsche Forschungsgemeinschaft DFG, Fachkollegien Chemie, "*Chemistry*" Review Boards on the handling of research data, **2021**, <https://www.dfg.de/resource/blob/175558/e4310513bf5e2d3bc3a8bfd611c3989c/handreichung-fachkollegien-chemie-forschungsdaten-data.pdf>, Accessed: 03.02.2025.
- [5] European Research Council, Scientific Council, *Open Research Data and Data Management Plans*, **2022**, https://erc.europa.eu/sites/default/files/document/file/ERC_info_document-Open_Research_Data_and_Data_Management_Plans.pdf, Accessed: 03.02.2025.
- [6] T. H. Vines, A. Y. K. Albert, R. L. Andrew, F. Débarre, D. G. Bock, M. T. Franklin, K. J. Gilbert, J.-S. Moore, S. Renaut, D. J. Rennison, *Curr. Biol.* **2014**, *24*, 94–97.
- [7] L. Bezuidenhout, *Dev. World Bioeth.* **2019**, *19*, 18–24.
- [8] R. G. Curty, K. Crowston, A. Specht, B. W. Grant, E. D. Dalton, *PLoS One* **2017**, *12*, e0189288.
- [9] D. R. Donaldson, J. W. Koepke, *Sci. Data* **2022**, *9*, 345.
- [10] T. Perrino, G. Howe, A. Sperling, W. Beardslee, I. Sandler, D. Shern, H. Pantin, S. Kaupert, N. Cano, G. Cruden, F. Bandiera, C. H. Brown, *Perspect. Psychol. Sci.* **2013**, *8*, 433–444.
- [11] D. G. Roche, L. E. B. Kruuk, R. Lanfear, S. A. Binning, *PLoS Biol.* **2015**, *13*, e1002295.
- [12] A. Subaveerapandiyan, *Science* **2023**.
- [13] M. D. Wilkinson, M. Dumontier, I. J. J. Aalbersberg, G. Appleton, M. Axton, A. Baak, N. Blomberg, J.-W. Boiten, L. B. Da Silva Santos, P. E. Bourne, J. Bouwman, A. J. Brookes, T. Clark, M. Crosas, I. Dillo, O. Dumon, S. Edmunds, C. T.

- Evelo, R. Finkers, A. Gonzalez-Beltran, A. J. G. Gray, P. Groth, C. Goble, J. S. Grethe, J. Heringa, P. A. C. 't Hoen, R. Hooft, T. Kuhn, R. Kok, J. Kok, S. J. Lusher, M. E. Martone, A. Mons, A. L. Packer, B. Persson, P. Rocca-Serra, M. Roos, R. van Schaik, S.-A. Sansone, E. Schultes, T. Sengstag, T. Slater, G. Strawn, M. A. Swertz, M. Thompson, J. van der Lei, E. van Mulligen, J. Velterop, A. Waagmeester, P. Wittenburg, K. Wolstencroft, J. Zhao, B. Mons, *Sci. Data* **2016**, 3, 160018.
- [14] B. Mons, C. Neylon, J. Velterop, M. Dumontier, L. O. B. Da Silva Santos, M. D. Wilkinson, *ISU* **2017**, 37, 49–56.
- [15] N. Bagdasarian, G. B. Cross, D. Fisher, *BMC Med.* **2020**, 18, 192.
- [16] Q.-H. Vuong, T.-T. Le, V.-P. La, H. T. T. Nguyen, M.-T. Ho, Q. van Khuc, M.-H. Nguyen, *Humanit. Soc. Sci. Commun.* **2022**, 9, 22.
- [17] K. Sijsma, *Never Waste a Good Crisis*, Chapman and Hall/CRC, Boca Raton, **2023**.
- [18] W. Stroebe, T. Postmes, R. Spears, *Perspect. Psychol. Sci.* **2012**, 7, 670–688.
- [19] Europäische Kommission, Generaldirektion Forschung und Innovation, *Turning FAIR into reality – Final report and action plan from the European Commission expert group on FAIR data*, **2018**, <https://data.europa.eu/doi/10.2777/1524>, Accessed: 08.02.2025.
- [20] European Commission: Directorate-General for Research and Innovation, *Horizon Europe, open science – Early knowledge and data sharing, and open collaboration*, **2021**, <https://data.europa.eu/doi/10.2777/18252>.
- [21] Rachel Janßen, *Synthesis of Novel Pyrroloquinoline Quinone Derivatives*, Master Thesis, Ludwig-Maximilians-Universität Munich, **2020**.
- [22] Violeta A. Vetsova, *Biomimetics for Lanthanide and Calcium Dependent Alcohol Dehydrogenases*, Dissertation, Ludwig-Maximilians-Universität Munich, **2023**.
- [23] J. A. Duine, R. A. van der Meer, B. W. Groen, *Annu. Rev. Nutr.* **1990**, 10, 297–318.
- [24] J. A. Duine, *J. Biosci. Bioeng.* **1999**, 88, 231–236.
- [25] M. Akagawa, M. Nakano, K. Ikemoto, *Biosci. Biotechnol.* **2016**, 80, 13–22.
- [26] V. Laurinavicius, J. Razumiene, B. Kurtinaitiene, I. Lapenaite, I. Bachmatova, L. Marcinkeviciene, R. Meskys, A. Ramanavicius, *Bioelectrochemistry* **2002**, 55, 29–32.
- [27] C. Anthony, M. Ghosh, C. C. Blake, *Biochem. J.* **1994**, 304 (Pt 3), 665–674.

- [28] A. Pol, T. R. M. Barends, A. Dietl, A. F. Khadem, J. Eygensteyn, M. S. M. Jetten, H. J. M. Op den Camp, *Environ. Microbiol.* **2014**, *16*, 255–264.
- [29] H. Lumpe, L. J. Daumann, *Inorg. Chem.* **2019**, *58*, 8432–8441.
- [30] H. Lumpe, A. Menke, C. Haisch, P. Mayer, A. Kabelitz, K. V. Yussenko, A. Guilherme Buzanich, T. Block, R. Pöttgen, F. Emmerling, L. J. Daumann, *Chem. Eur. J.* **2020**, *26*, 10133–10139.
- [31] V. A. Vetsova, K. R. Fisher, H. Lumpe, A. Schäfer, E. K. Schneider, P. Weis, L. J. Daumann, *Chem. Eur. J.* **2021**, *27*, 10087–10098.
- [32] R. Janßen, V. A. Vetsova, D. Putz, P. Mayer, L. J. Daumann, *Synthesis* **2023**, *55*, 1000–1006.
- [33] B. Jahn, A. Pol, H. Lumpe, T. R. M. Barends, A. Dietl, C. Hogendoorn, H. J. M. Op den Camp, L. J. Daumann, *ChemBioChem* **2018**, *19*, 1147–1153.
- [34] L. O. Björn, *Elements of Life and Death*, Cambridge Scholars Publishing, Newcastle upon Tyne, **2023**.
- [35] N. Nakamura, T. Kohzuma, H. Kuma, S. Suzuki, *Inorg. Chem.* **1994**, *33*, 1594–1599.
- [36] T. Ishida, M. Doi, K. Tomita, H. Hayashi, M. Inoue, T. Urakami, *J. Am. Chem. Soc.* **1989**, *111*, 6822–6828.
- [37] H. Mitome, T. Ishizuka, Y. Shiota, K. Yoshizawa, T. Kojima, *Dalton. Trans.* **2015**, *44*, 3151–3158.
- [38] R. S. McDonald, P. A. Wilks, *Appl. Spectrosc.* **1988**, *42*, 151–162.
- [39] C.-L. Lin, P.-C. Huang, S. Gräfle, C. Grathwol, P. Tremouilhac, S. Vanderheiden, P. Hodapp, S. Herres-Pawlis, A. Hoffmann, F. Fink, G. Manolikakes, T. Opatz, A. Link, M. M. B. Marques, L. J. Daumann, M. Tsotsalas, F. Biedermann, H. Mutlu, E. Täuscher, F. Bach, T. Drees, S. Neumann, S. S. Harivyasi, N. Jung, S. Bräse, *Sci. Data* **2025**, *12*, 130.
- [40] C. Anthony, *Antioxid. Redox Signal.* **2001**, *3*, 757–774.
- [41] P. D. Sarmiento-Pavía, M. E. Sosa-Torres, *J. Biol. Inorg. Chem.* **2021**, *26*, 177–203.
- [42] Z. Guo, O. Smutok, W. A. Johnston, C. E. Ayva, P. Walden, B. McWhinney, J. P. J. Ungerer, A. Melman, E. Katz, K. Alexandrov, *Angew. Chem.* **2022**, *134*, e202109005.
- [43] H. Lee, Y. J. Hong, S. Baik, T. Hyeon, D.-H. Kim, *Adv. Healthc. Mater.* **2018**, *7*, e1701150.

- [44] K. Satheeshkumar, P. Saravana Kumar, C. Nandhini, R. Shanmugapriya, K. N. Vennila, K. P. Elango, *Inorg. Chem. Commun.* **2022**, *139*, 109299.
- [45] K. Takeda, R. Kusuoka, M. Inukai, K. Igarashi, H. Ohno, N. Nakamura, *Biosens. Bioelectron.* **2021**, *174*, 112831.
- [46] A. Schäfer, V. A. Vetsova, E. K. Schneider, M. Kappes, M. Seitz, L. J. Daumann, P. Weis, *J. Am. Soc. Mass Spectrom.* **2022**, *33*, 722–730.
- [47] J. Nevarez, A. Turmo, J. Hu, R. P. Hausinger, *ChemCatChem* **2020**, *12*, 4242–4254.
- [48] K. Ikemoto, Y. Sakamoto, R. Tanaka, K. Ogata, N. Matsushita, S. Nakamura, *Cryst. Growth Des.* **2017**, *17*, 4118–4123.
- [49] H. Lumpe, P. Mayer, L. J. Daumann, *Acta Crystallogr. C Struct. Chem.* **2020**, *76*, 1051–1056.
- [50] Z. Zhang, L. M. V. Tillekeratne, R. A. Hudson, *Synthesis* **1996**, *1996*, 377–382.
- [51] E. J. Corey, A. Tramontano, *J. Am. Chem. Soc.* **1981**, *103*, 5599–5600.
- [52] S. Itoh, H. Kawakami, S. Fukuzumi, *J. Am. Chem. Soc.* **1997**, *119*, 439–440.
- [53] S. Itoh, M. Ogino, Y. Fukui, H. Murao, M. Komatsu, Y. Ohshiro, T. Inoue, Y. Kai, N. Kasai, *J. Am. Chem. Soc.* **1993**, *115*, 9960–9967.
- [54] S. Itoh, H. Kawakami, S. Fukuzumi, *Biochemistry* **1998**, *37*, 6562–6571.
- [55] G. Buchi, J. H. Botkin, G. C. M. Lee, K. Yakushijin, *J. Am. Chem. Soc.* **1985**, *107*, 5555–5556.
- [56] A. Roderick Mackenzie, C. J. Moody, C. W. Rees, *Tetrahedron* **1986**, *42*, 3259–3268.
- [57] J. A. Gainor, S. M. Weinreb, *J. Org. Chem.* **1982**, *47*, 2833–2837.
- [58] C. M. Glinkerman, D. L. Boger, *J. Am. Chem. Soc.* **2016**, *138*, 12408–12413.
- [59] J. B. Hendrickson, J. G. de Vries, *J. Org. Chem.* **1985**, *50*, 1688–1695.
- [60] J. V. Kempf, D. Gopal, W. Stalzer, US 2007/0072894 A1 **2007**.
- [61] J. A. Lewis, J. C. DiNardo, US 2014/0178316 A1 **2014**.
- [62] M. Ameyama, M. Hayashi, K. Matsushita, E. Shinagawa, O. Adachi, *Agric. Biol. Chem.* **1984**, *48*, 561–565.
- [63] A. H. Trotta, *Org. Lett.* **2015**, *17*, 3358–3361.
- [64] E. Fischer, F. Jourdan, *Ber. Dtsch. Chem. Ges.* **1883**, *16*, 2241–2245.
- [65] O. Doebner, W. v. Miller, *Ber. Dtsch. Chem. Ges.* **1883**, *16*, 2464–2472.

-
- [66] X. Zhang, Y. Zhang, C. Wang, X. Wang, *Signal Transduct. Target. Ther.* **2023**, *8*, 297.
- [67] C. Dupont, D. R. Armant, C. A. Brenner, *Semin. Reprod. Med.* **2009**, *27*, 351–357.
- [68] E. Jae Yoo, Y. Kyu Jang, M. Ae Lee, P. Bjerling, J. Bum Kim, K. Ekwall, R. Hyun Seong, S. Dai Park, *Biochem. Biophys. Res. Commun.* **2002**, *295*, 970–974.
- [69] J. Nakayama, J. C. Rice, B. D. Strahl, C. D. Allis, S. I. Grewal, *Science* **2001**, *292*, 110–113.
- [70] B. D. Strahl, C. D. Allis, *Nature* **2000**, *403*, 41–45.
- [71] T. Carell, M. Q. Kurz, M. Müller, M. Rossa, F. Spada, *Angew. Chem. Int. Ed.* **2018**, *57*, 4296–4312.
- [72] R. Jaenisch, A. Bird, *Nat. Genet.* **2003**, *33*, 245–254.
- [73] A. Jeltsch, R. Z. Jurkowska, *Nucleic Acids Res.* **2016**, *44*, 8556–8575.
- [74] G. R. WYATT, *Nature* **1950**, *166*, 237–238.
- [75] Y. Wang, F. C. C. Leung, *Bioinformatics* **2004**, *20*, 1170–1177.
- [76] J. K. Kim, M. Samaranayake, S. Pradhan, *Cell. Mol. Life Sci.* **2009**, *66*, 596–612.
- [77] F. R. Traube, T. Carell, *RNA Biol.* **2017**, *14*, 1099–1107.
- [78] M. Tahiliani, K. P. Koh, Y. Shen, W. A. Pastor, H. Bandukwala, Y. Brudno, S. Agarwal, L. M. Iyer, D. R. Liu, L. Aravind, A. Rao, *Science* **2009**, *324*, 930–935.
- [79] S. Ito, L. Shen, Q. Dai, S. C. Wu, L. B. Collins, J. A. Swenberg, C. He, Y. Zhang, *Science* **2011**, *333*, 1300–1303.
- [80] R. M. Kohli, Y. Zhang, *Nature* **2013**, *502*, 472–479.
- [81] M. L. Neidig, C. D. Brown, K. M. Light, D. G. Fujimori, E. M. Nolan, J. C. Price, E. W. Barr, J. M. Bollinger, C. Krebs, C. T. Walsh, E. I. Solomon, *J. Am. Chem. Soc.* **2007**, *129*, 14224–14231.
- [82] J. C. Price, E. W. Barr, B. Tirupati, J. M. Bollinger, C. Krebs, *Biochemistry* **2003**, *42*, 7497–7508.
- [83] P. J. Riggs-Gelasco, J. C. Price, R. B. Guyer, J. H. Brehm, E. W. Barr, J. M. Bollinger, C. Krebs, *J. Am. Chem. Soc.* **2004**, *126*, 8108–8109.
- [84] L. Hu, J. Lu, J. Cheng, Q. Rao, Z. Li, H. Hou, Z. Lou, L. Zhang, W. Li, W. Gong, M. Liu, C. Sun, X. Yin, J. Li, X. Tan, P. Wang, Y. Wang, D. Fang, Q. Cui, P. Yang, C. He, H. Jiang, C. Luo, Y. Xu, *Nature* **2015**, *527*, 118–122.

- [85] L. Hu, Z. Li, J. Cheng, Q. Rao, W. Gong, M. Liu, Y. G. Shi, J. Zhu, P. Wang, Y. Xu, *Cell* **2013**, *155*, 1545–1555.
- [86] S. Kal, L. Que, *J. Biol. Inorg. Chem.* **2017**, *22*, 339–365.
- [87] J.-U. Rohde, J.-H. In, M. H. Lim, W. W. Brennessel, M. R. Bukowski, A. Stubna, E. Münck, W. Nam, L. Que, *Science* **2003**, *299*, 1037–1039.
- [88] J. L. Que, M. Puri, *Bull. Jpn. Soc. Coord. Chem.* **2016**, *67*, 10–18.
- [89] T. Chantarojsiri, Y. Sun, J. R. Long, C. J. Chang, *Inorg. Chem.* **2015**, *54*, 5879–5887.
- [90] N. S. W. Jonasson, L. J. Daumann, *Chem. Eur. J.* **2019**, *25*, 12091–12097.
- [91] D. Schmidl, N. S. W. Jonasson, E. Korytiaková, T. Carell, L. J. Daumann, *Angew. Chem. Int. Ed.* **2021**, *60*, 21457–21463.
- [92] M. Hilbert, P. López, *Science* **2011**, *332*, 60–65.
- [93] J. Rothenberg, *Int. J. of Legal Inf.* **1998**, *26*, 1–22.
- [94] L. Ceze, J. Nivala, K. Strauss, *Nat. Rev. Genet.* **2019**, *20*, 456–466.
- [95] R. Heckel, G. Mikutis, R. N. Grass, *Sci. Rep.* **2019**, *9*, 9663.
- [96] N. Goldman, P. Bertone, S. Chen, C. Dessimoz, E. M. LeProust, B. Sipos, E. Birney, *Nature* **2013**, *494*, 77–80.
- [97] R. N. Grass, R. Heckel, M. Puddu, D. Paunescu, W. J. Stark, *Angew. Chem. Int. Ed.* **2015**, *54*, 2552–2555.
- [98] L. Organick, S. D. Ang, Y.-J. Chen, R. Lopez, S. Yekhanin, K. Makarychev, M. Z. Racz, G. Kamath, P. Gopalan, B. Nguyen, C. N. Takahashi, S. Newman, H.-Y. Parker, C. Rashtchian, K. Stewart, G. Gupta, R. Carlson, J. Mulligan, D. Carmean, G. Seelig, L. Ceze, K. Strauss, *Nat. Biotechnol.* **2018**, *36*, 242–248.
- [99] Y. Erlich, D. Zielinski, *Science* **2017**, *355*, 950–954.
- [100] V. Zhirnov, R. M. Zadegan, G. S. Sandhu, G. M. Church, W. L. Hughes, *Nature Mater.* **2016**, *15*, 366–370.
- [101] F. Sanger, S. Nicklen, A. R. Coulson, *PNAS* **1977**, *74*, 5463–5467.
- [102] D. R. Bentley, S. Balasubramanian, H. P. Swerdlow, G. P. Smith, J. Milton, C. G. Brown, K. P. Hall, D. J. Evers, C. L. Barnes, H. R. Bignell, J. M. Boutell, J. Bryant, R. J. Carter, R. Keira Cheetham, A. J. Cox, D. J. Ellis, M. R. Flatbush, N. A. Gormley, S. J. Humphray, L. J. Irving, M. S. Karbelashvili, S. M. Kirk, H. Li, X. Liu, K. S. Maisinger, L. J. Murray, B. Obradovic, T. Ost, M. L. Parkinson, M. R. Pratt,

- I. M. J. Rasolonjatovo, M. T. Reed, R. Rigatti, C. Rodighiero, M. T. Ross, A. Sabot, S. V. Sankar, A. Scally, G. P. Schroth, M. E. Smith, V. P. Smith, A. Spiridou, P. E. Torrance, S. S. Tzonev, E. H. Vermaas, K. Walter, X. Wu, L. Zhang, M. D. Alam, C. Anastasi, I. C. Aniebo, D. M. D. Bailey, I. R. Bancarz, S. Banerjee, S. G. Barbour, P. A. Baybayan, V. A. Benoit, K. F. Benson, C. Bevis, P. J. Black, A. Boodhun, J. S. Brennan, J. A. Bridgham, R. C. Brown, A. A. Brown, D. H. Buermann, A. A. Bundu, J. C. Burrows, N. P. Carter, N. Castillo, M. Chiara E Catenazzi, S. Chang, R. Neil Cooley, N. R. Crake, O. O. Dada, K. D. Diakoumakos, B. Dominguez-Fernandez, D. J. Earnshaw, U. C. Egbujor, D. W. Elmore, S. S. Etchin, M. R. Ewan, M. Fedurco, L. J. Fraser, K. V. Fuentes Fajardo, W. Scott Furey, D. George, K. J. Gietzen, C. P. Goddard, G. S. Golda, P. A. Granieri, D. E. Green, D. L. Gustafson, N. F. Hansen, K. Harnish, C. D. Haudenschield, N. I. Heyer, M. M. Hims, J. T. Ho, A. M. Horgan, K. Hoshler, S. Hurwitz, D. V. Ivanov, M. Q. Johnson, T. James, T. A. Huw Jones, G.-D. Kang, T. H. Kerelska, A. D. Kersey, I. Khrebtukova, A. P. Kindwall, Z. Kingsbury, P. I. Kokko-Gonzales, A. Kumar, M. A. Laurent, C. T. Lawley, S. E. Lee, X. Lee, A. K. Liao, J. A. Loch, M. Lok, S. Luo, R. M. Mammen, J. W. Martin, P. G. McCauley, P. McNitt, P. Mehta, K. W. Moon, J. W. Mullens, T. Newington, Z. Ning, B. Ling Ng, S. M. Novo, M. J. O'Neill, M. A. Osborne, A. Osnowski, O. Ostadan, L. L. Paraschos, L. Pickering, A. C. Pike, A. C. Pike, D. Chris Pinkard, D. P. Pliskin, J. Podhasky, V. J. Quijano, C. Racz, V. H. Rae, S. R. Rawlings, A. Chiva Rodriguez, P. M. Roe, J. Rogers, M. C. Rogert Bacigalupo, N. Romanov, A. Romieu, R. K. Roth, N. J. Rourke, S. T. Ruediger, E. Rusman, R. M. Sanches-Kuiper, M. R. Schenker, J. M. Seoane, R. J. Shaw, M. K. Shiver, S. W. Short, N. L. Sizto, J. P. Sluis, M. A. Smith, J. Ernest Sohna Sohna, E. J. Spence, K. Stevens, N. Sutton, L. Szajkowski, C. L. Tregidgo, G. Turcatti, S. Vandevondele, Y. Verhovsky, S. M. Virk, S. Wakelin, G. C. Walcott, J. Wang, G. J. Worsley, J. Yan, L. Yau, M. Zuerlein, J. Rogers, J. C. Mullikin, M. E. Hurles, N. J. McCooke, J. S. West, F. L. Oaks, P. L. Lundberg, D. Klenerman, R. Durbin, A. J. Smith, *Nature* **2008**, *456*, 53–59.
- [103] J. Clarke, H.-C. Wu, L. Jayasinghe, A. Patel, S. Reid, H. Bayley, *Nat. Nanotechnol.* **2009**, *4*, 265–270.
- [104] J. J. Kasianowicz, E. Brandin, D. Branton, D. W. Deamer, *PNAS* **1996**, *93*, 13770–13773.
- [105] Sandeep Shah, J. G. Elerath, *Annu. Reliab. Maintainability Symp. Proc.* **2004**, 163–167.
- [106] M. Meyer, Q. Fu, A. Aximu-Petri, I. Glocke, B. Nickel, J.-L. Arsuaga, I. Martínez, A. Gracia, J. M. B. de Castro, E. Carbonell, S. Pääbo, *Nature* **2014**, *505*, 403–406.
- [107] L. Orlando, A. Ginolhac, G. Zhang, D. Froese, A. Albrechtsen, M. Stiller, M. Schubert, E. Cappellini, B. Petersen, I. Moltke, P. L. F. Johnson, M. Fumagalli, J. T.

- Vilstrup, M. Raghavan, T. Korneliussen, A.-S. Malaspinas, J. Vogt, D. Szklarczyk, C. D. Kelstrup, J. Vinther, A. Dolocan, J. Stenderup, A. M. V. Velazquez, J. Cahill, M. Rasmussen, X. Wang, J. Min, G. D. Zazula, A. Seguin-Orlando, C. Mortensen, K. Magnussen, J. F. Thompson, J. Weinstock, K. Gregersen, K. H. Røed, V. Eisenmann, C. J. Rubin, D. C. Miller, D. F. Antczak, M. F. Bertelsen, S. Brunak, K. A. S. Al-Rasheid, O. Ryder, L. Andersson, J. Mundy, A. Krogh, M. T. P. Gilbert, K. Kjær, T. Sicheritz-Ponten, L. J. Jensen, J. V. Olsen, M. Hofreiter, R. Nielsen, B. Shapiro, J. Wang, E. Willerslev, *Nature* **2013**, *499*, 74–78.
- [108] D. Paunescu, R. Fuhrer, R. N. Grass, *Angew. Chem. Int. Ed.* **2013**, *52*, 4041.
- [109] L. Zhang, Z. Yang, K. Sefah, K. M. Bradley, S. Hoshika, M.-J. Kim, H.-J. Kim, G. Zhu, E. Jiménez, S. Cansiz, I.-T. Teng, C. Champanhac, C. McLendon, C. Liu, W. Zhang, D. L. Gerloff, Z. Huang, W. Tan, S. A. Benner, *J. Am. Chem. Soc.* **2015**, *137*, 6734–6737.
- [110] S. Hoshika, N. A. Leal, M.-J. Kim, M.-S. Kim, N. B. Karalkar, H.-J. Kim, A. M. Bates, N. E. Watkins, H. A. SantaLucia, A. J. Meyer, S. DasGupta, J. A. Piccirilli, A. D. Ellington, J. SantaLucia, M. M. Georgiadis, S. A. Benner, *Science* **2019**, *363*, 884–887.
- [111] A. W. Feldman, V. T. Dien, R. J. Karadeema, E. C. Fischer, Y. You, B. A. Anderson, R. Krishnamurthy, J. S. Chen, L. Li, F. E. Romesberg, *J. Am. Chem. Soc.* **2019**, *141*, 10644–10653.
- [112] D. A. Malyshev, K. Dhami, H. T. Quach, T. Lavergne, P. Ordoukhanian, A. Torkamani, F. E. Romesberg, *PNAS* **2012**, *109*, 12005–12010.
- [113] Y. Zhang, J. L. Ptacin, E. C. Fischer, H. R. Aerni, C. E. Caffaro, K. San Jose, A. W. Feldman, C. R. Turner, F. E. Romesberg, *Nature* **2017**, *551*, 644–647.
- [114] C. Switzer, S. E. Moroney, S. A. Benner, *J. Am. Chem. Soc.* **1989**, *111*, 8322–8323.
- [115] J. D. Bain, C. Switzer, A. R. Chamberlin, S. A. Benner, *Nature* **1992**, *356*, 537–539.
- [116] Z. Yang, D. Hutter, P. Sheng, A. M. Sismour, S. A. Benner, *Nucleic Acids Res.* **2006**, *34*, 6095–6101.
- [117] Z. Yang, A. M. Sismour, P. Sheng, N. L. Puskar, S. A. Benner, *Nucleic Acids Res.* **2007**, *35*, 4238–4249.
- [118] N. A. Leal, H.-J. Kim, S. Hoshika, M.-J. Kim, M. A. Carrigan, S. A. Benner, *ACS Synth. Biol.* **2015**, *4*, 407–413.
- [119] C. Mayer, G. R. McInroy, P. Murat, P. van Delft, S. Balasubramanian, *Angew. Chem. Int. Ed.* **2016**, *55*, 11144–11148.

- [120] M. Frommer, L. E. McDonald, D. S. Millar, C. M. Collis, F. Watt, G. W. Grigg, P. L. Molloy, C. L. Paul, *PNAS* **1992**, *89*, 1827–1831.
- [121] M. J. Booth, M. R. Branco, G. Ficz, D. Oxley, F. Krueger, W. Reik, S. Balasubramanian, *Science* **2012**, *336*, 934–937.
- [122] N. S. W. Jonasson, R. Janßen, A. Menke, F. L. Zott, H. Zipse, L. J. Daumann, *ChemBioChem* **2021**, *22*, 3333–3340.
- [123] E. Greco, A. E. Aliev, V. G. H. Lafitte, K. Bala, D. Duncan, L. Pilon, P. Golding, H. C. Hailes, *New J. Chem.* **2010**, *34*, 2634.
- [124] N. S. W. Jonasson, *Functional Models for Iron(II)/ α -Keto Acid Dependent Enzymes*, Doctoral dissertation, Ludwig-Maximilians-Universität Munich, **2021**.
- [125] G. Li, J. Chen, D.-Y. Zhu, Y. Chen, J.-B. Xia, *Adv. Synth. Catal.* **2018**, *360*, 2364–2369.
- [126] P. Ganapati Reddy, G. Kishore Kumar, S. Baskaran, *Tetrahedron Lett.* **2000**, *41*, 9149–9151.
- [127] C. Schwergold, G. Depecker, C. Di Giorgio, N. Patino, F. Jossinet, B. Ehresmann, R. Terreux, D. Cabrol-Bass, R. Condom, *Tetrahedron* **2002**, *58*, 5675–5687.
- [128] P. Xu, T. Zhang, W. Wang, X. Zou, X. Zhang, Y. Fu, *Synthesis* **2003**, *2003*, 1171–1176.
- [129] A. Vincze, R. E. Henderson, J. J. McDonald, N. J. Leonard, *J. Am. Chem. Soc.* **1973**, *95*, 2677–2682.
- [130] R. N. Salvatore, S. I. Shin, A. S. Nagle, K. W. Jung, *J. Org. Chem.* **2001**, *66*, 1035–1037.
- [131] D. Chaturvedi, S. Ray, *Monatsh. Chem.* **2006**, *137*, 127–145.
- [132] H. Sajiki, *Tetrahedron Lett.* **1995**, *36*, 3465–3468.
- [133] P. G. M. Wuts, T. W. Greene, *Greene’s protective groups in organic synthesis*, Wiley, Hoboken, 4th ed., **2007**.
- [134] K. L. Dueholm, M. Egholm, C. Behrens, L. Christensen, H. F. Hansen, T. Vulpius, K. H. Petersen, R. H. Berg, P. E. Nielsen, O. Buchardt, *J. Org. Chem.* **1994**, *59*, 5767–5773.
- [135] L. Liu, X. Ji, Y. Li, W. Ji, T. Mo, W. Ding, Q. Zhang, *Chem. Commun.* **2017**, *53*, 8952–8955.
- [136] R. Lopez, Y.-J. Chen, S. Dumas Ang, S. Yekhanin, K. Makarychev, M. Z. Racz, G. Seelig, K. Strauss, L. Ceze, *Nat. Commun.* **2019**, *10*, 2933.

- [137] A. Hofer, Z. J. Liu, S. Balasubramanian, *J. Am. Chem. Soc.* **2019**, *141*, 6420–6429.
- [138] S. A. Benner, A. M. Sismour, *Nat. Rev. Genet.* **2005**, *6*, 533–543.
- [139] J. W. Park, P. N. P. Lagniton, Y. Liu, R.-H. Xu, *Int. J. Biol. Sci.* **2021**, *17*, 1446–1460.
- [140] O. Andries, S. Mc Cafferty, S. C. de Smedt, R. Weiss, N. N. Sanders, T. Kitada, *J. Control. Release* **2015**, *217*, 337–344.
- [141] A. M. Sismour, S. A. Benner, *Nucleic Acids Res.* **2005**, *33*, 5640–5646.
- [142] G. S. Madugundu, J. Cadet, J. R. Wagner, *Nucleic Acids Res.* **2014**, *42*, 7450–7460.
- [143] A. Burdzy, K. T. Noyes, V. Valinluck, L. C. Sowers, *Nucleic Acids Res.* **2002**, *30*, 4068–4074.
- [144] J. Kaizer, E. J. Klinker, N. Y. Oh, J.-U. Rohde, W. J. Song, A. Stubna, J. Kim, E. Münck, W. Nam, L. Que, *J. Am. Chem. Soc.* **2004**, *126*, 472–473.
- [145] Y. Morimoto, J. Park, T. Suenobu, Y.-M. Lee, W. Nam, S. Fukuzumi, *Inorg. Chem.* **2012**, *51*, 10025–10036.
- [146] A. Barbieri, O. Lanzalunga, A. Lapi, S. Di Stefano, *J. Org. Chem.* **2019**, *84*, 13549–13556.
- [147] J. J. D. Sacramento, D. P. Goldberg, *Accounts Chem. Res.* **2018**, *51*, 2641–2652.
- [148] D. A. Proshlyakov, T. F. Henshaw, G. R. Monterosso, M. J. Ryle, R. P. Hausinger, *J. Am. Chem. Soc.* **2004**, *126*, 1022–1023.
- [149] A. D. Becke, *J. Chem. Phys.* **1993**, *98*, 5648–5652.
- [150] S. Grimme, J. Antony, S. Ehrlich, H. Krieg, *J. Chem. Phys.* **2010**, *132*, 154104.
- [151] R. Ditchfield, W. J. Hehre, J. A. Pople, *J. Chem. Phys.* **1971**, *54*, 724–728.
- [152] R. Krishnan, J. S. Binkley, R. Seeger, J. A. Pople, *J. Chem. Phys.* **1980**, *72*, 650–654.
- [153] A. Altun, F. Neese, G. Bistoni, *Beilstein J. Org. Chem.* **2018**, *14*, 919–929.
- [154] M. V. C. Greenberg, D. Bourc’his, *Nat. Rev. Mol. Cell. Biol.* **2019**, *20*, 590–607.
- [155] Y. He, J. R. Ecker, *Annu. Rev. Genom. Hum. G.* **2015**, *16*, 55–77.
- [156] Y.-F. He, B.-Z. Li, Z. Li, P. Liu, Y. Wang, Q. Tang, J. Ding, Y. Jia, Z. Chen, L. Li, Y. Sun, X. Li, Q. Dai, C.-X. Song, K. Zhang, C. He, G.-L. Xu, *Science* **2011**, *333*, 1303–1307.

- [157] A. Menke, R. C. A. Dubini, P. Mayer, P. Rovó, L. J. Daumann, *Eur. J. Inorg. Chem.* **2021**, 2021, 30–36.
- [158] J. Xiong, T.-T. Ye, C.-J. Ma, Q.-Y. Cheng, B.-F. Yuan, Y.-Q. Feng, *Nucleic Acids Res.* **2019**, 47, 1268–1277.
- [159] Y. Fu, G. Jia, X. Pang, R. N. Wang, X. Wang, C. J. Li, S. Smemo, Q. Dai, K. A. Bailey, M. A. Nobrega, K.-L. Han, Q. Cui, C. He, *Nat. Commun.* **2013**, 4, 1798.
- [160] J. Wu, H. Xiao, T. Wang, T. Hong, B. Fu, D. Bai, Z. He, S. Peng, X. Xing, J. Hu, P. Guo, X. Zhou, *Chem. Sci.* **2015**, 6, 3013–3017.
- [161] P. Barbaro, *Chemistry* **2006**, 12, 5666–5675.
- [162] C. Freire, C. Pereira, S. Rebelo in *Catalysis* (Eds.: J. J. Spivey, M. Gupta), The Royal Society of Chemistry, **2012**, pp. 116–203.
- [163] T. Chen, M. Qiu, Y. Peng, C. Yi, Z. Xu, *Coord. Chem. Rev.* **2023**, 474, 214863.
- [164] B. M. L. Dioos, I. F. J. Vankelecom, P. A. Jacobs, *Adv. Synth. Catal.* **2006**, 348, 1413–1446.
- [165] B. Altava, M. I. Burguete, E. García-Verdugo, S. V. Luis, *Chem. Soc. Rev.* **2018**, 47, 2722–2771.
- [166] I. Eş, J. D. G. Vieira, A. C. Amaral, *Appl. Microbiol. Biotechnol.* **2015**, 99, 2065–2082.
- [167] P. McMorn, G. J. Hutchings, *Chem. Soc. Rev.* **2004**, 33, 108–122.
- [168] L. M. Rossi, N. J. S. Costa, F. P. Silva, R. Wojcieszak, *Green Chem.* **2014**, 16, 2906.
- [169] H. Sand, R. Weberskirch, *Polym. Int.* **2017**, 66, 428–435.
- [170] M. Salavati-Niasari, M. Bazarganipour, *Appl. Surf. Sci.* **2009**, 255, 7610–7617.
- [171] A. R. Silva, K. Wilson, A. C. Whitwood, J. H. Clark, C. Freire, *Eur. J. Inorg. Chem.* **2006**, 2006, 1275–1283.
- [172] G.-J. Kim, J.-H. Shin, *Tetrahedron Lett.* **1999**, 40, 6827–6830.
- [173] M. L. Verma, S. Kumar, A. Das, J. S. Randhawa, M. Chamundeeswari, *Environ. Chem. Lett.* **2020**, 18, 315–323.
- [174] C. Ayats, A. H. Henseler, M. A. Pericàs, *ChemSusChem* **2012**, 5, 320–325.
- [175] R. P. Jumde, A. Di Pietro, A. Manariti, A. Mandoli, *Chem. Asian J.* **2015**, 10, 397–404.

- [176] A. R. McDonald, H. P. Dijkstra, B. M. J. M. Suijkerbuijk, G. P. M. van Klink, G. van Koten, *Organomet.* **2009**, *28*, 4689–4699.
- [177] A. R. McDonald, N. Franssen, G. P. van Klink, G. van Koten, *J. Organomet. Chem.* **2009**, *694*, 2153–2162.
- [178] R. A. Sheldon, R. Schoevaart, L. M. van Langen, *Biocatal. Biotransform.* **2005**, *23*, 141–147.
- [179] R. S. Khan, A. H. Rather, T. U. Wani, S.-U. Rather, T. Amna, M. S. Hassan, F. A. Sheikh, *Biotechnol. Bioeng.* **2023**, *120*, 22–40.
- [180] G. J. O'Neill, T. Egan, J. C. Jacquier, M. O'Sullivan, E. Dolores O'Riordan, *Food Chem.* **2014**, *160*, 46–52.
- [181] A. H. Chughtai, N. Ahmad, H. A. Younus, A. Laypkov, F. Verpoort, *Chem. Soc. Rev.* **2015**, *44*, 6804–6849.
- [182] R. de Paula, I. C. Santos, M. M. Simões, M. G. P. Neves, J. A. Cavaleiro, *J. Mol. Catal. A Chem.* **2015**, *404-405*, 156–166.
- [183] M. J. Sabater, A. Corma, A. Domenech, V. Fornés, H. García, *Chem. Commun.* **1997**, 1285–1286.
- [184] E. Serefoglou, K. Litina, D. Gournis, E. Kalogeris, A. A. Tziaila, I. V. Pavlidis, H. Stamatis, E. Maccallini, M. Lubomska, P. Rudolf, *Chem. Mater.* **2008**, *20*, 4106–4115.
- [185] C. Bianchini, P. Barbaro, V. Dal Santo, R. Gobetto, A. Meli, W. Oberhauser, R. Psaro, F. Vizza, *Adv. Synth. Catal.* **2001**, *343*, 41–45.
- [186] R. Zhai, B. Zhang, L. Liu, Y. Xie, H. Zhang, J. Liu, *Catal. Commun.* **2010**, *12*, 259–263.
- [187] A. Cunillera, C. Blanco, A. Gual, J. M. Marinkovic, E. J. Garcia-Suarez, A. Riisager, C. Claver, A. Ruiz, C. Godard, *ChemCatChem* **2019**, *11*, 2195–2205.
- [188] C. Vriamont, M. Devillers, O. Riant, S. Hermans, *Chem. Eur. J.* **2013**, *19*, 12009–12017.
- [189] D. Wang, D. Astruc, *Chem. Rev.* **2014**, *114*, 6949–6985.
- [190] L. Vaquer, P. Riente, X. Sala, S. Jansat, J. Benet-Buchholz, A. Llobet, M. A. Pericàs, *Catal. Sci. Technol.* **2013**, *3*, 706–714.
- [191] C. A. McNamara, M. J. Dixon, M. Bradley, *Chem. Rev.* **2002**, *102*, 3275–3300.
- [192] R. Akiyama, S. Kobayashi, *Angew. Chem. Int. Ed.* **2001**, *40*, 3469–3471.

- [193] R. B. Merrifield, *J. Am. Chem. Soc.* **1963**, *85*, 2149–2154.
- [194] X.-J. Huang, P.-C. Chen, F. Huang, Y. Ou, M.-R. Chen, Z.-K. Xu, *J. Mol. Catal. B Enzym.* **2011**, *70*, 95–100.
- [195] S. Datta, L. R. Christena, Y. R. S. Rajaram, *3 Biotech* **2013**, *3*, 1–9.
- [196] P. Piaggio, C. Langham, P. McMorn, D. Bethell, P. C. Bulman-Page, F. E. Hancock, C. Sly, G. J. Hutchings, *J. Chem. Soc. Perkin Trans. 2* **2000**, 143–148.
- [197] J. Jamis, J. R. Anderson, R. S. Dickson, E. M. Campi, W. Jackson, *J. Organomet. Chem.* **2001**, *627*, 37–43.
- [198] P. Riente, J. Yadav, M. A. Pericàs, *Org. Lett.* **2012**, *14*, 3668–3671.
- [199] P. Wang, F. Zhang, Y. Long, M. Xie, R. Li, J. Ma, *Catal. Sci. Technol.* **2013**, *3*, 1618.
- [200] Y. Wang, X. Song, S. Shao, H. Zhong, F. Lin, *RSC Adv.* **2012**, *2*, 7693.
- [201] N. E. Leadbeater, K. A. Scott, L. J. Scott, *J. Org. Chem.* **2000**, *65*, 3231–3232.
- [202] S. Sakai, Y. Liu, T. Yamaguchi, R. Watanabe, M. Kawabe, K. Kawakami, *Biotechnol. Lett.* **2010**, *32*, 1059–1062.
- [203] L. Zhu, X.-Q. Liu, H.-L. Jiang, L.-B. Sun, *Chem. Rev.* **2017**, *117*, 8129–8176.
- [204] A. Phan, A. U. Czaja, F. Gándara, C. B. Knobler, O. M. Yaghi, *Inorg. Chem.* **2011**, *50*, 7388–7390.
- [205] Z. Lin, Z.-M. Zhang, Y.-S. Chen, W. Lin, *Angew. Chem. Int. Ed.* **2016**, *55*, 13739–13743.
- [206] Y.-F. Chen, Y.-C. Ma, S.-M. Chen, *Cryst. Growth Des.* **2013**, *13*, 4154–4157.
- [207] G. Gelbard, *Ind. Eng. Chem. Res.* **2005**, *44*, 8468–8498.
- [208] G. Gelbard, F. Breton, M. Quenard, D. C. Sherrington, *J. Mol. Catal. A Chem.* **2000**, *153*, 7–18.
- [209] N. A. Paras, D. W. MacMillan, *J. Am. Chem. Soc.* **2001**, *123*, 4370–4371.
- [210] K. Hou, J. Börgel, H. Z. H. Jiang, D. J. SantaLucia, H. Kwon, H. Zhuang, K. Chakarawet, R. C. Rohde, J. W. Taylor, C. Dun, M. V. Paley, A. B. Turkiewicz, J. G. Park, H. Mao, Z. Zhu, E. E. Alp, J. Zhao, M. Y. Hu, B. Lavina, S. Peredkov, X. Lv, J. Oktawiec, K. R. Meihaus, D. A. Pantazis, M. Vandone, V. Colombo, E. Bill, J. J. Urban, R. D. Britt, F. Grandjean, G. J. Long, S. DeBeer, F. Neese, J. A. Reimer, J. R. Long, *Science* **2023**, *382*, 547–553.

- [211] N. S. W. Lindlar Né Jonasson, A. Menke, L. Senft, A. Squarcina, D. Schmidl, K. Fisher, S. Demeshko, J. C. Kruse, T. Josephy, P. Mayer, J. Gutenthaler-Tietze, P. Comba, F. Meyer, I. Ivanović-Burmazović, L. J. Daumann, *Inorg. Chem.* **2025**, *64*, 3719–3734.
- [212] D. Schmidl, N. S. W. Lindlar Né Jonasson, A. Menke, S. Schneider, L. J. Daumann, *ChemBioChem* **2022**, *23*, e202100605.
- [213] Y. Sun, J. P. Bigi, N. A. Piro, M. L. Tang, J. R. Long, C. J. Chang, *J. Am. Chem. Soc.* **2011**, *133*, 9212–9215.
- [214] R. Shelkov, A. Melman, *Eur. J. Org. Chem.* **2005**, *2005*, 1397–1401.
- [215] X.-C. Su, B. Man, S. Beeren, H. Liang, S. Simonsen, C. Schmitz, T. Huber, B. A. Messerle, G. Otting, *J. Am. Chem. Soc.* **2008**, *130*, 10486–10487.
- [216] R.-r. Tang, Q. Zhao, Z.-e. Yan, Y.-m. Luo, *Synth. Commun.* **2006**, *36*, 2027–2034.
- [217] C. R. Goldsmith, T. D. P. Stack, *Inorg. Chem.* **2006**, *45*, 6048–6055.
- [218] Michael Price, *AAAS Articles DO Group*, **2021**, <https://www.science.org/content/article/replicate-or-not-replicate>, Accessed: 02.03.2025.
- [219] L. J. Farrugia, *J. Appl. Crystallogr.* **2012**, *45*, 849–854.
- [220] Y. Li, R. Singh, A. Sinha, G. C. Lisensky, M. Haukka, J. Nilsson, S. Yiga, S. Demeshko, S. J. Gross, S. Dechert, A. Gonzalez, G. Farias, O. F. Wendt, F. Meyer, E. Nordlander, *Inorg. Chem.* **2023**, *62*, 18338–18356.
- [221] E. Guibal, *Prog. Polym. Sci.* **2005**, *30*, 71–109.
- [222] D. J. Macquarrie, J. J. E. Hardy, *Ind. Eng. Chem. Res.* **2005**, *44*, 8499–8520.
- [223] V. K. Mourya, N. N. Inamdar, *React. Funct. Polym.* **2008**, *68*, 1013–1051.
- [224] F.-L. Mi, C.-Y. Kuan, S.-S. Shyu, S.-T. Lee, S.-F. Chang, *Carbohydr. Polym.* **2000**, *41*, 389–396.
- [225] A. N. Singh, S. Singh, N. Suthar, V. K. Dubey, *J. Agric. Food. Chem.* **2011**, *59*, 6256–6262.
- [226] G. A. F. Roberts, K. E. Taylor, *Makromol. Chem.* **1989**, *190*, 951–960.
- [227] W. Kemp, *Organic Spectroscopy*, Macmillan Education UK, London, 3rd ed., **1991**.
- [228] B. Li, C.-L. Shan, Q. Zhou, Y. Fang, Y.-L. Wang, F. Xu, L.-R. Han, M. Ibrahim, L.-B. Guo, G.-L. Xie, G.-C. Sun, *Mar. Drugs* **2013**, *11*, 1534–1552.
- [229] O. A. Monteiro, C. Airoidi, *Int. J. Biol. Macromol.* **1999**, *26*, 119–128.

- [230] I. Migneault, C. Dartiguenave, M. J. Bertrand, K. C. Waldron, *BioTechniques* **2004**, *37*, 790–6, 798–802.
- [231] L. H. H. Olde Damink, P. J. Dijkstra, M. J. A. van Luyn, P. B. van Wachem, P. Nieuwenhuis, J. Feijen, *J. Mater. Sci.: Mater. Med.* **1995**, *6*, 460–472.
- [232] D. T. Cheung, M. E. Nimni, *Connect. Tissue Res.* **1982**, *10*, 187–199.
- [233] P. M. Hardy, G. J. Hughes, H. N. Rydon, *J. Chem. Soc. Perkin Trans. 1* **1979**, 2282.
- [234] T. Tashima, M. Imai, Y. Kuroda, S. Yagi, T. Nakagawa, *J. Org. Chem.* **1991**, *56*, 694–697.
- [235] P. Monsan, G. Puzo, H. Mazarguil, *Biochim.* **1976**, *57*, 1281–1292.
- [236] R. Karunanithy, T. Holland, P. Sivakumar, *Langmuir* **2021**, *37*, 5242–5251.
- [237] D. R. Walt, V. I. Agayn, *Trends Anal. Chem.* **1994**, *13*, 425–430.
- [238] J. H. Babler, M. C. Atwood, J. E. Freaney, A. R. Vizslay, *Tetrahedron Lett.* **2007**, *48*, 7665–7667.
- [239] X. Jie, Y. Shang, Z.-N. Chen, X. Zhang, W. Zhuang, W. Su, *Nat. Commun.* **2018**, *9*, 5002.
- [240] Akku&scdil, S. Çetinus, H. N. Öztıp, *Enzyme Microb. Technol.* **2000**, *26*, 497–501.
- [241] M. L. Foresti, M. L. Ferreira, *Enzyme Microb. Technol.* **2007**, *40*, 769–777.
- [242] M. Monier, D. M. Ayad, Y. Wei, A. A. Sarhan, *Int. J. Biol. Macromol.* **2010**, *46*, 324–330.
- [243] R. Muzzarelli, *Enzyme Microb. Technol.* **1980**, *2*, 177–184.
- [244] C.-Y. Chen, S. L. Burkett, H.-X. Li, M. E. Davis, *Microporous Mater.* **1993**, *2*, 27–34.
- [245] C.-Y. Chen, H.-X. Li, M. E. Davis, *Microporous Mater.* **1993**, *2*, 17–26.
- [246] F. Di Renzo, H. Cambon, R. Dutartre, *Microporous Mater.* **1997**, *10*, 283–286.
- [247] S. Bhattacharyya, G. Lelong, M.-L. Saboungi, *J. Exp. Nanosci.* **2006**, *1*, 375–395.
- [248] J. A. S. Costa, R. A. de Jesus, D. O. Santos, J. F. Mano, L. P. Romão, C. M. Paranhos, *Micropor. Mesopor. Mat.* **2020**, *291*, 109698.
- [249] G. Martínez-Edo, A. Balmori, I. Pontón, A. Del Martí Río, D. Sánchez-García, *Catal.* **2018**, *8*, 617.

- [250] D. P. Sahoo, D. Rath, B. Nanda, K. M. Parida, *RSC Adv.* **2015**, *5*, 83707–83724.
- [251] F. Adam, H. Osman, K. M. Hello, *J. Colloid. Interface Sci.* **2009**, *331*, 143–147.
- [252] C. Baleizão, B. Gigante, M. J. Sabater, H. Garcia, A. Corma, *Appl. Catal. A Gen.* **2002**, *228*, 279–288.
- [253] L. A. Carpino, E. M. E. Mansour, J. Knapczyk, *J. Org. Chem.* **1983**, *48*, 666–669.
- [254] C. Haensch, C. Ott, S. Hoepfner, U. S. Schubert, *Langmuir* **2008**, *24*, 10222–10227.
- [255] K. Soai, M. Watanabe, A. Yamamoto, *J. Org. Chem.* **1990**, *55*, 4832–4835.
- [256] P. Sutra, D. Brunel, *Chem. Commun.* **1996**, 2485.
- [257] Y. Li, C. M. Santos, A. Kumar, M. Zhao, A. I. Lopez, G. Qin, A. M. McDermott, C. Cai, *Chem. Eur. J.* **2011**, *17*, 2656–2665.
- [258] M. D. Driessen, H. L. Junghans, L. Hartmann, U. I. M. Gerling-Driessen, *Chem. Eur. J.* **2022**, preprint. doi: 10.1101/2022.10.24.513273.
- [259] R. M. Fratila, M. Navascuez, J. Idiago-López, M. Eceiza, J. I. Miranda, J. M. Aizpurua, J. M. de La Fuente, *New J. Chem.* **2017**, *41*, 10835–10840.
- [260] J. G. Großmann, *Synthesis of New Derivatives of a Pentapyridine Ligand with Functionalities for Immobilization of the Respective Iron Complexes*, Master thesis, Heinrich-Heine-University Düsseldorf, **2025**.
- [261] J. Lee, H. Kim, S. Han, E. Hong, K.-H. Lee, C. Kim, *J. Am. Chem. Soc.* **2014**, *136*, 12880–12883.
- [262] H. E. Gottlieb, V. Kotlyar, A. Nudelman, *J. Org. Chem.* **1997**, *62*, 7512–7515.
- [263] G. M. Sheldrick, *Acta Crystallogr. A Found. Adv.* **2015**, *71*, 3–8.
- [264] B. Bechlars, D. M. D’Alessandro, D. M. Jenkins, A. T. Iavarone, S. D. Glover, C. P. Kubiak, J. R. Long, *Nature Chem.* **2010**, *2*, 362–368.
- [265] J. Cong, D. Kinschel, Q. Daniel, M. Safdari, E. Gabrielsson, H. Chen, P. H. Svensson, L. Sun, L. Kloo, *J. Mater. Chem. A* **2016**, *4*, 14550–14554.
- [266] I. M. Bell, J. M. Erb, R. M. Freidinger, S. N. Gallicchio, J. P. Guare, M. T. Guidotti, R. A. Halpin, D. W. Hobbs, C. F. Homnick, M. S. Kuo, E. V. Lis, D. J. Mathre, S. R. Michelson, J. M. Pawluczyk, D. J. Pettibone, D. R. Reiss, S. Vickers, P. D. Williams, C. J. Woyden, *J. Med. Chem.* **1998**, *41*, 2146–2163.
- [267] P. Stoss, E. Kaes, G. Eibel, U. Thewalt, *J. Heterocycl. Chem.* **1991**, *28*, 231–236.
- [268] J. R. Bartels-Kelch, J. B. Mahoney, A. J. Puttick, *J. Org. Chem.* **1985**, *50*, 980–987.
- [269] T. T. Sakai, A. L. Pogolotti, D. V. Santi, *J. Heterocycl. Chem.* **1968**, *5*, 849–851.